DESIGN, DEVELOPMENT AND ANALYSIS OF THE FRICTION STIR WELDING PROCESS

Calvin Blignault

Design, Development and Analysis of the Friction Stir Welding Process

Submitted to

FACULTY: ELECTRICAL, INDUSTRIAL &
MECHANICAL ENGINEERING
PORT ELIZABETH TECHNIKON

For the proposed research in the programme

Magister Technologiae: Mechanical Engineering

by

Calvin Blignault, B. Tech. Mech. Eng.

Date of Submission: **Promoters: Dr. D. G. Hattingh**

Friday, 13 December 2002 **Prof. T. I. van Niekerk**

I Calvin Blignault hereby declare that:

- the work done in this thesis is my own;
- all sources used or referred to have been documented and recognized; and
- this theses has not been previously submitted in full or partial fulfillment of the requirements for an equivalent or higher qualification at any other educational institution.

Author Signature: **Date:**

2002-12-13

I wish to acknowledge the contributions by the following:

The Lord Jesus Christ for the persons and systems he timelessly put in place, and for giving me the strength and dedication to complete this project to the best of my ability.

My promoters, Dr. D. G. Hattingh and Dr. T. I. van Niekerk for their guidance and encouragement.

All the team members in the Manufacturing Technology Research Centre as well as Mrs. A. els Botes and Mr. C. du Preez for guidance in strength of materials; Mr. J. Wang and Mr. I. Clark for all their guidance and support on the electrical modifications and control development of the machine.

The National Research Foundation and research committee of the Port Elizabeth Technikon for financial assistance. This enabled the purchasing of hardware and software required for the experimental set-up and to make a visit to another international institution possible.

The library staff of the Port Elizabeth Technikon for their friendly assistance.

All members of rectorate of the Port Elizabeth Technikon for providing climate and means for performing my research.

My family, Aubrey, Noeline and Craig Blignault as well as my girlfriend Sharon Farnworth for their love and support throughout the duration of my research.

ABSTRACT

The development of a CNC-based technology FSW machine to accurately produce friction stir weld samples that can be analyzed for research purposes is implemented and discussed. A process diagnosis and control scheme to improve the process monitoring and weld evaluation capabilities of an FSW machine are proposed and implemented. Basic CNC-based hardware implementation such as optical encoders and inverters for process control are explained and verified. The control scheme and framework of interfaces to the digital I/O cards for PC user interface are explained. An advanced monitoring system which senses process performance parameters such as tool temperature, 3-axis tool forces, torque and spindle speed are explained. Mechanical designs and manufacturing techniques such as tool, clamp and backing plate designs are explained and verified. The process parameters for quality optimization are investigated and optimized by making use of Correlation and Regression Analysis. The statistical data and analytical relationships between welding parameters (independent) and each of the performance parameters (dependent) are obtained and used to simulate the machining process.

The weld research samples are tested for strength and integrity making use of various scientific testing techniques. The reliability of the samples are also evaluated and compared to that of other institutions. Process variables and the optimum operating range of the Friction Stir Welding machine is determined and a framework for further research into weld quality optimization is set.

Introduction

Friction Stir Welding (FSW) is a solid-phase joining technique invented and patented at TWI (UK) for the butt and lap welding of ferrous and non-ferrous metals and plastics. FSW is a continuous process that involves plunging a portion of a specially shaped rotating tool between the abutting faces of the joint. The relative motion between the tool and the substrate generates frictional heat that creates a plasticised 'third-body' region around the immersed portion of the tool. The contact of the shouldered region of the tool with the work pieces also generates significant frictional heat, as well as preventing plasticised material from being expelled. The tool is

moved (relatively) along the joint line, forcing the plasticised material to coalesce behind the tool to form a solid-phase joint.

At present, Friction Stir Welding has found various applications in a number of areas. Potential applications are space shuttle fuel tanks, aluminum decking for car ferries, manufacturing of compound aluminum extrusions and automotive structural components. Most of the applications are on aluminum alloys although several facilities have reported experiments on titanium alloys and steels. The process is not yet fully understood and further research is required to optimize this technology.

To improve quality and increase welding speed a better understanding of tool geometry and interaction with material behavior would be necessary. Historically, the criteria for development of an advanced tool tip have largely been qualitative due to difficulty generalizing the design. It is important to investigate the relationship between the different welding parameters and their influence on material behavior since the material being welded endures a high range of static and dynamic frictional forces.

Objective of Research

Development of a FSW machine

The development of the FSW machine will be made possible by converting a conventional milling machine into an adequate, functional, workstation where experimental friction stir welded joints may be performed on various base materials.

Process Monitoring

Process parameters such as welding speed and feed must be monitored and evaluated to obtain various comparisons between process characteristics and welded material characteristics.

Material Characterization

The welded joints must be analyzed to determine their metallurgical behavior. Comparisons must be made to other methods of welding techniques to prove the advantages of using FSW.

Problem Statement

To develop a FSW facility for analysis of the interaction between friction stir weld parameters and thin aluminum plate behavior.

Subproblems

Various subproblems will have to be addressed in order to successfully accomplish the intended purpose and objective of this research project. These will include the following:

Subproblem 1 (Conversion)

Conversion of a conventional vertical milling machine to a structural multifunctional workstation in order to perform experimental friction stir weld samples on thin aluminum plate

Subproblem 2 (Tool Design)

Design and development of a tool that will also lead to a better understanding of the interfacing of the tool tip with the material

Subproblem 3 (Clamp Design)

Design and manufacture of clamping surfaces and backing plates to support the base material being welded

Subproblem 4 (Process Monitoring)

Investigate, evaluate and control of process welds with the aid of embedded sensors

Subproblem 5 (Weld Evaluation)

To determine and evaluate the weld capabilities and performance of the FSW facility at the MTRC

Hypothesis

To develop an experimental set-up for a friction stir welding unit using a process design methodology based on theoretical and experimental analysis from a standard vertical milling machine that will produce acceptable research samples.

Delimitations

The development of the FSW unit will purely be for research purposes.

Only longitudinal butt welds on aluminum alloy plate ranging with plate thickness of 1 to 20mm will be considered since the machine power is limited. Development of profile welds will not be considered until we fully understand the characteristics involved during normal longitudinal butt welds.

Mechanical tests (ex. fatigue and tensile tests) will be carried out on welded specimens to compare various property behaviors but this project will not aim to broach further in advanced material research such as Synchrotron Radiation for Residual Stress Measurement.

For the purpose of the investigation into the characteristic behavior of the welded joints we will use Aluminum alloy 5083 H321 since comparable information is available on these types of alloys and is used readily in industrial applications.

Assumptions

- The standard vertical milling machine will have adequate power to produce a friction stir weld.

- The increment adjustment for feed and speed will be adequate for accurate adjustment of the welding process.

- Adequate analysis of the weld for comparison of property behavior produced can be conducted by means of fatigue, tensile, hardness and impact testing alone.

- At the time when experimental welding should be addressed basic electrical equipment will be operational.

- Background literature will be available for accessing certain parameters on friction stir welding techniques.

- The result and outcome will be similar to that expected from other friction stir welding machines.

- It is assumed that the investigation will lead to a better understanding of the welding process and that the material properties achieved will be in close approximation to that what is expected.

Importance of the Research

Within the Technikon

It would be a Technikon based research project that would expand the research to further areas in friction stir welding. A fundamental research framework in this field will be launched.

A research workstation for multidisciplinary research into FSW will be set up on which researchers will be able to do hands-on experimental welding on various types of materials as well as intelligent control.

This research project will contribute to the development of fields in design, intelligent machining, mechatronics and materials research at the Technikon.

General

Improved material fatigue life and reduction in crack growth are only two of many other advantages that friction stir welding introduced. Further development and more advanced application for FSW will assist in establishing FSW as a more acceptable joining technique.

Advantages of friction stir welding have resulted in widespread interest and rapid development of the application thereof in industry. The friction stir welding techniques are playing an increasingly important role in manufacturing industries.

Other researchers and industries can benefit from possible new and better methodology developed by the Technikon researchers.

The project could make a contribution to other research fields by encouraging other academic institutions to also develop a better understanding in FSW.

Summary of Related Literature and Discussions

The study of literature has been concentrated on the mechanical response of friction stir welds. The property characterization of materials being welded depends on certain weld parameters and tool designs.

The FSW process

A wear resistant rotating tool is used to join sheet and plate materials such as aluminum, copper, lead and others. In laboratory experiments, magnesium, zinc, titanium and steel have also been friction stir welded. The welds are made below the melting point in the solid state.

Designs of tool tips

The ability to weld faster at a given thickness relates critically to the FSW tool design. At TWI a new development, reported by *Dawes*[3,13], has been the introduction of a scroll profile on the tool shoulder. *Thomas and Gittos*[4,13] reported the development of two new types of tools known as Whorl and Triflute. Mostly new inventions in tool manufacture arise at TWI since they hold the patent.

The other well-known development was from NASA[14] and Boeing for the invention of a retractable tool tip. Related papers of these new achievements are available.

Material Characterization

Some of the comparisons, related to material characterization, have already been analyzed and documented in papers. Some of the latest papers released are as follows:

- Latest publication 2001 to be released: Y.J. Chao and K.W. Miller., Friction Stir Welding Effects on Dynamic Properties of AA2024-T3 and AA7075-T351, Welding Journal.

- Year 2000 release: Y.J. Chao., Heat Transfer Analysis and Test of Friction Stir Joining of AA-2195 Plates, Presentation at Aeromat, Bellevue, WA.

- A.P. Reynolds., W.D. Lockwood and T.U. Seidel., Processing-Property Correlation on Friction Stir Welds, Materials Science Forum, Vols. 331-337, (2000) pp. 1719-1724, 2000 Trans Tech Publications, Switzerland Proceedings of ICAA-7, Charlottesville, VA, (April 2000)

Other related literature on latest technology and findings are available on CD's. The 1st, 2nd and 3rd International FSW Symposiums held on 1999,2000 and 2001 are available.

Research Methodology

This project is envisaged to comprise of the following stages:

- Investigation and development of criteria describing the welding process and basic procedure

- Establishment of important parameters to create a friction stir weld. Such parameters will include feed range, vertical force application, temperature regulation, material and tool sizes that will indicate the specification of material and weld speed limits for the proposed machine.

- Design and manufacturing of a tool tip that can perform a friction stir weld

- Design and manufacture of clamping devices to ensure stability and accuracy of the welding process

- Conversion and development of a conventional milling machine into a friction stir welding unit with an appropriate workstation to analyze data

- Creating successive butt welds on aluminum plates by using CNC technology

- Revision on previous tool designs and welding techniques so that possible improvements to the process can be made

- The selection and installments of embedded sensors for the monitoring of process behavior

- Development of a conceptual design methodology for the welding process and procedure by monitoring certain parameters such as weld temperature, process speed, axial force and vibration

- Comparing and evaluating FSW joint characteristics in certain aluminum plates to that specified by other institutions

The Researcher's Qualifications

- National Diploma in Mechanical Engineering – N Dip Mech Eng - Port Elizabeth Technikon (2000)

- Bachelor of Mechanical Engineering – B Tech Mech Eng - Port Elizabeth Technikon (2001)

The FSW Process

The main objective of this chapter is to obtain a better understanding of the Friction Stir Welding Process and current developments. In this chapter fundamental knowledge will be presented and in so doing will provide insight to some basic operational issues, which relates to the welding process. The principal of operation, development and reasons for using this welding technique with relevance to the advantage of this process for future manufacturing of metal joining, will be discussed.

Background to FSW and related processes

Friction stir welding is a solid state joining technique, which has made possible the welding of a number of materials that were previously extremely difficult to weld reliably without voids, cracking or distortion. The method was derived from conventional friction welding.

The earliest reference to the use of friction heat for solid-phase welding and forming appeared over a century ago in a United States patent.[1] A period of fifty years then passed before any significant advancement in friction technology took place namely a British patent in 1941 that introduced what is now known as friction surfacing.[2] Yet another fifty years went by before friction stir welding (FSW) was invented and patented in Cambridge at TWI (The Welding Institute of UK) in 1991.[3] This relatively recent innovation has permitted friction technology to be used to produce continuous welded seams for plate fabrication, particularly in light alloys.

Aluminum alloys are used in many applications today where the combination of high strength and low weight are attractive. Shipbuilding is one in which the low weight can be of significant value. In fact, the first aluminum boat was built in 1891 and the first welded aluminum ship in 1953.[4] The two most frequently used aluminum alloys for shipbuilding are AA5083 (AlMg4.5Mn) for plates and AA6082 (AlSi1Mg) for extrusions. The main alloying element in the 5000 series is magnesium.

MIG welding is a flexible and productive method and is therefore widely used for welding of aluminum alloys in shipbuilding. However, two disadvantages with MIG welding are deformation of the base material and a decrease in strength within the heat affected zone. Other fusion welding techniques like TIG and plasma welding are also widely used. However, these methods have the same weakness as MIG welding. FSW presented an alternative welding/joining technique to existing fusion welding methods.

Friction stir welding techniques have developed to a stage, in the early 21st century, where they are applied in small-scale production. Currently 51 organizations hold non-exclusive licenses to use the process. Most of them are industrial companies, and

several of them exploit the process in commercial production, e.g. in Scandinavia, USA, Japan and Australia.[5] They have filed more than 285 patent applications related to FSW.

The characteristics of the FSW technique can be compared with other friction process variants. For example, when Continuous Drive Rotary, Inertia, Linear, Orbital and Arcuate friction welding variants are used to join two bars of the same material and same diameter or aligned cross-section, axial shortening (consumption of the bars) occurs equally from each bar to form a common plasticised 'third body'. However, differences in diameter or section, lead to preferential consumption of the smaller component. Differences of material in one of the parts to be joined also lead to preferential consumption of the comparatively softer material.[6] The unequal consumption and temperature distribution in rotary friction welding between different diameter bars has already been studied[7,8] and is illustrated in Figure 2.1.

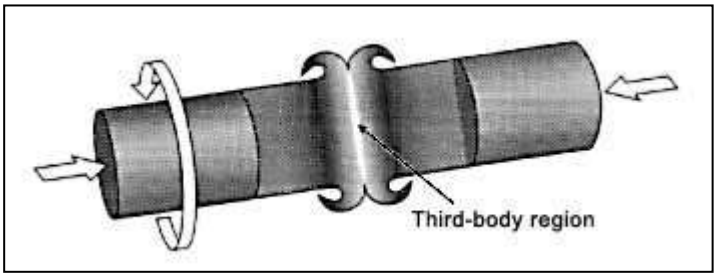

This preferential consumption and reprocessing of one component in a friction system has been put to good use in the development of Friction Surfacing, as illustrated in Figure 2.2. Other related processes are Friction Hydro Pillar Processing and Friction Pillaring, Radial Friction Welding and Friction Plunge Welding.

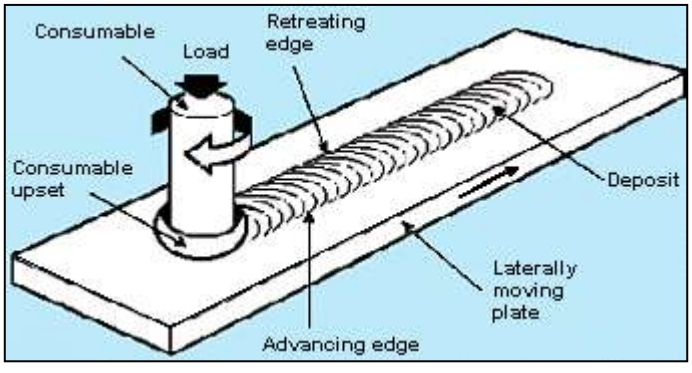

Figure 0.2 Friction Surfacing[15]

Friction Stir Welding is a further development in that only the workpiece weld region is processed, to form a solid-phase welded joint. Friction Extrusion and Friction Third-body are exceptions to the latter variants in that the consumed and reprocessed material is introduced into the friction system. This introduced material, which has a comparatively lower thermal softening temperature than the components being welded are frictionally treated or extruded to provide a 'third-body' material. Suitably conditioned, this 'third-body' material can be harnessed either as an extruded product or be used as a joining medium.

By introducing new workpiece material at a nominally ambient temperature, the lateral movement in Friction Surfacing[8,9] and FSW modifies the already unequal temperature distribution. This is due to the comparatively small diameter rotating consumable bar in Friction Surfacing and the rotating tool in FSW. Both these techniques rely on producing suitable temperature and shear conditions within the 'third-body' transient region. In Friction Surfacing it exists between the consumable bar and the substrate while it exists between the tool and the workpiece in FSW.

In Friction Surfacing any increase in temperature differential (by the intrusion of cold substrate material) enhances the deposition mechanism and allows comparatively harder materials to be deposited onto nominally softer materials.[9,10,11]

Principal of Operation

FSW uses a non-consumable tool to generate frictional heat at the point of welding, inducing gross plastic deformation of the workpiece, resulting into a complex mix

across the joint. The plates to be joined are placed on a rigid backing plate and clamped in a manner that prevents the abutting joint faces from separating. A cylindrical-shouldered tool, with a specially projecting pin (probe) with a screw thread, is rotated and slowly plunged into the joint line. The pin length is similar to the required weld depth.[12] The shoulder of the tool is forced against the plates. The rotating tool causes friction heating of the plates which in turn lowers their mechanical strength. The threads on the pin assist in ensuring that plastically deformed material flows around the pin as the tool advances along the joint line. As the tool proceeds along the joint line, frictional heating is maintained ahead of the tool ensuring the required plastic state. It subsequently stirs and recombines the plasticized material to the side of the tool where the material cools to form a solid state weld. At the end of the weld, the tool is retracted from the plate and leaves a hole at the end of the weld.

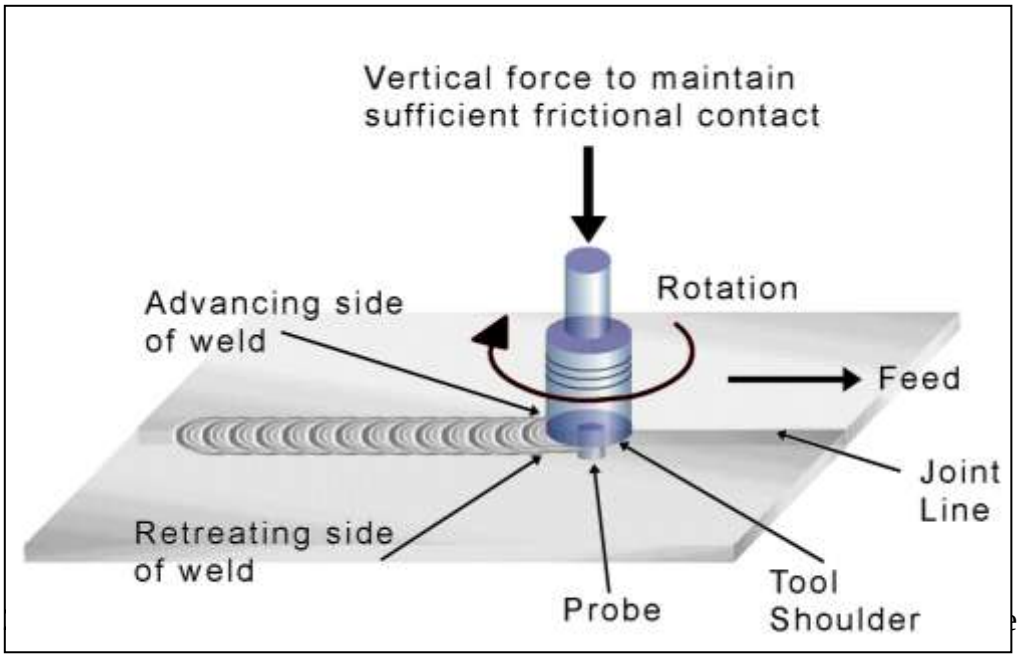

Figure

to the tool rotation, friction stir welds are not symmetric about the weld centerline. The side of the weld on which the rotational velocity of the tool has the same direction as the welding velocity (X-axis) is designated the advancing side of the

weld. The side of the weld on which the two velocities have opposite direction is designated the retreating side of the weld. This onion flow pattern that the tool leave is also schematically illustrated in Figure 2.4. Friction stir welding can be regarded as an autogenous keyhole joining technique without the creation of liquid metal. The consolidated weld material is thus free of typical fusion welding defects. No consumable filler material or profiled edge preparation is normally necessary.

Figure 0.4 Schematic illustrating flow pattern[15]

The microstructure of a friction stir weld is unlike that of a fusion weld in that no solidification products are present and the grains in the weld region are equiaxed and highly refined. Indeed, the FSW microstructure is that of a wrought rather than a cast product.

Welding Parameters

Welding Speed

Depending on the thickness and type of material, the tool rotational speed is between 200 to 1000 revolutions per minute. The pin section of the tool is forced into the material under 15 000 to 45 000 N of force.[14] The pin continues rotating and moves forward at an average rate of 80 to 250 mm/min. The highest feed rate possible depends on various parameters e.g. tool geometry, spindle speed and the downward force (Z-axis). As the pin rotates, friction heats the surrounding material and rapidly produces a softened 'plasticized' region around the pin. As the pin travels forward, the material behind the pin is forged under the pressure from the tool shoulder and consolidates to form a bond. Unlike fusion welding, no actual melting occurs in this process and the weld is left in the same fine-grained condition as the parent metal.

TWI established an empirical formula that determines the relationship between welding speed, material thickness, tool geometry and material type. The following formula indicates the relationship between these parameters[45]:

$$V = \phi . \frac{\beta}{t} \qquad \textbf{(0-1)}$$

V = feed rate mm/min
ϕ = material factor
β = tool factor
t = material thickness (mm)

Certain factors such as tool and material factors are implemented in the formula to compromise for error in process performance. Factors are experimentally pre-determined to make the use of various tool and material geometries compatible with the formula. The following tool factors are provided:

Initial tool designs with no special pin and shoulder profiles have $\beta = 1$
Improved tool designs will have $\beta = 2$

For material factors, the following has been designated:

Lead = 3700
Copper = 300
Aluminum 6xxx = 1200
Aluminum 7xxx and 2xxx = 600
Magnesium = 400
Titanium = 100
Aluminum 5xxx = 700

This project focuses on the welding of 5000 series aluminum with plate thickness of 6mm. Since the researcher does not know the efficiency of the tool geometry at this stage, a factor of 1 and/or 2 is used. The estimated welding speed can be calculated as follows:

$$V = 700 \times \frac{1 \text{ or } 2}{6} = \xrightarrow{116 \text{ or } 233 \text{ mm / min}}$$

Software related packages are also available that determine the outcome of certain parameter settings according to this empirical formula.

Weld Quality

Thomas W.M.[16] describes the optimization for the friction stir welding process as follows:

"*For a given tool shape and tool inclination, the process only involves, rotational speed and travel rate, which enables the FSW to be readily optimized*."

To make the optimizing process intelligent, plunge force and other variables will have to be measured and controlled. The contribution of this research project will focus on factors that determine the possibility of the weld such as the tool geometry, spindle and feed rates as well as downward axial force of the tool shoulder. When thicker material is being welded more attention must be given to the pin or probe design of the tool since adequate mixing of the plasticized material is essential. Parameters like

temperature, torque and force profiles that change during the welding process will be sensed and monitored. This then provides a scope for further research into intelligent welding techniques. Many uncertainties also arise along related FSW parameters and weld quality for various materials. The development of an FSW facility with monitoring capabilities will enhance research into weld quality.

Relationship of viscosity levels to welding parameters

In order to reduce tool wear, increase weld quality and minimize welding defects it is important for the friction stir welding technologist to understand the close relationship between friction stir welding parameters and the viscosity levels reached in the base material during a welding trial. This relationship gives us a better understanding around the visual characterization of material flow during a weld.

During the welding trial the welding parameters can be adjusted to correspond to weld quality to a certain degree. Looking at obstacles like side flash, onion ring flow pattern, plunge depth and plastisized material flow, it is possible to adjust the parameter settings accordingly. This plastisized third body needs to be controlled by adjusting some parameters.

Development of a satisfactory 3-dimensional process model for FSW depends on determination of the material properties in the fully-plasticised (third body) region. The material viscosity is determined using plunge testing, where the forces that act on a rotating steel pin as it penetrates the aluminum alloy base material are measured and converted into effective viscosities and temperature output.[31] Since this process was already addressed in the past by other institutions the researcher will only be concerned about the relationship between the viscosity and welding parameters obtained by these inspections.

A relation involving material viscosity and key welding parameters was developed based on the requirement that satisfactory joining depends on the formation of a plasticised layer immediately ahead of the moving tool. The width of the plasticised region formed ahead of the traversing tool is inversely proportional to the travel speed and is also dependent on the amount of preheat available prior to the FSW.[31] The width of the plasticised region ahead of the rotating pin also depends on the ratio of the square of the angular velocity and the travel speed as well as the thermal conductivity of the aluminum alloy base material.[31]

The width of the plasticised region (φ) formed ahead of the moving pin is determined by the relation[31]:

$$\xi = \mu\beta\alpha\varpi \left(\frac{R\varpi}{V_{welding}}\right)\left(\frac{R}{k_{th}\left(T_{solidus} - T_{ambient}\right)}\right) \qquad \textbf{(0-2)}$$

where,

R :	tool radius
μ :	material viscosity
α :	thermal diffusivity
ϖ :	angular velocity of the tool
$V_{welding}$:	the travel speed
$T_{solidus}$:	solidus temperature of the substrate
k_{th} :	thermal conductivity of the substrate
ν :	viscosity of the plasticised region
β :	Constant

The one dimensional model equation above is explained in detail in reference [31].

In conclusion the material viscosity values for 6061 aluminum base material were determined using combination of numerical modeling and experimental testing. These material properties are critical during the development of a satisfactory 3-dimensional process model for FSW. The following has been concluded from the

investigations done by the department of Metallurgy and Materials Science, University of Toronto, Ontario, Canada:

1. The viscosity of the base material decreases when the rotational speed of the tool increases. The decrease in relative viscosity values corresponded well with a well-known fluid flow relation indicating that the material viscosity would be inversely proportional to the angular velocity.[31]

2. The calculated and experimentally measured temperature values were in close agreement during plunge testing, with the calculated peak temperature at the periphery of the rotating pin corresponding with the solidus temperature (582 °C) of 6061-T6 base material. It is worth emphasizing that this peak temperature was calculated without applying any *a priori* assumptions during the numerical modeling process.[31]

3. A relation was developed based on the requirement that satisfactory friction stir welding depends on the formation of a plasticised layer immediately ahead of the moving tool. The width of the plasticised region formed immediately ahead of the traversing tool was inversely proportional to the travel speed, the preheat level prior to FSW and the thermal conductivity of the aluminum alloy base material. The width of the plasticised region ahead of the rotating pin also depended on the ratio of the square of the angular velocity and the travel speed.[31]

During the experimental weld trials on 6mm aluminum and 6.35mm brass plate interesting results were found that could be closely linked to the formation of this plasticised layer or region. As mentioned earlier, the width of this region depended

on various factors like travel speed, preheat level and the thermal conductivity of the material. During our evaluation we found that the spindle speed (related to angular velocity) had a great influence on the heat being dissipated throughout the material.

From Figure 2.5, welding the 6mm thick A5083 H321 at a relatively low spindle speed of 400rpm and feed rate of 60mm/min complete penetration was obtained. From the backing end of the plate the TMAZ is about 3mm apart on either side of the joint line. This then proves that the heat flow is dissipated throughout the entire plate thickness when using these parameters.

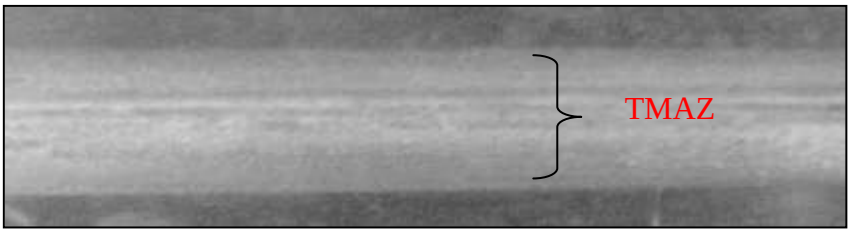

Figure 0.5 Figure illustrating the complete penetration of the heat throughout the plate viewing it from the backing end (Alluminum - 400rpm @ 60mm/min)

When keeping all welding parameters constant and only increasing the spindle speed to 650rpm a drastic change in weld quality and surface finish exists. From the surface discoloring, viewed in Figure 2.6, it can be seen that the surface temperature increases but still not creating enough heat distribution throughout the entire plate thickness. This lack of fusion can be verified when viewing the backing end of the plate in Figure 2.6 and 2.7 where the TMAZ decreases considerably. Materials of rubbing components cannot warm up throughout during the short-term process of high speed friction, and the heat is absorbed by thin surface layers only.[39]

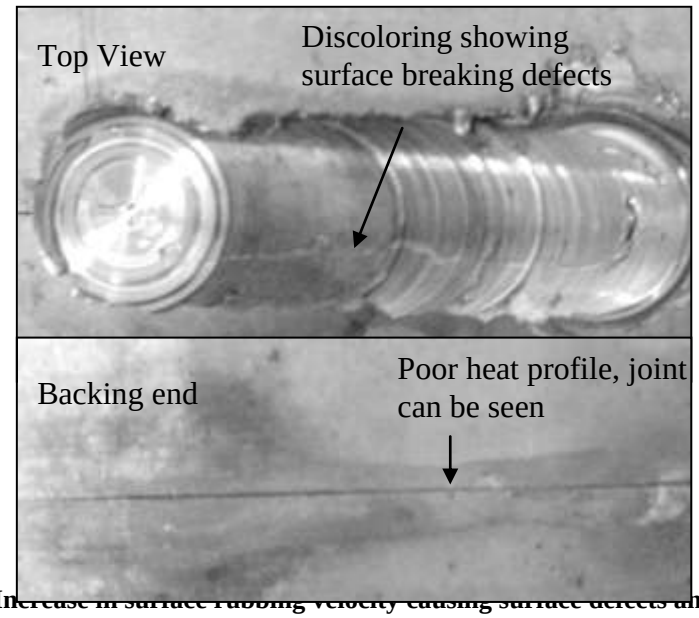

Figure 0.6 Increase in surface rubbing velocity causing surface defects and incomplete temperature distribution (Brass - 850rpm @ 40mm/min)

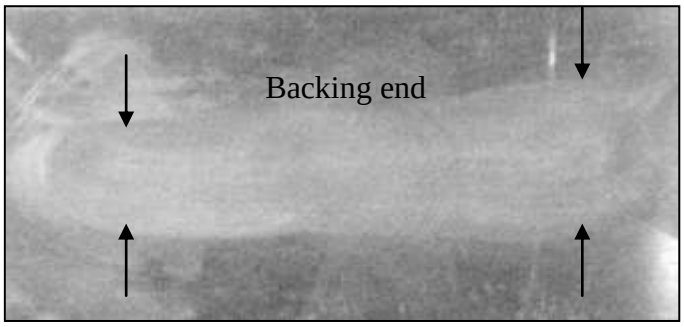

Figure 0.7 Increase in surface rubbing velocity causing incomplete temperature distribution and a decreasing heat pattern (Aluminum 650rpm @ 60mm/min)

In conclusion the philosophy would be to establish a certain critical point or limitation of maximum surface rubbing velocity (or rpm) with respect to time whereas the researcher can control this width of the plasticised region or heat distribution pattern by means of spindle speed only, since it will be preferred to keep other parameters such as welding speed and plunge depth constant. Further research into this area is necessary to verify this philosophy and preliminary phenomenon.

Weld formation and flow patterns

In friction joining and forming, the process is similar to a fluid layer of high viscosity between solid components in relative motion and under significant compressive

loading. The thixotropic properties and fluid flow features that occur in conventional friction welding have been reported, along with friction induced 'third body' conditions and superplasticity that occur as a result of extreme plastic deformation. Thus the science of these processes, in some respects, is probably closely allied to that of rheology.[17,18,19]

The relative motion between the tool and the substrate generates sufficient frictional heat to reduce the yield strength of the material. As the temperature rises the yield strength falls below the applied shear stress so that a 'third body' region of highly deformed plasticised material forms around the immersed and contacting regions of the tool.

The outer edges of the weld track only experience limited friction from the periphery of the tool shoulder. In contrast, and depending on the degree of tool tilt, most of the shoulder acts upon the central region of the weld track. Inevitably, it is the central region that receives most friction as well as the stirring due to the probe.[15]

This highly plasticised 'third-body' material provides some hydrostatic effect. As the rotating tool moves along the joint, this hydrostatic effect helps the plasticised weld material to flow around the tool. The plasticised weld material then coalesces behind the tool, to form a solid phase joint as the tool moves away.

Figure 2.8 provides evidence that hydrostatic pressure leads to displacement of plasticised material. The recovery of the through-thickness dimension was proven during the welding of dissimilar metal produced by TWI. Figures 2.9 & 2.10 show

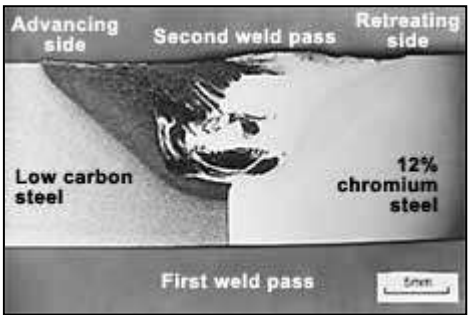

that even where the trailing edge (heel part of the shoulder) is sunk below the plate surface recovery in plate thickness is possible.

Figure 0.8 Transverse macrosection of dissimilar 12% chromium alloy steel/carbon steel. First weld pass showing increased hydrostatic effect with 12% chromium alloy shallow ridge above the plate surface[15]

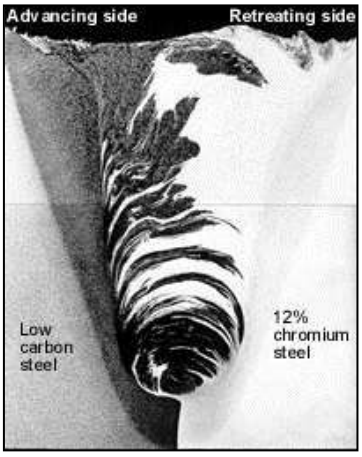

Figure 0.9 Transverse taper macrosection of dissimilar 12% chromium/low carbon steel FSW joint showing cyclic flow pattern[15]

In the case of dissimilar materials, preferential recovery occurs with the more plasticised material, especially when positioned on the retreating side of the weld. The presence of a shallow bulge above the plate surface, as shown in Figure 2.10, confirms this effect.

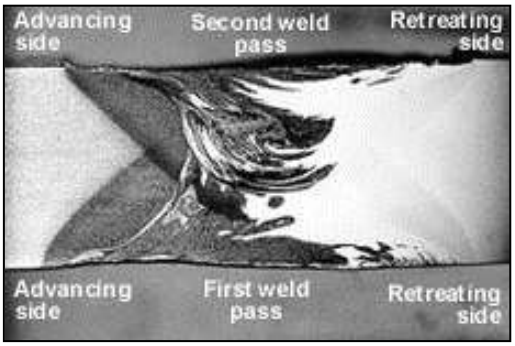

Figure 0.10 Transverse macrosection of dissimilar 12% chromium alloy steel/low carbon steel FSW double sided weld (First pass hand ground flat)[15]

More of these appearances and surface related weld features are dealt with in subset chapters.

Both friction stir welding and friction surfacing processes show some lack of symmetry. The use of optimized conditions however, virtually ensures that differences between the advancing side and retreating side do not cause any adverse effects. However, with less suitable conditions, the asymmetric nature of the process can lead to defects. In friction surfacing lack of symmetry can lead to excess expulsion of material at the retreating edge of the deposit, as shown in Figure 2.11. In FSW, defects can be found such as buried voids, "worm holes" or a surface-breaking groove that usually runs along the advancing side. Figure 2.6 illustrates the surface breaking defect and Figure 2.12 illustrates the "worm hole" defect that was produced during the first welding trials at PE Technikon.

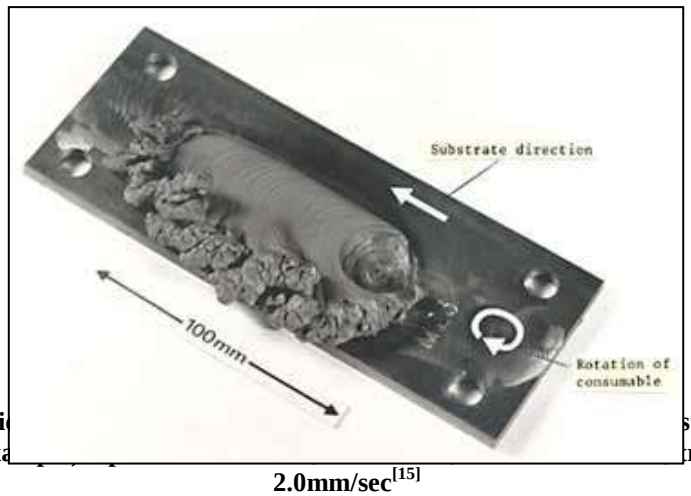

Figure 0.11 Fri sticised material (extreme exa raverse rate 2.0mm/sec[15]

The inherent lack of process symmetry causes a differential pressure around the probe such that the rotating tool tries to veer away from the retreating side of the weld

towards the advancing side[15]. This phenomenon can be verified by future development in polar force plots that can be generated to graphically illustrate the force pattern around the tool while welding. This 2D force pattern will be explained in Chapter 5. Secure fixturing and robust machine tool equipment prevent any noticeable sideways deflection.[1,2]

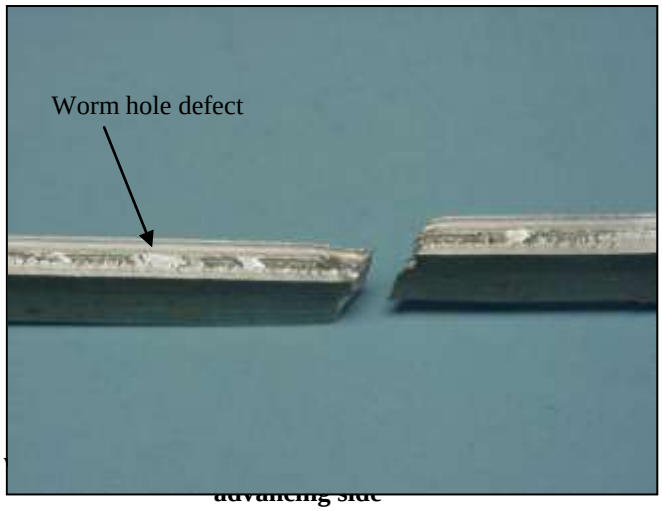

Figure 0.12 An all [illegible] defect on the advancing side

Improving Thermal Management

Investigations are continuing to study the value of preheating ferrous and other comparatively high temperature materials to improve welding speed and minimize tool wear.

Before frictional contact is made the workpiece material will be at its hardest, and therefore, be more prone to tool wear and damage. Therefore the plunging of the tool into the material is regarded as the most critical.

It may be beneficial, for the higher temperature materials, to preheat the touch down region of workpieces so as to condition this region before plunging the probe into the work piece. The welding process can then progress without further additional

heating. It is expected that this simple procedure will significantly reduce tool wear during plunging.

Depending on the properties of the workpiece material and its thermal diffusivity, it can also be beneficial to continue the preheating throughout the welding operation. Conversely, cooling or even welding certain materials underwater is found to be beneficial.[15]

Preheating of the tool is also recommended for certain tool materials that are brittle at room temperature, so that they become more ductile and thus better suited for carrying out the welding process. It is considered that any suitable heating process can be adopted for heating the workpiece. Heating techniques may include the use of flame, coherent or incoherent radiation, friction, induction resistance or arc/plasma. High frequency induction heating and high frequency resistance heating may be of particular advantage since they can achieve heating through the thickness of the workpiece, rather than just surface heating.

Processes such as TIG, MIG, sub-arc and hot wire welding methods as well as resistance hot wire can be used to fill gaps between plates just in front of the FSW tool. This hybrid approach effectively allows the FSW technique to become a gap filling and a post fusion welding process to refine and improve the weld from the prior fusion process.

In some cases, where the FSW process is used at high temperatures, a non-oxidising gaseous atmosphere may be needed to protect the joint from atmospheric contamination and to prevent certain tool and workpiece materials becoming oxidised.

The FSW process seems ideally suited to the welding of hot plate where the entire plate or product is raised to a higher temperature e.g. hot plate welding in the steel mills or hot strip tube manufacture in pipe mills.

Advantages and Disadvantages of FSW

Generically friction welding and its related process variants are characterized by being thermo-mechanically energy efficient solid-phase joining techniques. Friction stir welding is no exception and in addition the welding operation is simple and operator friendly. The following lists some of the advantages of the process at present: -

- The process is machine tool technology based, which can be semi-or fully automated.
- The surface appearance approaches to that of a rough machined surface. In most cases this reduces production costs in further processing and finishing.
- For most materials the process does not normally require a shielding gas.
- High integrity welds are produced for an increasing range of materials.
- Parent metal chemistry is retained without any gross segregation of alloying elements.
- The process is essentially an autogeneous non-consumable keyhole technique. (Therefore, eliminating the problems associated with the selection and storage of consumables.)
- Plain low carbon steel and 12% chromium alloy steel can be welded in a single pass in thickness from 3-12mm.
- Steel thickness up to 25mm can be welded from two sides. (Similarly to arc welding, the double sided weld joint is more process tolerant.)

- Welding is carried out without spatter, ozone formation, or visual radiation associated with fusion welding techniques.
- The process is relatively quiet.
- The process is solid-phase, with process temperature regimes much lower than fusion techniques, thus avoiding problems which can occur with the liquid phase, such as alloy segregation, porosity and cracking.
- The process can be carried out in all positions - vertical and overhead.
- No special edge preparation is required (only nominally square edged abutting plates are needed for a butt joint), so it saves consumable material, time and money.
- A feature associated with FSW weldments is the comparatively reduced distortion levels.
- FSW is easy to automate, and user friendly.
- Equipment is simple with relatively low running costs.
- Once established optimized process conditions can be pre-set and subsequent in-process monitoring can be used as a first line check that weld quality is being maintained.
- Like most friction techniques the process can be operated underwater.

The following lists some of the disadvantages:

- It is necessary to clamp the workpiece materials firmly. Suitable jigging and backing bars are needed to prevent the abutting plates moving apart or material breaking out through the underside of the joint.
- An end of run hole is left as the probe is withdrawn.
- To overcome the latter feature run-on/run-off plates which take the end of the run hole from the substrate joints are sometimes used or the hole can be left in

a suitable region. In addition, one of the friction hole filling techniques, such as taper plug and friction hydro pillar welding can be considered.

- At present for plain low carbon and 12% chromium steels the welding traverse speed is typically in the order of 1.7 to 4 mm/sec which could be considered comparatively slow for relatively thin plate material.
- For plain low carbon steels and to a lesser extent 12% chromium alloy steels tool wear is a limiting feature.

Industrial Applications

The process has been used for the manufacture of butt welds, overlap welds, T-sections, fillet, and corner welds. For each of these joint geometries specific tool designs are required which are being further developed and optimized. Longitudinal butt welds and circumferential lap welds of Al alloy fuel tanks for space flights have been friction stir welded and successfully tested.[24]

The FSW process can also cope with circumferential, annular, non-linear, and three-dimensional welds. Since gravity has no influence on the solid-phase welding process, it can be used in horizontal, vertical, overhead and orbital configurations. Current investigations at GKSS are to improve profile, or welds made on curvatures. Figure 2.13 shows typical joint configurations possible to FSW:

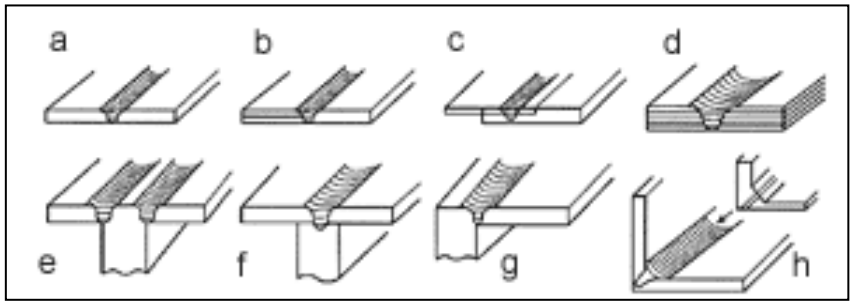

Figure 0.13 Joint configurations[24]

a. Square butt
b. Combined butt and lap
c. Single lap
d. Multiple lap
e. 3 Piece T butt
f. 2 Piece T butt
g. Edge butt
h. Possible corner fillet weld

Shipbuilding and marine industries

The shipbuilding and marine industries are two of the first industry sectors that have adopted the process for commercial applications. The process is suitable for joining panels for decks and floors, aluminum extrusions, hulls and superstructures, helicopter platforms, offshore accommodation, marine and transport structures, masts and booms for sailing boats and refrigeration plants. Some of these applications are illustrated in Figure 2.14.

Aerospace industry

Currently the aerospace industry is welding prototype parts by friction stir welding. Opportunities exist to weld skins to spars, ribs, and stringers for use in military and civilian aircraft. This offers significant advantages compared to riveting and machining from solid, such as reduced manufacturing costs and weight savings. Longitudinal butt welds and circumferential lap welds of Al alloy fuel tanks for space vehicles have been friction stir welded and successfully tested. The process could also be used to increase the size of commercially available sheets by welding them before forming. The friction stir welding process can therefore be considered for wings, fuselages, empennages, cryogenic fuel tanks for space vehicles, aviation fuel tanks, external throw away tanks for military aircraft, military and scientific rockets and repair of faulty MIG welds.

Railway industry

The commercial production of high speed trains made from aluminum extrusions which may be joined by friction stir welding has been published. Applications include high speed trains, underground carriages, railway tankers and container bodies.

Land transportation

The friction stir welding process is currently being experimentally assessed by several automotive companies and suppliers to this industrial sector for its commercial application. A joint EWI/TWI Group Sponsored Project is investigating joint designs for automotive lightweight structures. Potential applications are engine and chassis cradles, wheel rims, attachments to hydroformed tubes, tailored blanks, truck bodies, tail lifts for trucks, mobile cranes, armour plate vehicles, fuel tankers, caravans, buses and airfield transportation vehicles, frames and personnel bridges. Figure 2.15 illustrates this application.

Construction industry

The use of portable FSW equipment is possible for aluminum bridges, facade panels made from aluminum, copper or titanium, window frames, aluminum pipelines, aluminum reactors for power plants and the chemical industry, heat exchangers, air conditioners and pipe fabrication.

Electrical industry

The electrical industry shows increasing interest in the application of friction stir welding for electric motor housings, busbars, electrical connectors, and encapsulation of electronics.

Other industry sectors

Friction stir welding can also be considered for refrigeration panels, cooking equipment, white goods, gas tanks and gas cylinders, connecting of aluminum or copper coils in rolling mills and various furniture.

Figure 0.14 Esab SuperStir machine at Hydro Marine Aluminum to weld aluminum extrusions for shipbuilding panels[22]

Available Machines and Equipment for FSW

If one is to consider building a friction stir welding machine, it will be advisable to first do a thorough literature review on currently available FSW machines in order to expand knowledge on machine and construction parameters. A range of modified machines now exists at TWI, which is briefly discussed below.

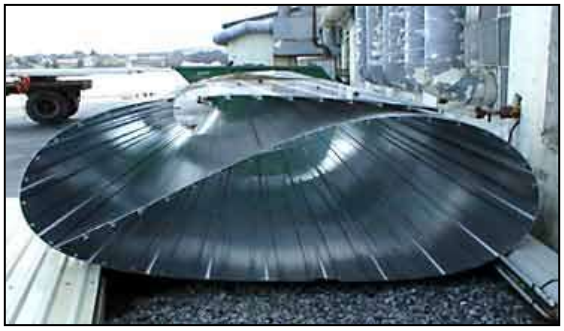

Figure 0.15 Prefabricated FSW panel for catamaran side-wall, rolled for road transport (at Hydro Marine Aluminum)[22]

Modular machine FW22 to weld large size specimens

A laboratory machine was built in October 1996 to accommodate large sheets and to weld prototype structures. The modular construction of FW22 enables it to be easily enlarged for specimens with even larger dimensions. This machine is illustrated in Figure 2.16.

Figure 0.16 FW22 to weld large size sheet metal[23]

The machine specifications can briefly be described as follows:

- Sheet thickness: 3mm-15mm aluminium
- Maximum welding speed: up to 1.2m/min
- Current maximum sheet size: 3.4m length x 4m width
- Current maximum working height: 1.15m

Moving gantry machine FW21

The purpose built friction stir welding machine FW21 was built in 1995. This machine uses a moving gantry with which straight welds up to 2m long can be made. It was used to prove that welding conditions can be achieved which guarantee constant weld quality over the full length of long welds.

Figure 0.17 FW21, the moving gantry machine to weld long continuous welds[23]

Machine specifications as follows:

- Sheet thickness: 3mm-15mm aluminum
- Maximum welding speed: up to 1.0m/min
- Current maximum sheet size: 2m length x 1.2m width

Heavy duty Friction Stir Welding machines FW18 and FW14

Two existing machines within TWI's Friction and Forge Welding Group have been modified exclusively to weld thick sections. The following thickness range has been experimentally investigated but the machines are not yet at their limits.

- Sheet thickness: 5mm-50mm aluminum from one side
  10mm-100mm aluminum from two sides
  5mm thick titanium from one side
- Power: max 22kW
- Welding speed: max 1m/min

High rotation speed machine FW20

For welding thin aluminum sheets TWI equipped one of its existing machines with an air cooled high speed head which allows rotation speeds of up to 15,000rev/min.

- Sheet thickness: 1.2mm-12mm aluminum
- Maximum welding speed: up to 2.6m/min, infinitely variable

Friction Stir Welding demonstrator FW16

TWI's small transportable machine produces annular welds with hexagonal aluminum alloy discs. It has been exhibited on fairs in USA, Sweden, Germany, and the United Kingdom in recent years. It is an eye catcher which enables visitors to produce their first friction stir weld themselves. It can be operated with 110V or 220V-240V and has been used by TWI and its member companies to demonstrate the process.

Other machines

Portable CRC machine

TWI commissioned a prototype machine, which was designed and manufactured by their CRC partners at the Department for Mechanical Engineering of the University of Adelaide, Australia. This machine can be carried and aligned by two operators without the use of a crane or other lifting device. It has been used to weld curved sheets under site conditions in a shipyard.

Commercially available FSW machines

Purpose built friction stir welding machines have been designed, manufactured, and commissioned. One of them, which is installed at Marine Aluminum Aanensen, Norway, is capable of making 16m long welds. It was built by ESAB in Laxå, Sweden and is used for the mass production of panels, which are made by joining extruded profiles. The machine and the welding procedure have been approved by Det Norske Veritas and Germanischer Lloyd. Several shorter machines, some of them with CNC systems of up to 5 axes, have been built for experiments and for the production of prototype parts. ESAB demonstrated FSW with a welding speed of 750mm/min in 5mm thick aluminum (6000 series) at the 14th International Welding Fair in Essen. Even friction stir welds with very rigid robots were successful and demonstrated the possibility of non-linear welds.

ESAB in Laxå (Sweden) started in December 2000 with the manufacture of two new SuperStir^{TM} machines. These machines are representing the state of the art of commercially available FSW equipment and will be used in the EuroStir Project[23] which is part funded by the Eureka program and focuses on 'European Industrialisation of Friction Stir Welding'. The first contract was signed between

ESAB and TWI. The equipment has a gantry type design with a welding area of 8 x 5m and two heads of different sizes. The first head will be used for welding thin sheets with high rotation speeds. The second head can be used for thick sheets while applying high downward forces. The machine will be capable of welding aluminum alloys of 15mm and larger. Up to 25mm thick aluminum plates can be welded in the centerline of the machine. At a later stage the machine will be used for welding full size industrial prototypes. The machine is large enough to weld for example a complete side panel of a double-decker bus.

ESAB received also another order from the first European FSW "job" shop, DanStir ApS in Copenhagen (Denmark). This machine is of the same gantry type design as that for TWI but is designed for a welding area of 5 x 3m and has one welding head. It has a vertical clearance under the gantry of 0.85m. It is equipped with a high-power main drive and a hydraulic actuator for vertical spindle movements. The versatile control system allows for numerous operations modes including position or force control and/or various combinations thereof. The power-full design facilitates up to 100kN (10t) downward force on the parts to be welded, and up to 40kN (4t) transverse thrust on the welding head. This allows the welding of all aluminum alloys in thickness up to 15mm and beyond.

A Powerstir machine has been tailor-made by Crawford Swift in Halifax (UK) and delivered in autumn 1999 to BAE Systems in Filton (UK) where it is being used for fabricating prototype aluminum wings and fuselage skins for large aircraft, among them the future Airbus A380. The FSW machine was named '360' which refers to its 3-axis CNC capability and 60kW spindle power. This machine can be viewed in Figure 2.19. The mechanics of the machine withstand a 100kN (=10t) downward

force with minimum deflection. The machine is 11.5m long x 5.7m wide x 4.7m high and takes the basic form of a moving table machine. The table, onto which the workpieces are clamped, moves underneath the gantry and is accelerated by the latest servomotor and ball-screw technology to speeds of up to 8m/min.

Figure 0.18 Crawfo ndle power.

Another SuperStir™ machine has been installed at Sapa and is used for the production of large panels and heavy profiles with a welding length of up to 14.5m and a maximum width of 3m. This machine has three welding heads, which means that it is possible to weld from two sides of the panel at the same time, or to use two welding heads (positioned on the same side of the panel) starting at the center of the workpiece and welding in opposite directions. Using this method, the productivity of the FSW installation is substantially increased.

Conclusion

The advantages and disadvantages for FSW in industry were mentioned. This gave the researcher a good idea on what the process is capable of doing and in what direction research must lead to. Although machines are currently made for friction stir welding our knowledge about the process from an academic point of view is still limited. Only aluminum alloys are currently being welded in a limited industry and

South Africa, as such has never done FSW related processes nor any investigations into this welding process. There are no tables of related parameter settings available for producing a good weld on certain materials and thus proves that research in this field needs more attention.

This chapter provided the researcher with grounding knowledge about machine capacities and what need to be controlled during the FSW process. Important aspects were addressed which will provide the welding enthusiast with a good idea on what the process is capable of doing and how to go about building or creating a friction stir weld. If one is to consider building a specialized FSW machine, this chapter will provide a good foundation on general machine requirements and capacity. Basic formula is introduced in this chapter to provide the researcher with a starting point on what parameters to use. At this stage the researcher performed small preliminary studies to get more familiar with the welding procedure and the type of plasicized flow patterns to expect. These studies were done with manual pushbutton operations, thus improved control schemes have not yet been implemented.

Development of FSW Equipment, Hardware Implementation and Advanced Process Control Schemes

There are many important FSW machines currently in production. A background survey gave the researcher a good idea of machine parameters and required power consumption necessary to make a friction stir weld. This chapter will provide a description of the refurbishing of a conventional milling machine into a CNC machine so that it can function as an advanced FSW machine for research purposes.

Refurbishing Process

Figure 3.1 shows a conventional milling machine as purchased. The machine was not electrically connected and the outdated electronic controls and contactors restricted the flexibility required for FSW. Please view Appendices A for a basic specification sheet on this machine.

Figure 0.1 **Conventional Milling Machine as purchased**

The minimum requirements that need to be considered when purchasing a milling machine with the intention of transforming it into a friction stir welding machine are:

- Sufficient horsepower to generate constant torque at various spindle speeds

- High Z-force capability (At least 1.5 tons depending on material thickness)
- Vertical spindle rotation
- Fairly big feed bed for welding big sheet-metal alloys
- Stable machine with rigid bed that can handle heavy vibration
- Spindle head (quill) that can tilt to a preferred angle of 0-5^{o}
- Wide variety of feed and spindle speed ratios
- Preferably a second Z-axis that can be controlled individually during the weld.

The diagram in Figure 3.2 illustrates the control configuration and interfaces between the drive controllers/inverters and other system hardware.

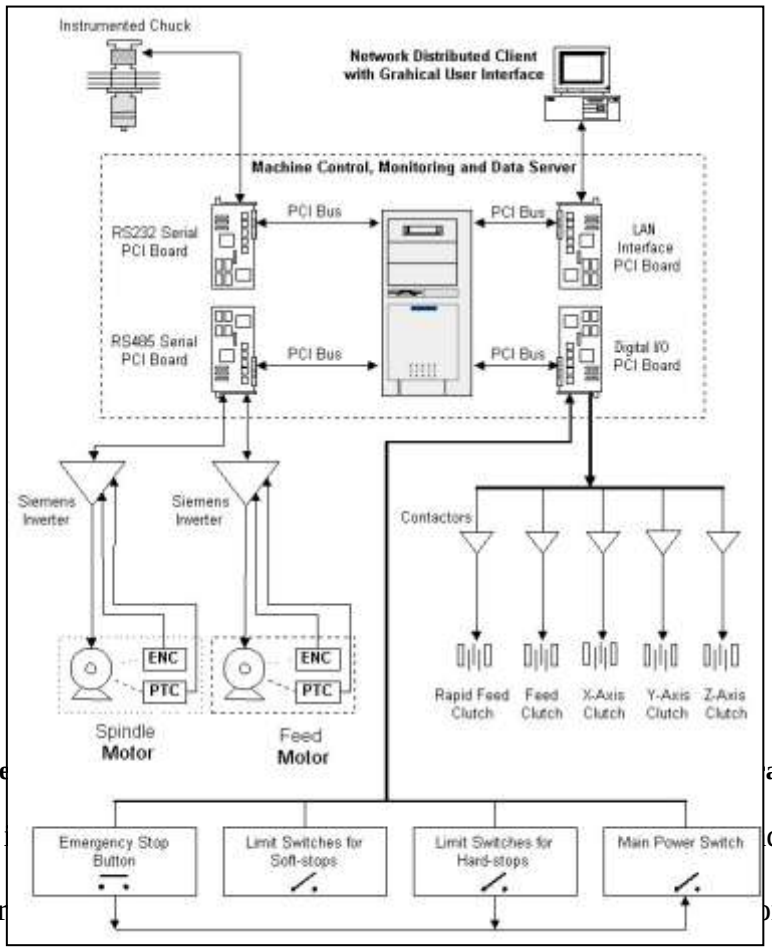

Figure **ation**[39]

The system d feed motor. These motor ons that make interface possible with a PC. Feedback for positioning purposes is given by means of optical encoders providing pulses related to linear movement. The Spindle motor is rated at 5.5kW and the Feed bed motor is rated at 1.5kW. Both these motors use mechanical gearboxes to increase the torque on the output shaft. The main spindle motor provides the spindle rotation while the feed bed motor supplies power to all the three axes movements of the bed. The various axes of the bed namely X, Y and Z are

engaged with 24V electromagnetic clutches. The clutches are in tern controlled by contactors that are linked to the PC with digital I/O boards as illustrated in Figure 3.2. Limit switches and emergency stop buttons are also linked to the PC with the PCI boards. Further details on the hardware implementation are explained in Section 3.2.

First it had to be verified that the machine would be capable of performing a friction stir weld. Previous parameter settings established by other institutions, such as feed rate and force distributions during weld trials gave good indications of the requirements expected. For 6mm aluminum plate an average vertical force of 1 to 1.5 tons is required to maintain a good quality weld.[26] An experimental setup was made by means of strain gauging a short length of square bar using two quarter bridge diagonal circuits as shown in Figure 3.3. The two bridges were completed to a full bridge in a UPM 40 Amplifier. The system was calibrated by compressing the bar in a tensile machine. The test results revealed that for every 1μ strain change a 215N of compressive force was induced.

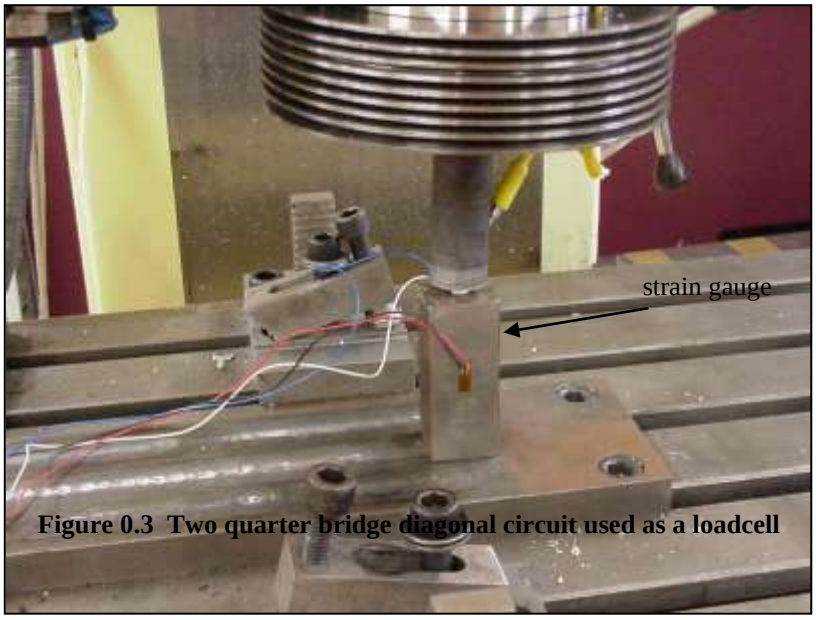

Figure 0.3 Two quarter bridge diagonal circuit used as a loadcell

The loadcell was compressed in the milling machine by first using the bed vertical feed. It was noted that the Z-force was climbing easily to over 3tons of force. The quill downward force power provided by the spindle motor could deliver over 2 tons. In both cases the machine did not run to its full potential, thus preventing any damage due to overload. From these results it was concluded that the machine was capable of performing a good quality weld on 6mm thick aluminum plate. For details on the experimental setup see Appendix A. Other mechanical aspects of the process e.g. clamp and tool designs, which also are major role players, will be dealt with in Section 3.3 and in Chapter 4.

Motion Control Implementation

The machine was automated with CNC capabilities making use of inverters or drive controllers, which in turn are controlled by a computer. For reliability and safety, all bed axis movements, spindle speeds and feed speeds were critical from a control point of view. The controls of the original milling machine were outdated consisting of numerous contactors, push buttons and pin boards for programming. A detailed report on the electric circuit diagrams and automation software is available in a Master Dissertation by Mr. G. Kruger to be published early in 2003. The following subsections will report briefly on all modifications made during the conversion and re-design process.

Spindle Motor

The 5.5kW main spindle motor had to be accurately controlled to establish consistency in each weld trial. The drive controllers or inverters, communicate with the PC via RS 485 connections. An optical encoder mounted at the back of the motor shaft gives parameter feedback of the actual spindle speed. This in tern is build into a

closed loop control system. The drive has a fixed torque setting that will maintain a constant torque input on the motor. Built-in safety features like ramp-up and ramp-down time are implemented on the inverters in case of emergencies. All drives are protected against overload but an additional emergency push button is installed that will allow the power supply to the drive controllers to be shut down in case of emergencies.

Feed Motor for Position Control

Figure 3.4 shows a closed loop system also referred to as a servo or feedback system. The control system issues commands to the drive controllers, which then compares the results of these commands as measured by the movement or location of the machine component, such as the table or spindlehead. The feedback devices normally used for measuring movement or location of the component are called resolvers, encoders, Inductosyns, or optical scales.

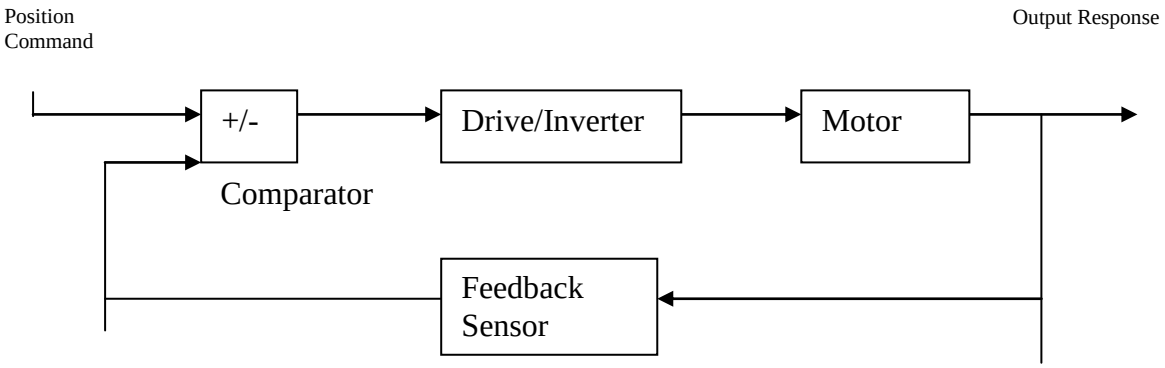

Figure 0.4 General Arrangement of a Closed-Loop Control System

Optical incremental encoders were retrofitted to the rotating shaft of the motors via a special coupling. These encoders will supply feedback by means of a series of pulses, which relates to linear bed movement. Position control was established by controlling

the bed movement using the motor speeds. Figure 3.5 illustrates the position of the encoder.

Figure 0.5 Incremental Optical Encoder connected to the shaft of the feed motor. The cowl of the motor is custom-made to accompany a forced convection fan of 220V

Drive (Inverter) Controls Layout and Description

Figure 3.6 illustrates the layout of the motor drives, contactors and electrical safety mechanisms installed for the control of the FSW process. The following items are numbered in the figure as follows:

1. Main 3 phase power switch
2. Main 3 phase power contactor with 24V DC coil
3. Fuses
4. Siemens 24V power supply
5. Manual 24V power switch
6. Transformer
7. Input choke for primary drive controller
8. Input choke for secondary drive controller
9. Siemens drive controller for main spindle 5.5kW (Primary)
10. Siemens drive controller for feed motor 1.5kW (Secondary)
11. 24V Contactors
12. Connection terminal block

From the left the nine contactors are: Auxiliary contactor for power supply, Rapid Feed, Normal Feed, X-Brake, Y Brake, Z-Brake, X-Feed, Y-Feed and Z-Feed.

The main 3phase power supply leads to the main power switch (1) which is connected in parallel with the main power contactor (2) and the set of fuses (3) that leads to the 24V power supply (4).

The 24V DC coil of the main 3phase contactor (2) can be switched via two methods. The first option is manually with switch 5. Second option is with auxiliary contactor (11) via the digital interface from the I/O card of the PC. Once this coil is excited the contactor will switch 3 Phase to the transformer and the input chokes via a set of fuses.

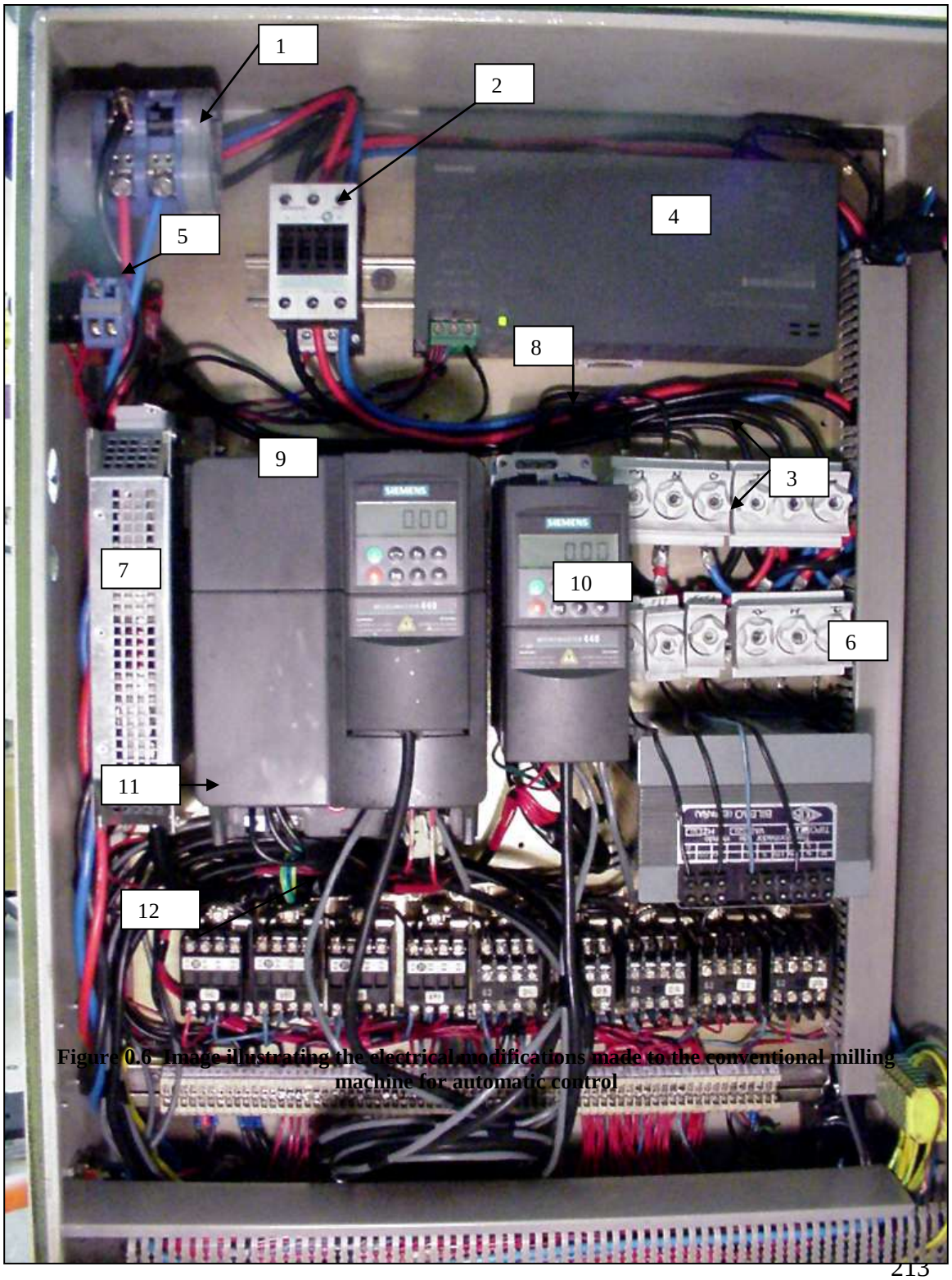

Figure 0.6 Image illustrating the electrical modifications made to the conventional milling machine for automatic control

The 3 Phase power supply is filtered for noise reduction by means of the input chokes before it is supplied to the drive controllers. The transformer (6) supplies an output of 220V to the two cooling fans, one on each motor. The drive controllers are programmed and controlled via the RS485 interfaces.

The digital inputs from the PC I/O cards are connected to the terminal block (12) that will supply the excitation to the appropriate contactor coil that will switch the 24V power supply to the various brakes and electromagnetic clutches.

The drive controllers and contactors are fully integrated and are controlled from a computer by the end user. The integrated software will monitor and log data from the monitoring unit and also use the data feedback from the optical encoders to control the process through a closed loop system as mentioned in the previous section. Chapter 6 will address the data logging device and its operation in more detail.

Design and Development of Mechanical Fixtures

The main purpose of a fixture for friction stir welding is to hold the workpieces in position during welding. However, there is limited published information that details the fixture design requirements. The main reason for having appropriate clamps or fixtures is to prevent the specimens from moving while being welded. Obtaining good stability during the process is important since any deflection or major vibration would affect the quality of the weld. A logical representation of the forces to expect during this process gives the researcher a good idea of clamp or fixture design requirements.

Clamping Requirements

The forces that act on the base plates as a result of transversal and rotational movement of the tool can be summarized and built into a clamping design.[25,26] The

initial plunge of the tool, before welding feed (cold start), transfers forces to the base material. Firstly the tool generates a moment while rotating against the frictional surface of the base material. This frictional moment or shearing force is assisted by the downward thrust of the tool increasing the linear force vector at every increment of rotation. The probe that is sunk into the joint line wants to push the two base plates apart. Movement of the tool through the joint line also produces translational forces that tend to push the plates in the x-axis direction. The magnitude of these forces will depend on the viscosity level reached as well as the feed rate that the process commences at.[25,26] The other forces to be under attention are the transverse forces produced by the rotating tool due to the shearing action. An important aspect to consider then is the relationship between the transvers and translational forces. Vanderbilt University stated that the transverse (force perpendicular to the direction of travel) is the dominant force over the tranlational force (force opposite the direction of travel).

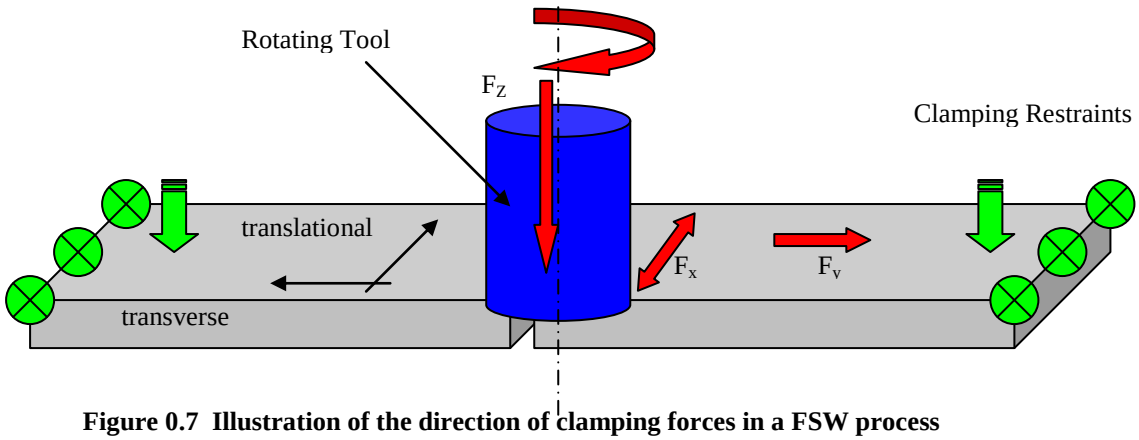

Figure 0.7 Illustration of the direction of clamping forces in a FSW process

Figure 3.7 illustrates the force model and important concepts related to the clamping techniques.

Key features that a FSW weld fixture must have are as follows:

- **Welding tool's axial force and deflection**

The forces in action during FSW are significant, and proper fixture design is critical to the success of the weld. The axial force applied to the welding tool, keeping it embedded in the workpiece, is commonly from 20kN to 60kN.[26] This depends on the welding tool, workpiece alloy, thickness, travel speed, etc. This force must be controlled with minimal deflection, since it is necessary to control the position of the welding tool precisely in relation to the surface of the workpiece.

- **Joint or workpiece separation**

During the initial plunge of the welding tool into the workpieces load is transferred laterally to separate the plates along the joint line where large forces are required to prevent this separation. The magnitude of this force has not been published in any literature. In addition, during the course of welding plates tend to separate under the thermal expansion/contraction associated with passage of the welding tool. This produces an in-plane moment that opens the unwelded section in front of the welding tool. In the case of the plate separation due to the plunge of the welding tool at the start of the weld, restraining the plates laterally immediately adjacent to the plunge location is most effective. As the weld progresses, the thermal expansion that causes plate separation in front of the welding tool is most effectively counteracted by clamping at the end of the plate, producing the maximum in-plane moment to counter the separation with minimal force.

- **Workpieces buckling due to thermal expansion**

While constraining plate separation produced by thermal expansion, workpiece plates can sometimes buckle upward into a convex profile, rising around the welding tool

and making the tool appear to be diving into the workpiece when actually the surrounding plate is lifting off the backingplate. This results in a weld with "dropout", a term borrowed from fusion welding, where the weld zone protrudes from the back of the welded panel. The effect is often worse with thin plates, in the 3mm to 10mm range, since these plates are less able to resist the in-plane moment without buckling. To counteract this, clamping is required to apply out-of-plane forces that prevent buckling. This is best applied as close as is practical to the weld zone, usually about 50mm on either side of the joint. This clamping also serves the purpose of deflecting plates that may not be perfectly flat so that the plates are in contact with the backingplate at all points along the joint.

- **Preventing the longitudinal sliding of workpieces**

Preventing workpiece plates from sliding longitudinally is not usually important for flat butt welds, since the large axial load applied by the welding tool tends to pin the workpiece to the backingplate. However, in making corner welds it is necessary to pin one of the two plates being welded to prevent sliding in the direction of the weld. Restraining only one plate is adequate to prevent sliding of the pair, since the pair of plates are sufficiently welded at completion of the initial plunge of the workpiece to prevent the unrestrained plate from sliding on its own.

Concept clamp design

A recommended advantage on the engineering design side was a universal clamp that would characterize easy manufacturing; good stability and quick disassembling characteristics. The first prototype design concentrated on easy disassembling methods as well as universal applications i.e. clamping of wider and thicker material. After the initial concept design it was realized that the clamping strength was not

adequate. Since the clamp was only bolted down with one T-nut it could not prevent any rotational (moments) movement of the clamp base. Figure 3.8 illustrates this clamp model.

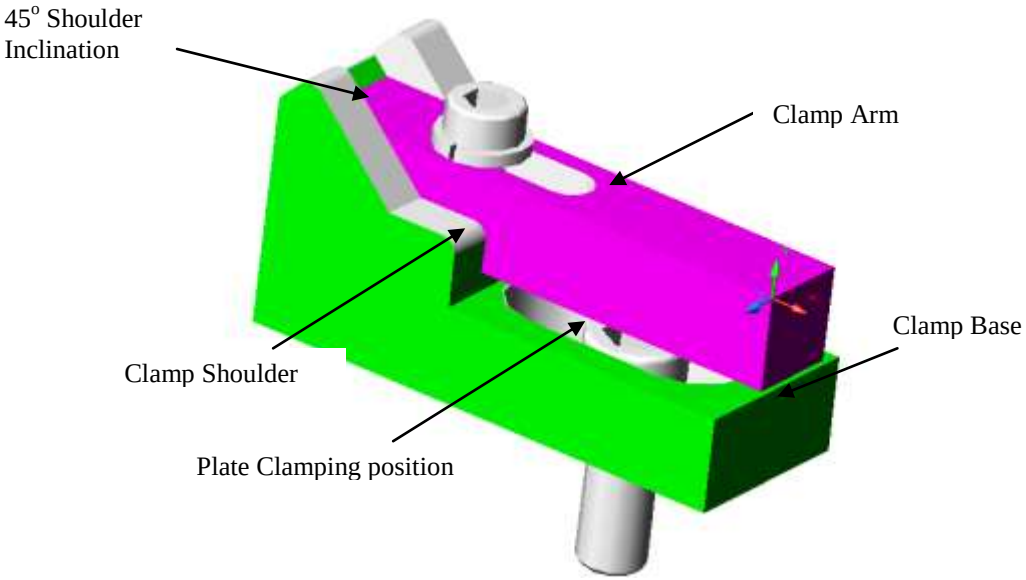

Figure 0.8 First clamping model

This clamp had a 45° shoulder inclination on the one side so that the clamping arm could be adjusted to suite the appropriate plate thickness. Complete manufacture drawings of this clamp design can be viewed in Appendix A.

Final clamp design

Figure 3.9 illustrates the assembly bed for the clamping configuration. The exact dimensions were copied from the actual feed bed so that the model could be drawn to full scale. Objects like T-nuts, allen cap bolts, clamp adjustment lengths and the backing plate sizes were also drawn to scale. The two flat plates shown are the 6 x 120 x 800mm Aluminum plate specimens to be welded on the first weld trial.

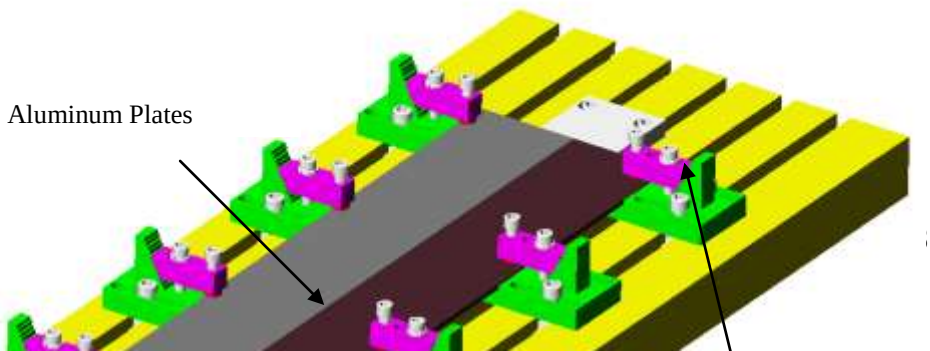

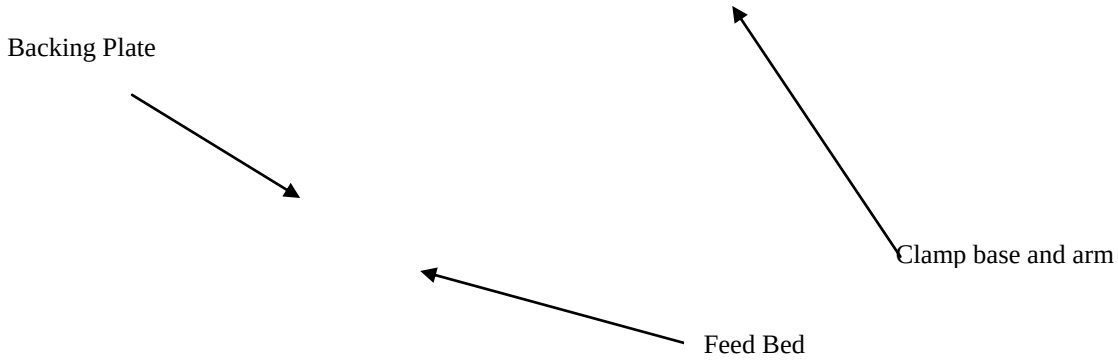

Figure 0.9 Assembly bed of clamping method

For this clamp a 5mm shouldered step is designed to prevent the plates being forced apart when the probe penetrates the specimens. The clamping arm prevents the plates from moving or sliding in any direction. Figure 3.10 illustrates the clamping configuration where the design is easy to manufacture, universal, quick and easy to adjust and disassemble.

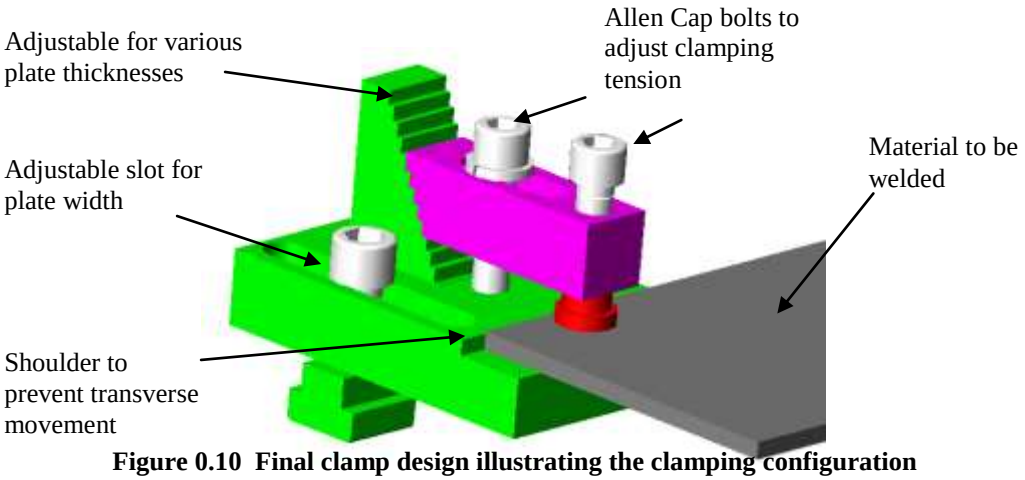

Figure 0.10 Final clamp design illustrating the clamping configuration

Backing Plate Design

The design of the fixtures had to be based around a backing plate size. This 'backing plate' is a piece of material, normally made out of a medium carbon steel, placed at the bottom (back) of the plates to be welded. The main purpose of this backing plate is to prevent the welded material being forced out of the joint line during a weld run. Since the tool shoulder applies a downward force on the plasticised material the backing plate must support the welded plate and resist any thermal deflection. Advise

on backing plate design was given from a personal e-mail letter from Dr. A. P. Reynolds (University of South Carolina). From past experience he suggested that the plate should be manufactured from medium carbon steel since copper-backing plates will conduct too much heat away from the joint line. In some cases this is not an advantage since more frictional heat needs to be generated to accomplish a weld. The backing plate designed was 1000 x 100 x 20mm and not heat treated. The clamping base and the backing plate height are both 20mm thick to support the two plates being welded. The backing plate manufacture drawings can be viewed in Appendix A.

Tool holder for Sensor and Data Transmission System

The first few weld trials were made by using a standard milling machine chuck with a ϕ19.05mm (¾ inch) tool shank & cullet. This tool clamping method, taper cullet, was not of the latest methods available but the required accuracy and eccentricity error were in allowable limits. The tool ran very true to the axis of rotation and therefore concentric limits approved. A continuous welding trial of 800mm in total length was made to investigate the heat load on the standard chuck. The estimated temperature of the chuck at the end of the weld trial ranged from 100 to 200 degree Celsius. This was estimated by simply placing an external temperature probe on the surface of the chuck. Since it is a transient heat transfer process, the temperature of the chuck walls will increase as weld length increases. This temperature gradient will follow its trend until it reaches the steady state temperature of 300 to 400 degree Celsius, depending on the maximum tool temperature. This practical evaluation proved that the chuck surface would reach high temperature values and that any electrical equipment would fail under these conditions.

A custom-made tool holder with a strain gauge based sensor system was to be designed that can accurately monitor important process parameters during the welding trials. The measurement system consisted of strain gauges and a telemetry system to transfer data from the rotating unit to a stator arm. High temperature strain gauges were available on the market but also still out of our temperature range required. The outcome was to design a tool holder with a heat sink in order to lower the temperature gradient on the areas were the gauges would be applied. In Section 5.1 more detail on the measuring unit and its capabilities are given. Figure 3.11 illustrates the mechanical model of the custom tool holder system with its appropriate heat sink theory.

The Heat Sink Design

The tool holder is designed so that it could withstand high tensile and compressive forces but still produce a high enough stimulation to detect a small enough change in strain readings from the gauges applied at the position indicated in Figure 3.11. The main shaft of the chuck, where the strain gauges will be applied, is 50mm in diameter. The heat sink portion was to be separate from the chuck but also robust in design since the tool collet will fit in it. The entire system had to be manufactured in close tolerances since concentricity of the unit was of great importance. Good alloy steel, EN19, was selected and not need to be heat-treated since it already had high strength and ductile characteristics. An additional 5mm Tufnol disc with a very low thermal conductivity “k” was implemented in the design to isolate the heat flow even further. The chuck or tool holder is manufactured so that it can be retrofitted to the current milling machine quill. The full manufacture drawings of the model are available in Appendix A.

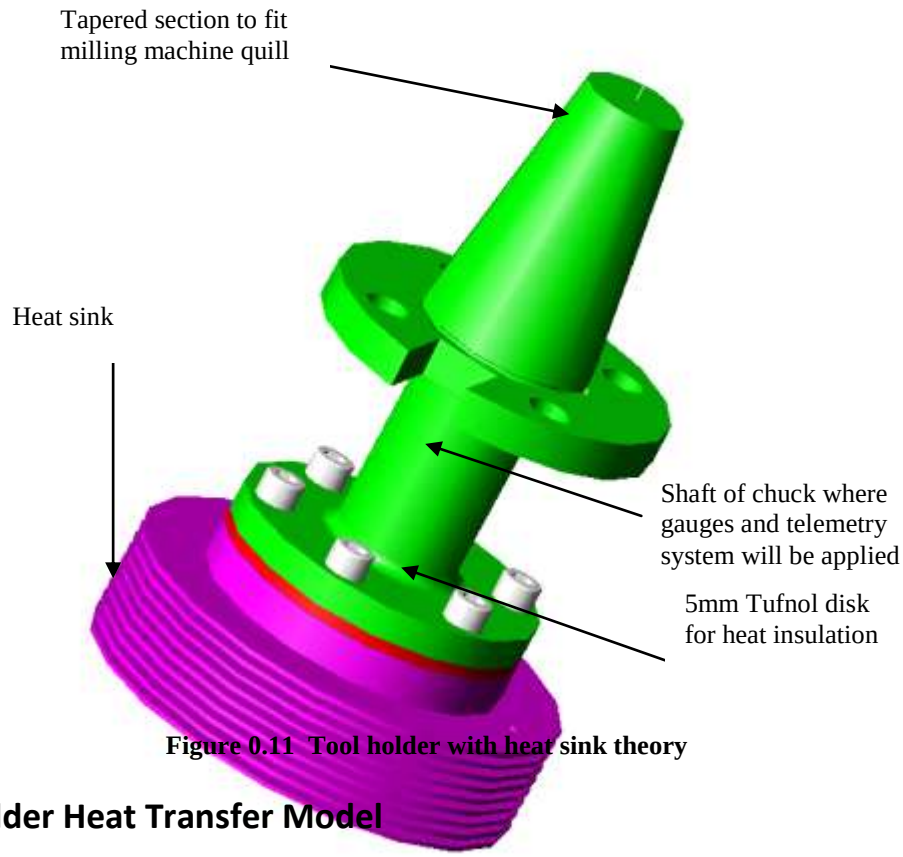

Figure 0.11 Tool holder with heat sink theory

Tool Holder Heat Transfer Model

The rate of heat transfer from a surface at a temperature T_s to the surrounding medium at T_∞ is given by Newton's law of cooling as[28]:

$$\dot{Q}_{conv} = hA\,(T_s - T_\infty) \qquad \textbf{(0-1)}$$

Where 'A' is the heat transfer surface area and 'h' is the convection heat transfer coefficient. When the temperatures T_s and T_∞ are fixed by design considerations, as is often the case, there are two ways to increase the rate of heat transfer: to increase the convection heat transfer coefficient h or to increase the surface area A. Increasing h may require the installation of a pump or fan, or the replacement of the existing one with a larger one, and this approach may or may not be practical. Besides, it may not be adequate. The alternative is to increase the surface area by attaching extended surfaces called fins made of highly conductive materials such as aluminum. For this

project it would complicate the manufacturing of the chuck considerably if a different material for the fins than that of the tool holder was to be used. For manufacturability and mechanical strength purposes, the complete unit was made out of alloy steel, EN19. Fins enhance heat transfer from a surface by exposing a larger surface area to convection. In the analysis of fins the researcher considers steady operation with no heat generation in the fin, and assuming the thermal conductivity "k" of the material to be constant. Another assumption made is that the convection heat transfer coefficient "h" is constant and uniform over the entire surface of the fin for calculations purposes.

In reality, however, the temperature of the fin will drop along the fin, and thus the heat transfer from the fin will be less because of the decreasing temperature difference T(x)- T: towards the fin tip. To account for the effect of this decrease in temperature on heat transfer, we define fin efficiency. In text to follow we will see that the fin design of the chuck is 2mm thick. Normally fins are very small in cross-section since limited space is available and more surface area is required. The reasons for the thicker fin surface are to simplify manufacturability, lower manufacturing costs, create a more stronger and rigid assembly and to absorb a higher heat load during a longer weld trial. Already from this data the researcher can expect a fairly big temperature drop across the fins and thus relative low fin efficiency.

Fin efficiency is defined as follows[28]:

$$\eta_{fin} = \frac{\dot{Q}_{fin}}{\dot{Q}_{fin,\max}} = \frac{actual\ \ heat\ \ transfer\ \ rate\ \ from\ \ the\ \ fin}{ideal\ \ heat\ \ transfer\ \ rate\ \ from\ \ the\ \ fin\ \ if\ \ the\ \ entire\ \ fin\ \ was\ \ at\ \ base\ \ temperatur\ \ e} \qquad \textbf{(0-2)}$$

or

$$\dot{Q}_{fin} = \eta_{fin} Q_{fin,\max} = \eta_{fin} hA_{fin} (T_b - T_\infty) \quad \textbf{(0-3)}$$

where A_{fin} is the total surface area of the fin. This relation enables us to determine the heat transfer from a fin when its efficiency is known. Fin efficiency relations are developed for fins of various profiles. This relationship can be obtained from Figure 3.12.

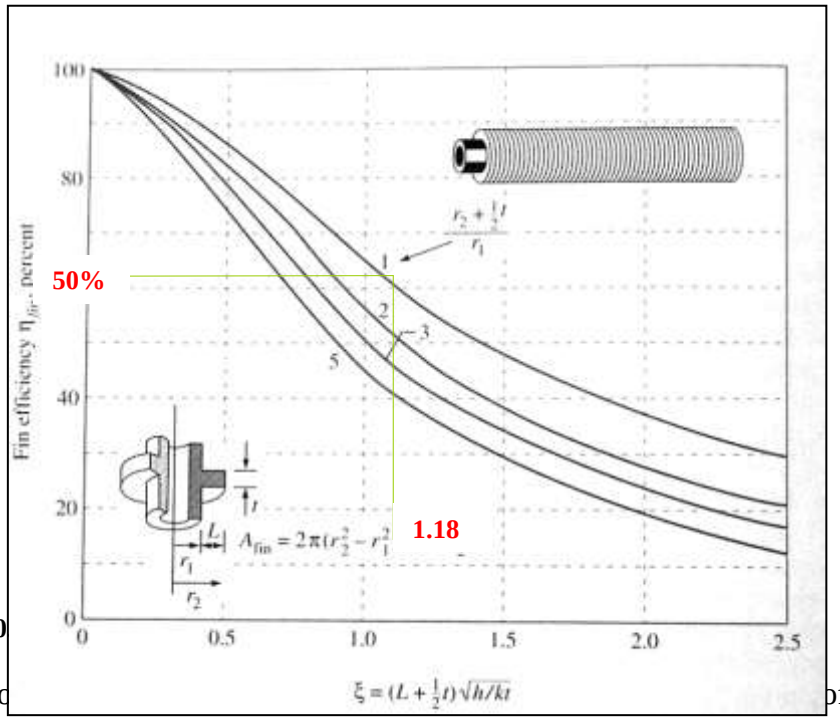

Figure 0

An important co of the proper fin length L. Normally the longer the fin, the larger the heat transfer area and thus the higher the rate of heat transfer from the fin. But also, the larger the fin, the bigger the mass, the higher the price, and the larger the fluid friction. Therefore, increasing the length of the fin beyond a certain value cannot be justified unless the added benefits outweigh the added cost. Also, the fin efficiency decreases with increasing fin length because of the decrease in fin temperature with length.

Another important element in fin design is the fin effectiveness. Fins are used to enhance heat transfer, and the use of fins on a surface cannot be recommended unless

the enhancement in heat transfer justifies the added cost and complexity associated with the fins. In fact, there is no assurance that adding fins on a surface will enhance heat transfer. The performance of the fins is judged on the basis of the enhancement in heat transfer relative to the no-fin case, and expressed in terms of the fin effectiveness ε_{fin} defined as:

(0-4)

Here A_b is the cross-sectional area of the fin at the base, and $Q_{no\ fin}$ represents the rate of heat transfer from this area if no fins are attached to the surface. An effectiveness of $\varepsilon_{fin}=1$ indicates that the addition of fins to the surface does not affect heat transfer at all. An effectiveness $\varepsilon_{fin} < 1$ indicates that the fin actually acts as insulation, slowing down the heat transfer from the surface. This situation can occur when fins made of low thermal conductivity materials are used. An effectiveness $\varepsilon_{fin} > 1$ indicates that the fins are enhancing heat transfer from the surface, as they should. Finned surfaces are designed on the basis of maximizing effectiveness for a specified cost, or minimizing cost for a desired effectiveness.

When determining the rate of heat transfer from a finned surface, the unfinned as well as the fin portion of the surface must be considered. Therefore, the rate of heat transfer for a surface that contains "n" fins can be expressed as:

$$\begin{aligned}\dot{Q}_{total\ ,\ fin} &= \dot{Q}_{unfin} + \dot{Q}_{fin} \\ &= hA_{unfin}\,(T_b - T_\infty) + \eta_{fin}\, hA_{fin}\,(T_b - T_\infty) \\ &= h(A_{unfin} + n\,\eta_{fin}\,A_{fin})(T_b - T_\infty)\end{aligned}$$

(0-5)

The overall effectiveness for a finned surface is the ratio of the total heat transfer from the finned surface to the heat transfer from the same surface if there were no fins,

$$\varepsilon_{fin\ overall} = \frac{\dot{Q}_{total\ \ fin}}{\dot{Q}_{total\ \ no\ \ fin}} = \frac{h(A_{unfin} + \eta_{fin} A_{fin})(T_b - T_\infty)}{hA_{no\ \ fin}(T_b - T_\infty)} \quad \textbf{(0-6)}$$

Where $A_{no\ fin}$ is the area of the surface when there are no fins, A_{fins} is the total surface area of all the fins on the surface, and A_{unfin} is the area of the unfinned portion of the surface. Note that the overall fin effectiveness depends on the fin density (number of fins per unit length), as well as the effectiveness of the individual fins. A small value of thermal resistance indicates a small temperature drop across the heat sink, and thus a high fin efficiency.

Design verification

Design considerations for fin effectiveness and fin efficiency were revised and then combined to bring forward a custom-made heat sink-design concept that would suit our FSW process. Although this is a transient heat conduction process it was considered to be at maximum steady state heat transfer conditions in order to simplify calculations. This estimate will be very close to the true value and will be acceptable to verify and conclude the design to be appropriate for the application. The following theoretical calculations were made to estimate the heat sink potential:

Note: The combined heat transfer coefficient of h = 60W/m^2.^{o}C is a good estimate to compare the fin and no-fin heat transfer comparison and will not influence the overall result. (The ratio of heat transfer between fins included and excluded will remain the same.)

Design Specifications: Approximate operating conditions of our finned cylinder

D_1 = 7.6cm (Outer diameter of shaft)

D_2 = 17 cm (Outer diameter of fins)

t = 2mm thick

n = fins per meter, 10 fins in 43mm thus 232 fins in 1 meter

$T_{:}$ = 25 ^{o}C

T_b = 400 ^{o}C

h = 60 W/m^2.^{o}C

To be Determined: Increase in heat transfer associated with using fins

Proof heat sink to be an advantage for the application

Schematic:

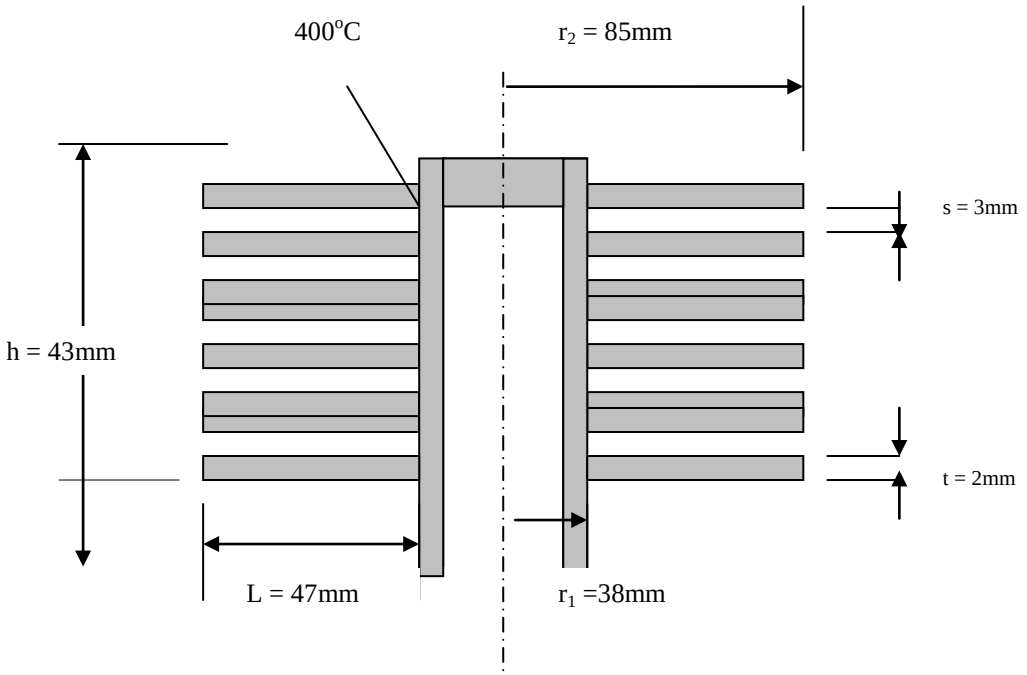

Solution:

In the case of no fins, heat transfer from the tube per meter of its length is determined from Newton's law of cooling to be:

$$A_{no\ fin} = \pi D_1 L = \pi (0.076)(1) = 0.23876\ \ m^2$$

$$Q_{no\ fin} = hA_{no\ fin}(T_b - T_\infty)$$

$$= 60 \times 0.23876\ \ (400 - 25)$$

$$= \underline{5372\ .1W}$$

The efficiency of the circular fins attached to a circular tube is plotted in Figure 3.12.

Note that:

$$L = 0.5(D_2 - D_1)$$

$$= 0.5(0.17\text{-}0.076)$$
$$= \underline{0.047m} \quad \text{thus:}$$

$$\frac{r_2 + 0.5t}{r_1} = \frac{(0.085 + 0.5 \times 0.002)}{0.038} = \underline{2.26}$$

$$(L + 0.5t)\sqrt{\frac{h}{kt}} = (0.047 + 0.5 \times 0.002) \times \sqrt{\frac{60}{50 \times 0.002}}$$
$$= \underline{1.18}$$

From Figure 3.12: $\eta_{fin} = \underline{0.5}$

Also

$$A_{fin} = 2\pi(r_2^2 - r_1^2) + 2\pi r_2 t$$
$$= 2\pi(0.085^2 - 0.038^2) + 2\pi(0.085)(0.002)$$
$$= 0.0374\ m^2$$

$$Q_{fin} = \eta_{fin} Q_{fin\,max} = \eta_{fin} hA_{fin}(T_b - T_\infty)$$
$$= 0.5[60 \times 0.0374](400 - 25)$$
$$= \underline{421\ W}$$

Note if the space between the two fins is 3mm, heat transfer from the un-finned portion of the tube is:

$$A_{unfin} = \pi D_1 S = \pi(0.076)(0.003) = 0.0007163\ m^2$$
$$Q_{unfin} = hA_{unfin}(T_b - T_\infty)$$
$$= 60 \times 0.0007163 \times (400 - 25)$$
$$= \underline{16.12\ W}$$

If there are 232 fins and thus 232 interfin spacings per meter length of the tube, the total heat transfer from the finned tube becomes:

$$Q_{total\ fin} = n(Q_{fin} + Q_{unfin}) = 232\ (421 + 16.12)$$
$$= 101.41\ kW$$

Therefore, the increase in heat transfer from the tube per meter of its length as a result of the addition of fins is:

$$\begin{aligned} Q_{increase} &= Q_{total\ \ fin} - Q_{no\ \ fin} \\ &= (101\ .41 \times 10^{3}) - 5372\ .1 \\ &= \underline{\underline{96\ 038\ W}} \qquad (\ per\ \ meter\ \ \ tube\ \ \ length\ ) \end{aligned}$$

For this case the tube length is 43mm and thus $Q_{increase}$ = 4129.6W

Discussion: The overall effectiveness of the finned tube is:

$$\begin{aligned} \varepsilon_{fin\ \ overall} &= \frac{Q_{total\ \ fin}}{Q_{total\ \ no\ \ fin}} = \frac{101\ .41 \times 10^{3}}{5.3721\ \times 10^{3}} \\ &= \underline{18\ .88} \rightarrow \end{aligned}$$

This overall effectiveness value demonstrates that the rate of heat transfer from the tube will increase by a factor of almost 19 as a result of adding fins. This verifies the design and provides insurance that the fins will be appropriate for the application.

Safety considerations

The safety for operators and fellow researchers involved during the FSW process is always of utmost importance. During the machining process safety on the electrical and mechanical side was important. From the electrical point of view an emergency stop switch on the control board that is linked with the main power contactor is installed. The drive controllers that will control the various motors have a build-in safety device for overload protection. An additional safety feature for overload protection was the installation of temperature gauges or better known as thermistors on the motor windings. The three thermistors, one on each winding, are connected in series to each other and are directly connected to the drive controllers. The total

change in resistance will be signaled back to the controllers and if this change exceeds the limit it will shut down the power supply to the motors. The thermistors that were installed are rated 130^{o}C.

The mechanical safety was also to be controlled for rapid deceleration of the spindle. The time that the spindle will take to stop or decelerate was to be controlled by the drive ramp down time. The drive controllers had a build-in feature for electrical braking of the motors.

To isolate the operator from the spindle movement while machining a safety screen or barrier (thickness of 10mm) was mounted around the feed bed. The clear Perspex shield is designed so that it could easily be disassembled but still be rigid during the machining process. Further more the feedbed with multi-axis movement has soft stops and hard stops (mechanical trip dogs) that function as limit switches to protect the bed against over-feed.

Additional Modifications

Motor cowls

Since the process will be controlled via the drive controllers some method of tracking is necessary. For control purposes it was necessary to know exactly where the bed was at any time in order to maintain a closed loop control system. In order to keep track of the movement of the axes, optical encoders were coupled to each shaft of the motors. The encoders gave incremental outputs that were calibrated with linear bed movement. Forced convection cooling had to be implemented on each motor since the motor windings will reach higher temperature gradients at lower speeds. This could be expected since the motor current will increase at lower rpm in order to

maintain a constant torque setting. The original fan cowls were replaced by custom-made housings in order to accommodate the encoders as well as the electrical fans.

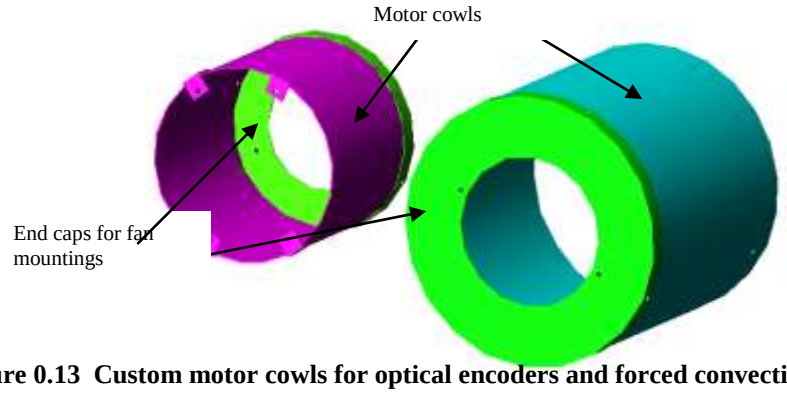

Figure 0.13 Custom motor cowls for optical encoders and forced convection cooling

The manufacture drawings of the fan cowls with the encoder brackets can be viewed in Appendix A.

Other small modifications made were the bracket arm for the stator unit of the telemetry system. This measuring system is explained in Chapter 5 and the bracket can be viewed in Figure 5.5. The manufacture drawings are also available in Appendix A.

Future modifications

Installing a mechanical "movement" arm that will apply a certain load on the material onto the backing plate can assist in future development for the downward pressure application onto the joint line. The arm will be mounted onto the spindle head and thus move with the joint line while applying the downward force. This arm will also be capable of controlling the plunge depth of the tool shoulder into the parent metal, therefore maintaining good weld consistency. Figure 3.14 illustrates the mechanical movement arm that Gemcor has introduced.

Figure 0.14 Mechanical movement arm from Gemcor [36]

Another future modification that needs to be considered will be the control of the downward (Z-direction) force during traverse. The intention will be to install an additional servomotor and controller on a separate axis that will be interfaced to the personal computer. This motor will control the Z-axis accurately and make force control possible during the machining process.

Conclusion

This chapter concentrated on the design and development process that had to be addressed during the modification of a conventional milling machine in order to convert it into a reliable friction stir welder that can be used for research purposes. The modifications made consisted mainly out of hardware although software changes were also done but are not explained in detail in this report. The reader should now have a better understanding of the machine development side and important changes that were made for improved machine control. The machine will be capable of monitoring the important welding parameters such as temperature, force and torque changes while the process can be accurately controlled via a computer. The design and basic concept of the measurement system's mechanical structure was also introduced. The weld data and parameter settings will be captured and analyzed for the assessment of weld quality making use of this newly developed measuring system. More about this measurement system and tool holder will be dealt with in Chapter 5.

The structural design of components was explained and developed and can now be manufactured and installed. The safety mechanisms and future development under machine modifications were also addressed.

Tool Technology

Friction stir welding uses a non-consumable rotating tool, which moves along the joint line of two plates to produce high-quality butt or lap welds. The FSW tool is generally made with a profiled pin, which is contained in the center of a larger diameter shaft. For butt joints the length of the pin is approximate the thickness of the workpiece. The pin is traversed through the joint line while the shoulder is in contact

with the top surface of the workpiece. The contact area of the tool shoulder is determined by the tool tilt angle.

The tools are manufactured from a wear resistant material with good static and dynamic properties at elevated temperature. Tool technology has advanced considerably over the last few years and tool tips that can last up to 1000m of weld length on 5mm thick aluminum extrusions have been developed. Since the tool creates frictional heat, high temperature gradients exit at the tool tip and shoulder. Some of the important properties that the tool material should have are good hot hardness, toughness and good high temperature strength in order to minimize tool wear.

Tools with specially profiled pins and optimized shoulder designs that provide large tolerance envelopes have been developed and are common in industrial applications.[13] Tool designs, optimized welding parameters and specialized clamping techniques have been developed during a large number of confidential studies to serve the industrial demands. Since advanced technical information on tool designs is mainly the privilege of the patent holders, the research team in the MTRC had to develop their own tool designs and manufacturing technology.

Tool Functionality

The designing principal of the local developed tool was based on the MX Triflute tool that can be viewed in Figure 4.1. In general terms, the tool as shown in the figure comprises of a shoulder and a probe.

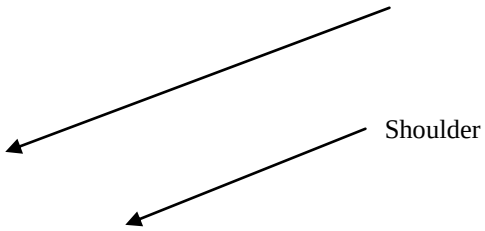

Figure 0.1 MX Triflute TM tool with frustrum shaped probe and triflutes and additional helical ridge around the triflute lands[13]

The probe/pin

As the workpiece thickness increases, more heat needs to be generated through friction between the rotating probe and the workpiece. The probe needs to ensure sufficient stirring of the material at the weld line and also needs to control the flow of the material around the tool to form a satisfactory weld. The probe generally has a profiled or threaded surface to facilitate a downward augering effect. This augering effect can be defined as the gripping movement of the rotating tool, pulling the plasticisized material in a downward direction.

The shoulder

The shoulder compresses the surface of the workpiece and contains the plasticised weld region. Heat is generated on the surface by friction between the rotating shoulder and the workpiece surface and, when welding thin sheets, this is the primary source of heat. The secondary source of heat will be from the rotating tool pin in the material.

For tools positioned perpendicular to the workpiece the leading edge of the shoulder in effect provides some preheat and hence thermal softening of the workpiece in front of the probe, which can be of advantage when dealing with harder or difficult to weld

materials. The greater the area of the shouldered region making contact with the work surface the greater the preheat available, but this becomes less effective for substantially thick plate. Increasing the diameter of the shouldered region, however, has practical limitations and tends to produce side flash on the weld surface.[13] On the other hand, as the tool tilt angle increases the surface contact area of the shoulder decreases thus lowering the energy efficiency of the system. The system efficiency can be defined as electrical energy input over thermal heat energy output. The tools can be manufactured so that it would have a degree of tilt on the surface to be welded thus compromising for the zero degree tilt position. In our case the tools are manufactured concentrically and aligned with the central axis of rotation and therefore in most cases some degree of tilt angle will be beneficial.

The machine quill (head) is tilted at a specified angle between 0 and 5 degrees to establish a better hydrostatic pressure and flow path on the tool shoulder surface. Inclined tools are used, where the trailing edge of the shoulder is set slightly below the workpiece top surface, which helps to consolidate the weld. Essentially hydrostatic pressure within the third-body region leads to subsequent recovery of the joint through-thickness as the FSW tool moves away as illustrated in Figure 4.2.

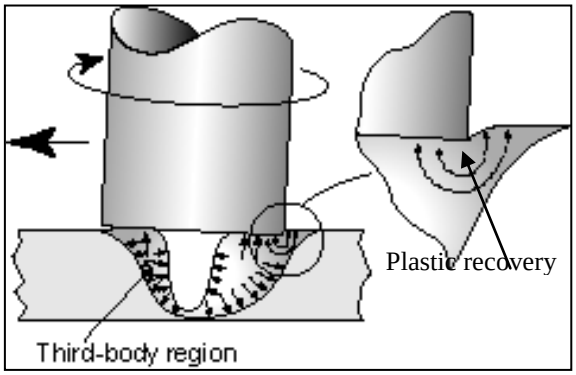

Figure 0.2 Hydrostatic pressure leads to plastic recovery[16]

This degree of tilt then also determines the stagnating point of mixing of the probe in the third-body region, also illustrated in Figure 4.2. The hydrostatic pressure and point of mixing are very important parameters to be evaluated when it comes to creating a complete fusion weld with no defects.

Tool Profiles and Design Theory

A major factor in achieving weld integrity and process efficiency is the design characteristics of the tool to provide a suitable ratio between the volume of the probe swept during rotation to the volume of the probe itself. This relationship is also termed the dynamic to static volume flow ratio.[16] This can be explained better if one is to push a stationary (static) tool probe through a liquid and then obtaining the difference in material volume displaced to that when the same tool is rotated (dynamic) through the material. With conventional tools, the dynamic to static volume ratio is achieved by the design of the probe geometry.

Early in the development of FSW, it was realized that the form of the welding tool was critical in achieving sound welds with good mechanical properties.

Preferably, the probe has an odd number (tri-flute) of equally spaced flutes to maintain maximum cross-section opposite to any re-entrant feature. Examples of these designs can be viewed in Figure 4.1 and Figure 4.3 respectively. This sort of design is more effective when welding thicker materials. It should also be noted that the change in section between the shoulder and the probe is well radiused in order to reduce stress concentration. In essence, the probe is tapered to maintain approximately a uniform stress distribution owing to torsion and the forward thrust. The helical flutes of the MX Triflute tool are comparatively steeply angled and this,

together with a coarse outer thread provides a significant augering effect and flow path.

This tapered design of the probe will not be that critical tool design for the welding of thin (6mm) plate. For this project a short probe with a circular profile was selected which will be explained further in Section 4.6.1.

The MX Triflute tools were designed so that the probe was not parallel sided but frustum shaped. Together with re-entrant features, the MX Triflute probe displaces substantially less material during welding (approximately 70%) than the cylindrical pin type probe.[13] This provides for a more uniformly stressed tool and allows for a more efficient flow path. The coarse helical ridge around the triflute lands reduces the tool volume further, (and therefore aid material flow), and thus breaks up and disperses surface oxides. The re-entrant helical flutes and thread features used on these probes are responsible for increasing the surface area of the probe. This increases the interface between the probe and the plasticised material resulting in a more complete stirring effect.

The high performance and the superiority of the MX Triflute probe over the conventional cylindrical pin type probe (especially for thick plate welding), can be attributed to the ratio of the volume of the probe swept during rotation to the volume of the probe itself. As mentioned earlier it is the ratio between 'dynamic volume' as opposed to the static volume that is important in providing a sufficient flow path. Typically, this ratio for similar root diameter and length probes was 1.1:1 for conventional pin probes and 2.6:1 for MX Triflute probes.[13]

The frustum shaped tool probes incorporate a helical ridge profile designed to augur the plasticised weld metal in a downward direction. Some probes also have side flats, or re-entrant features, to enhance the weld metal flow path.

Figure 4.3 illustrates the various designs that will improve welding speed and weld quality on that of thicker materials because of the improved pin profiles which allows better mixing or stirring of the plasticised material. The manufacturing of these helical ridges and flute lands on smaller probes (6mm and less pin lengths) will be very difficult, if not impossible, because of their small dimensions.

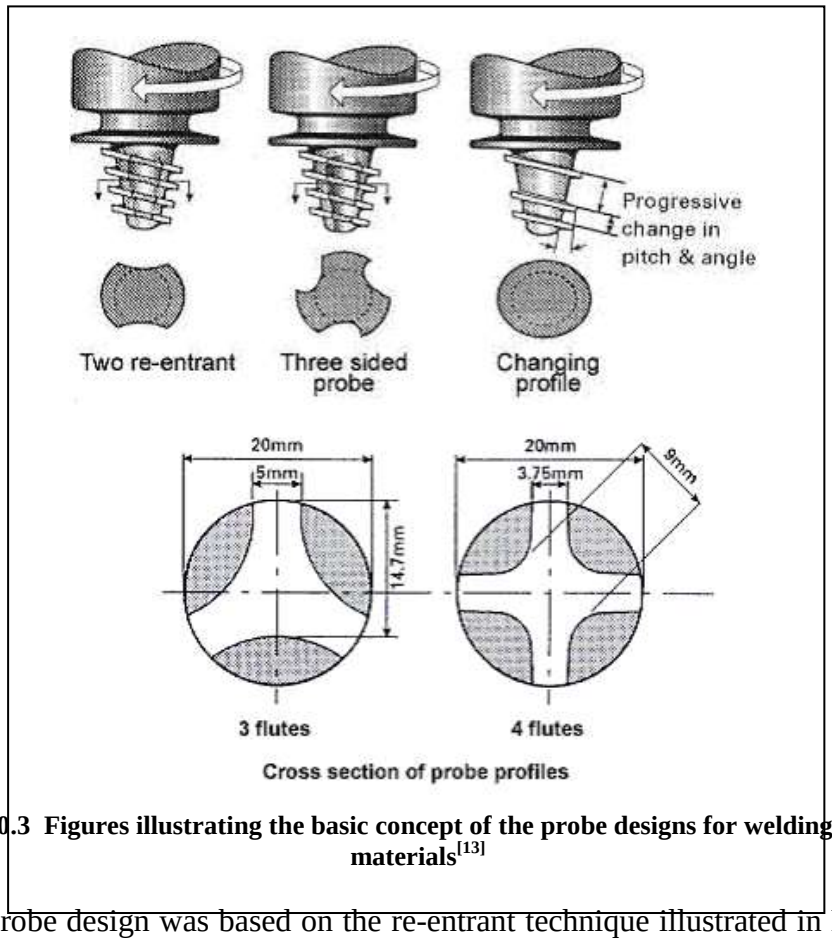

Figure 0.3 Figures illustrating the basic concept of the probe designs for welding thicker materials[13]

The first probe design was based on the re-entrant technique illustrated in Figure 4.3. The figures also illustrate that tool designs with good stirring effect is necessary. Things to consider are the type of flute lands, the pitch and angle of these flutes as

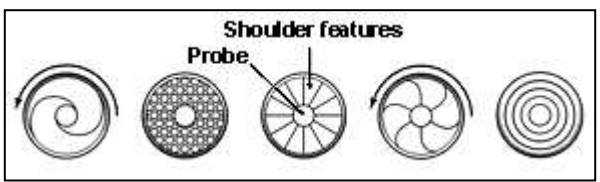

well as the various design geometries possible. Figure 4.4 illustrates shoulder designs that exist for welding thinner sheet metal alloys.

Figure 0.4 Tool shoulder geometries, viewed from underneath the shoulder[13]

These shoulder profiles improve the coupling between the tool shoulder and the workpiece by entrapping plasticised material within special re-entrant features. This essentially provides frictional contact and improves weld closure by helping prevent plasticised material from being expelled.

General considerations on tool design

Past experience shows that the middle of the tool shoulder should be in contact with the workpiece, therefore; pin lengths must be designed according to the plunge depth that will be used during welding to ensure full weld penetration. If the material plate thickness is 6mm and a shoulder plunge depth of 0.2mm is to be used then a tool pin length of approximately 5.7mm is necessary. Figure 4.5 illustrates the shoulder plunge depth of 0.2mm from a tool tilt angle of 2.5 degrees.

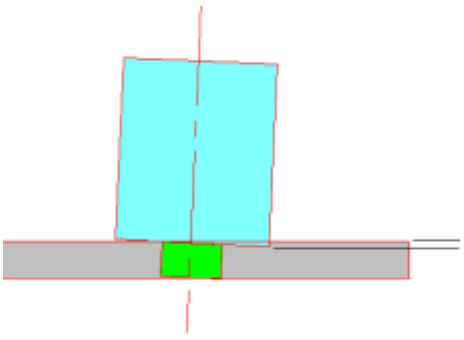

Figure 0.5 Figure illustrating a shoulder plunge depth of 0.2mm below the plate surface

The classification of Tool Steels

As a cooperative industrial effort under the sponsorship of AISI and SAE, a tool steel classification system has been developed in which the commonly used tool steels are

grouped into seven major categories. These categories, several of which contain more than a single group, are listed in Table 4.1 with the symbols used for identification. Suffix numbers following the letter symbols identify the individual types of tool steels within each category.

Category Designation	Letter Symbol	Group Designation
High-Speed Tool Steels	M T	Molybdenum types Tungsten types
Hot-Work Tool Steels	H_1-H_{19} H_{20}-H_{39} H_{40}-H_{59}	Chromium types Tungsten types Molybdenum types
Cold Work Tool Steels	D A O	High carbon, high chromium types Medium alloy, air hardening types Oil hardening types
Shock Resisting Tool Steel Mold Steels	S P	… …
Special Purpose Tool Steels	L F	Low alloy types Carbon tungsten types
Water Hardening Tool Steels	W	…

Table 0.1 Classification of Tool Steels

Selection of Tool steel for Aluminum 5083 H321

From to the various options of steels and alloys available it was necessary to select an appropriate steel with specific characteristic behaviors that would apply to joining Aluminum 5083 H321 plate. During the welding process the tool will reach temperatures in the range of 500 ^{o}C at tool tip depending on the type of material being welded. The tool material must have good hardness, toughness and wear resistant properties at elevated temperatures.

A hot-work tool steel that comprises of outstanding high temperature strength, high temperature toughness, high temperature wear resistance and good machineability is W302. This tool steel selection was also motivated by its cost and availability.

Thermal treatment of W302 (H13)

Since this tool steel has a very specific tempering phase, great precaution had to be followed during the heat treatment stage in order to produce a high quality tool. Two specimens were prepared with the same diameter of that of the machined tool to be tempered. The dimensions of the test specimens were &30.5mm x 20mm long. The specimens were heat treated by the following specifications supplied by Bohlersteels in order to produce the required hardness.

Stress relieving: 600 to 650^{o}C Slow cooling in furnace; intended to relieve stresses set up be extensive machining, or in complex shapes. After through heating, hold in neutral atmosphere for two hours.

Hardening: 1020 to 1080 Oil, salt bath (500 to 550^{o}C), air holding time after temperature equalisation: 15 to 30 minutes Obtainable hardness: 52 - 54 HRc (Oil or Salt Bath), 50 - 54 HRc (Air).

Tempering: Slow heating to tempering temperature immediately after hardening / time in furnace. One hour for each 20mm of workpiece thickness but at least two hours cooling in air. It is recommended to temper at least twice. A third tempering cycle for the purpose of stress relieving may be advantageous. 1ST TEMPER: Approx. 30^{o}C above maximum secondary hardness. 2ND TEMPER: Temper to desired working hardness. 3RD TEMPER: For stress relieving, at a temperature 30 - 50^{o}C below highest tempering temperature.

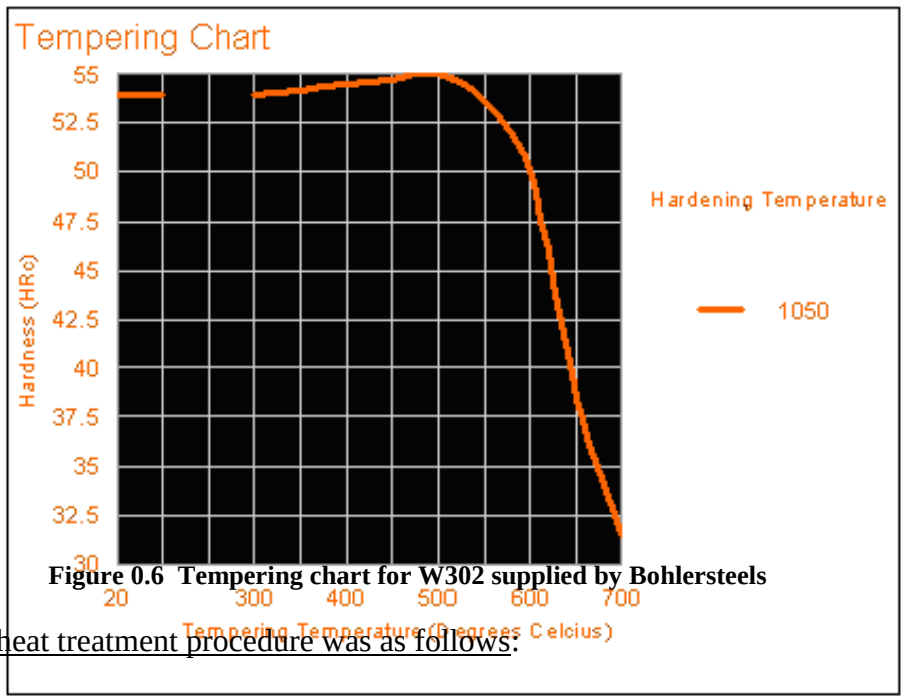

Figure 0.6 Tempering chart for W302 supplied by Bohlersteels

The actual heat treatment procedure was as follows:

1. Specimens in furnace: 0.5 hour @ 1050 ^{o}C - Actual time in 25min at 1050 ^{o}C from equalization.

2. Quench in oil directly after heating.

3. *1st Temper*: Placed in second furnace equalization temperature @ 530 ^{o}C. – Actual time in 1hour.

4. Cool in air for 2hours.

5. *2nd Temper*: Placed in furnace equalization temperature @ 600 ^{o}C – Actual time in 1 hour.

6. Cool in air for 2hours.

7. *3rd Temper*: Place in furnace equalization temperature @ 550 ^{o}C – Actual time in 1 hour.

The product must be slowly heated in furnace until temperature reaches equalization point, time taken from there onwards.

The tempering procedure of the test specimens was done according to Figure 4.6 and then Related Vickers hardness tests were performed on each specimen to establish the hardness of the material. Table 4.2 and 4.3 illustrate the related Vickers results obtained before and after respectively.

Specimen 1 @ 30kg Vickers	Specimen 2 @ 30kg Vickers
1.) 210.6	1.) 205.7
2.) 207.3	2.) 204.2
3.) 213.9	3.) 205.7
Average: <u>210.6</u>	**Average: <u>205.2</u>**

Table 0.2 Specimen hardness before heat treatment

Specimen 1 @ 30kg Vickers	Specimen 2 @ 30kg Vickers
1.) 583	1.) 575
2.) 525	2.) 583
3.) 563	3.) 517
Average: <u>557</u>	**Average: <u>558</u>**

Table 0.3 Specimen hardness after heat treatment

The equivalent to the Rockwell C scale is about **RC 52**.[27] Since the experimental test run with the specimens produced the required properties and characteristics, the same procedure was used for the heat treatment of the final tools.

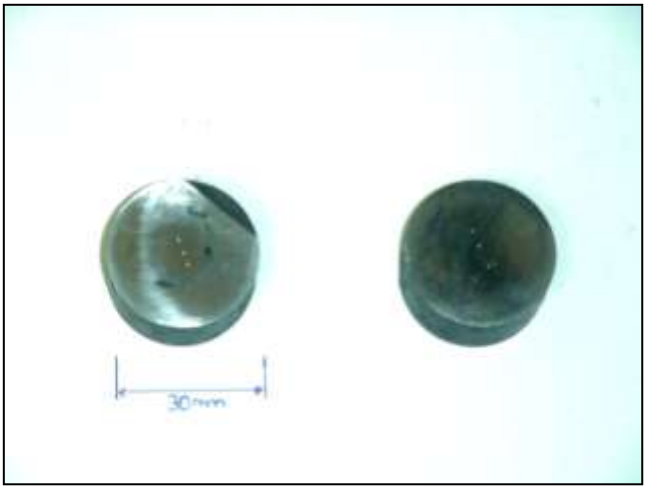

Figure 0.7 Two specimens tested at tempered condition

Tool Characteristics

Most welds made by institutions are evaluated by their characteristic external appearance during and after a weld. The welding parameters are then adjusted to eliminate any surface defect features that appear. Weld appearance and the preliminary quality of the weld can be evaluated by the type of footprint pattern, amount of side flash build-up, concave plunge depth, discoloring of HAZ, amount of plasticised material flow in front and rear end of tool and also the bottom or backing end joint line visibility after the weld. The next couple of tool designs were investigated with respect to these external appearance factors.

Tool Design – FSW1

The first tool design that was manufactured by the MTRC was based on the following criteria:

- 6mm Aluminun Plate to be welded
- Diameter of shoulder 25.4mm
- Diameter of probe 10mm
- Re-entrant probe configuration
- Shoulder design – Concentric ring type

As illustrated in Figure 4.4 the shoulder design with concentric rings was selected since machineability was easier and a better dimensional accuracy was possible during manufacturing.

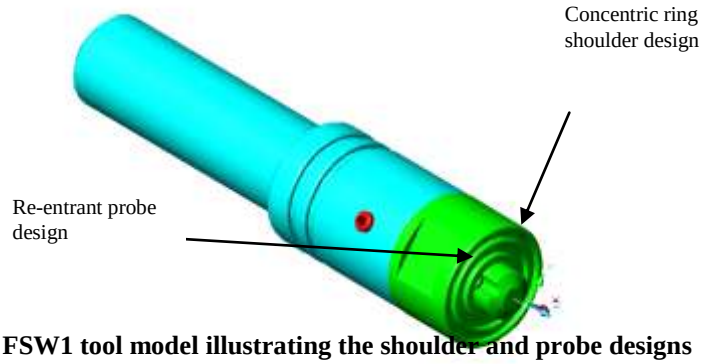

Figure 0.8 FSW1 tool model illustrating the shoulder and probe designs

The tool model shown in Figure 4.8 has a probe length of 5.5mm intended to weld only 6mm plate since the probe length governs the plate thickness of the weld.

Figure 0.9 First FSW tool manufactured by PE Technikon

In Figure 4.9 the tool was designed so that it consists out of two components: The tool housing and the tool tip. The intention of this design, although more costly to manufacture, was to use the tool housing section and just replace the tool tip section by new designs. The manufacturing drawings can be viewed in Appendix B.

Tool (FSW1) Preliminary Performance Evaluation

The very first welds that were made using this tool profile produced interesting results. External surface evidence indicate that this tool geometry produced enough

surface contact to produce a good friction stir weld although there was still room for improvement on probe design. The first welding trials were made with a 0^{o} tilt of the tool axis. During these welding trials an increase or build-up of aluminum, termed "side flash", on the retreating side was produced. This can be attributed to the increasing downward pressure.

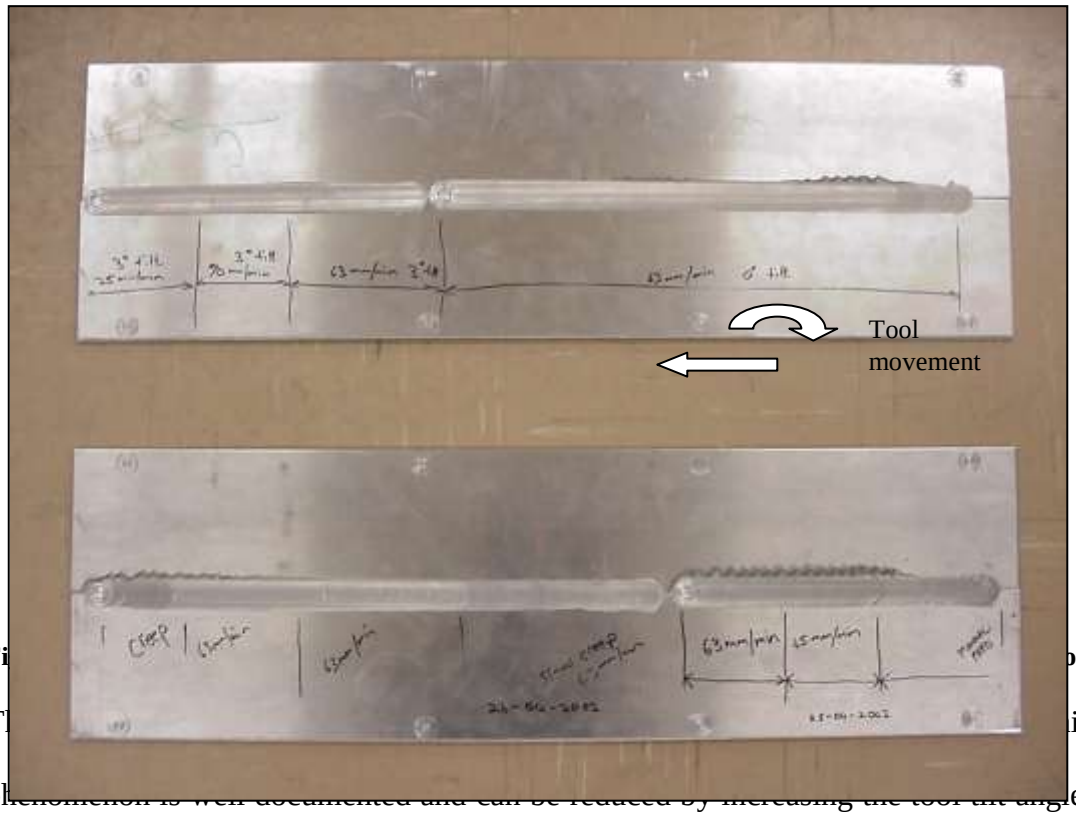

Fi **on**

Th is

ph e,

ranging from 1 to 5 degrees or using a helical or spiral ridge profile on the tool shoulder.[5][13]

Figure 4.10 illustrates that by increasing the Z-force at a 3-degree tilt results in an increasing hydrostatic pressure of the tool shoulder and eliminates side flash build up. It is important to note that the hydrostatic pressure on the tool surface has to be increased if a faster traverse feed rate is required.

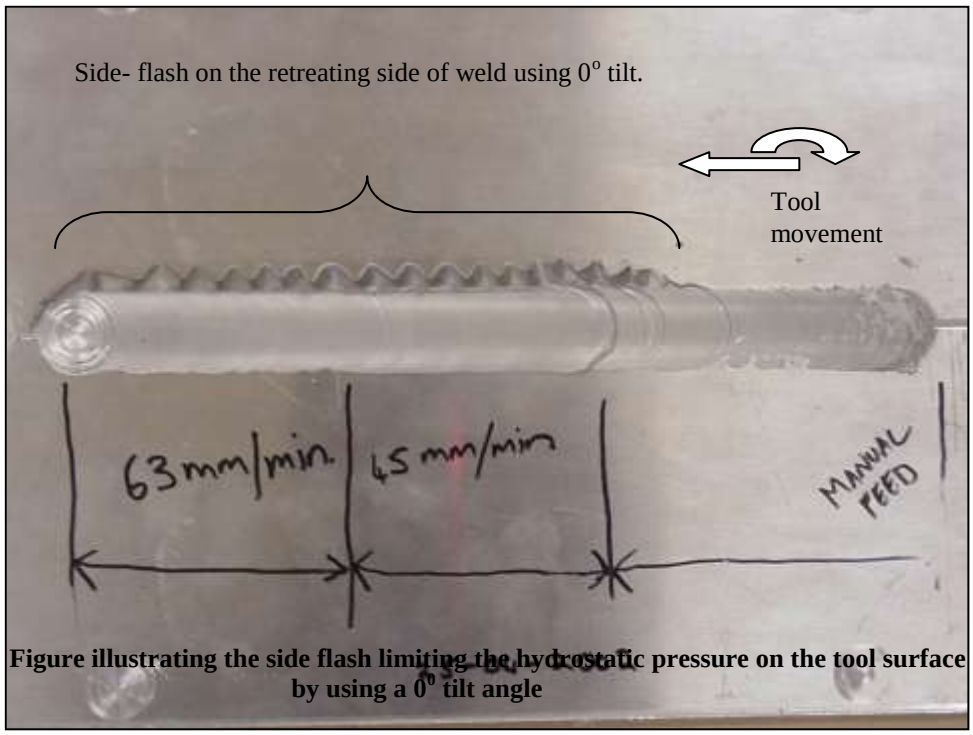

Figure 0.11 Figure illustrating the side flash limiting the hydrostatic pressure on the tool surface by using a 0^0 tilt angle

During studies done at the University of South Carolina (UOSC) by Dr. A. P. Reynolds it was found that for a zero degree tilt a special tool shoulder profile design could reduce side flash build up. A specially shaped shoulder with a scroll type feature must be implemented so that the clockwise rotation of the tool will produce the anti-clockwise scroll profile to auger the movement of the plasticized material away from the retreating side keeping the material in the region of the flow path.[13] This tool design will be investigated in Section 4.6.1.

The higher feed rates are only possible by a 2-3 degree set tilt angle with this tool geometry. It seems that the flow path of the plasticised material is well controlled by this tool shoulder since the weld flow pattern and footprint are of uniform nature.

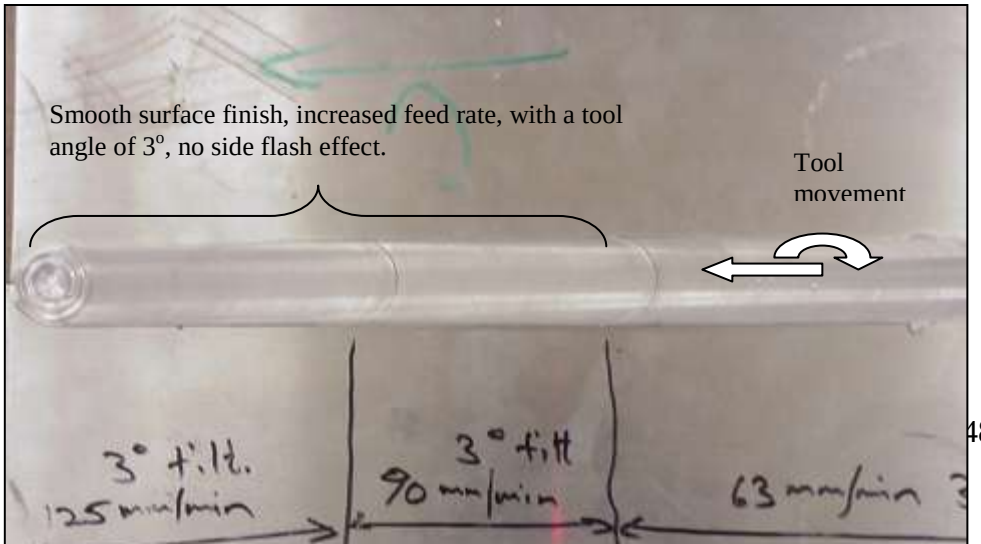

Figure 0.12 Figure illustrating the surface finish produced by a 3^0 tilt angle of the tool axis

Tool Design - FSW2

The second tool concept was based on the following criteria:

- 6mm Aluminun Plate to be welded
- Diameter of shoulder 25.4mm
- Diameter of probe 10mm x 5mm
- Paddle type probe design
- Shoulder design – Concentric ring type

The main reason for this configuration was to evaluate and create a better stirring effect of the plasticized material. This paddle type design is also mentioned in reference [16]. Although the static to dynamic volume ratio of the probe/pin to material flow is low it was important to estimate the effect it has on the material welding parameters especially for thin plate welding. Figure 4.13 illustrates the model of the concept shoulder and pin profile of the second tool design.

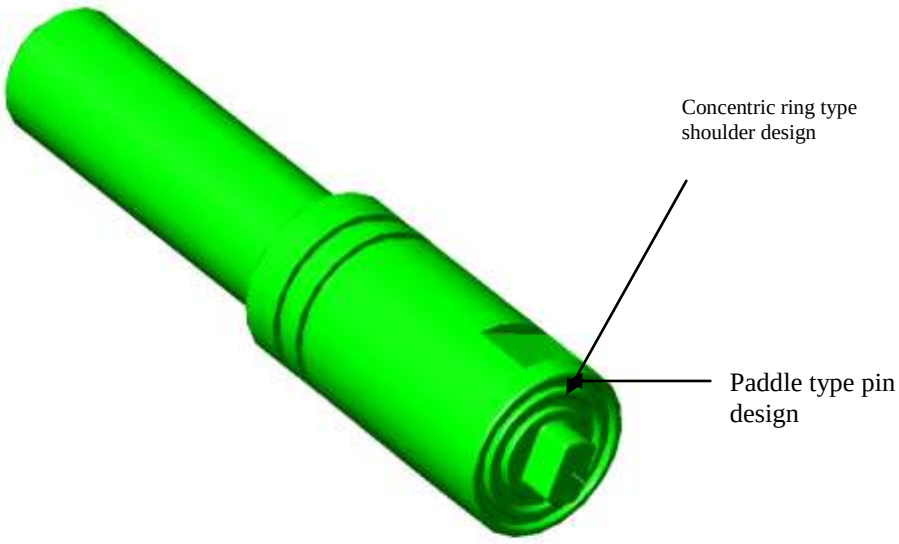

Figure 0.13 FSW2 tool model illustrating the shoulder and probe designs

The full manufacture drawings can be viewed in the Appendix B.

Tool (FSW2) Preliminary Performance Evaluation

The paddle type concept did not work as well as expected. During this welding trial we could clearly see the drastic effect of the low static to dynamic volume flow ratio. The tool seemed to have produced enough friction on the tool shoulder to rapidly reach plasticized conditions in the material but the probe design was inadequate. By using the same spindle speed and feed as in the first tool design we found that a big wormhole or surface-breaking groove existed all along the joint line. The incomplete fusion can be explained because of the probe pushing the material away from the flow path and not causing it to mix and combine at the trailing edge of the tool shoulder. It can clearly be seen in Figure 4.14 that this probe design causes less mixing than expected and actually pushes the material away from the joint line rather than bringing the material together.

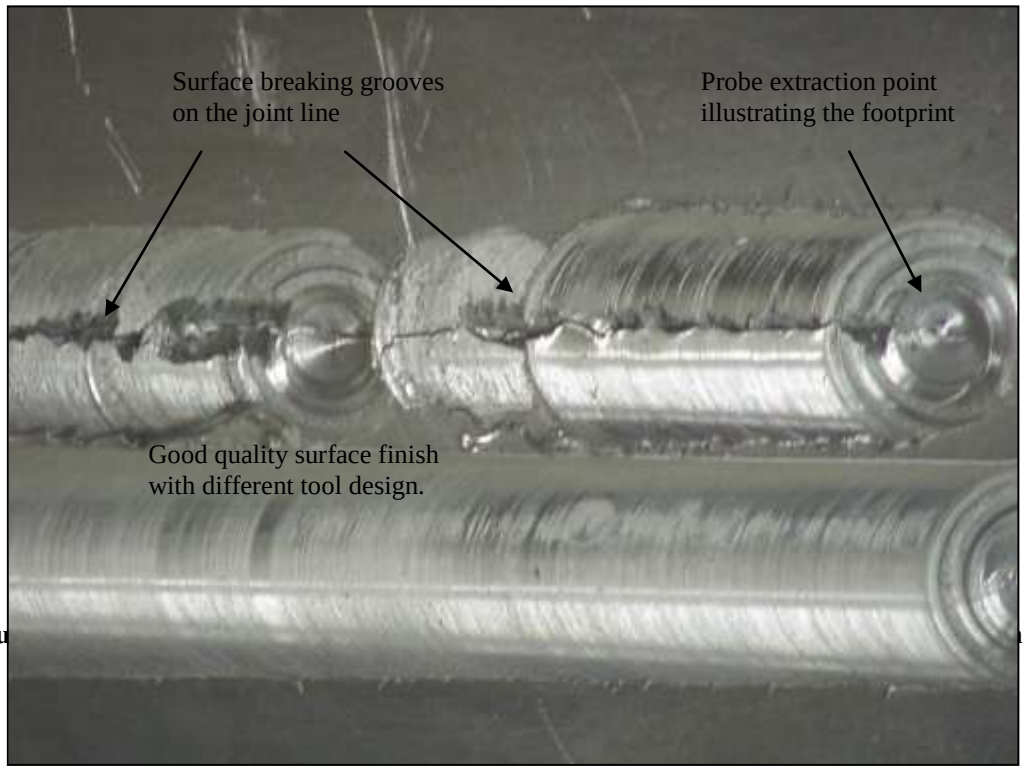

Figu

Tool Design – FSW3

The third tool design is based on the following criteria:

- 6mm Aluminun Plate to be welded
- Diameter of shoulder 25.4mm
- Major diameter of probe 10mm
- Accommodate a thermocouple
- Single flute configuration on probe
- Threaded probe design
- Shoulder design – Recess type

In Section 4.2 the functionality of the tool was explained in detail. The aim of this tool design was to meet these requirements. Firstly a new shoulder design was used to create a better flow path for the plasticized material on the surface and to also reduce side flash.

The probe has a single flute and threaded surface that will help improve the static to dynamic volume flow ratio and assist in the downward auguring effect respectively. The probe has a better stirring effect since the single flute has a bigger surface area and taper angle. This tool design was made to work under a preferred tool tilt angle of 2.5 degrees. Figure 4.15 illustrates this tool design before it was heat treated.

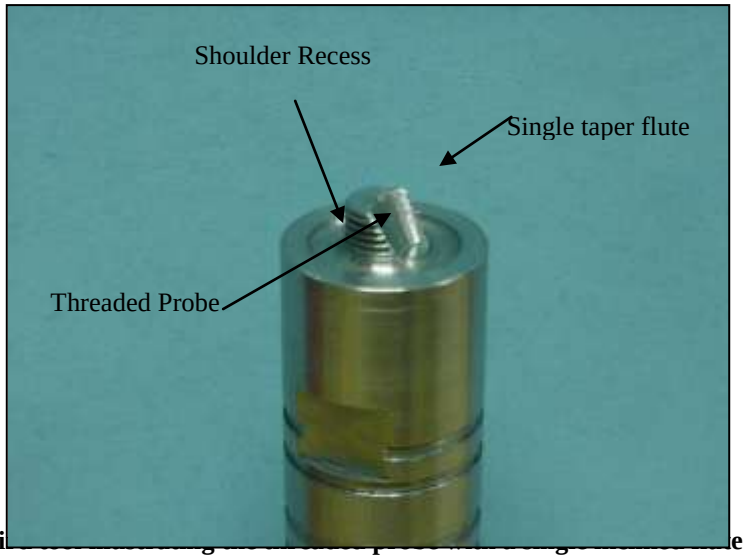

Figure 0.15 Thi e and a recessed shoulder design

Further more the tool can accommodate a thermocouple that will give us an indication of the tool operating temperature. The full manufacturing drawings can be viewed in Appendix B.

Tool (FSW3) Preliminary Performance Evaluation

The surface finish of the weld is slightly concave due to the hydrostatic pressure effect of the tool shoulder. Further more the plasticized flow formation around the tool seemed to be controlled and maintained in the direction of flow although it was observed that the plasticized region (third-body) is maintained in the central region of the tool. This will not always be an advantage since the probe will then experience more X-force due to the forging action rather than to mix the plasticized material around the tool on the leading edge. No surface breaking grooves or worm-hole defects were observed at this stage. Figure 4.16 illustrates the surface finish on the face and root respectively.

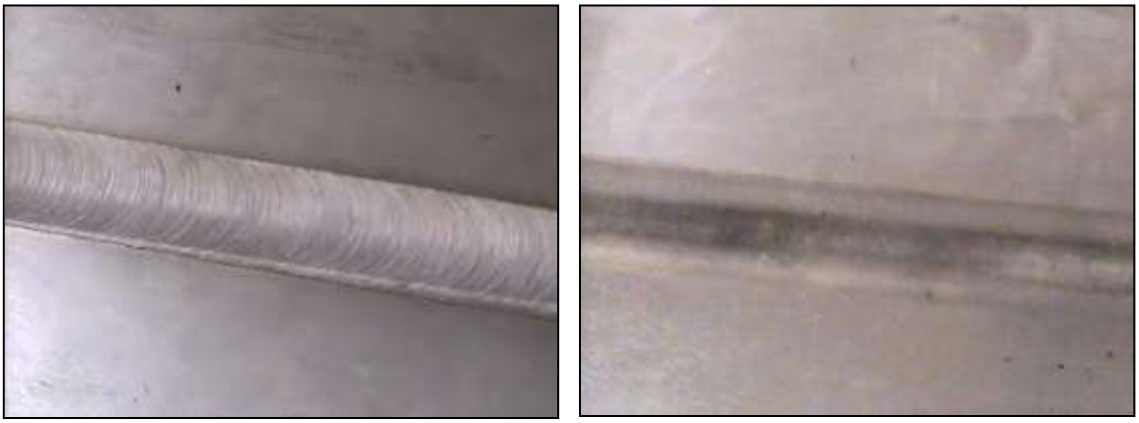

Figure 0.16 Results produced by the third concept tool. Figure illustrating the surface finish of the face and root weld respectively.

Future Developments under attention

Tool Design – FSW4

The fourth tool design is based on the following criteria:

- 6mm Aluminun Plate to be welded
- Diameter of shoulder 25.4mm
- Major diameter of probe 10mm
- Accommodate a thermocouple
- Single flute configuration on probe
- Threaded probe design
- Shoulder design – Scroll type

This tool design must still be evaluated by using various welding parameters. The shoulder is designed so that it can augur the material flow path during the weld in a radial inward direction towards the stirring region. This auguring effect should reduce the side flash build up and make welding at a 0^o tilt angle possible. The advantage of using a 0^o tilt angle in certain alloys was observed during a visit to the University of South Carolina. It was understood that the angle plays an important role during the heating of the material in front of the tool during the weld. Since the tool is now flush with the material, the heat input is better during a weld run. A negative factor that could play a role during the quality of the weld will be the change in hydrostatic pressure between the tool shoulder and substrate. This change must be proportionally controlled to ensure a good quality surface finish. Further investigation into this matter must still be done. Figure 4.17 illustrates the manufactured tool (FSW4) intended for 0^o welding. The full manufacture drawings of this tool are also available in Appendix B.

Figure 0.17 FSW4 Tool illustrating the scroll profile tool shoulder with an embedded thermocouple

Skew-Stir

Currently under investigation at TWI[13] are improvements relating the dynamic to static volume ratio of the tool by use of a skew motion.

The Skew-stir variant of friction stir welding differs from the conventional method in that the axis of the tool is given a slight inclination (skew) from that of the machine spindle. As shown in Figure 4.18 the face of the shoulder is produced such that it is at 90° to the axis of the machine spindle. The intersection of the two axes can occur above the plate, through the plate thickness, and to a position below the plate being welded. This intersection, or focal point, can be varied to suit the material, the process parameters and the tool geometry.

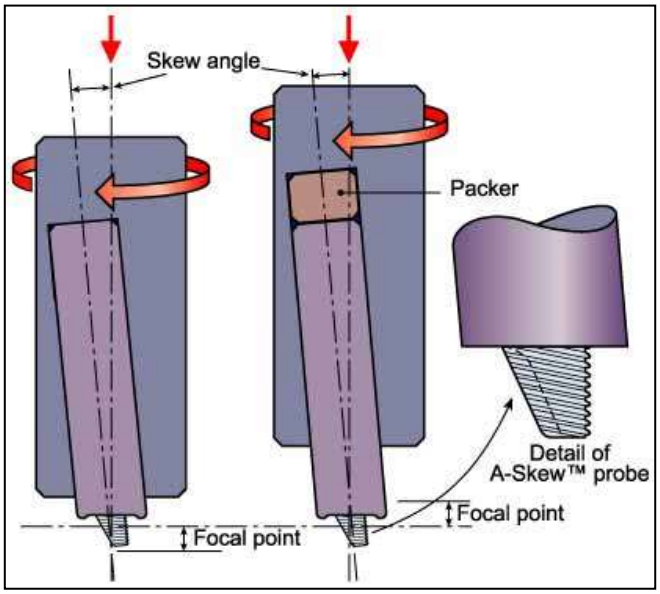

Figure 0.18 Basic principle of Skew-Stir showing different focal points[30]

Tilting the plate substrate or machine spindle with respect to the shoulder can then additionally produce a plate to tool tilt, similar to that often used in conventional FSW.

When the focal point is positioned slightly above the top surface of the plate, at any position through the thickness of the plate, or slightly below the plate, the shoulder contact face makes a nominally orbital movement. This orbital motion of the shoulder is dependent on the angle of skew and the focal point. The greater the skew angle and the greater the distance of the focal point from the top of the plate, the greater is the shoulder orbit.

This tool does not rotate on its own axis, and therefore only a specific part of the face of the probe surface is directly involved in working the substrate component material. Consequently, the inner part of the tool can be cut away to improve the flow path of material during welding. This results in an asymmetric shaped probe as shown in Figure 4.15. The skew-stir technique provides an increase flow path, and the width of the weld nugget region is greater than the diameter of the probe. This feature is ideally suited for lap and T-joints and similar welds, where the interface is 90^{o} to the machine axis, i.e. parallel with the work piece surface.

Friction Skew-stir welding increases the extent of the plasticized material surrounding the probe. The Skew-stir technique, therefore, provides a method of increasing the 'dynamic to static volume ratio' of the probe by the skew motion of the tool. Traditionally, the 'dynamic to static volume ratio' is provided by the geometry of the probe because of its re-entrant features. Skew-stir, therefore, can be used to the advantage where complex shaped tools cannot be employed. Moreover, the skew action results in a greater volume of plasticized material within which the disrupted surface oxide layer can be dispersed. This should minimize the risk of undesirable joint remnant features.[13]

Conclusion

It can be seen from Section 4.5 that the tool designs have a great influence on weld appearance and quality. The probe of the tool plays an important role during the flow path of the plasticized material. If this flow path is not controlled by the mixing and downward auguring effect of the probe, major defects will arise such as surface breaking grooves and worm holes. The tool profile must firstly be linked to the possibility of creating a weld before any attempts are made to improve the weld quality. When a good welded joint is obtained with the specific tool design, it will be up to the process parameters settings and interactions, such as spindle speed and feed-rate, to optimize the weld quality. The importance of the tool geometry is conducted and verified in Chapter 5. The non-profiled tools produced high welding loads and very poor quality. Welds were not possible when using non-profiled tool geometries, thus simply rotating a pin in the material will not produce a welded joint. The surface finishes of the profiled and non-profiled tool geometries can be viewed in Appendix C. From the FSW3 tool geometry it can be seen that good welds are achievable, making faster feed-rates possible with lower loads. The pin and shoulder plays a very important role in the design as well as the type of tool material used. The tool material should be chosen according to the base material being welded. Tool material that need to be considered when welding base materials such as 12% Chromium alloy steel will be tools manufactured out of Tungsten Carbide alloys that can resist heat generated at shoulders whith temperature ranges from about 1000^0C. Aluminum alloys have low melting points (600^0C), thus normal tool steel may be used and selected by their toughness and strength characteristics.

The heat of the process, which is directly related to tool temperature, must be controlled in order to maintain good plasticized conditions. The tool shoulder and

geometry will affect this heat input since it is the rotating tool shoulder and pin surface that create the heat. Many different tool geometries can be used but must still be tested for quality, such as the FSW4 tool. The optimum condition that all FSW researchers would like to meet will obviously be to weld at the highest feed-rate possible with the best quality and strength.

Good welds are now made possible making use of improved tool technology such as the FSW3 tool. In order to improve the quality of the weld, better process parameters such as spindle speed and feed-rate must be adopted. For the researcher to determine what optimal parameters to use, a measuring system had to be implemented to monitor real time process variables such as tool temperature and vertical Z-force. This monitoring system will be explained in detail in Chapter 5.

Advanced Monitoring Equipment for Process Optimization

In order to monitor torque and forces F_x, F_y and especially F_z on the rotating tool, specialized measuring techniques had to be implemented. A thorough investigation was made to determine the best practical methods for monitoring the crucial parameters during the FSW process and then selecting the best and most economical sensor and transducer application method. For all the various forces, X, Y, Z and Torque, measurements will be conducted by means of strain gauging in one form or another. An initial method was to strain gauge the backing plate itself or to strain gauge the rotating shaft. Figure 5.1 demonstrates the concept model for measuring the forces applied by strain gauging the backing plate.

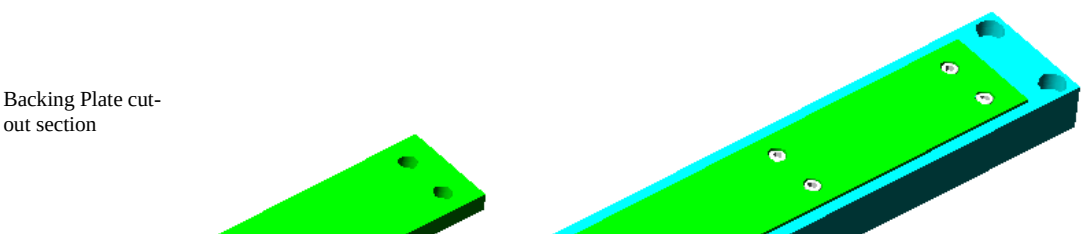

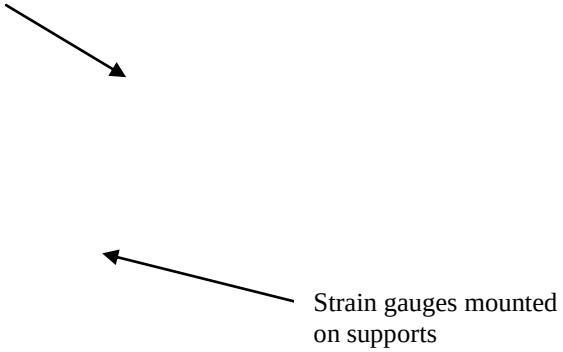

Figure 0.1 Alternative concept for measuring weld forces

On the other hand temperature of the tool could be monitored using an infrared thermal imaging camera, embedded sensors in the parent plate or simply embedding a thermocouple in the rotating tool. All these options also have its limitations, mainly being cost.

It was decided to make use of a non-contact measuring system on the rotating tool-chuck since this method will enable us to monitor all the relative variables including temperature and torque directly form the actual tool. The system is illustrated schematically in Figure 5.2.

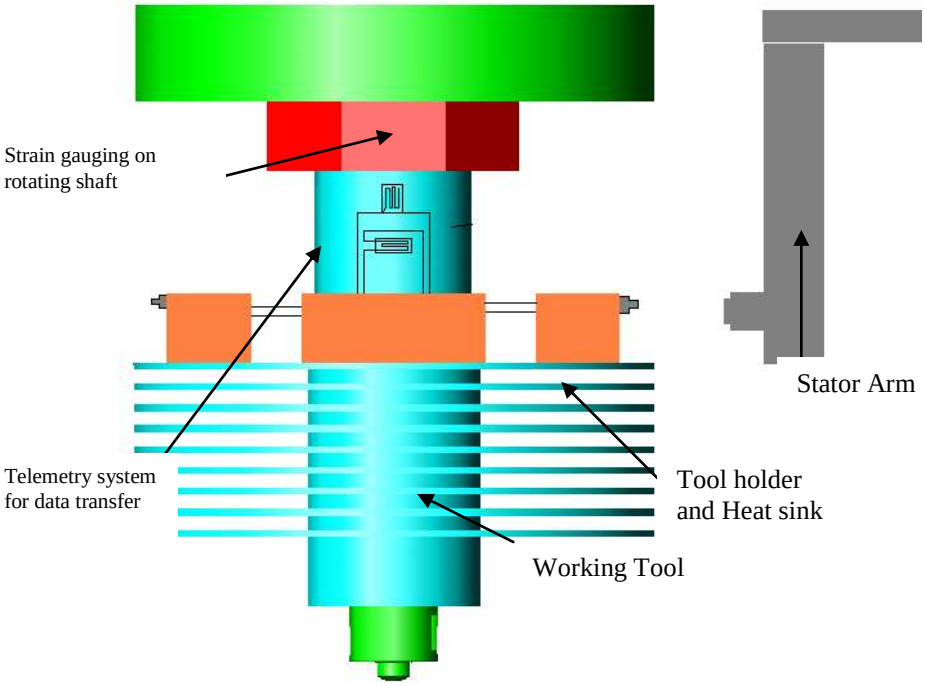

Figure 0.2 Improved concept model for measuring weld parameters

A few non-contact measuring systems are available on the market. Custom-made sliprings and dynamometers are available for selected milling machines but the process needs at least one additional built-in channel for temperature measurement. To mention a few that were under investigation are: from Kistler, the rotating cutting force dynamometer 9123C and 9124B; from Microstrain, the Strainlink (TM) a multichannel digital strain transmitter; from Kraustelemetry, the MT32 and RT8/16 mini telemetry systems. Most of these where unsuitable because of their poor response time, were costly and had limited flexibility in terms of building in additional channels.

A local company called LMI (Libra Measuring Instruments)[40] builds custom telemetry units making use of inductive/capacitance transmission. In this chapter the measuring system; its operation and capabilities will be described.

Operation of the Data Measuring System

An instrumented chuck for the machine was developed to measure realtime process data. The mechanical structure and design can be viewed in Section 3.5. Strain gauges were mounted on the shaft and a thermocouple was inserted near the tool pin. This unit provides a direct stream of data (process variables) during a welding run. The following data are the conditioned data that can be obtained using this system.

- Tool rotational speed
- Tool torque
- Tool temperature
- Tool vertical force on material
- Tool 360^{o} polar force footprint around the tool

The configuration of the measuring system can be better explained with the aid of the diagram as illustrated in Figure 5.3.

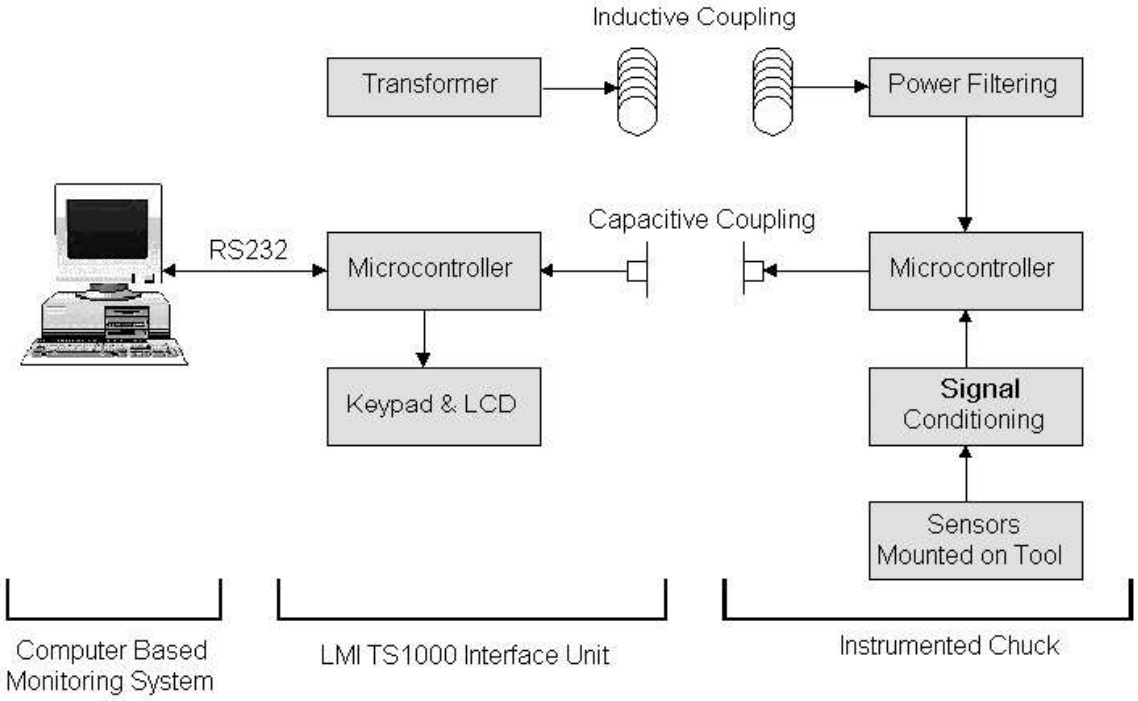

Figure 0.3 Block diagram illustrating the basic control configuration of the measuring system[40]

The electronics mounted on the chuck allow all the required variables to be sampled, the raw sensor data is signal conditioned and passed to a microprocessor, where it is prepared for transmission to the TS1000 interface unit. Electrical power is transferred to the chuck using induction and the sampled data is transferred off the chuck in a digital format, using a capacitive technique. The power coil and capacitive receiver can be seen on Figure 5.5. There are two of the above systems installed on the chuck, as each system can only support four channels of sampled data. Both systems share the same power coil and capacitive receiver.[40]

The channels of sampled data are received by the microcontroller housed in the interface unit, for processing. When the interface unit receives a request for data, it

transfers the information via the RS232 serial interface to the requesting device (the computer). The two interface units can be viewed in Figure 5.4.

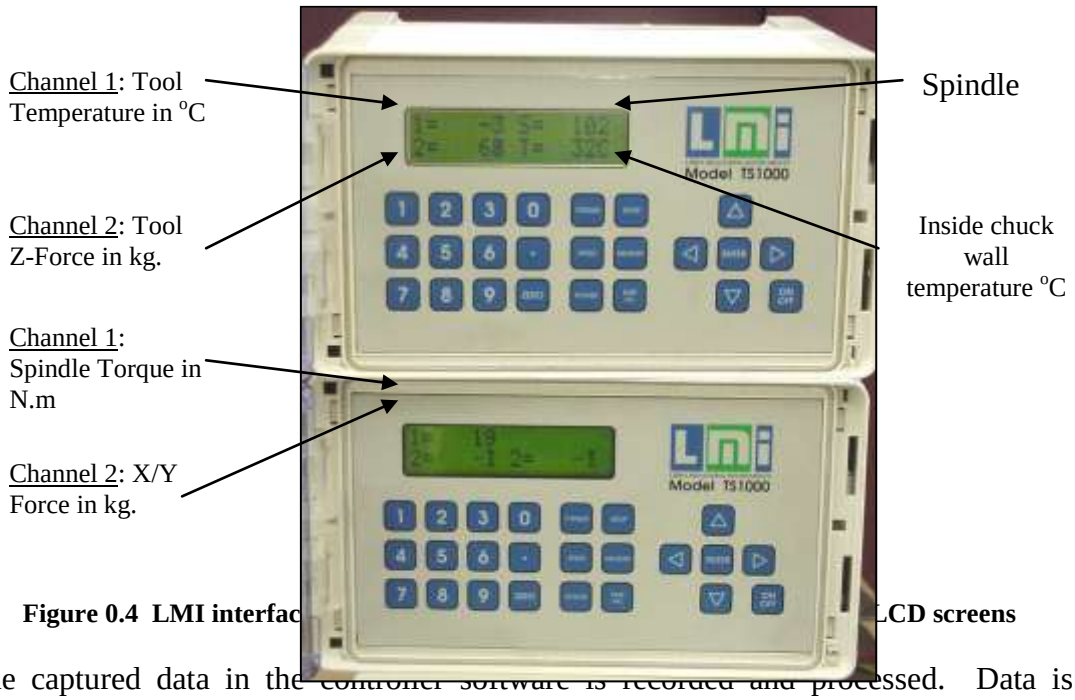

Figure 0.4 LMI interfac LCD screens

The captured data in the controller software is recorded and processed. Data is displayed on the user interface in real-time to enable the operator to make control decisions or to be used as inputs to a fuzzy logic controller. The fuzzy logic controller's rule base can be modified and new process control schemes can be tested.[39] The two interface units display the rotor voltage of the two systems and must be checked before each weld trial. These voltage settings are typically in the range of 5.1 V for each unit and must not fluctuate during weld trials. These settings can be checked on the setup menu on the LMI unit display. Figure 5.5 illustrates the final design and the measuring unit currently in operation.

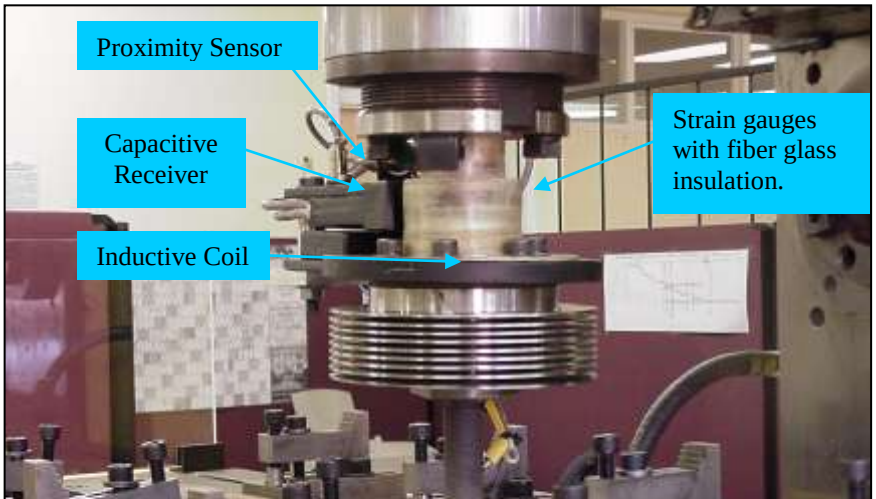

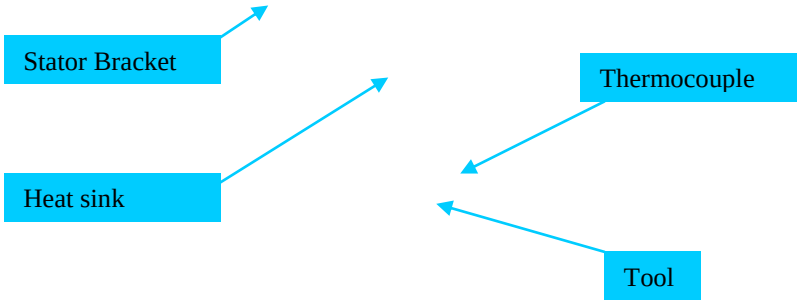

Figure 0.5 Non Contact FSW Data measuring system

The shaft of the custom-made chuck is strain gauged making use of standard strain gauging procedure. Detailed information regarding the strain gauging procedure, selection and application thereof can be viewed in references [37] and [38].

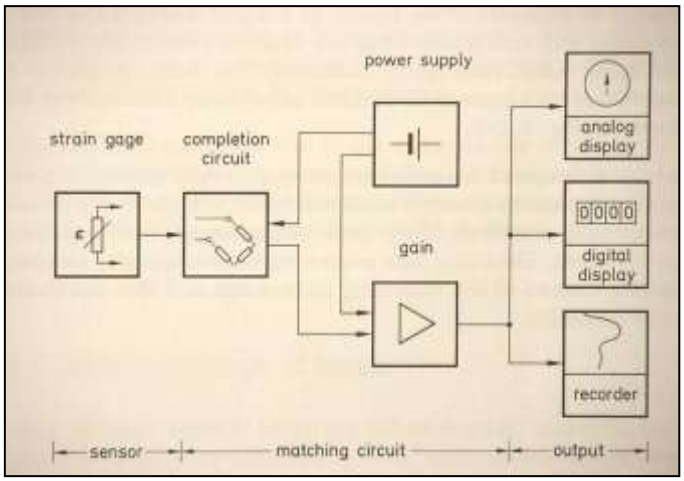

Figure 0.6 Diagram of a measurement system making use of strain gauges[37]

A typical strain gauge measurement system is illustrated in the diagram shown in Figure 5.6. There are three Wheatstone full bridge configurations implemented on the rotating shaft.[38,41] One bridge for Torque, one for Z-force and the other for X/Y-force measurement[41]. All the above circuits do compensate for temperature fluctuations. An additional temperature gauge is also mounted within the rotating electronic unit of the tool holder for safety purposes in case of overheating. The system will shut down if the threshold level of 70^{o}C is reached within the unit. A proximity sensor mounted on the receiver measures the exact rotational speed of the tool holder and is displayed in revolutions per minute. A type K thermocouple with a

3mm diameter probe is imbedded within the tool, close in contact with the tool shoulder. The thermocouple will measure the tool temperature during operation and it is calibrated to the signal conditioner reflecting a change with 0-43mV. This range will be the typical operating range from 0-1000^{o}C.

Calibration

LMI calibrated the equipment and the interface thereof to the display unit. The researcher double checked the measured strain readings and made sure that they are in the correct proportion to the applied loadings. The Z-force was checked by the custom-made two quarter bridge diagonal loadcell mentioned in Section 3.1.

During the calibration procedure the most difficulty was experienced during the calibration of the 2D force profile on a 360^{o} polar pattern. This was to be obtained when applying a constant force on the rotating tool. Firstly the theory behind the experimental approach will be explained.

Since measuring is by means of strain gauges on a rotating chuck arm, it can be closely related to the existing theory on a bar (square or tubular) in tension or compression. The maximum of the tension or compressive stresses act in the direction in which the forces act. In all other directions the stresses are smaller and follow the relationship as shown in Equation 5.1.[37]

$$\sigma = f(\phi) = \frac{1}{2}\sigma_{max}(1 + \cos 2\phi). \qquad \textbf{(0-1)}$$

ϕ = angle between the active direction of force, i.e. the principal direction, and the direction under consideration.

In Figure 5.7 this relationship is represented in a polar diagram for the tension bar.

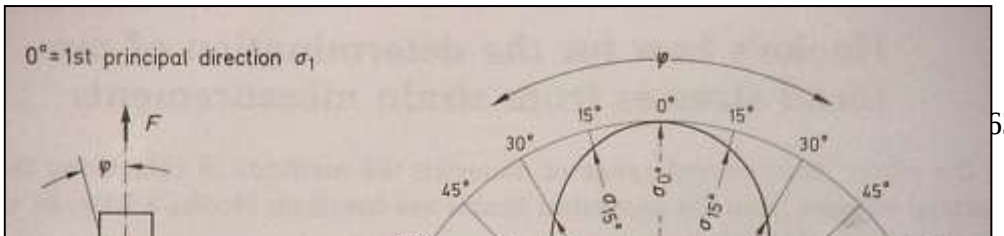

Figure 0.7 Stress distribution on the tension bar[37]

Figure 5.8 shows the relationship (Figure 5.7) for the compression bar.

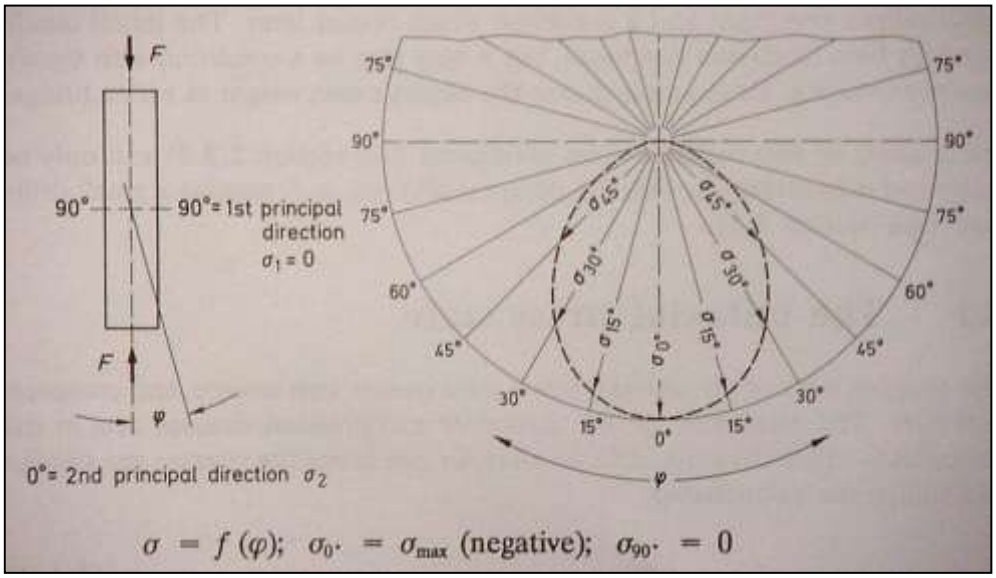

Figure 0.8 Stress distribution on the compression bar[37]

Both principal directions are always perpendicular to one another. The first Principal direction is always that with the algebraically larger numerical value; therefore there is a change in the indexing of the tension and compression bars.

If the **strain** distribution is regarded in a similar manner as with the stress distribution, a biaxial strain is found despite the uniaxial stress state. There are two defined directions, one in the active direction of the force (0^o) and the other perpendicular to it

$$\varepsilon = f(\phi) = \frac{1}{2}\varepsilon_1[1 - \nu + \cos 2\phi \cdot (1 + \nu)]$$

(90^o). Starting from the principal strain $\varepsilon_0 = \varepsilon_1$, the strains ε_ϕ, which occur at the angle $0^o < \phi < 90^o$ to the direction, can be calculated according to Equation 5.2[37]:

(0-2)

The relation of the two principal strains is expressed by the transverse strain factor 'm' or its reciprocal, Poisson's ratio ν.

$$\varepsilon_2 = -\nu . \varepsilon_1 \qquad \textbf{(0-3)}$$

In Figures 5.9 and 5.10 the relationship is shown for a tension bar and a compression bar respectively. These diagrams are drawn for a material with a Poisson's ratio ν = 0.3. Typical EN19 steel, the tool holder steel, reflects the same Poisson's ratio of approximately 0.3. In this case the strain becomes zero at an angle $\phi = 61^o$, i.e. the zero crossover between the positive and the negative strain regions is in this direction.

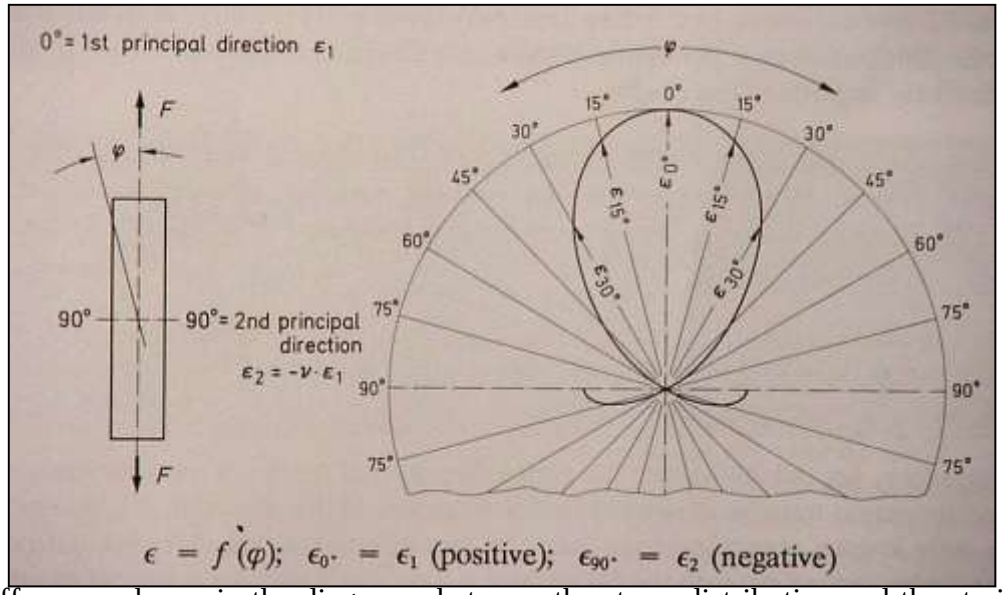

The difference, shown in the diagrams, between the stress distribution and the strain distribution in dependence of the active direction of the force leads to an extremely important conclusion: The material stress σ should be calculated from the measured strain only according to Hooks's Law for the uniaxial stress state as in Equation 5.4.

$$\boxed{\sigma = \varepsilon E .} \qquad \textbf{(0-4)}$$

In the transverse direction (90^o direction) there is no material stress present despite the measurable strain (transverse contraction, transverse dilation). Therefore for reliable results the active direction of the force must be known and the strain must be measured in this direction.

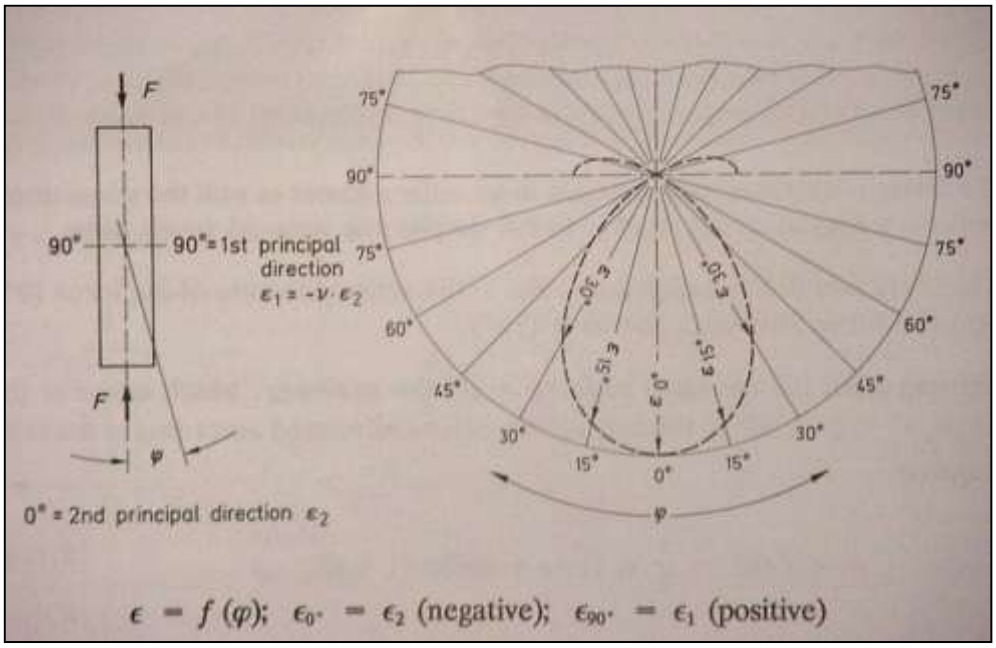

The calibration of the polar force pattern is based on this theory. A force was applied in a known direction on a non-profiled tool to ensure symmetrical readings. The strain was recorded from the measuring unit and transferred via RS 232 cabling to the computer software program were further conditioning took place. Since only a certain number of samples are available per revolution and due to certain limitations of the LMI software, a linear interpolation average had to be taken between certain degrees in order to obtain precise 10^o incremental readings. More of these limitations will be explained in Section 5.3. When the maximum principal strain reading or load reading is obtained, Equation 5.2 is applied to obtain each individual strain/load reading at a specific interval (degree). Firstly a one directional force was applied on the tool shoulder (Figure 5.12) and the corresponding force profile, plotted as shown

in Figure 5.11. Also shown in this figure is the corresponding force profile (dashed line) of the calculated data obtained when using Equation 5.2.

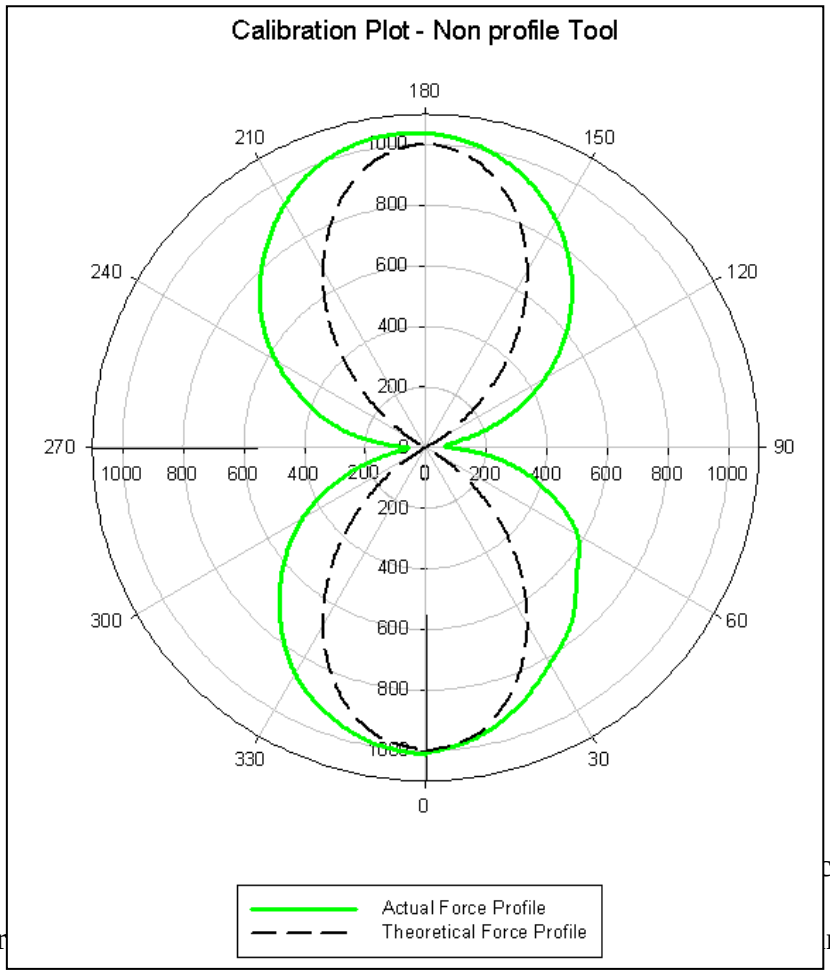

A comparison ce trend lines. They ar nterval. The narrower gradient of the calculated curve (dashed) is due to the fact that a sharper point load is applied on a flat theoretical surface. This dampen effect is schematically illustrated in Figure 5.12.

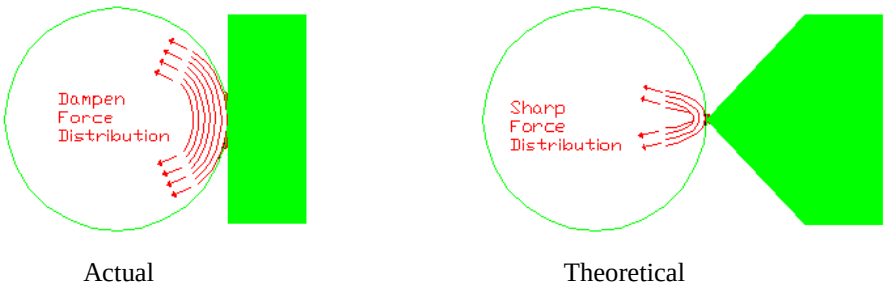

Figure 0.12 Figures illustrating the difference between the force distribution obtained when load is applied with a sharp point, and a flat surface

The more rounded gradient of the actual force plot (solid) is due to the load that is applied on a round, rotating, surface giving a more dampen gradient. This calibration plot proves the biaxial theory behind the tensile and compressive force relationships.

After the calibration of the measuring unit, three tests were performed to verify the repeatability of the system. The three tests conducted were all done at 560rpm, 0.1mm plunge depth and with a feed rate of 80mm/min with a non-profiled tool. The shape of the non-profile tool as well as the three calibration polar plots can be viewed in Appendix C. These plots represent the same orientation and profile of forces around the tool in all three tests conducted. It must be emphasized that the readings do fluctuate now and then due to the sensitivity setting on the signal conditioner. The discrepancy in the last 50 degrees is due to system limitations explained in Section 5.3. The accuracy and repeatability are estimated to be in the range of 100 to 150N of X/Y force and 200N Z-Force due to the amplifier gain setting. Other possible reasons for the small discrepancies in magnitudes ranging from tensile to compressive forces are the fact that the tool is rotating and a frictional, rubbing velocity vector could cause an additional force apposing the direction of travel. It is not the main objective of this report to investigate all these forces and the shape of the profiles obtained, thus comment on these plots are restricted. The tool eccentricity factor may also have an influence in non-symmetrical profiles. This scenario must still be further investigated to verify these statements.

Limitations

The following limitations were encountered during the calibration and experimental procedure of the measurement system:

Machine vibration

Excess machine vibration during the weld trials can cause instability of the stator arm. This results in induced voltage fluctuations and therefore loss in communication. In order to overcome this problem a more rigid mounting bracket for the stator arm can be used as well as an improvement on the stability of the machine base.

Limited Sampling Rate

The number of samples possible during one revolution of the tool is inversely proportional to the rotational speed of the tool. The maximum sample period allowed by the measuring system is 5 milliseconds due the communication baud rate of 28800 bytes per second. This can't be changed since it is a fixed specification of the purchased unit.

Fluctuation of communication response times

Response times vary when data is transferred between the measurement system and the PC, due to the design of the purchased hardware. This is not controllable and results in deviations of the sampling periods expected.

Machine and Equipment Limitations

- Excess vibration of the traverse bed can cause measured tool forces to deviate.
- Tool eccentricity can cause major deviations in force profiles if not correctly inserted in the tool holder.
- Tool slippage in the tool holder during excessive forces causes the 2D polar force plot to shift orientation.
- Although the profile and magnitude of the polar force plots stay constant during tool changes, the angle of orientation changes with respect to the gauge reference marker on the tool holder.

- During multiple tests conducted and results obtained via the statistical analysis procedure, it can be concluded that the machine is limited to welding maximum plate thickness ranging from 6 to 8mm. This is due to the fact that the machine spindle and feed motor will not support the high loads that will be required during welding of thicker plate sections.

Statistical Analysis using Linear Correlation and Regression

Experiments planning

When designing experiments, very often researchers resort to approaches such as the evaluation of the effects of one factor at a time or to a factorial design.[33] The latter design would obviously lead to a large number of tests. In contrast, the use of an efficient testing strategy such as the orthogonal arrays (OAs) developed by Taguchi[34,35] would minimize this number of tests. In addition, an advantage of an OA design is its equal representation of all factors; some combinations of factors and factor levels are tested which otherwise would not have been investigated. Accordingly, the OAs will be used here for the design of experiments and models.

As shown in Appendix C, in the design of experiments table, weld parameters N, f and D were assigned four different levels varying from 300 to 600rpm, 40 to 100 mm/min and 0.1 to 0.4mm, respectively. These ranges are chosen so to ensure maximum deviation of dependent variables.

The Process cause-effect diagram for the design of experiments is illustrated in Figure 5.13. The Process Conditions each have two level inputs. The following are the designations given for the two levels, used as input symbols in the experiments table.

Material Properties	**Tool Type**
P1: Oxide layer	Y1: Profiled
P2: No-oxide layer	Y2: Non-profiled

Material thickness	**Dwell time**
s1: 6mm	t1: 16s
s2: 8mm	t2: 8s

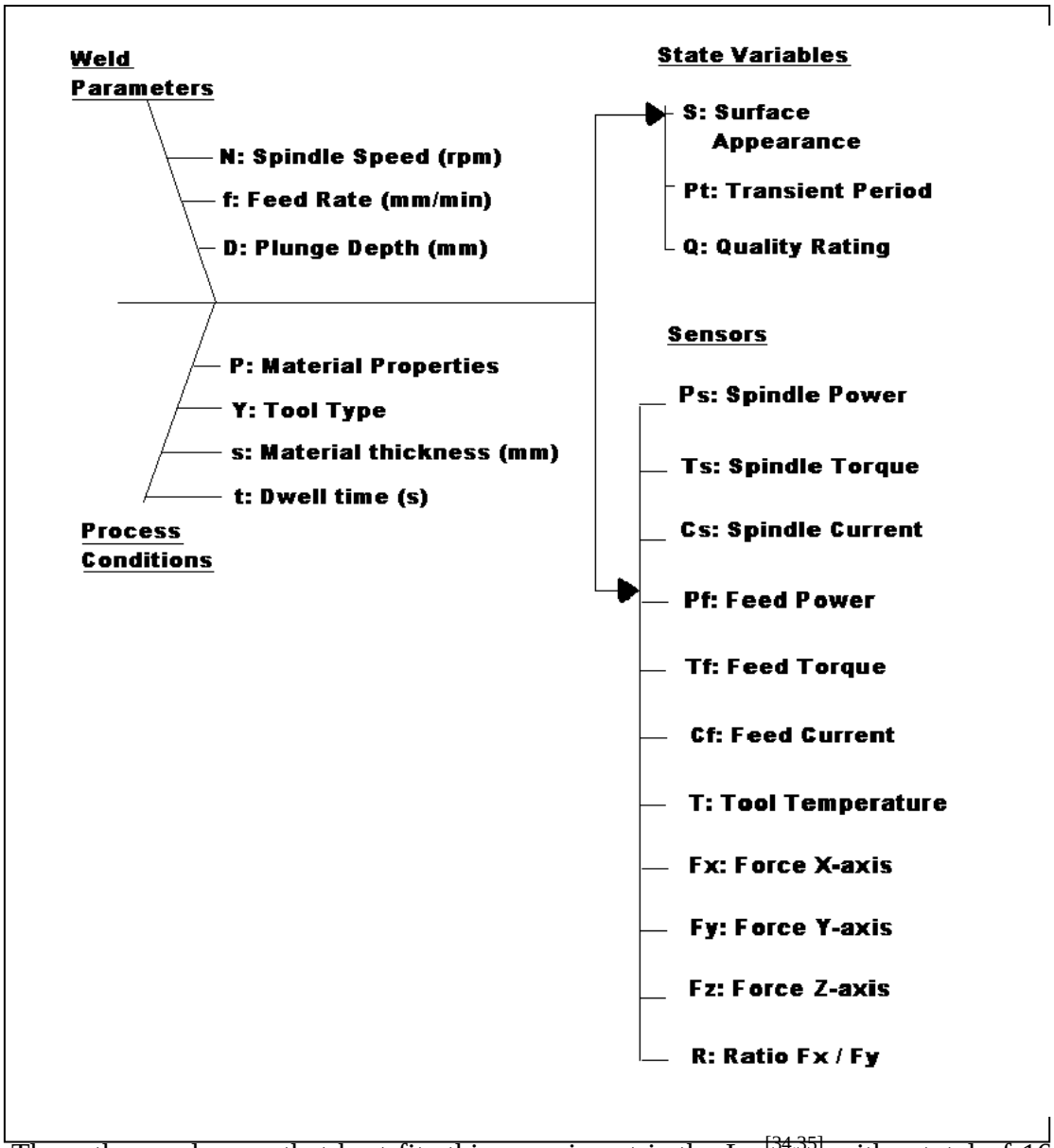

The orthogonal array that best fits this experiment is the L_{16}[34,35] with a total of 16 tests. This first level analysis is to determine how all these parameters, mentioned in Figure 5.13, relate to one another. In order to test the repeatability of the sensors and

eventually evaluate the capacity of our fusion model, a set of three tests were designed as mentioned in Section 5.2.

Introduction to Correlation and Regression Analysis

Correlation and regression refer to the relationship that exist between two variables, X and Y, in the case where each particular value of X_i is paired with one particular value of Y_i.[43] In this case an example can be taken from the Correlation Matrix table were 'ps' and 'ts' are the two correlation variables. Obviously 'ps' related to itself will result in a 100% correlation that reflects a value of 1 as can be seen in Figure 5.14. From the table it can be seen that 'ps' and 'ts' have a strong correlation coefficient of 0.58.

Variable	Correlations (Weld data Results for analysis.sta) Marked correlations are significant at p < .05000 N=16 (Casewise deletion of missing data)										
	ps	ts	cs	pf	tf	cf	t	fx	fy	r	fz
ps	1.00	0.58	0.95	0.32	0.52	-0.40	0.15	0.31	-0.26	0.42	-0.68
ts	0.58	1.00	0.76	0.47	0.38	-0.19	-0.15	0.37	-0.04	0.25	-0.60
cs	0.95	0.76	1.00	0.32	0.47	-0.34	0.01	0.32	-0.19	0.39	-0.64
pf	0.32	0.47	0.32	1.00	0.26	-0.05	-0.38	0.15	-0.16	0.10	-0.57
tf	0.52	0.38	0.47	0.26	1.00	-0.59	-0.10	0.92	-0.50	0.82	-0.86
cf	-0.40	-0.19	-0.34	-0.05	-0.59	1.00	0.02	-0.43	0.12	-0.34	0.51
t	0.15	-0.15	0.01	-0.38	-0.10	0.02	1.00	-0.21	0.30	-0.26	0.02
fx	0.31	0.37	0.32	0.15	0.92	-0.43	-0.21	1.00	-0.40	0.77	-0.72
fy	-0.26	-0.04	-0.19	-0.16	-0.50	0.12	0.30	-0.40	1.00	-0.74	0.36
r	0.42	0.25	0.39	0.10	0.82	-0.34	-0.26	0.77	-0.74	1.00	-0.59
fz	-0.68	-0.60	-0.64	-0.57	-0.86	0.51	0.02	-0.72	0.36	-0.59	1.00

Figure 0.14 Correlation Matrix Table illustrating significant correlations between variables

Fundamentally, it is a variation on the theme of quantitative functional relationship.[43] The more you have of this variable, the more you have of that one. Or conversely, the more you have of this variable, the less you have of that one. This can be seen when viewing the Matrix Plot in Figure 5.15 where 'ps' and 'ts' are related. As 'ps' increase so will 'ts' and from the plot 'fx' vs 'fz' it is seen that as 'fx' decreases, 'fz' increases.

Figure 0.15 Matrix Plot illustrating various quantitative functional relationships between variables

In the first case (the more of this, the more of that), you are speaking of a positive correlation between the two variables; and in the second kind (the more of this, the less of that), you are speaking of a negative correlation between the two variables.

Correlation and regression are two sides of the same coin. In the underlying logic, you can begin with either one i.e. 'ps' and end up with the other i.e. 'ts' or vice versa.

In examining the relationship between two causally related variables, the **independent variable** is the one that is capable of influencing the other, and the **dependent variable** is the one that is capable of being influenced by the other. For example, spindle speed will tend to increase the tool temperature, whereas a change in tool temperature will have no systematic effect on spindle speed. In this relationship

between spindle speed and tool temperature, spindle speed is the independent variable and tool temperature is the dependent variable. The welding parameters and process conditions are both independent variables and the sensor measurements such as tool temperature and ‘fx’ are dependent variables.

For cases where the distinction between "independent" and "dependent" does not apply, it makes no difference which variable is called X and which is called Y (ex. ‘ps’ & ‘ts’).

The basic possibilities are: (i) positive correlation; (ii) negative correlation; and (iii) zero correlation. In the case of zero correlation, the coordinate Matrix plot will look something like the rather patternless jumble like ‘ps’ and ‘t’, reflecting the fact that there is no systematic tendency for ‘ps’ and ‘t’ to be associated, either the one way or the other. This correlation plot between ‘ps’ and ‘t’ can be seen in Figure 5.15. The plot for a positive correlation, on the other hand, will reflect the tendency for high values of X_i to be associated with high values of Y_i, and *vice versa*; hence, the data points will tend to line up along an upward slanting diagonal, as ‘ps’ and ‘cs’. The plot for negative correlation will reflect the opposite tendency for high values of X_i to be associated with low values of Y_i, and *vice versa*; hence, the data points will tend to line up along a downward slanting diagonal, as ‘fy’ and ‘fz’ in Figure 5.15. The line, called the regression line, fits the best line possible between the data points thus linking the mean of X and the mean Y intersections on the graph.[44]

The slant of the line upward or downward is what determines the sign of the correlation coefficient (**r**), positive or negative; and the degree to which the data points are lined up along the line, or scattered away from it, determines the strength of the correlation ($\mathbf{r}^2$).[43]

The primary measure of linear correlation is the **Pearson product-moment correlation coefficient**, symbolized by the Roman letter **r**, which ranges in value from **r** = +1.0 for a perfect positive correlation to **r** = —1.0 for a perfect negative correlation. Note that this letter 'r' is replaced by a capital letter 'R' in the Regression Table but has the same meaning. The midpoint of its range, **r** = 0.0, corresponds to a complete absence of correlation. Values falling between **r** = 0.0 and **r** = +1.0 represent varying degrees of positive correlation, while those falling between **r** = 0.0 and **r** = —1.0 represent varying degrees of negative correlation.

A closely related companion measure of linear correlation is the **coefficient of determination**, symbolized as $\mathbf{r}^2$, which is simply the square of the correlation coefficient. The coefficient of determination can have only positive values ranging from $\mathbf{r}^2$ = +1.0 for a perfect correlation (positive or negative) down to $\mathbf{r}^2$ = 0.0 for a complete absence of correlation. The advantage of the correlation coefficient, **r**, is that it can have either a positive or a negative sign and thus provide an indication of the positive or negative direction of the correlation. The advantage of the coefficient of determination, $\mathbf{r}^2$, is that it provides an equal interval and ratio scale measure of the strength of the correlation. In effect, the correlation coefficient, **r**, gives you the true direction of the correlation (+ or —) but only the square root of the strength of the correlation; while the coefficient of determination, $\mathbf{r}^2$, gives you the true strength of the correlation but without an indication of its direction. Both of them together give you the whole works.[44]

For purposes of interpretation, you can translate the coefficient of determination into terms of percentages (i.e., percentage = $\mathbf{r}^2$x100), which will then allow you to state that, for example, the correlation in the regression table for 'ps' ($\mathbf{r}^2$ = 0.609) is 60.9%

as strong as it possibly could be, whereas the one for regression table 'ts' ($\mathbf{r}^2 = 0.869$) is 86.9% as strong as it possibly could be.

An adjusted $\mathbf{r}^2$ will be the more accurate value to use since it incorporates a factor of penalty related to the number of tests conducted to that of dependant variables used. This Adjusted $\mathbf{r}^2$ will become closer to the original **r** if more tests are conducted thus following a bigger orthogonal array or simply using less dependant variables in the experimental design.

What needs to be added is a measure of **probable error**, something that reflects the strength of the observed correlation, hence the strength of the tendency for actual values of Y_i to approximate their predicted values. Within the context of linear regression, the measure of probable error is a quantity spoken of as the **standard error of estimate**. Essentially, it is a kind of standard deviation. This error of estimate can be incorporated in the linear regression formula to adjust for error as follows[43,44]:

$$\textbf{predicted } Y_i = a + bX_i \pm SE \qquad (0\text{-}5)$$

Results obtained

Section 5.4.2 explains important terms and concepts used during the analysis that will now be used in the next sub-section for the explanation of the results.

The Correlation Matrix

Values that are highlighted in the table have a significant correlation between each other. All these values have a correlation significance of 95% or higher ($p < 0.05$). The bold values show no significance since their values are much lower than 1. From the Correlation Matrix table in Figure 5.14 it can be seen which significant, and by

what magnitude, correlations exist between dependant variables. The following examples will explain the advantage of the Correlation Matrix table illustrated in Figure 5.14:

‘ps’ and ‘ts’: 0.58 – Average strength positive correlation exists
‘ps’ and ‘cs’: 0.95 – Very strong positive correlation exists (as expected)
‘ps’ and ‘tf’: 0.52 - Lower strength positive correlation exists
‘ps’ and ‘fz’: 0.68 – Strong negative correlation exists

From the above it is seen that ‘ts’, ‘cs’, ‘tf’ and ‘fz’ are the only strong correlations that existed between themselves and ‘ps’. All the other 10 variables can be evaluated in exactly the same manner.

The Matrix Plot

The matrix plots in Figure 5.15 are all illustrated as a mirror image of the top half to the bottom half section. This mirror image explains the corresponding plots in a different direction i.e. regression line ‘ps’ to ‘ts’ and *vice versa* ‘ts’ to ‘ps’. The regression line will determine the best fit and direction of the correlation that exists as explained in Section 5.4.2. The histograms of data points inside the graphs give an indication of data input trends. The purpose of the plots can be explained better by means of the following examples that are taken from Figure 5.15:

‘ps’ and ‘ts’: have a positive correlation, as ‘ps’ increases so will ‘ts’
‘ps’ and ‘cs’: a strong correlation exists because the data points form a good regression line that also indicates a positive correlation
‘ps’ and ‘tf’: not a very strong correlation since regression line deviates quite a bit from the regression line
‘ps’ and ‘fz’: strong negative correlation exists, regression line illustrating as ‘ps’ decreases ‘fz’ will increase

All the other plots can be analyzed in exactly the same manner as demonstrated above.

The Regression Summary table

All the regression tables are listed in Appendix C but an example is given in Figure 5.16 and Figure 5.17.

Regression Summary for Dependent Variable: ps (Weld data Results for analysis.sta)
R= .78064883 R²= .60941259 Adjusted R²= .26764861
F(7,8)=1.7831 p<.21752 Std.Error of estimate: 909.68

N=16	Beta	Std.Err. of Beta	B	Std.Err. of B	t(8)	p-level
Intercept			-675.597	2263.135	-0.29852	0.772911
rpm	0.413695	0.234969	5.016	2.849	1.76064	0.116333
feed	0.333957	0.232332	15.727	10.941	1.43741	0.188539
plunge	0.134740	0.313676	1178.528	2743.625	0.42955	0.678857
oxide	-0.085124	0.223182	-175.224	459.412	-0.38141	0.712829
type	0.047781	0.286687	98.355	590.134	0.16666	0.871769
thick	0.666961	0.242850	1372.913	499.897	2.74639	0.025199
time	-0.255301	0.228895	-525.528	471.172	-1.11536	0.297076

Figure 0.16 Regression Table relating dependant variable 'ps'to independent variables

In the regression summary tables (Appendix C) the dependent variables 'ps', 'ts', 'cs' etc. are correlated with each independent variable such as rpm, feed, plunge etc. In Section 5.4.2 the theory around r, r^2, adjusted r^2 and standard error of estimate are explained. With the aid of the following examples the purpose of these functions will be made clearer.

In the regression summary table illustrated in Figure 5.16 it can be concluded that the factorial table is only accurate or reliable within 26.7% if the corresponding factors are to be used. All the individual factors relating the independent variables with the dependent variable 'ps' have various efficiency factors for accuracy in data available i.e. 'p-values.' A low p-level will be a significant correlation and is highlighted in the table. For 'ps' in Figure 5.16, thickness (of the plate) is the significant correlation. The error of estimate in this linear equation will be in the range of 909.68Watts.

It is important to remember that since we have a very low adjusted r^2 value it could mean that other factors also determine the change in 'ps' and thus p-values with an average (relative lower) p-level must not be neglected at this stage.

Another example can be taken from the regression table for 'ts' as illustrated in Figure 5.17, where a better-adjusted r^2 is obtained showing more reliability in the equation factors. Four p-levels are highlighted showing that all of them had a dominant correlation between themselves and 'ts.' The error of estimate in the total equation will be in the range of 3.84Amps.

Regression Summary for Dependent Variable: ts (Weld data Results for analysis.sta)
R= .93237423 R²= .86932170 Adjusted R²= .75497818
F(7,8)=7.6027 p<.00520 Std.Error of estimate: 3.8479

N=16	Beta	Std.Err. of Beta	B	Std.Err. of B	t(8)	p-level
Intercept			33.11654	9.57293	3.45939	0.008575
rpm	-0.455522	0.135910	-0.04039	0.01205	-3.35164	0.010056
feed	0.475613	0.134386	0.16380	0.04628	3.53917	0.007629
plunge	-0.016836	0.181436	-1.07690	11.60538	-0.09279	0.928350
oxide	0.020301	0.129093	0.30560	1.94329	0.15726	0.878938
type	-0.032017	0.165825	-0.48196	2.49623	-0.19307	0.851712
thick	0.559358	0.140469	8.42024	2.11453	3.98208	0.004050
time	-0.088104	0.132397	-1.32626	1.99303	-0.66545	0.524481

Figure 0.17 Regression Table relating dependant variable 'ts' to independent variables

Formulas for Intelligent Control

In order to control the system intelligently in the future, a control algorithm with a set of rules need to be implemented.[40] A foundation for these rules can now already be established making use of the results obtained from the preliminary studies done. The regression analysis made it possible for the researcher to obtain a set of formulas that link the dependent variables with the independent variables. It must be emphasized that most of the regression tables have relative low adjusted r^2 values meaning that other variables, not taken into account in this design, must still be introduced. To improve the design reliability, a higher-level orthogonal array or factorial design must

be followed. At this stage the formulas are adequate to give a good indication of the correlation that exists between variables, what significant effect they have on the total formula as well as by how much they compare with each other.

The final results of the regression formulas that link the variables with each other are displayed in Table 5.1.

Since the p-levels give a good indication whether the variables have a strong correlation it is a good estimate of what to leave out in the next design or in the predicted formula for that regression summary. Also to note that if all the variables, with low and high p-levels, are to be implemented in the regression formula it will only be an advantage to consider in the next design. For future development of these formulas, only p-levels are implemented that seem to have average correlation strengths since it might still show a better significance in future analysis.

Regression Formulas	Units
ps = -675.597+(5.016.rpm)+(15.727.feed)+(1372.913.thick)-(525.528.time)	W
ts = 33.11654-(0.04039.rpm)+(0.1638.feed)+(8.42024.thick)-(1.32626.time)	N.m
cs = 4.03186+(0.03666.feed)+(3.10006.thick)-(1.03066.time)	A
pf = 30.44096-(0.01084.rpm)+(5.34155.feed)+(1.79081.oxide)-(4.48396.thick)+(5.08189.time)	W
tf = -1.1805+(0.00218.rpm)+(0.00994.feed)+(1.03749.type)+(0.74877.thick)-(0.5997.time)	N.m
cf = 2.662-(0.000224.rpm)-(0.1552.plunge)-(0.0456.type)-(0.0412.thick)+(0.0861.time)	A
t = 406.775+(0.1371.rpm)-(0.6647.feed)+(107.455.plunge)+(27.8745.thick)	°C
fx = -341.862+(3.479.feed)-(121.73.oxide)+(658.081.type)+(404.503.thick)-(273.969.time)	N
fy = 589.722-(0.212.rpm)-(211.222.plunge)-(118.357.type)-(30.837.thick)-(23.352.time)	N

r = -16.806+(0.0137.rpm)+(9.3477.type)+(4.3665.thick)-(2.856.time)	
fz = 7.34152-(0.01218.rpm)-(0.12607.feed)-(4.57352.type)-(5.26259.thick)+(2.31748.time)	**kN**

Table 0.1 Formulas obtained for Regression Summary of Dependent Variables

Surface Plots

Variables that influence the process quality such as tool temperature and vertical Z-Force can now be displayed on 3D Surface Plots where further deductions in process trends can be made. All the surface plots are illustrated in Appendix C but only the significant plots will now briefly be discussed in the following sub-sections:

The Tool Temperature Plot (t)

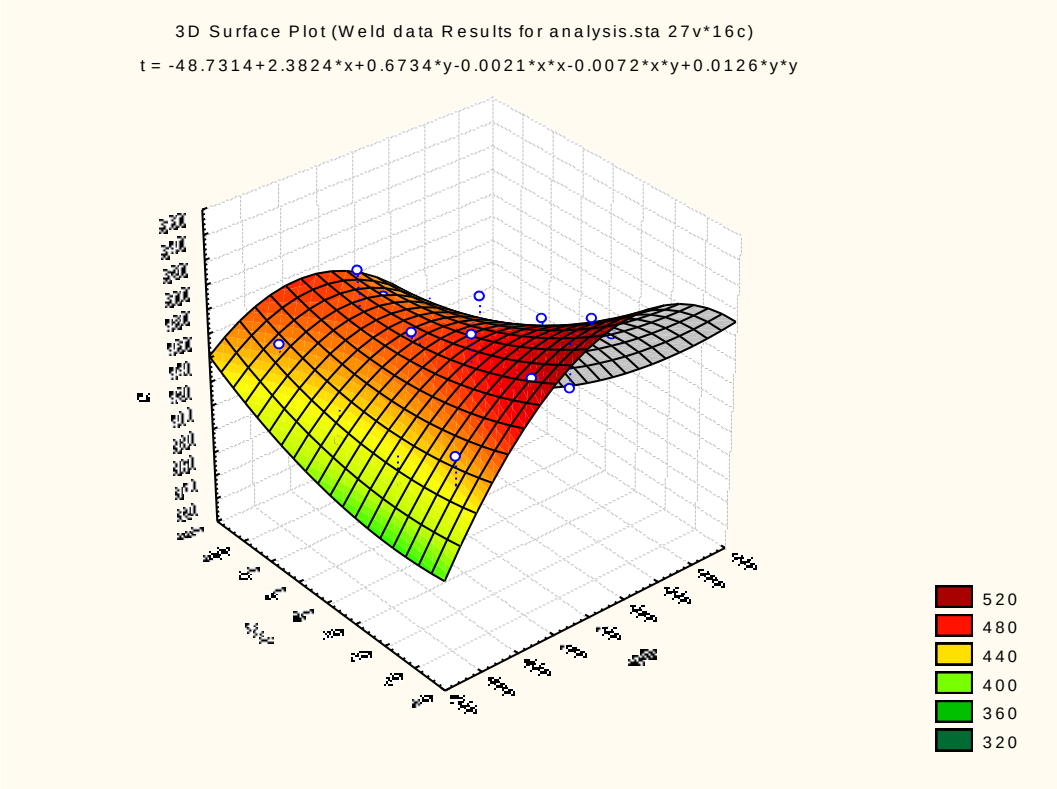

Figure 0.18 3D Surface Plot for Tool Temperature 't'

The curves given on the plot illustrates two possible optimum design points for welding at lower temperatures. Either increasing rpm and feed-rate or by decreasing

the feed rate as well as the rpm, these points may be reached. Medium range settings for rpm and feed tend to results in higher temperature values.

The X-Force Plot (fx)

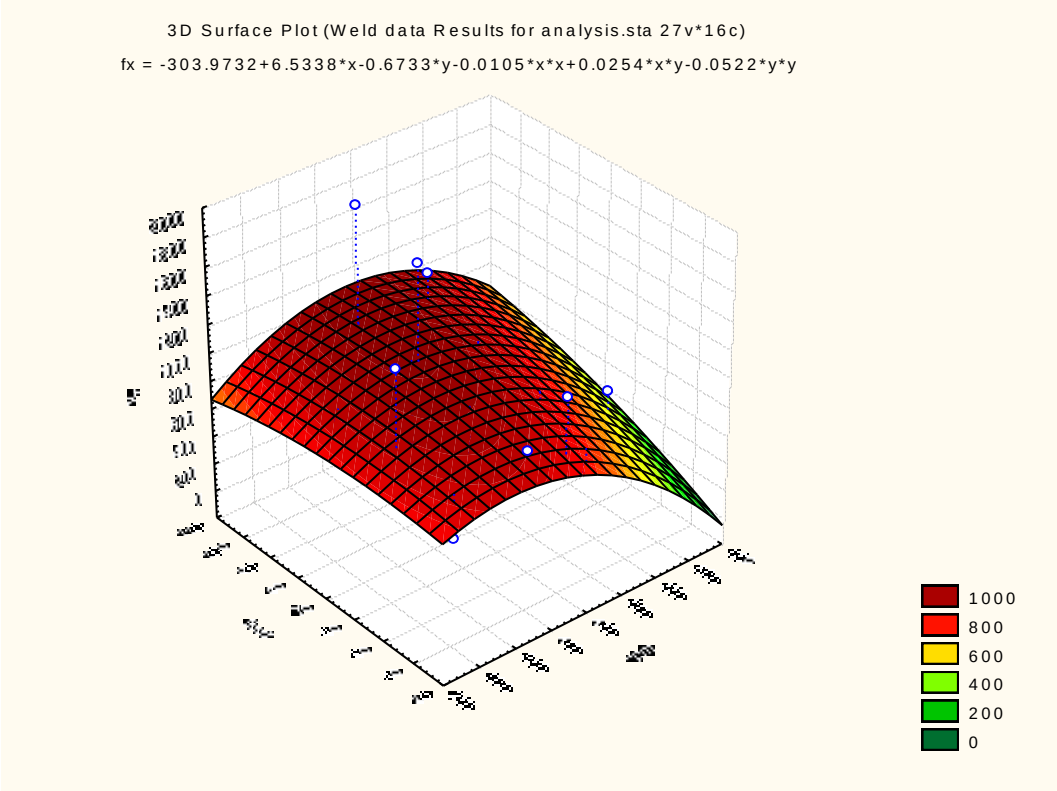

Figure 0.19 3D Surface Plot for X-Force 'fx'

It seems that by increasing the rpm and decreasing the feed-rate results in a lower 'fx' value. When evaluating the temperature curve to this high rpm range it can be seen that an increase in temperature results in a lower 'fx.' This can then also prove that the degree of plasticized flow is influenced by the temperature gradient.

The Z-Force Plot (fz)

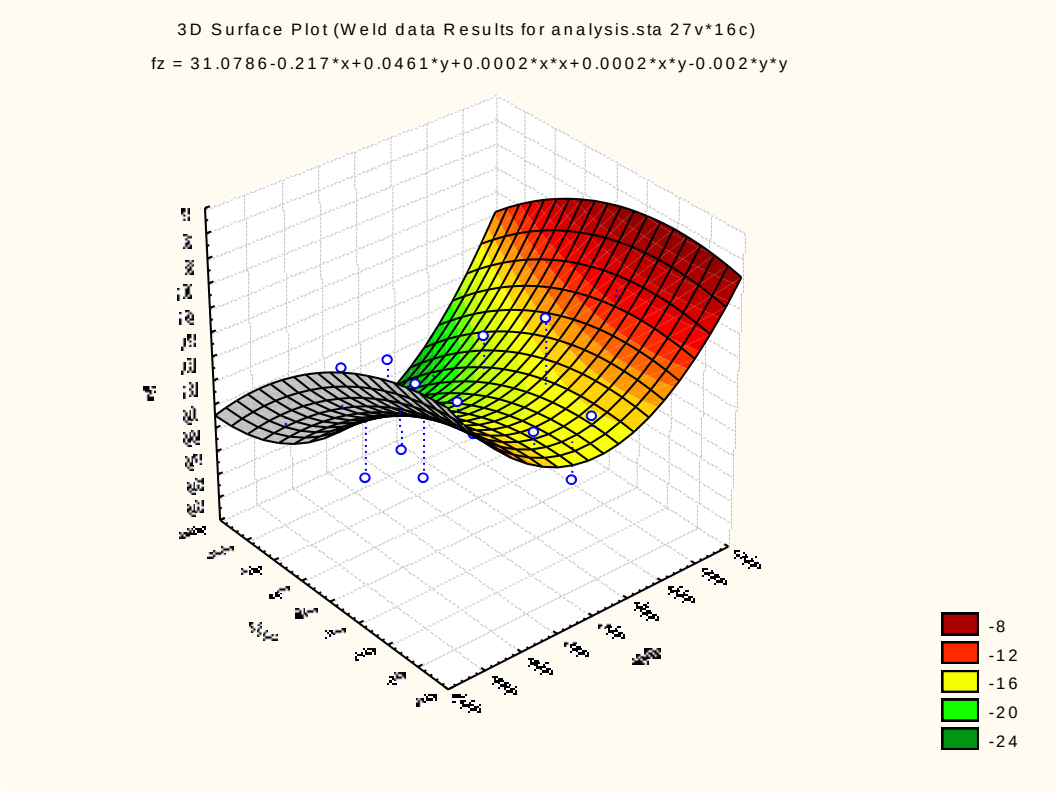

Figure 0.20 3D Surface Plot for Z-Force 'fz'

If to be welded at a lower Z-force it will be advised to increase the rpm and decrease the feed-rate slightly. The surface plot illustrates a lesser effect of feed-rate on 'fz' than that of rpm. The conclusion can be made that the welding speed can be increased, resulting in only a slight change in 'fz.'

The Y-Force Plot (fy)

Again in the corresponding force plot the researcher can conclude that welding at a higher rpm and lower feed-rates will result in lesser force, in this case 'fy.'

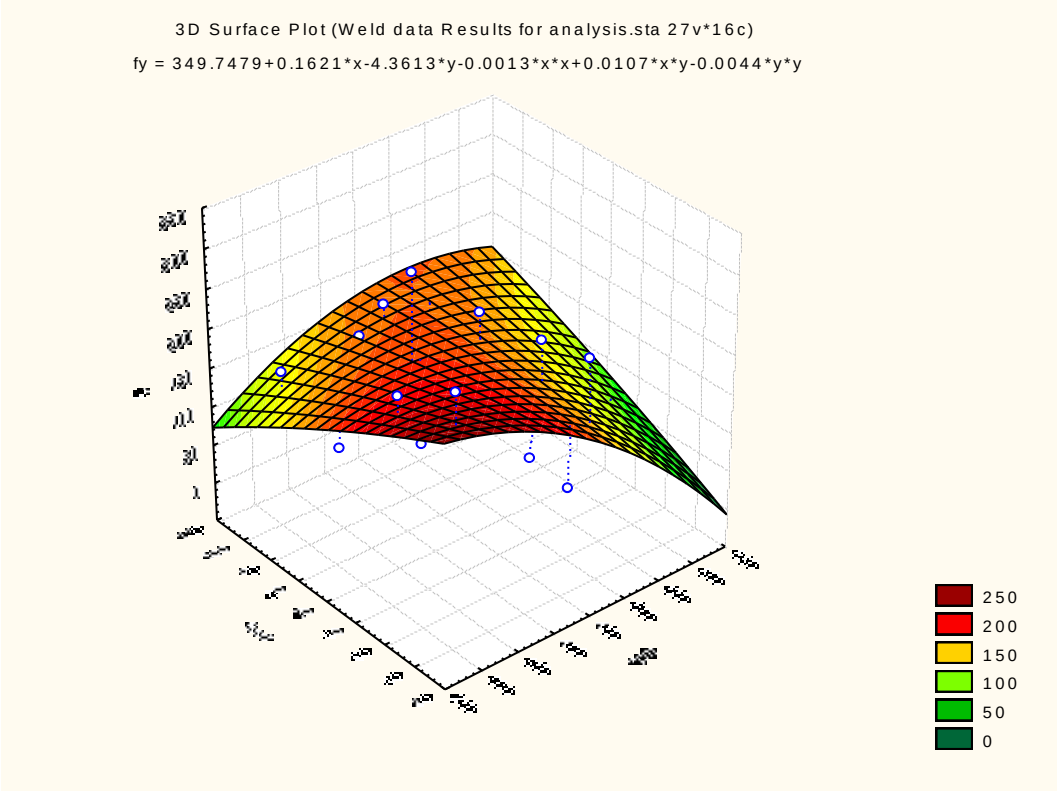

Figure 0.21 3D Surface Plot for Y-Force 'fy'

The Spindle Torque Plot (ts)

The dominant variable that will influence 'ts' on this plot is feed. It seems that by lowering the feed-rate a lower torque is being applied on the spindle. The increase in rpm has a small significance but a noticeable change in the gradient of 'ts' can be seen.

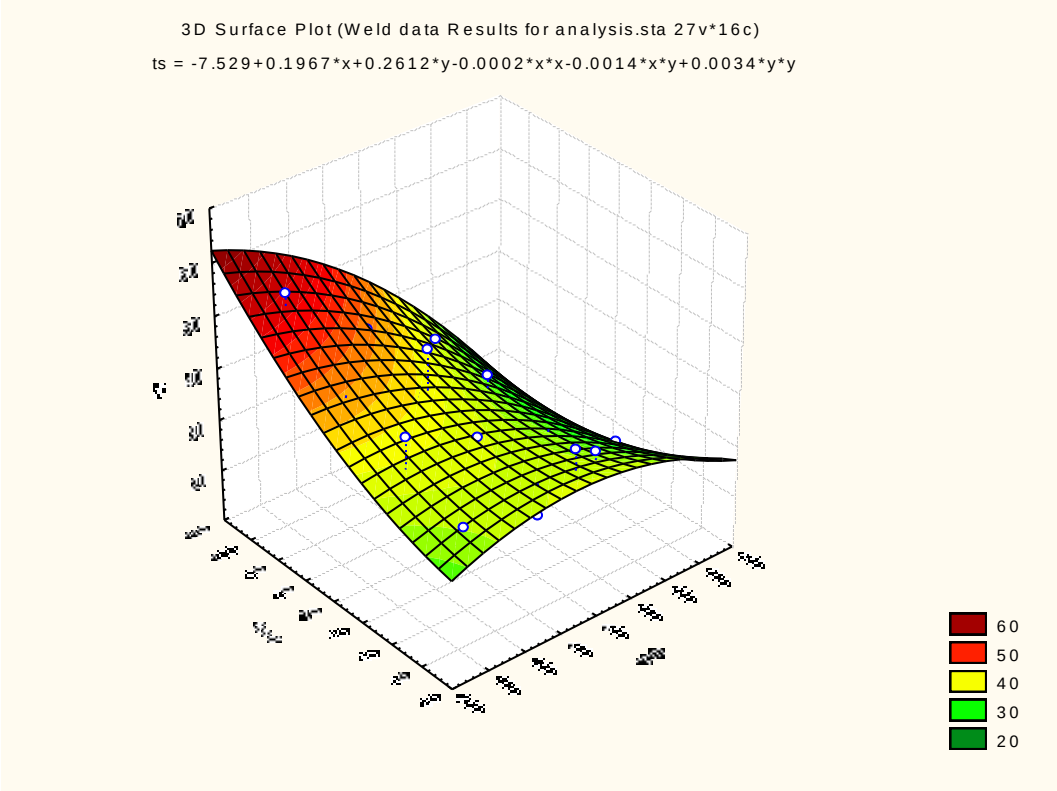

Figure 0.22 3D Surface Plot for Spindle Torque 'ts'

Optimal Operating Range of the PET FSW machine

From the surface plots discussed in Section 5.4 it can be seen that all the forces during the process are very much influenced by the spindle speed and feed rate. In all the plots it was concluded that an increase in rpm and a decrease in feed-rate, result in lower applied forces during the process weld. The Z-Force (fz) is the pre-dominant force under consideration since it is of the highest magnitude and thus determines the capacity and weld capabilities of the machine. When welding at higher rpm and lower feed-rates these forces can be lowered which would be an advantage during machine selection. Machine capacity can be lowered and thus save money. On the other hand there are disadvantages in welding at lower feed-rates and increased rpm's. Firstly, it results in increasing the production costs of each weld run since welding is done at slower feed-rates. Secondly, if welding is done at higher rpm's it can be seen on the surface plots that the temperature increases dramatically. The increase in

temperature plays an important role during the quality achieved by the welded joints as discussed in Section 6.2.2 and will be a disadvantage if excess heat is applied.

It must now be concluded that welds must either be made with relative lower temperatures for improved weld quality or welds at faster feed-rates but resulting in higher forces. In Section 6.2.2 it was seen that welding at tool temperatures in excess of 500^0C resulted in surface defects. This statement is purely based on the specific weld parameters that correspond with it. It is then safe to approximate an optimal operating temperature in the range of 420^0C for this particular alloy. The researcher can then also by evaluating the machine structure and motor power capability estimate a safe load of 2tons for the Z-force. These variables can now be implemented in the formulas specified in Table 5.1 to obtain a simultaneous equation that will solve the approximate optimal operating range for the machine as follows:

Set Parameters Considered

t = 420^0C
fz = 20kN
Plate thickness = 6mm
Plunge = 0.2mm
Dwell time (16s) = 1
Profile Tool Used (FSW3) = 1
Oxide Layer Present = 1

t = 406.775+(0.1371.rpm)-(0.6647.feed)+(107.455.plunge)+(27.8745.thick) ± Error

420 = 406.775+(0.1371 x rpm)-(0.6647 x feed)+(107.455 x 0.2)+(27.8745 x 6)

$$-175.513 = (0.1371 \times rpm) - (0.6647 \times feed) \quad \textbf{(0-6)}$$

fz = 7.34152-(0.01218.rpm)-(0.12607.feed)-(4.57352.type)-(5.26259.thick)+ (2.31748.time) ± Error

20 = 7.34152-(0.01218 x rpm)-(0.12607 x feed)-(4.57352x1)-(5.26259x6)+(2.31748x1)

$$46.49006 = -(0.01218 \times rpm) - (0.12607 \times feed) \quad \textbf{(0-7)}$$

When solving Equation 5.6 and 5.7 simultaneously it is found that:

Feed-rate = (-) <u>166.9 mm/min</u>

Rpm = (-) <u>471 rpm</u>

From the above the machine optimum design point for the corresponding process parameters is established.

Verification of Optimal Design Point

From the Regression Formulas an optimum design point for the machine was established. From the previous section the optimum design point was to weld at a temperature of 420^0C with a vertical Z-Force not exceeding 20kN. The researcher made a weld using these values provided (spindle speed of 471rpm and a feed rate of 167mm/min). The weld was made of a slightly longer weld length than that performed in the original array for the design of experiments. The weld was 300mm long but the results obtained were of an exceptional standard. The good surface finish of the weld can be seen in Figure 5.23 and it can be noted that no surface defects are visible. The tool temperature at the 80mm marker was 478.9^0C and the Z-Force was –19.4kN. The error of estimate given in the regression tables are for t: 27.752^0C and for Fz: 3.1524kN. This means that it is in the acceptable limit and is very close to the predicted weld of 420^0C and Fz of 20kN. This then provides a good confidence level for making use of the regression formulas in weld lengths of up to 100mm. After the 100mm marker is reached, temperatures and forces need to be controlled with

artificial intelligence via the computer, in order to remain in the desired operating conditions.

Figure 0.23 Figure illustrating the good surface finish with no surface defects. Weld was made to evaluate the regression formula reliability.

The actual force plots and temperature profile for this weld evaluation can be seen in Figure 5.24.

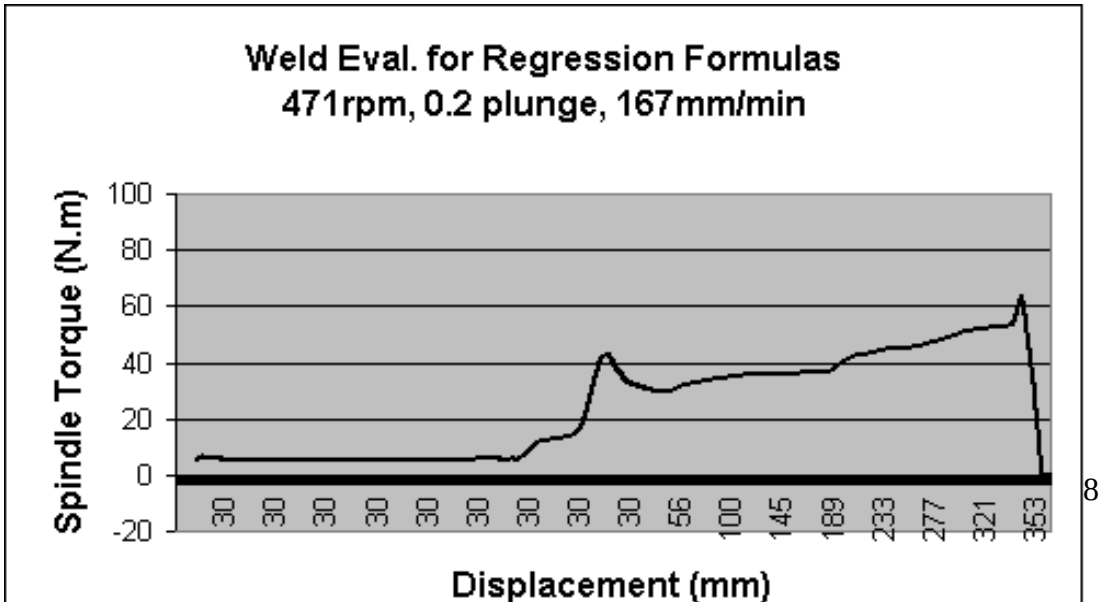

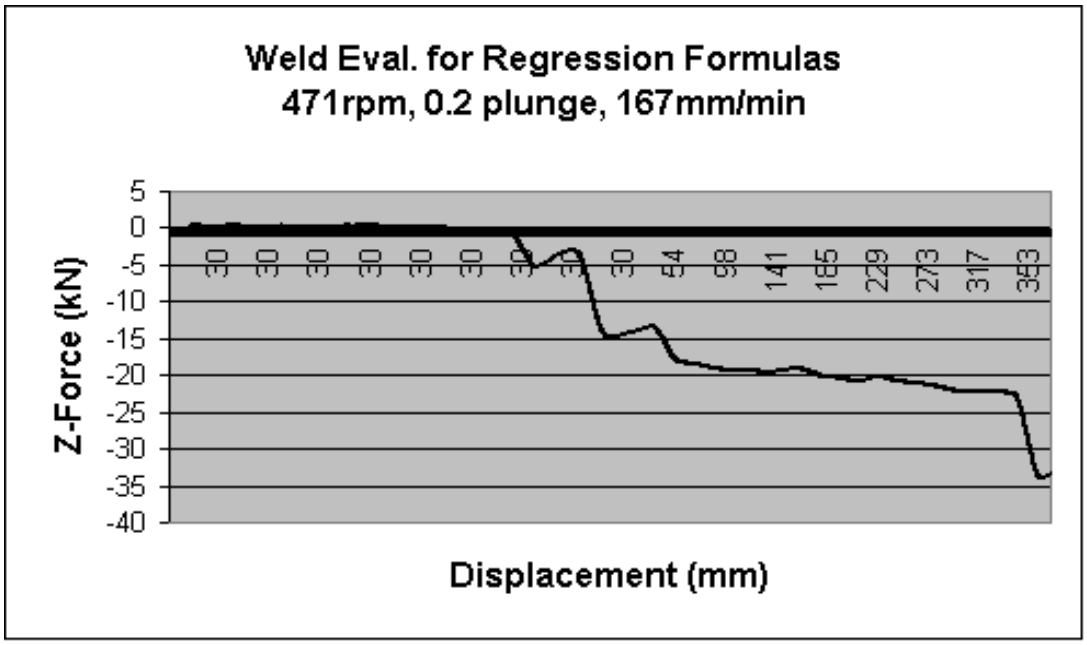

Figure 0.24 Figures illustrating the Spindle Torque and Z-Force distribution during a weld evaluation

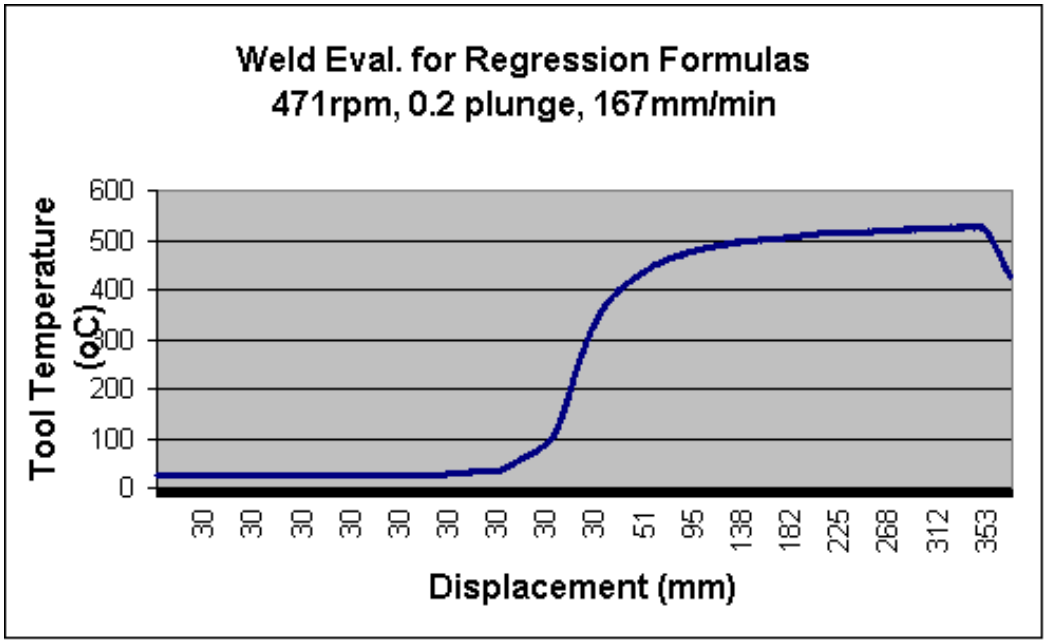

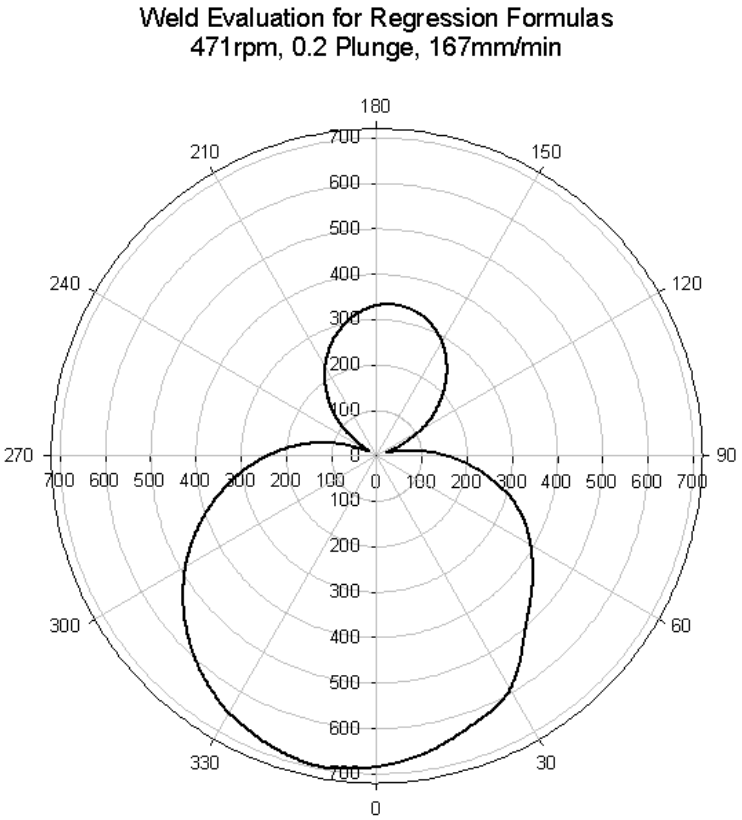

Figure 0.25 Figures illustrating the Tool Temperature and 2D Force Plot obtained during the evaluation of a weld for the Regression Formulas

Conclusion

With the measuring system up and running many process variables can now be reliably monitored. Improved experimental designs can now be implemented to create a better understanding about the process characteristic behavior. Welds can be made and process variables can be linked to the quality of the welded joints. Since the main objective for the FSW researcher was to obtain good quality welds, the importance of having a reliable measuring system was critical. With this new measurement system new doors are opened for future researchers since opportunities in further quality analysis and intelligent control of the process are now made possible. Parameters can now be monitored and make the visualization of various process interactions possible. With the linkage provided between process interactions improvement can be made to process control. Many graphs, from the raw data captured, can now be analyzed to provide a link between process parameter settings and weld quality. These graphs can include spindle power, spindle torque, spindle current, feed power, feed torque, feed current, tool temperature, tool Z-force, 2D X/Y polar force around tool, spindle torque, spindle rpm and many more. It can thus be said that without the measuring system, good quality and improvement into FSW research will be impossible. This chapter also provided a framework for future development in statistical and multiple regression analysis. The optimum design point for the machine was established for welding 6mm and 8mm aluminum plate. Further evaluation and characterization of welds made by PET will be addressed in Chapter 6.

Friction Stir Weld Evaluation

In this Chapter a preliminary evaluation of the weld strengths and structure will be done to determine the usefulness of the FSW samples produced by PET.

The parent plates that are being used are 6mm thick Aluminum 5083 H321 alloy plate. This specific alloy has its own chemical composition and behavior under mechanical conditions and therefore evaluation of the material prior to the test welds is necessary.

5000 series: Magnesium is one of the most effective alloying elements for aluminum. When it is used as the major alloying element or with manganese, the result is a moderate to high strength non-heat-treatable alloy. Magnesium is considerably more effective than manganese as a hardener, about 0.8% magnesium being equal to 1.25% manganese, and it can be added in considerably higher quantities. Alloys in this series have good welding characteristics and resistance to corrosion in marine atmospheres. However, certain limitations should be placed on the amount of cold work and the safe operating temperatures permissible for the higher magnesium content alloys (over about 3.5% for operating temperatures over about 66^{o}C.) to avoid susceptibility to stress corrosion.[27]

Mechanical Properties of Al5083-H321

The 'H3' temper applies to products which are strain hardened and then stabilized by a low temperature heating to slightly lower their strength and increase ductility. This designation applies only to the magnesium-containing alloys, which unless stabilized, gradually age-soften at room temperature. The number following this designation indicates the degree of strain-hardening remaining after the product has been strain-hardened a specific amount and stabilized.

Parent Plate

The Tensile test specimens from the parent plate were taken in both the transverse and parallel plane to that of the rolling direction. Dimensions for these specimens are specified by the ASTM standards reference [32]. Figures 6.1 and 6.2 illustrate some of the tensile test data obtained during the analysis of the parent plate. Appendix D provides more graphs.

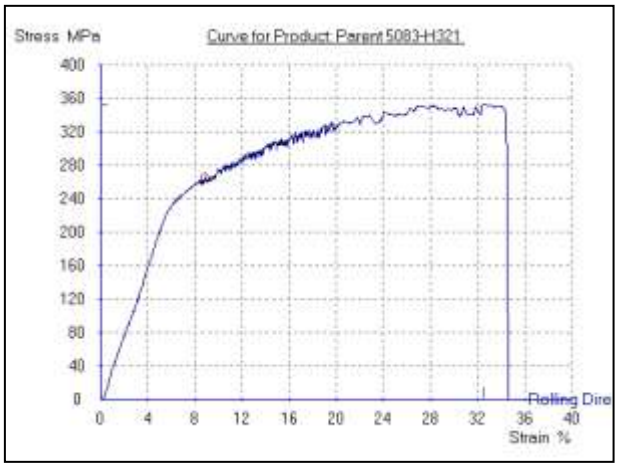

Figure 0.1 Stress-strain curve for parent plate tensile test taken parallel to rolling direction

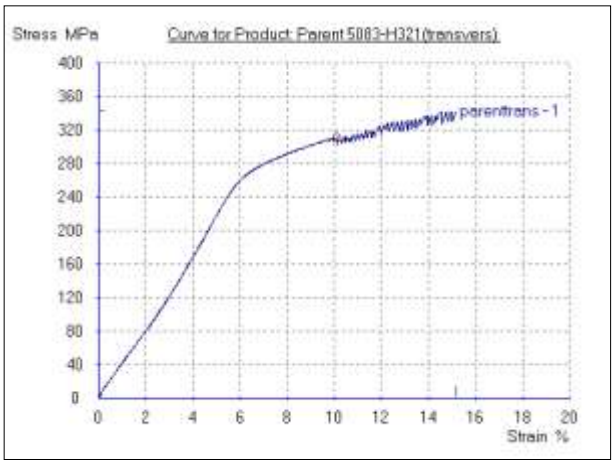

Figure 0.2 Stress-strain curve for parent plate tensile test taken in the transverse direction

The average of the three parent plate tensile tests conducted, parallel and transverse to the rolling direction is reflected in Table 6.1:

Measured Values		
0.2% Proof Stress, Mpa	Tensile strength, Mpa	Thickness, mm

Parallel to Rolling Direction	267	348	6
As per Specification	250	340	6
Transverse to Rolling Direction	305	350	6
As per Specification	250	340	6

Table 0.1 Tensile properties for the parent material parallel and transverse to the rolling direction

As-welded Tensile

Tensile properties of the weld will obviously change dramatically depending on the tool geometry as well as the corresponding process parameters used. In this report the scope is to compare a typical FSW weld made by PET to that of another institution and then to comment on the results obtained. The weld to be investigated was done with the FSW3 tool using the following parameters:

- Spindle rpm: 400rpm Feed rate: 100mm/min Plunge depth: 0.2mm

Figure 6.3-6.5 illustrates the corresponding stress-strain graphs obtained when tensile samples were taken at various intervals on a 200mm weld run.

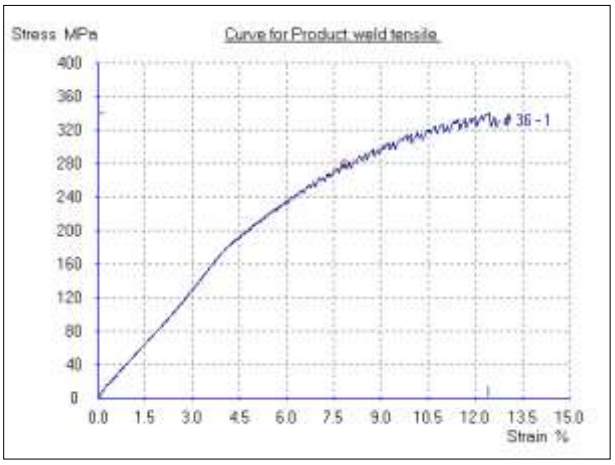

Figure 0.3 Tensile Test data – 20mm from plunge (start) position (UTS 340Mpa)

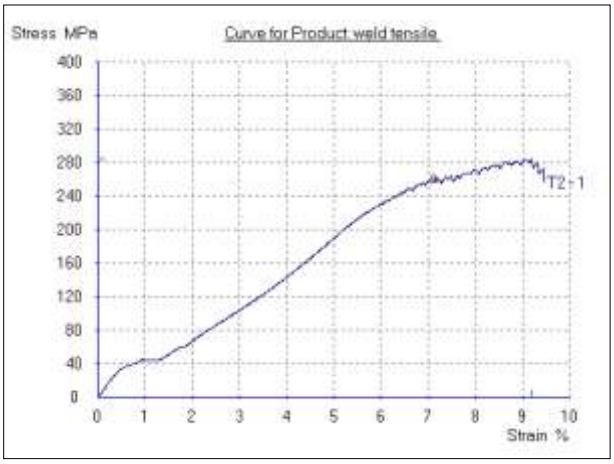

Figure 0.4 Tensile Test data – 80mm from plunge (start) position (UTS 290 Mpa)

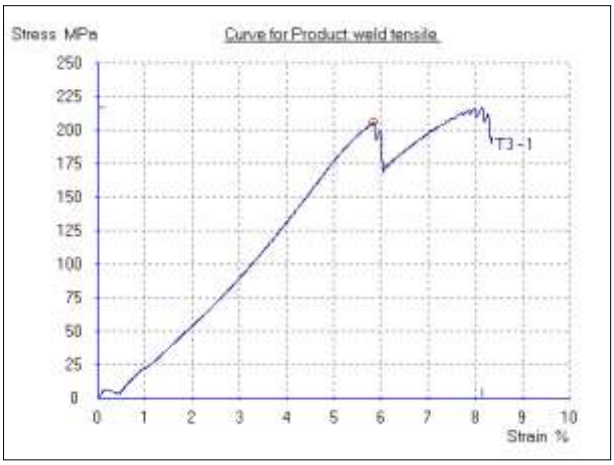

Figure 0.5 Tensile Test data – 140mm from plunge (start) position (UTS 216 Mpa)

From the results it can be seen that the UTS decreases as the weld length increases. As the weld length increases it is clearly noted that the temperature of the tool increases and that the surface appearance of the welded flow path changes after a certain temperature range is met. The tool temperature profile can be viewed in Figure 6.7. Near the end of the weld trial, where the tool temperature is the highest, the surface tends to create a defect like feature at the retreating side of the tool shoulder as if the shoulder almost burns the surface. This defect is illustrated in Figure 6.6. Point A will be the start of the weld and point C the end. These points are

more or less where the actual tensile samples were taken. The corresponding temperature graph (Figure 6.2) shows that the temperature of the tool at intervals 20, 80 and 140mm are 446, 487 and 510^{0}C respectively.

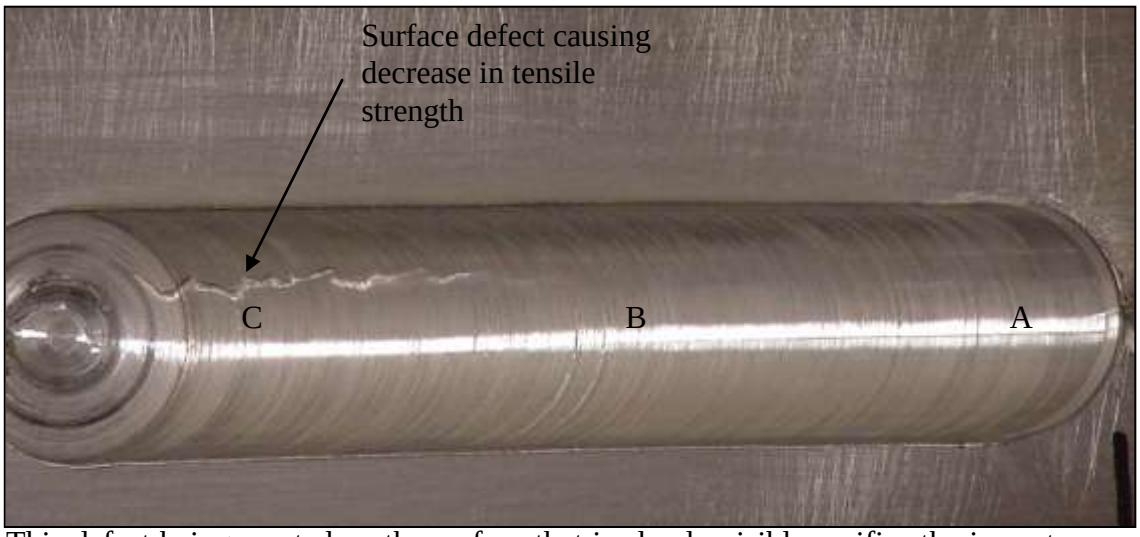

This defect being created on the surface that is clearly visible verifies the importance and need for intelligent control of process variables. Other related graphs and data pertaining this weld i.e. Z-Force, Spindle Torque and the Polar Force Plot can be viewed in Appendix D.

<u>The UTS of the welds made are</u>

At 20mm Marker (A): 340Mpa
At 80mm Marker (B): 290Mpa
At 140mm Marker (C): 216Mpa

From Tensile tests conducted at the University of Plymouth[42], using the same alloy 5083 H321 a typical UTS of 300 to 350Mpa is obtained. Other institutions that produced similar results are ESAB AB in Sweden.[47]

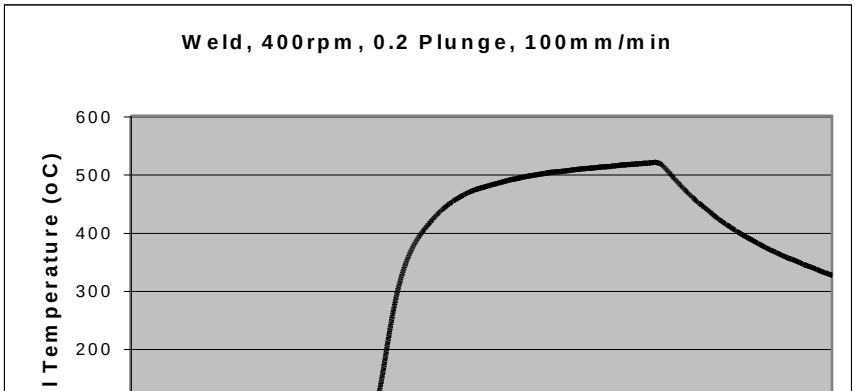

Figure 0.7 Tool temperature profile during a 200mm weld run

From the similar test results shown it can now be verified that the PET Friction Stir Welder is more than capable of producing good quality test samples.

Microstructure Classification of weld

The first attempt at classifying microstructures was made by P L Threadgill (Bulletin, March 1997).[16] His work was based solely on information available from aluminum alloys. However, it has become evident from work on other materials that the behavior of aluminum alloys is not typical of most metallic materials, and therefore the scheme cannot be broadened to encompass all materials. It is therefore proposed that the following revised scheme is used. This has been developed at TWI, but has been discussed with a number of appropriate people in industry and academia, and has also been provisionally accepted by the Friction Stir Welding Licensees Association.[16] The system divides the weld zone into distinct regions as follows:

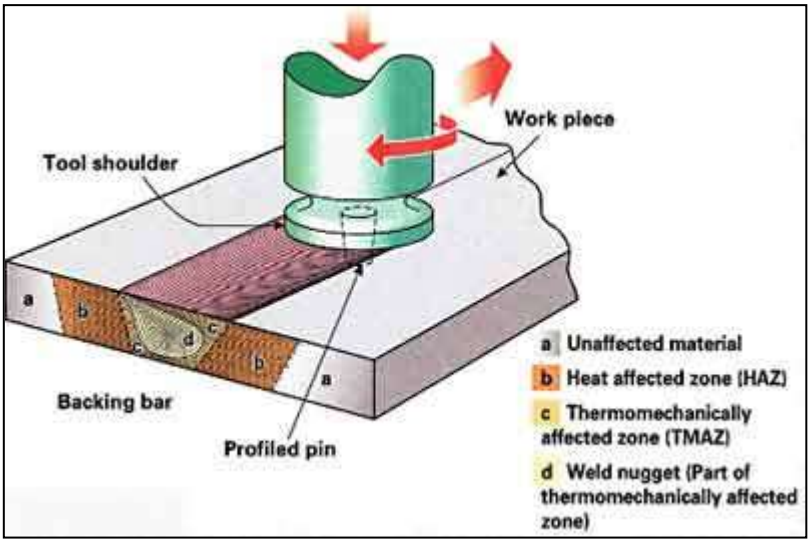

Figure 0.8 Friction stir welding principle and microstructure[16]

Unaffected material or parent metal: This is material remote from the weld, which has not been deformed, and which although it may have experienced a thermal cycle from the weld is not affected by the heat in terms of microstructure or mechanical properties.

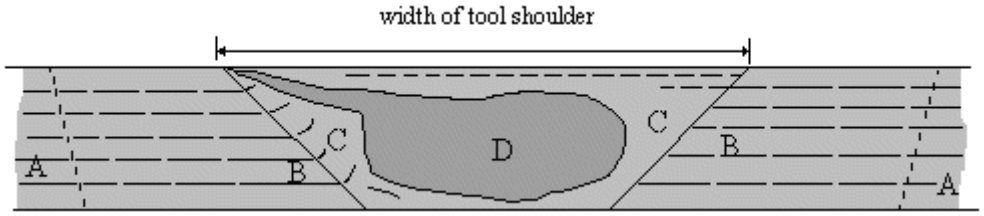

A. Unaffected material
B. Heat affected zone (HAZ)
C. Thermo-mechanically affected zone (TMAZ)
D. Weld nugget (Part of thermo-mechanically affected zone)

Figure 0.9 Classification of weld zone[16]

Heat affected zone (HAZ): In this region, which clearly will lie closer to the weld centre, the material has experienced a thermal cycle, which has modified the microstructure and/or the mechanical properties. However, there is no plastic deformation occurring in this area. In the previous system, this was referred to as the "thermally affected zone". The term heat affected zone is now preferred, as this is a direct parallel with the heat affected zone in other thermal processes, and there is little justification for a separate name.

Thermo-mechanically affected zone (TMAZ): In this region, the material has been plastically deformed by the friction stir welding tool, and the heat from the process will also have exerted some influence on the material. In the case of aluminium, it is possible to get significant plastic strain without recrystallisation in this region, and

there is generally a distinct boundary between the recrystallised zone and the deformed zones of the TMAZ. In the earlier classification, these two sub-zones were treated as distinct microstructural regions. However, subsequent work on other materials has shown that aluminium behaves in a different manner to most other materials, in that it can be extensively deformed at high temperature without recrystallisation. In other materials, the distinct recrystallised region (the nugget) is absent, and the whole of the TMAZ appears to be recrystallised. This is certainly true of materials, which have no thermally induced phase transformation, which will in itself induce recrystallisation without strain, for example pure titanium, b titanium alloys, austenitic stainless steels and copper. In materials such as ferritic steels and a-b titanium alloys (e.g.Ti-6Al-4V), the understanding of the microstructure is made more difficult by the thermally induced phase transformation, and this can also make the HAZ/TMAZ boundary difficult to identify precisely.[16]

Weld Nugget: The recrystallised area in the TMAZ in aluminium alloys has traditionally been called the nugget. Although this term is descriptive, it is not very scientific. However, its use has become widespread, and as there is no word, which is equally simple with greater scientific merit, this term has been adopted. A schematic diagram is shown in Figure 6.4, which clearly identifies the various regions. It has been suggested that the area immediately below the tool shoulder (which is clearly part of the TMAZ) should be given a separate category, as the grain structure is often different here. The microstructure here is determined by rubbing by the rear face of the shoulder, and the material may have cooled below its maximum. It is suggested that this area is treated as a separate sub-zone of the TMAZ. Figure 6.10 illustrates the typical weld nugget obtained when using the FSW3 tool geometry and weld parameters set to 400rpm, 100mm/min and plunge depth of 0.2mm. References [48]

and [49] indicates similar macrographs illustrating the same nugget and TMAZ formation.

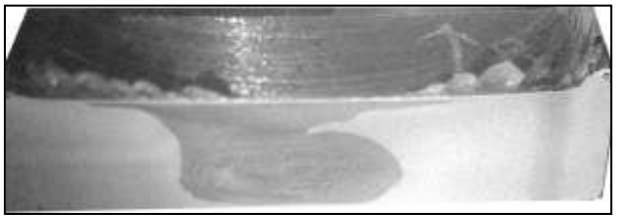

Figure 0.10 Macrograph of a SP friction stir weld transverse cross-section illustrating the distinct weld zone. Welding direction is inward and the right hand side is the retreating side.

Bend tests

Bend tests always give a good indication of the strength capability of the welded joint. Sections of the weld are cut out in the transverse plane (perpendicular to the weld) in order to make an 180^0 bend test. The total length of the sample is 240mm and about 25mm in width. The bend is made around a 40mm diameter roller.

A clear split of the root or crack on the face will determine whether the samples pass or fail.[46] All three face and root samples tested, passed and no flaws or lack of penetration (fusion) were visible. The successful bend tests performed are illustrated in Figure 6.11. It must be noted that the tool pin length will play an important role in obtaining a good weld penetration throughout the entire plate thickness as well as the plunge depth of the tool shoulder. The required plunge depth of the tool shoulder is important to consider when designing for a certain pin since the plunge depth governs the pin length.

Figure 0.11 Successfu a weld made at

Microhardness Evaluation

Figure 6.12 illustrates a micro hardness profile of the welded transverse cross-section of the weld. The results were as expected, similar to that specified by other institutions.[42,47] Since aluminum alloy 5083-H321 is a strain hardened alloy (Section 6.1) the welded joint, TMAZ and weld nugget region (Section 6.2), are 'work soften' during the weld and lower the mechanical strength of the alloy. This then also being the main reason for the tensile specimens to all fail within the TMAZ for an H temper (strain hardened) and in the parent material for the O (annealed) condition.[46] The parent plate hardness under a 200g load drop is 105 and in the weld nugget region this hardness value can drop to the lower 70's as can be seen in Figure 6.12. The typical hardness in the weld region for 5083 aluminum alloys is known to be ±75HV.[47]

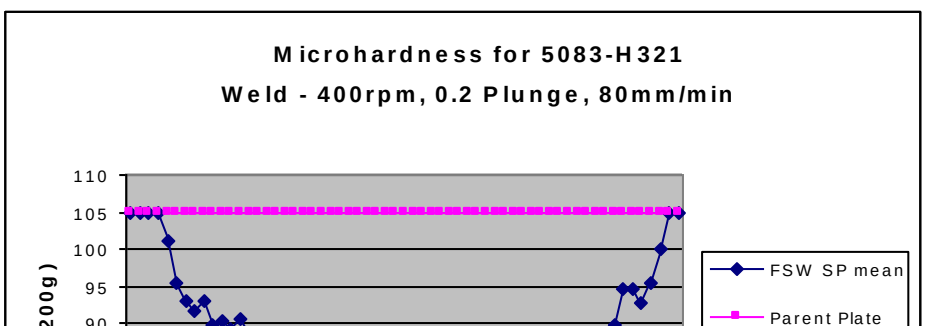

Figure 0.12 Microhardness data for a single pass (SP) weld in 5083-H321 aluminum plate

Future work must thus accentuate welding at lower temperatures in order to increase the related hardness number in the TMAZ.

Conclusion

In this chapter fundamental background is provided on the characterization of aluminum alloys. The 5000 series aluminum alloys were the ones particular of interest. The FSW process is a stirring and forging process where the rotating tool work softens the material in order to reach plasticized conditions. After the welds are made the mechanical strength is thus lowered by a certain degree. The ideal would be to optimize the process so that a welding strength as close as possible to that of the parent material can be obtained. From the microstructural verifications made, the welded zone is known to be grain refined and not related to grain growth as some other welding techniques introduced. This grain refinement of the weld nugget will be an advantage for improvement in fatigue life. Future evaluations will look into the fatigue life of the welds since this is the main advantage of the FSW process. From the tensile graphs obtained it can be seen that the actual tensile strength lowers as the weld length increases. This will be the case when the temperature of the tool gets too hot and start to cause surface defects. In the future the process variables such as tool

temperature must be intelligently controlled in order to maintain a constant weld quality. From the microhardness tests conducted the softer region of the weld is in the TMAZ. The researcher must thus try to weld with the lowest temperature possible so that the hardness of the TMAZ may be improved. Future research is required to establish this optimal welding temperature range.

Conclusion and Future Developments

It can now be concluded that the PET Friction Stir Welder is complete. The process was started from scratch where a conventional milling machine was transformed into a FSW machine by means of numerous control modifications. The modifications made were in combination with mechanical and electrical engineering aspects, covering various fields of knowledge such as mechatronics, mechanics, mathematics, electronics and many more. The main reasons for the major machine modifications made were to improve the controllability of the welding process. This was made possible by installing two inverters or drive controllers to directly control the main motor speeds. Related software programs were developed to assist with the control and monitoring of process parameters. When the machine control side was completed and the machine could accurately be controlled by a personal computer more time was put into the development of welding tools and the measuring of weld parameters.

Information on tool designs and process parameter settings are very much limited since the process is patented. The PET developed new tool designs and only experimental evaluations would determine the outcome of the design. Eventually an improved tool design was developed that makes welding at faster feed-rates with lower forces possible. The FSW3 tool is capable of making good butt welds on Aluminum plate ranging from 6 to 8mm in plate thickness. This tool can now be used with all other process parameters settings to determine the related weld qualities. Other than the control modifications made on the machine, tool fixturing and material clamping techniques had to be designed and manufactured. The clamping of the workpieces plays an important role during the welding process since it must prevent any deflection or movement of the base material. The clamps must be so designed that it is easy to disassemble and also easy to manufacture. The mechanical structure of the tool holder must also be able to withstand the high welding forces of each weld

trial. Other small modifications made on the machine will be things like motor cowls, couplings, telemetry brackets and safety screens.

For the measuring of crucial weld parameters a specialized sensor and data transmission system was developed. This unit can measure realtime process data directly from the rotating tool holder while welding. It enables the researchers to link process variables, such as tool temperature, with that of process parameter settings such as spindle speed and feed-rate. Further advanced studies can now be made to link weld quality with that of process variables and then improve on the design for optimal operating points.

After a range of comprehensive tests conducted by the researchers a good knowledge was built on process optimization. The weld quality can vary considerably with only a slight change in one or two variables. A method was to be designed that could link process parameters to that of process variables so that the researcher will know what to change to influence what and by how much during the process. An experimental approach was followed to determine the correlations that existed between these variables. A regression summary was now also established and related mathematical formula links the dependent variables with that of the independent variables. These formulas are being used to establish the optimal operating point of the PET friction stir welder when a number of parameters such as spindle speed and feed-rate are set. Successful welds were made on 6mm and 8mm thick aluminum plates. At this stage the machine is limited to welding plate thickness of not more than 8mm because of the spindle and feed-motor power availability.

Future developments at the PET will be to *improve weld quality*. Since the MTRC specializes in manufacturing, weld quality will be a high priority. Quality of the welds is mainly related to mechanical properties obtained by tests such as fatigue and tensile testing thus the aim will be to improve these properties. At the moment it is preferable to obtain a higher tensile strength, closer to that of the parent material. Temperature will be a good starting point to evaluate weld quality since FSW is a heat related process. Other variables that can be linked to weld quality are the tool forces generated during a welding trial. Polar force plots generated around the tool can be linked to the characterization of material flow. The optimum will be to weld at lower feed forces since it will save money during machine selection and availability.

Other important developments that need attention will be to weld at *higher feed-rates*. This is important since it will drop the production cost and make FSW a more efficient process.

Profile welding on thin sheets need to be further investigated to make the process more industry related. Profile welding will have to be done through advanced control algorithm and will be a problem on its own. Much work still need to be done in this field of study.

A *'bobbin' tool* used to make welding without a backing plate was recently invented. This is not everyday technology yet and work in this field also needs attention. If the process can operate at lower Z-Forces and without any backing plates it will make many other weld configurations possible.

Improvement in tool design will always be an advantage since it plays an important role during weld quality. A new tool that can weld at lower forces, achieve better surface finishes and improve the tensile strength of the joint, are to be considered.

A portable welder that industry can use will be a future concept under attention. Since the process is energy efficient, the motor industry should be interested in the process if a relatively low priced aluminum welder can be introduced.

The researcher is planning to investigate the effects that temperature and force-distribution profiles have on the residual stress and fatigue life of FSW.

Attached please find the CD containing a FSW video that will demonstrate the operation of the PET Friction Stir Welder.

GLOSSARY OF TERMS

A

augering effect – the gripping movement of the rotating tool in FSW where the tool shape or profile pulls or stirs the plasticized material in a downward direction.

alloying element **– an element added to and remaining in metal that changes structure and properties.**

annealing – heating to and holding at a suitable temperature followed by cooling at a suitable rate.

as manufactured – pertains to sheet metal plate in it as manufactured form.

B

bending stress **– if a beam is subjected to a bending moment the fibres in the upper part are extended and those in the lower part are compressed. Tensile and compressive stresses are thereby induced which vary from zero at the neutral axis of the beam to a maximum at the outer fibres. These stresses are called bending stresses.**

D

drop-out – **a term borrowed from fusion welding where the weld zone protrudes from the back of the welded panel.**

E

eccentricity **– displacement or off-set adjustment with reference to the center position.**

elastic region **– a material is said to be stressed within the elastic region when the working stress does not exceed the elastic limit.**

etchant – a chemical solution used to etch a metal to reveal structural details.

etching – subjecting the surface of a metal to preferential chemical or electrolytic attack to reveal structural derails for metallograhic examination.

F

fatigue – a phenomenon which results in the sudden fracture of a component after a period of cyclic loading in the elastic regime.

fatigue life – the number of load cycles a component can withstand prior to failure.

G

grain growth – an interface separating two grains at which the orientation of the lattice changes from that of one grain to that of the other. When the orientation change is very small the boundary is sometimes referred to as a sub-boundary structure.

H

hardness – a term used for describing the resistance of a material to plastic deformation under the action of an indenter.

hardening – increasing hardness by suitable treatment, usually cold working.

homogeneous – a chemical composition and physical state of any physical small portion are the same as those of any other portion.

hot working – deformation under conditions that result in re-crystallization.

hot hardness – this property designates the steel's resistance to the softening effect at elevated temperatures.

hydrostatic pressing – the application of liquid pressure directly to a perform which has been sealed, e.g. in a plastic bag. It is characterized by equal pressure in all directions maintaining perform shape to reduced scale.

I

incremental steps – refers to the small amount of movement during positioning or control of a process or part thereof.

incremental optical encoders – electrical device coupled to a rotating motor shaft. This unit provides a set of pulses that are related to linear movement.

longitudinal plane – is a plane that is normal to the longitudinal axis.

longitudinal axis – that direction parallel to the direction of maximum elongation in a worked material.

M

macrograph – a graphic reproduction of a prepared surface of a specimen at a magnification not exceeding 25x.

macrostructure – the structure of metals as revealed by macroscopic examination of the etched surface of a polished specimen.

magnification – the ratio of the length of a line in the image plane to the length of a line on the imaged material.

maximum bending strain – a cylindrical shaft is said to be subject to pure torsion when the torsion is caused by a couple, applied so that the axis of the couple coincides with the axis of the shaft. The state of stress, at any point in the cross-section of the rod, is one of pure shear, and the strain is such that one cross-section of the shaft moves relative to another.

microsturcture – the structure of a prepared surface of a metal as revealed by a microscope at a magnification exceeding 25x.

O

onion-skin flow pattern – a characteristic weld pattern featuring a cyclic ring or onion skin-like profile.

oxidation – the addition of oxygen to a compound. More generally, any reaction involving the loss of electrons from an atom.

P

plastic deformation – deformation that remains or will remain permanent after release of the stress that caused it.

plasticity – capacity of a metal to deform non-elastically without rupturing.

polished surface – a surface that reflects a large proportion of the incident light in a specular manner.

principal strains – the maximum and minimum direct strains in a material, subjected to complex stress are called Principal Strains. These strains act in the directions of the principal stresses.

principal stresses – at any point within a stressed material it will be found that there exist three mutually perpendicular planes on each of which the resultant stress is a normal stress (i.e. no shear stresses occur on these planes). These mutually perpendicular planes are called principal planes, and the resultant normal stresses are called Principal Stresses.

plunge force – during the plunging stage of the tool pin in FSW, the vertical force in the direction of the Z-axis movement is normally referred to as the plunging force.

Q

quantitative – identification of relative amounts making up a sample.

quench hardening – in ferrous alloys, hardening by austenitising, then cooling at a rate so that a substantial amount of austenite transforms to martensite.

quill – the mechanical section of a milling machine head that contains the chuck or tool holder.

R

re-crystallisation – a change from one crystal structure to another, such as that occurring upon heating or cooling through a critical temperature.

relieved – allowing for freedom of movement or relaxation.

residual stress – are stresses inherent in a component prior to service loading conditions.

restrained – hold back movement in any direction.

rolling direction – refers to the direction in which the billet was rolled during the sheet metal plate manufacture.

S

side-flash – in FSW, a build-up of weld material, normally on the retreating side of the rotating, which has a ‘peal like’ effect is termed side-flash.

solid-phase – a physically homogeneous and distinct portion of a material system in the solid state.

spindle speed – the speed of the work holding device (chuck), measured in revolutions per minute.

stagnation point – the point, at or near the nose of a body in motion in a fluid, where the flow divides and where, in a viscous fluid pressure is at a maximum, and in an inviscid one the fluid is at rest.

strain – strain is a measure of the deformation of a body acted upon by external forces and can be expressed as a change in dimension per unit of original dimension or in the case of shear as a change in angle between two initially perpendicular planes.

strain amplifier – the ratio of the voltage supplied to the voltage delivered by the Wheatstone Bridge as a result of the unbalance caused by a change of strain gauge resistance is equivalent to the strain and is amplified into a suitable voltage or current which can be fed into an analogue or digital indicator or graphic recorder.

stress – load applied to a piece of material tends to cause deformation which is resisted by internal forces set up within the material which are referred to as stresses. The intensity of the stress is estimated as the force acting on the unit area of the cross-section, namely as Newtons per square meter or Pascals.

sub-surface – a location just beneath the surface of a component.

T

telemetry system – a system making use of non-contact methods such as radio and capacitive transmission, normally used for measuring and data transfer purposes.

tempering – in heat treatment, reheating hardened steel to some temperature below the eutectoid temperature to decrease hardness and/or increase toughness.

Tensile strength (UTS-ultimate tensile strength) – maximum load in tension which a material will stand prior to fracture. For ductile iron = 414MPa to 1380 MPa.

$$UTS = \frac{Maximum \quad Load}{Cross \quad Sectional \quad Area}$$

threshold level – generally the lowest intensity of an effect, which is detectable.

thixotropic – a property of fluids and plastic solids, characterized by a high viscosity at low stress, but a decreased viscosity when an increased stress is applied.

toughness – in tool steels, this property expresses ability to sustain shocks, suddenly applied loads and relieved loads, or major impacts, without breaking.

transverse direction – refers to the perpendicular direction in which the billet was rolled during sheet plate manufacture.

Triflute Tool – a TWI trademark tool.

third-body region – area where recrystalization took place of the parent and/or filler metal due to the plastic flow of material during a weld. This region contains the weld nugget within the TMAZ.

V

viscosity – the resistance of a fluid to shear forces, and hence to flow. Such shear resistance is proportional to the relative velocity between the two surfaces on either side of a layer of fluid, the area in shear, the coefficient of viscosity of the fluid and the reciprocal of the thickness of the layer of fluid.

void – the space that exist between particles or grains. Normally in welding voids are associated with defects and incomplete penetration.

W

Whorl tool – a TWI trademark tool.

worm holes – a sub-surface defect in a Friction Stir weld, normally on the advancing side of the rotating tool, due to the lack of mixing and re-bonding of plasticized material.

wear resistance – the gradual erosion of the tool's operating surface, most conspicuously occurring at the exposed edges, is known as wear.

X

x-axis – relating to a specific axis (Horizontal) or a fixed line determining the direction of movement or placement in a 2D or 3D coordinate system.

Y

y-axis – relating to a specific axis (perpendicular to x-axis)or a fixed line determining the direction of movement or placement in a 2D or 3D coordinate system.

Z

z-axis – relating to a specific axis (vertical) or a fixed line determining the direction of movement or placement in a 2D or 3D coordinate system.

(**Note**: For other definitions and nomenclature please see text.)

Table of Contents

LIST OF ABBREVIATIONS

Al	Aluminum
CNC	Computer Numerical Control
DC	Direct Current
FSW	Friction Stir Welding
HAZ	Heat Affected Zone
HRc	Rockwell C Hardness
I/O	Input and Output
LMI	Libra Measuring Instruments
MIG	Metal Inert Gas welding
MTRC	Manufacturing Technology Research Center
PC	Personal Computer
PET	Port Elizabeth Technikon
TIG	Tungsten Inert Gas welding
TMAZ	Thermal Mechanical Effected Zone
TWI	The Welding Institute of the United Kingdom
UOSC	University of South Carolina

LIST OF FIGURES

LIST OF TABLES

References:

Bevington, J., ‘Spinning tubes mode of welding the ends of wire, rods, etc, and mode of making tubes’. US Patent 463134 January 13, 1891.

Klopstock, H., Neelands A.R., ‘An improvement method of joining or welding metals’. British Patent specification 572789, October 17, 1941.

Thomas, W.M., Nicholas E.D., Needham J.C., Murch M.G., Temple-Smith P., Dawes C.J., ‘Improvements relating to friction stir welding’. European Patent Specification 0615 480 B1.

Thomas W.M., International Patent Application No PCT/GB92/02203, 10 June, 1993.

‘Second Intenational Symposium on Friction Stir Welding’. 26-28 June 2000, Gothenburg, Friction Stir Welding at TWI.

McMullan D.J., Bahrani A.S., ‘The mechanics of friction welding dissimilar metals’. Second International Symposium of the Japan Welding Society on Advanced welding technology, 25-27 August, 1975, Osaka, Japan.

Hasui A., ‘Effect of the relative difference of bar diameter on the friction welding of different diameter bars’. IIW Doc. III-679-81.

Fukakusa K., Satoh T., ‘Travelling phenomena of potational plane during friction welding. Application of Friction Hardfacing’. International Symposium on Resistance Welding and Related Welding Processes. 10th-12th July 1986, Osaka.

Nicholas E.D., Thomas W.M., ‘Metal deposition by friction welding’. Welding Journal, August 1986, pp17-27.

Bedford G.M., ‘ Friction surfacing for wear applications’. Metals and Material, November 1990, pp 702-705

Thomas W.M., ‘Solid phase cladding by friction surfacing’. Welding for the Process Industries, International Symposium, April 1988

Dr. Edward A. Metzbower., " Friction Stir Welding" ASM International. Online.Internet.WWW:http://www.asmintl.org/content/Chapters_Committees/FellowsForum/stirwelding.htm

Thomas W.M., Nicholas E.D., Smith S.D. "Friction Stir Welding- Tool Developments." Aluminum Proceedigs 2001, TMS 2001. Also Online Available: www.twi.co.uk/j32k/protected/band_8/spwmtfeb2001.html

United States of America. NASA, Marshall Space Center. (2001). Space Shuttle Technology Summary, Friction Stir Welding. USA: Government printer.

Thomas W.M., Threadgill P.L., Nicholas E.D. "The feasibility of Friction Stir Welding steel." Online. Internet. Available WWW: http://www.twi.co.uk/j32k/protected/band_8/spwmtfeb99.html

Thomas W.M., "Friction stir welding and related friction process characteristics." International Conference 7th, April 1998, Joints in Aluminum: Inalco'98, 1999.

Godet M., 'The Third-Body approach: A mechanical view of wear.' Wear, Vol No 100, (1984) pp 437-452

Singer Irwan L., 'How Third-Body Process Effect Friction and Wear' MRS Bulletin 1998.

Khazanov I.O., Fomin N.I., (Tomsk Polytechnical Insitute)., 'Friction Welding in the temperature range of superplasticity of High-Speed Tool Steel', Welding International 1990 4 8 633-634 (Selected from Svarochnoe 1989 36 4-5, Reference SP/89/3/4, Translation 860)

Benson P.G., Backlund J., 'Possibilities with aluminium extrusions joined by friction stir welding'. 4th Int Forum on Aluminium Ships, New Orleans, 10-11 May 2000.

Kumagai M., Tanaka S., 'Properties of aluminium wide panels by friction stir welding'. First International Symposium on Friction Stir Welding, Thousand Oaks, CA, USA, 14-16 June 1999.

Midling O.T., Kvåle J.S., Dahl O., 'Industrialisation of the friction stir welding technology in panels production for the maritime sector'. 1st Int Symp on FSW, Thousand Oaks, CA, June 1999.

"Friction Stir Welding – Equipment" Online. Internet. Available WWW: http://www.twi.co.uk/j32k/protected/band_8/spwmtapr98.html

"Friction Stir Weld Geometries" Online. Internet. Available WWW: http://www.twi.co.uk/j32k/unprotected/band_1/fswjoint.html

Backlund, J., Norlin, A., Anderson, A., 'Friction stir welding-weld properties and manufacturing techniques.' International Conferance 7th – 1998 April, Joints in aluminum : Inalco 1998, pp.184 -196

Johnson R., 'Forces in Friction Stir Welding Alluminum Alloys'. Proceedings of the Third International Friction Stir Welding Symposium, Kobe Japan, 27-28 Sept 2001.

Oberg E., Jones D.F., Holbrook L., Ryffel H., Machinery's Handbook, 25th Edition, Industrial Press Inc. New York, 1996.

Cengel Y. A., Introduction to Thermodynamics and Heat Transfer. International Edition. The McGraw-Hill Companies, Inc. New York, 1997.

Incropera F. P., DeWitt D. P., Fundamentals of Heat and Mass Transfer, Fourth Edition. John Wiley & Sons, New York, Brisbane, 1996.

"Skew-stir a Friction stir welding variant" Online. Internet. Available http://www.twi.co.uk/j32k/protected/band_3/ksskew_stir.html

North T. H., Bendzsak., G. J., Smith C., 'Material Properties Relevent to 3-D FSW Modelling'. Proceedings of the Second International Friction Stir Welding Symposium, Gothenburg, Sweden, 26-28 June 2000.

1988 Annual book of ASTM Standards, Section 3, Metals Test Methods and Analytical Procedures, Volume 03.01. American Society for Testing and Materials, Easton, MD, U.S.A., 1988.

Azouzi R., Guillot M., 1997, On-Line Prediction of Surface Finish and Dimensional Deviation in Turning using Neural Network Based Sensor Fusion, Vol. 37, No. 9, pp. 1201-1217.

Ross, P. J., Taguchi Techniques for Quality Engineering. McGraw-Hill, New York, 1988.

Sung, H. P., Robust Design and Analysis for Quality Engineering. Chapman and Hall, London, 1996.

Online Internet: Available www.gemcor.com/FSW.html

Hoffmann, K., An Introduction to Measurements using Strain Gages. Hottinger Baldwin Messtechnik Gmbh, Darmstadt, 1989.

Hoffmann, K., Applying the Wheatstone Bridge Circuit. Third Edition. Hottinger Baldwin Messtechnik Gmbh, 1986.

I.V. Kragelsky., V.Alisin., First, second and third Edition 1981. Friction Wear Lubrication., Tribology Handbook. Mir publishers Moscow 1982.

G. Kruger., Research associate., work conducted during his research in compliance with his Master Degree in Electrical Engineering at Port Elizabeth Technikon.

M. Herselman., Company, Libra Mearuring Instruments. Personal Interview and System Manual supplied, October 2002.

M. N. James., D. G. Hattingh., 'Influence of travel speed on fatigue life of friction stir welds in 5083 Alluminium'., Proceedings of the Eight International Fatigue Congress, Stockholm, Sweden, June 2002.

Online Internet available http://vassun.vassur.edu/~lowry/ch3pt1.html, 'Introduction to Linear Correlation and Regression'.Chapter 3, Part 1, 2 & 3.

B. Zeelie., Workshop: Statisctical Analysis, 4 December 2002, Personal interviews, Lecture Notes:. PE Technikon.

S. Kallee., D. Nicholas., H. Powell., J. Lawrence., 'Knowledge-based software package for friction stir welding'. Presented at 7TH International Conference, Abington, Cambridge, UK, 15-17 April 1998

C. J. Dawes., W. M. Thomas., E. D. Nicholas., 'Friction Stir Welding'. TWI, Cambridge, CB1 6AL UK.

L. Karlsson., L. E. Svensson., H. Larsson., 'Characteristics of Friction Stir Welded Aluminum Alloys'. Trends in Welding Research, International Conference 5th , 1998 June, pg 574-579. Esab AB, Gottenburg, Sweden

T. Hashimoto., N. Nishikawa., S. Tazaki., M. Enomoto. 'Mechanical Properties of Joints for Aluminum Alloys with Friction Stir Welding Process'. International Conference 7th, 1998 April, Joints in Aluminum: Inalco 1998. pg247-260, 1999.

H. Larsson., L. Karlsson., L.E. Svensson., 'Friction Stir Welding of AA5083 & AA6082 Aluminum'. JOM International Conference, 1999, Vol 9, pg242-247.

Appendix A:

In Combination with Chapter 3

TECHNICAL CHARACTERISTICS

TECHNICAL CHARACTERISTICS				F3U-E	F3U-E CM
TABLE	Surface	Length	mm.	1400	1400
		Width	mm.	340	500
	Width of T slots		mm.	18H8	18H8
	Number of T slots			4	6
	Distance between T slots		mm.	71	71
AUTOMATIC TRAVERSES	Longitudinal		mm.	1100	1100
	Table cross		mm.	375	290
	Overarm cross		mm.	–	760
	Vertical		mm.	485	485
MAIN SPINDLE	Main spindle nose as per ISO R-297			ISO-50	ISO-50
	Diameter of horizontal spindle on front bearing		mm.	90	90
SPEEDS AS PER ISO R-229	Number of speeds in geometric progression			18	18
	Range (on machine and motorized overarm)		R.P.M.	28/1400	28/1400
FEEDS AS PER ISO R-229	Number of feeds in geometric progression			13	13
	Longitudinal and teble cross feed range		mm./min	11,2/710	11,2/710
	Vertical feed range		mm./min.	4/250	4/250
	Number of overarm feeds			–	6
	Overarm cross feed range		mm./min.	–	16/500
RAPID FEEDS	Longitudinal and table cross		mm./min.	3000	3000
	Overarm cross		mm./min.	–	2000
	Vertical		mm./min.	1000	1000
MOTORS	Machine main spindle		H.P.	10	10
	Overarm main spindle		H.P.	–	7,5 (10)
	Machine feeds		H.P.	2	2
	Overarm feeds		H.P.	–	1,5
	Motor pump		H.P.	0,15	0,15
	Total installed output		H.P.	12,15	21,15 (23,65)
OTHER DATA	Height		mm.	1750	2193
	Weight		Kgs.	3600	4300

Standard equipment
Complete electrical equipment and motors. Cutter arbor. Set of wrenches. Grease gun. Drawbar. Coolant equipment. Arm supporting head (except on F3U-E with motorized overarm). Two arbor supports. Service and spare parts book.

Technical characteristics chart of the conventional milling machine as purchased.

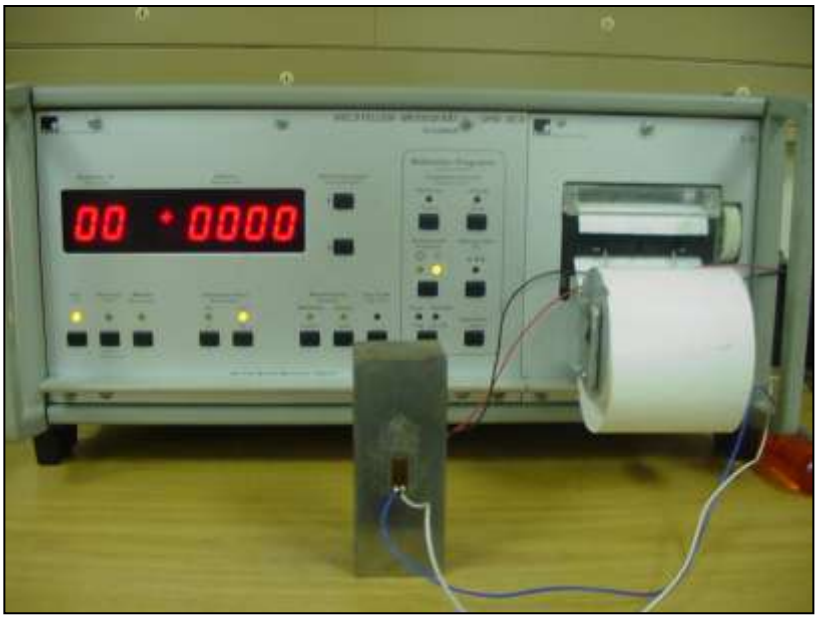

Loadcell setup for two diagonal quarter bridge circuits.

Full bridge conditioned and completed in UPM 40 amplifier.

Encoder housing (motor cowl) with an internal force convection fan and safety grid, system mounted on the feed bed motor.

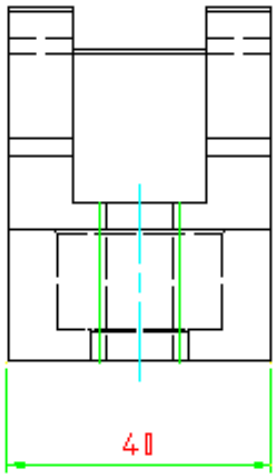

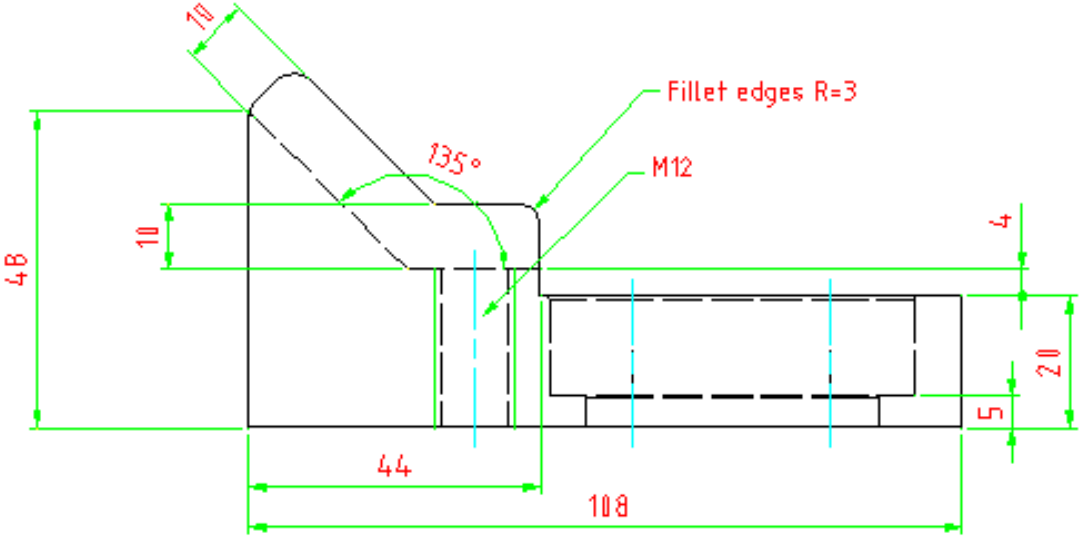

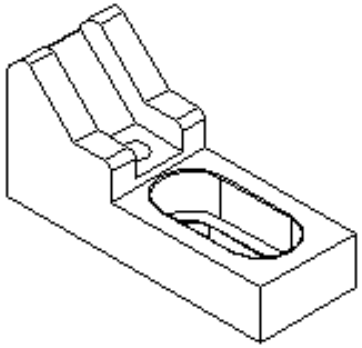

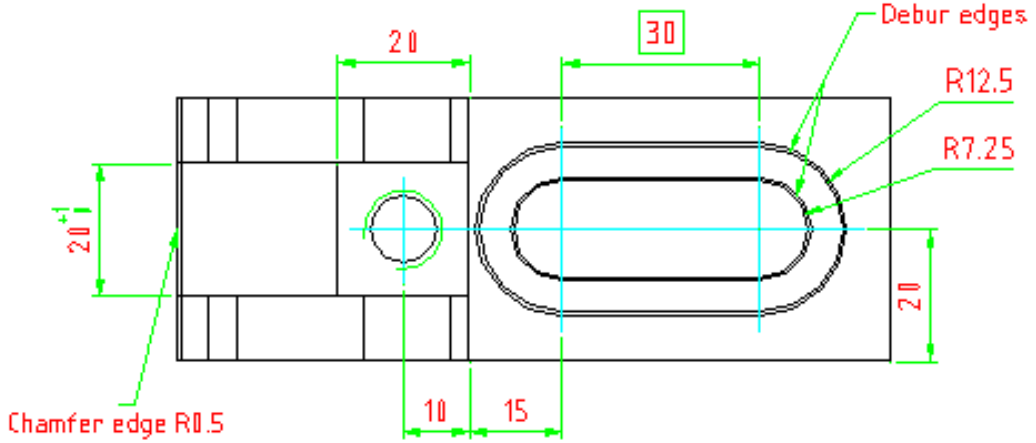

CLAMPING BLOCK 1

Refer to : Calvin Blignault
tel. 504 3003

Page 1-2

NOTE: Debur all sharp edges
Surface finish in the range of 6.3

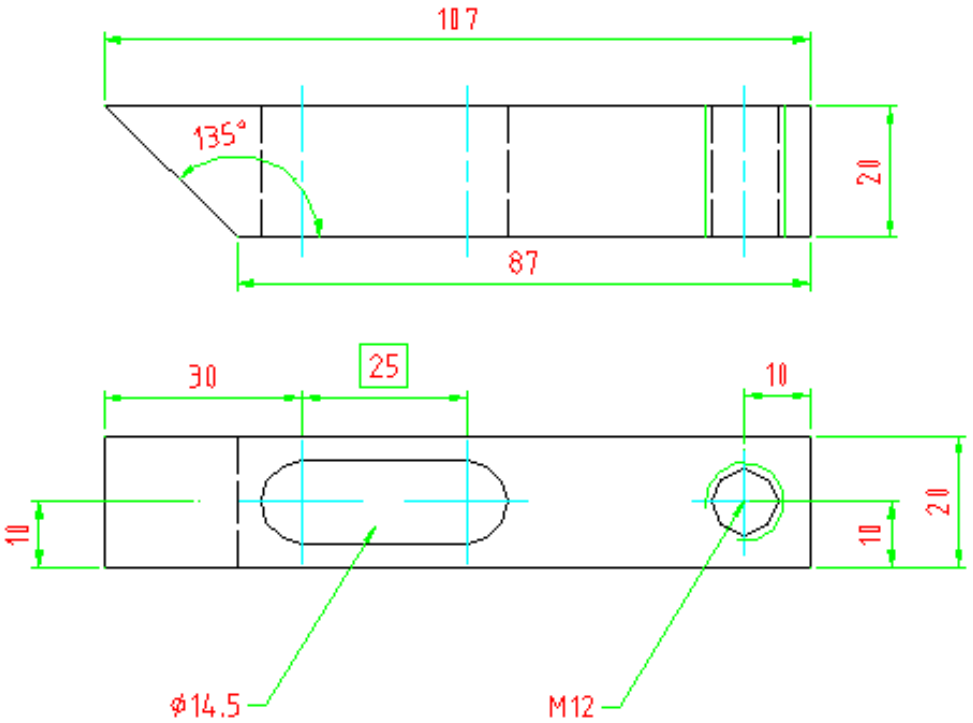

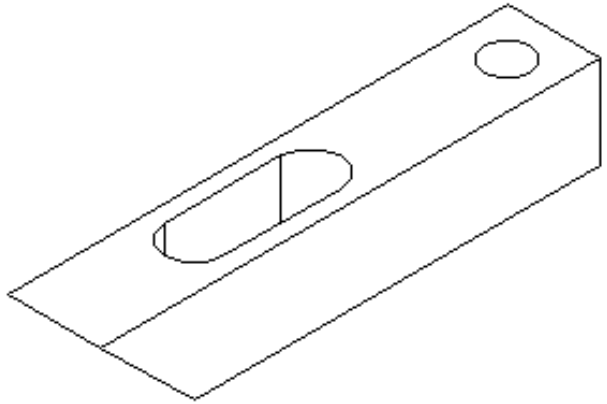

CLAMPING ARM 1

Refer to : Calvin Blignault
tel. 504 3003

Page 2-2

NOTE: Debur all sharp edges
Surface finish in the range of 6.3

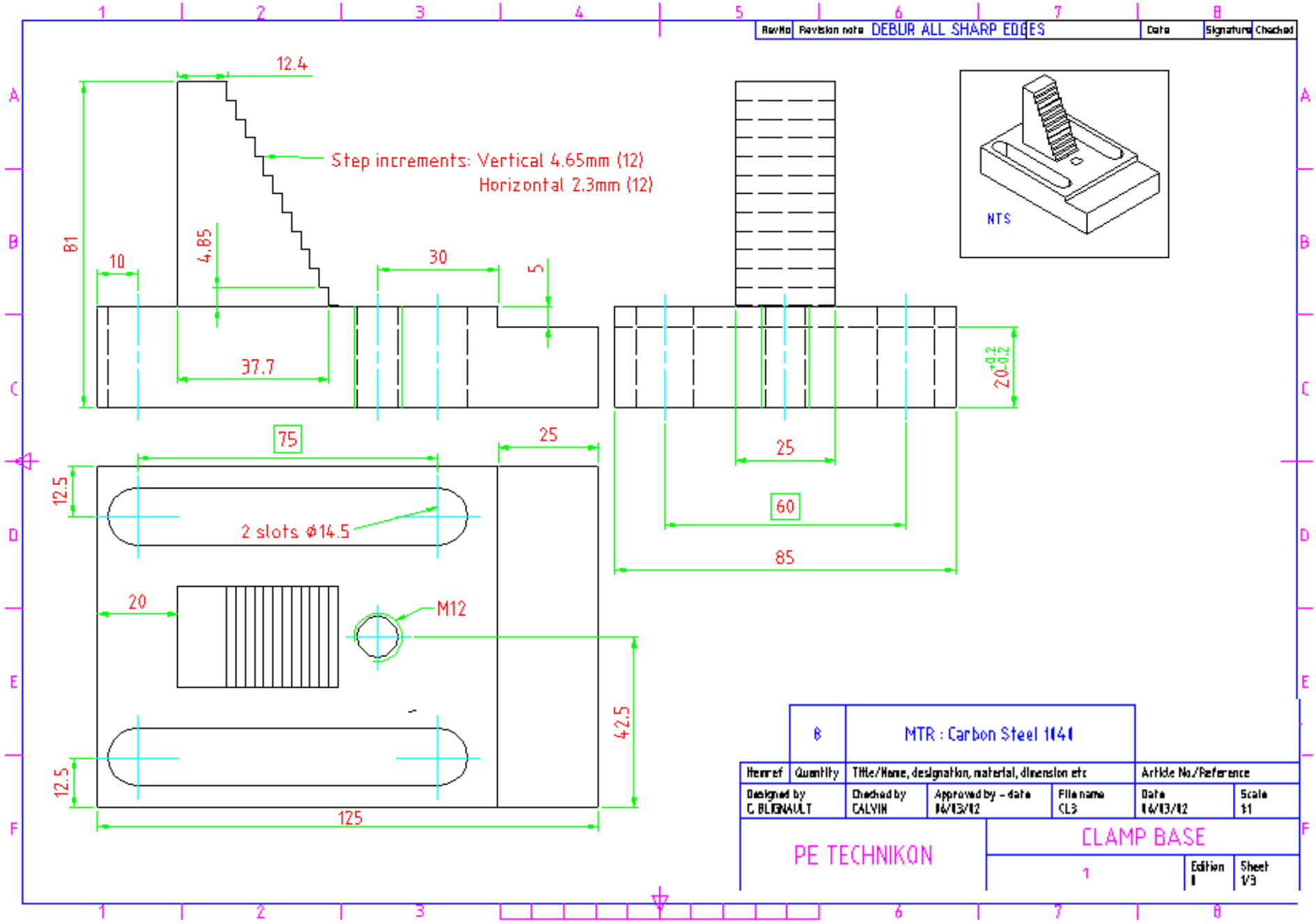
Rev No
Revision note DEBUR ALL SHARP EDGES
Date
Signature
Checked
12.4
Step increments: Vertical 4.65mm (12)
Horizontal 2.3mm (12)
B1
10
4.85
30
5
37.7
NTS
20 +0.2 -0.2
25
60
85
75
25
12.5
2 slots ⌀14.5
20
M12
42.5
12.5
125
B
MTR : Carbon Steel 1141
Item ref
Quantity
Title/Name, designation, material, dimension etc
Article No./Reference
Designed by
C BLIGNAULT
Checked by
CALVIN
Approved by - date
14/03/12
File name
CL3
Date
14/03/12
Scale
1:1
PE TECHNIKON
CLAMP BASE
1
Edition
1
Sheet
1/3

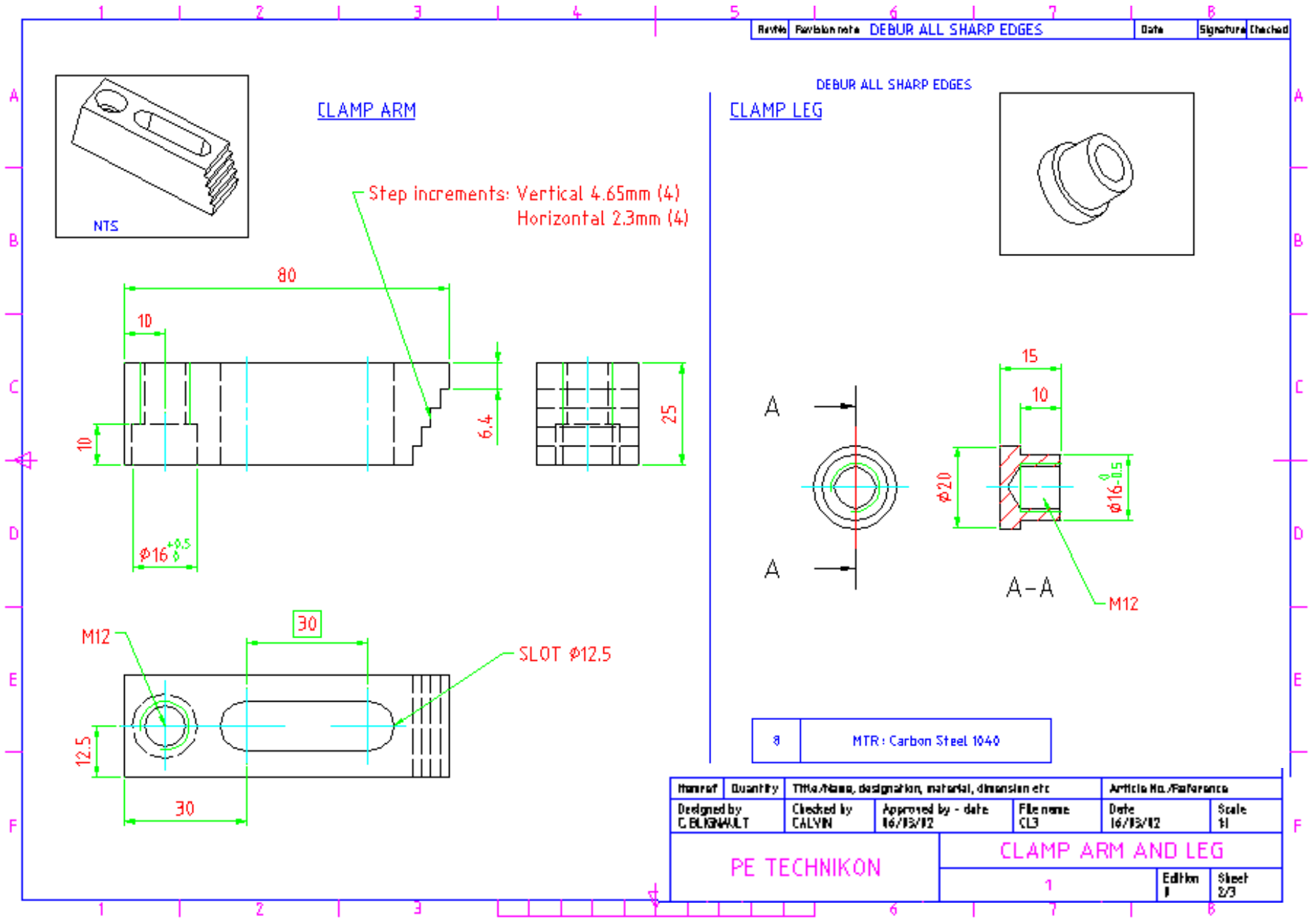
Revision note DEBUR ALL SHARP EDGES
Date
Signature
Checked
DEBUR ALL SHARP EDGES
CLAMP ARM
NTS
Step increments: Vertical 4.65mm (4)
Horizontal 2.3mm (4)
80
10
10
6.4
25
ϕ16 +0.5 0
M12
30
SLOT ϕ12.5
12.5
30
CLAMP LEG
15
10
A
A
ϕ20
ϕ16 -0 -0.5
A-A
M12
8
MTR : Carbon Steel 1040
Item ref
Quantity
Title/Name, designation, material, dimension etc
Article No./Reference
Designed by
C.BLIGNAULT
Checked by
CALVIN
Approved by - date
16/03/12
File name
CL3
Date
16/03/12
Scale
1:1
PE TECHNIKON
CLAMP ARM AND LEG
1
Edition
1
Sheet
2/3

Part No	Part Name / note	DEBUR ALL SHARP EDGES	Date	Signature	Checked

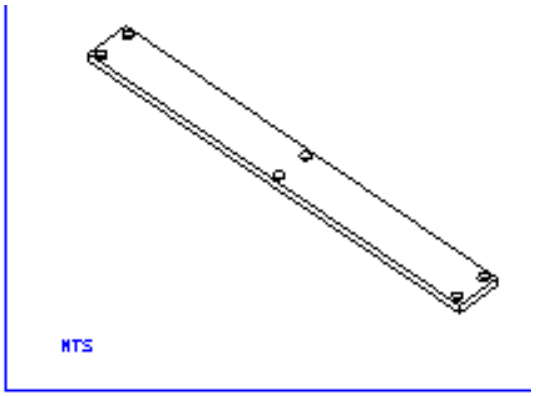

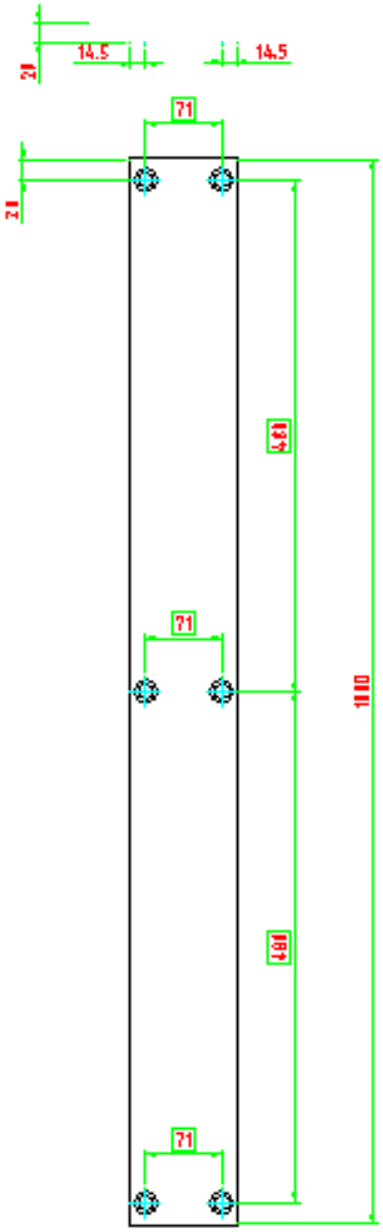

6 HOLES Ø14.5

COUNTER BORE Ø22 x 15 DEEP

Issue nr	Quantity	Title/Name, designation, material, dimension etc			Article No/Reference	
	1	NTS Datum Sheet 11x8				
Designed by C. BLIGHAULT		Checked by CALVIN	Approved by – date 06/03/12	File name CL3	Date 06/03/12	Scale 1:6
PE TECHNIKON		BACKING PLATE				
		3			Edition 1	Sheet 3/3

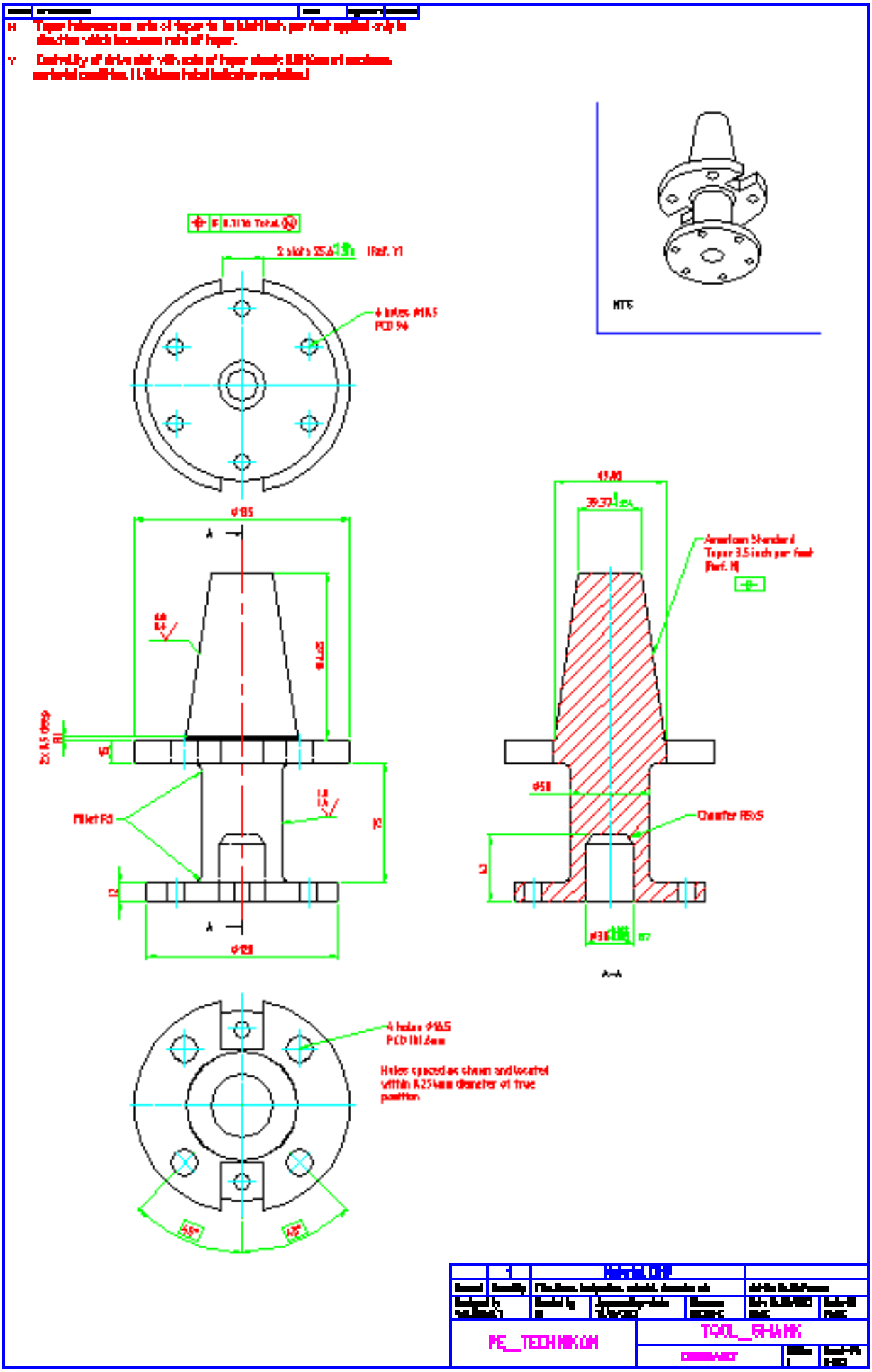
MT5
Chamfer R6x5
A–A

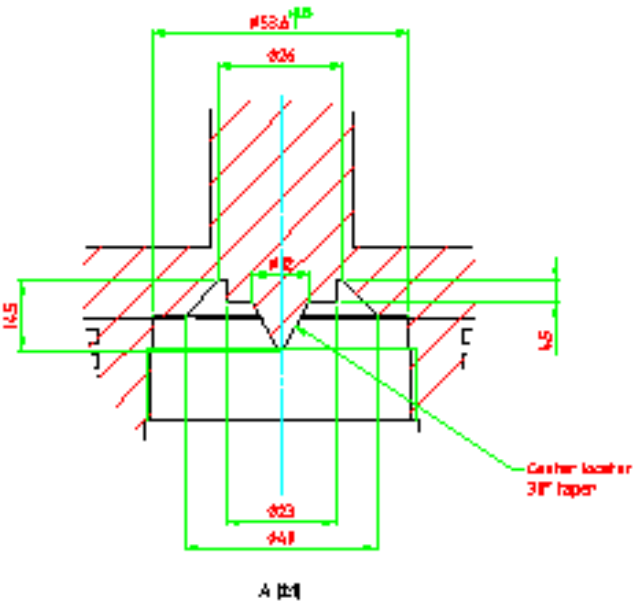

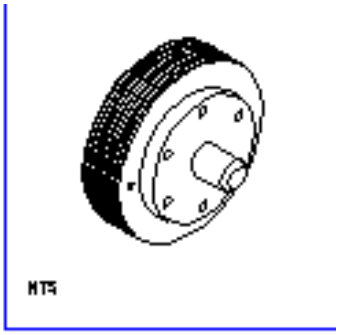

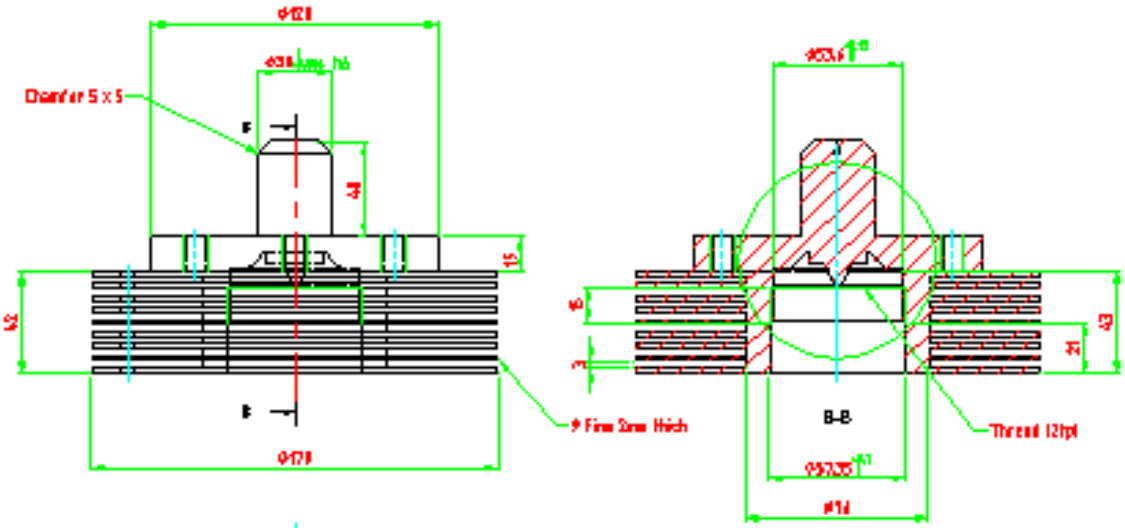

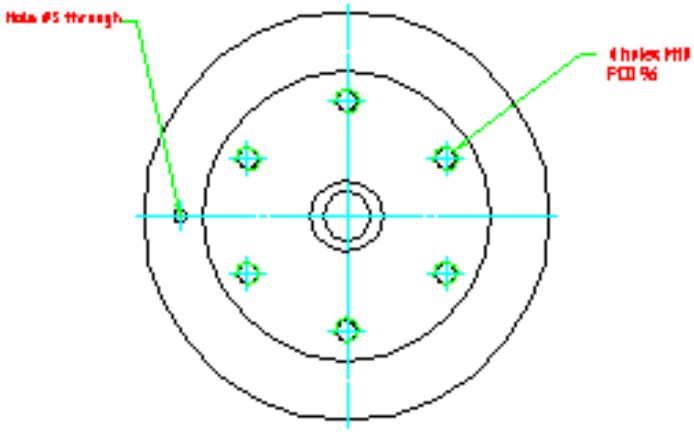

PE_TECHNIKON			HEAT_SINK		

Scale 2:1

1 off required MS

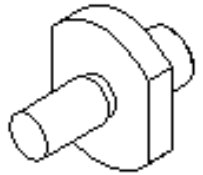

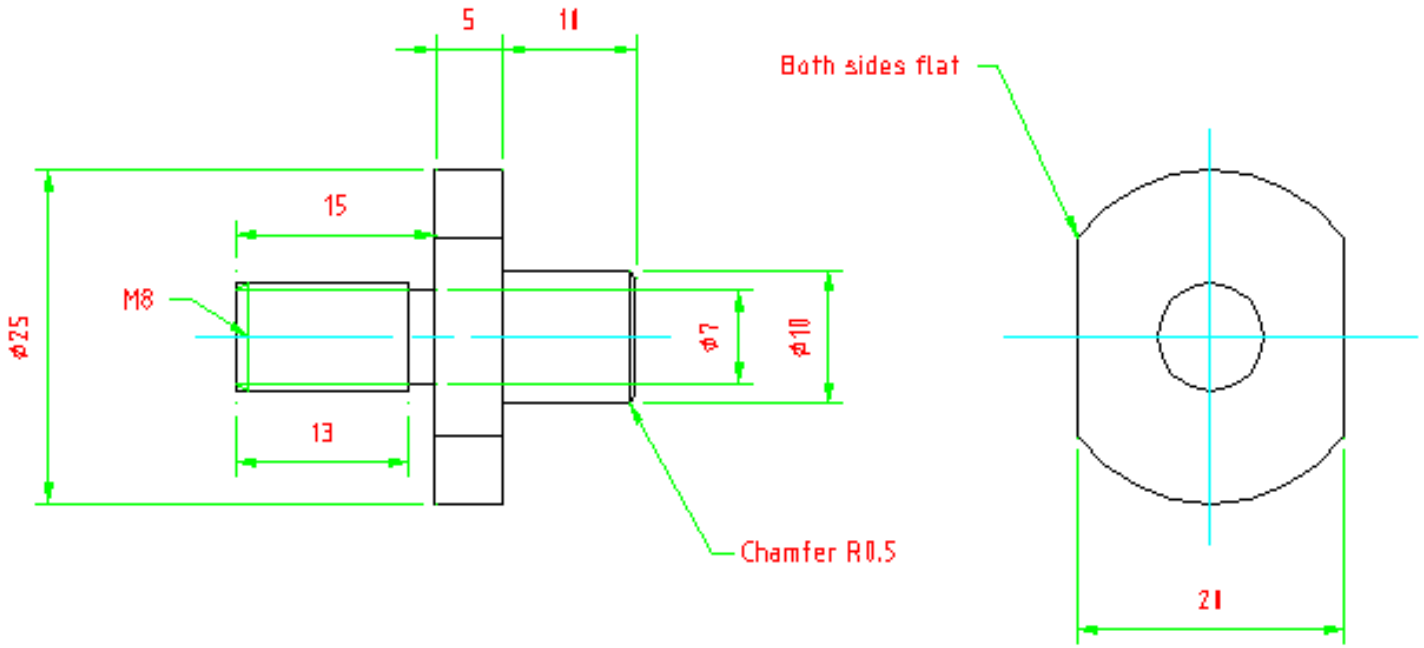

Encoder Coupling

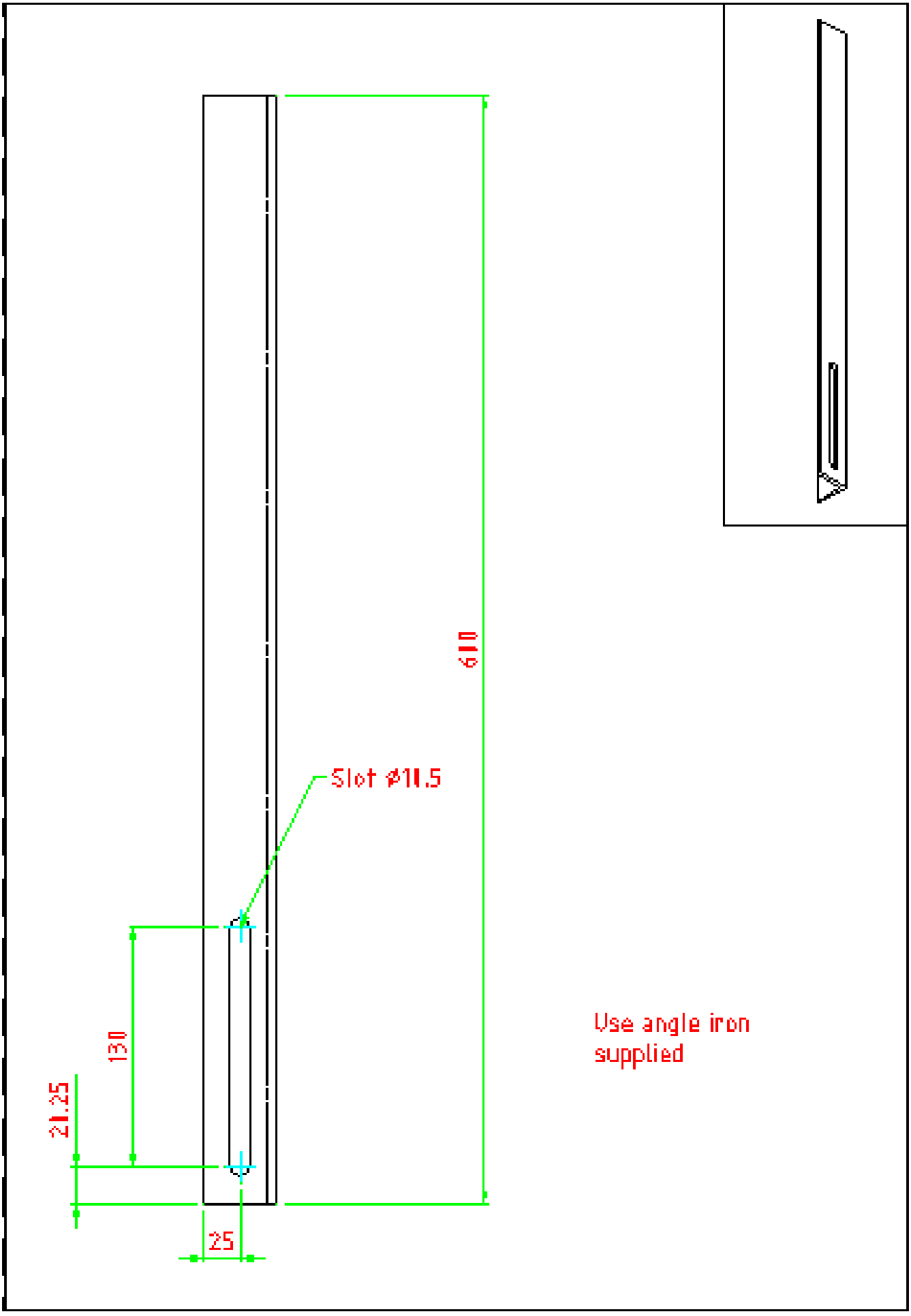
610
Slot ø11.5
130
21.25
25
Use angle iron
supplied

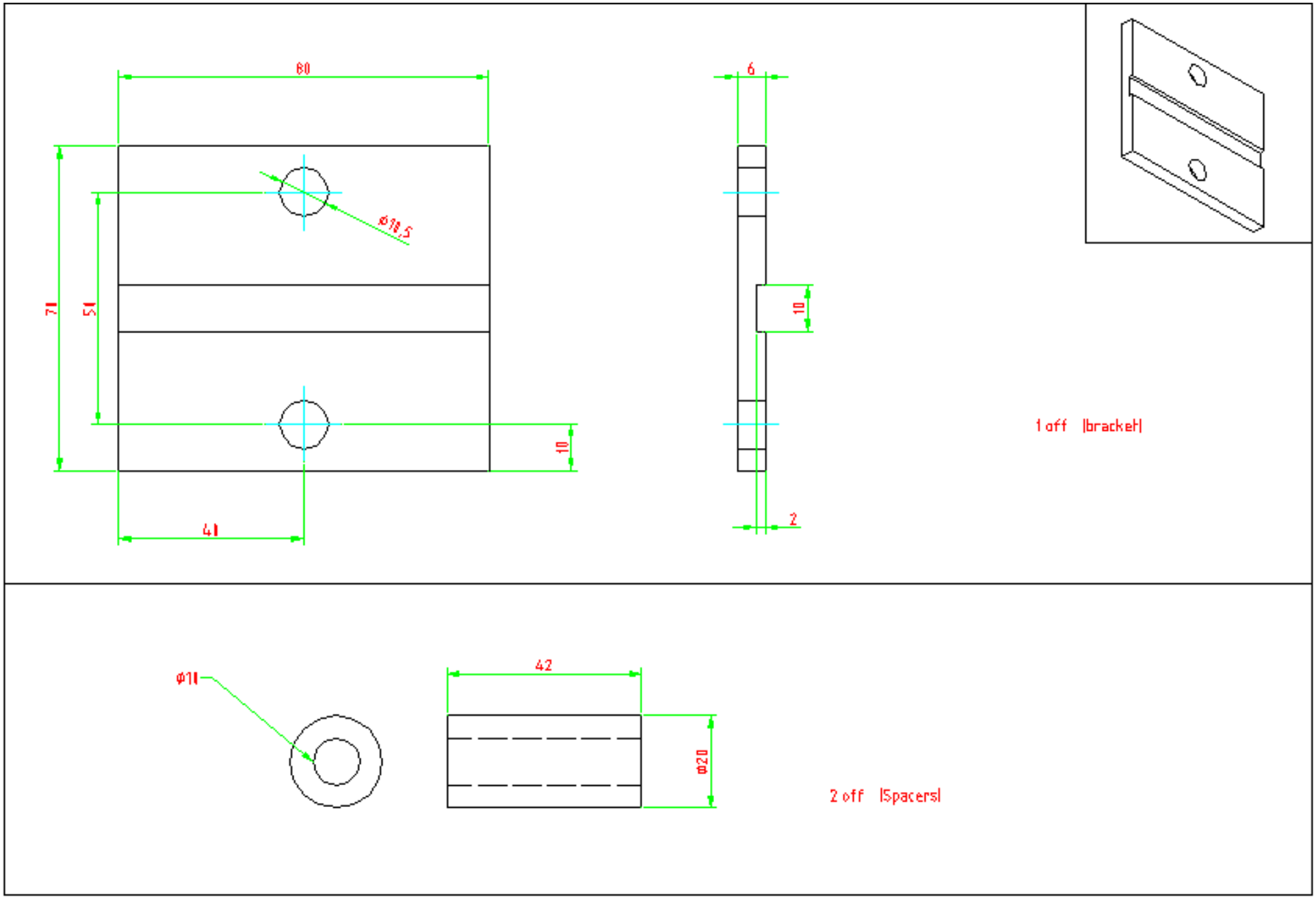
80
71
51
41
10
6
10
2
1 off (bracket)
φ11
42
φ20
2 off (Spacers)

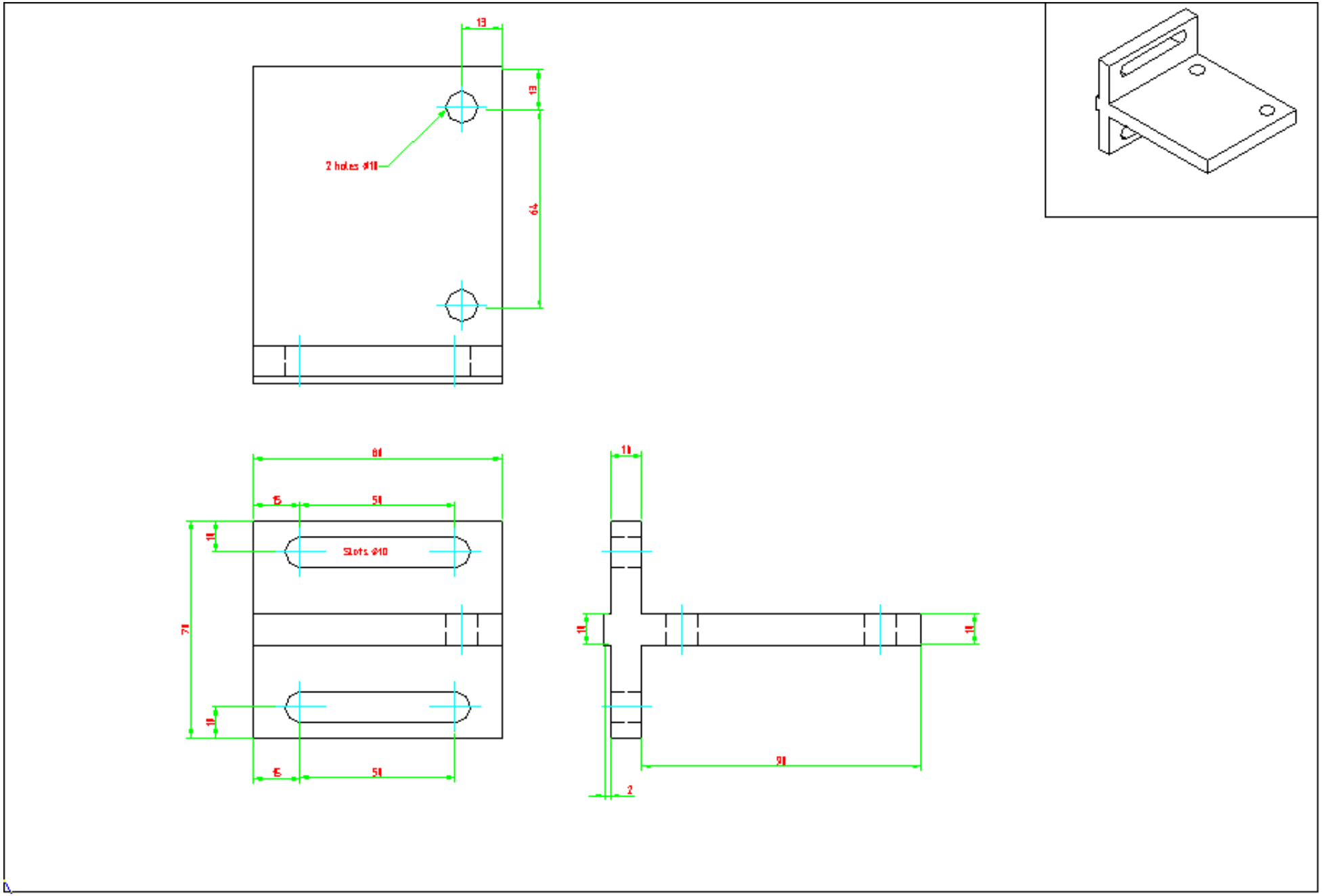
13
13
2 holes ⌀11
64
81
15
51
11
Slots ⌀10
71
11
15
51
11
11
11
91
2

ITEM 1 SCALE 1@

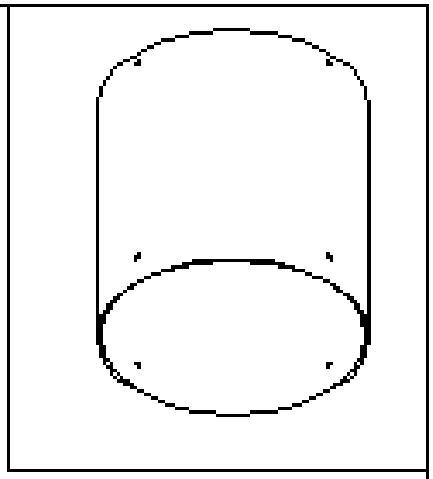

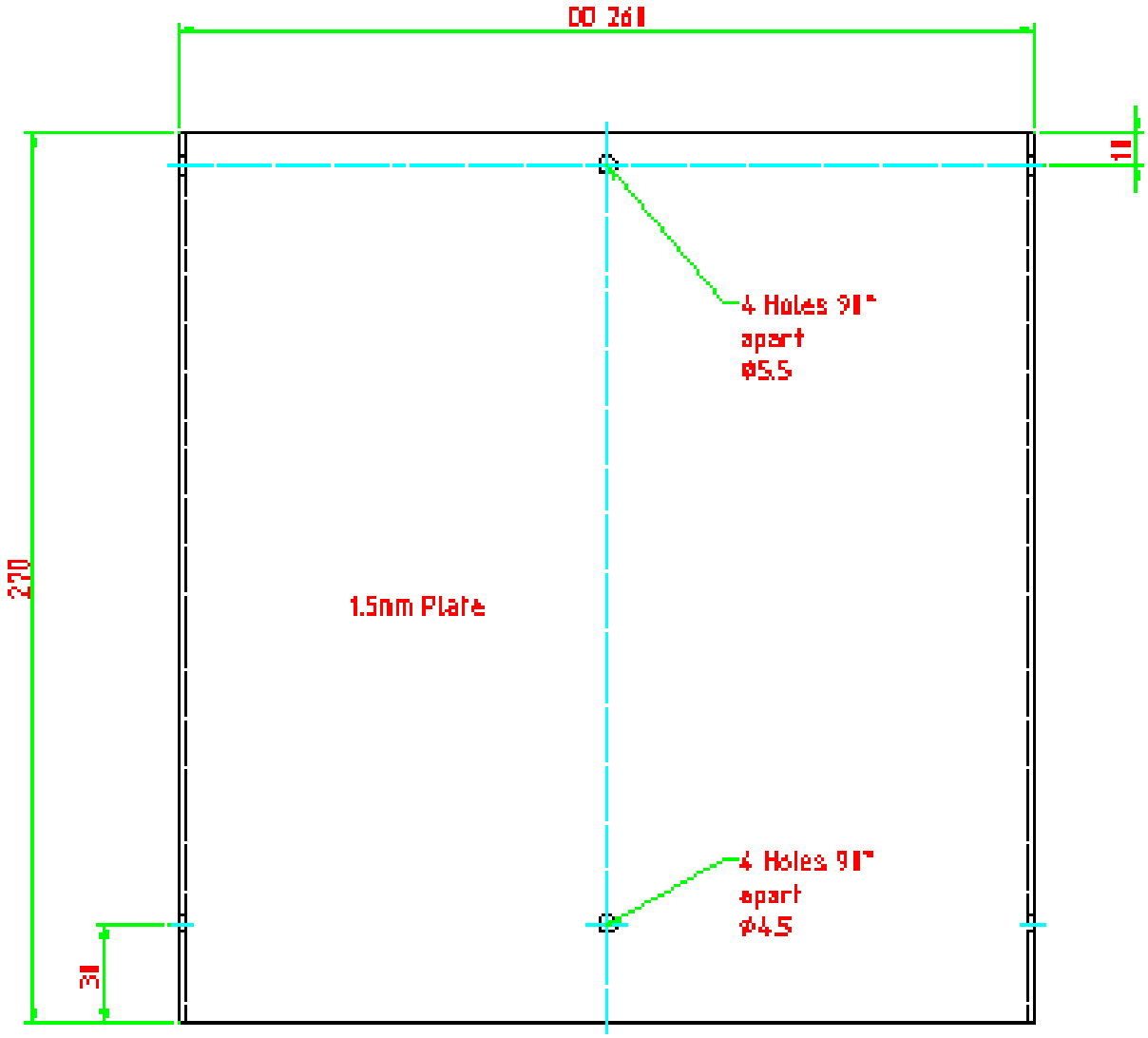

ITEM 2 SCALE 1:2

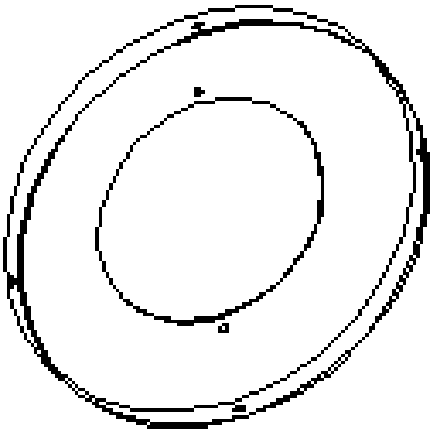

1.5mm Plate

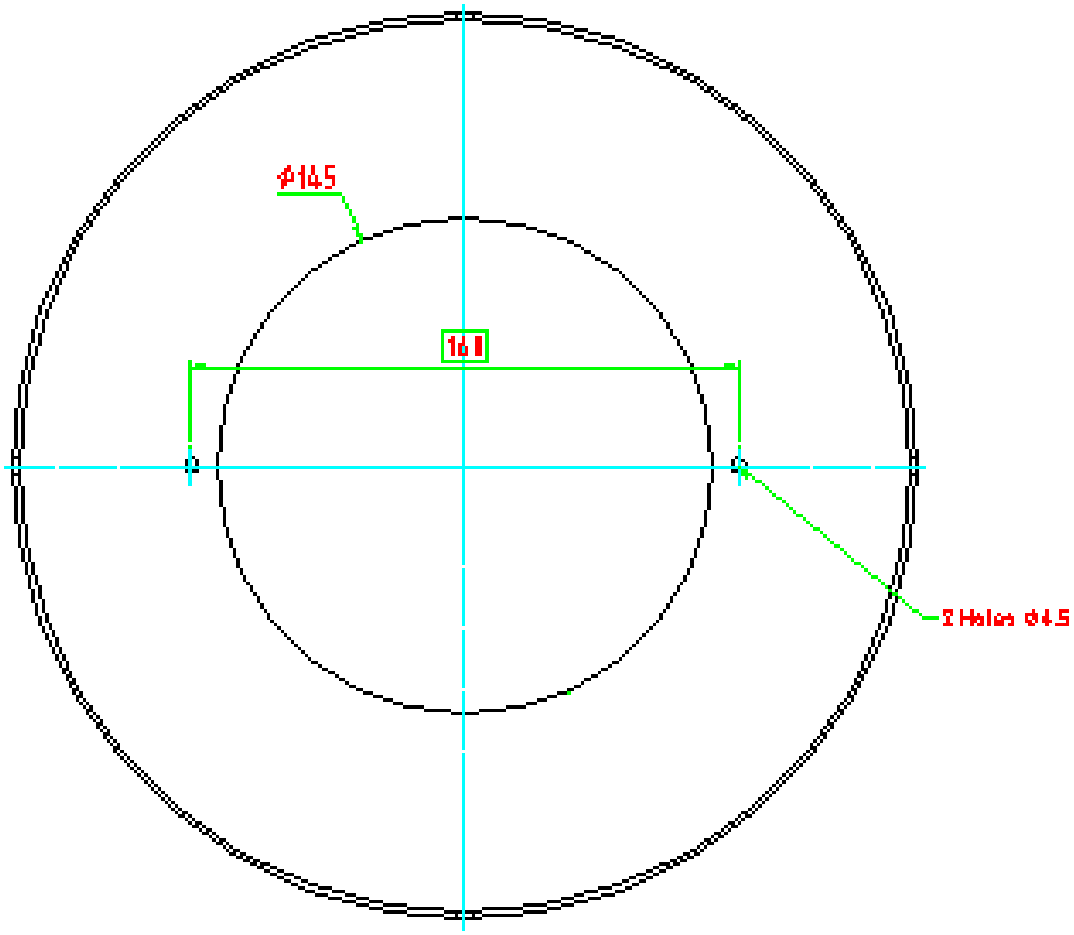

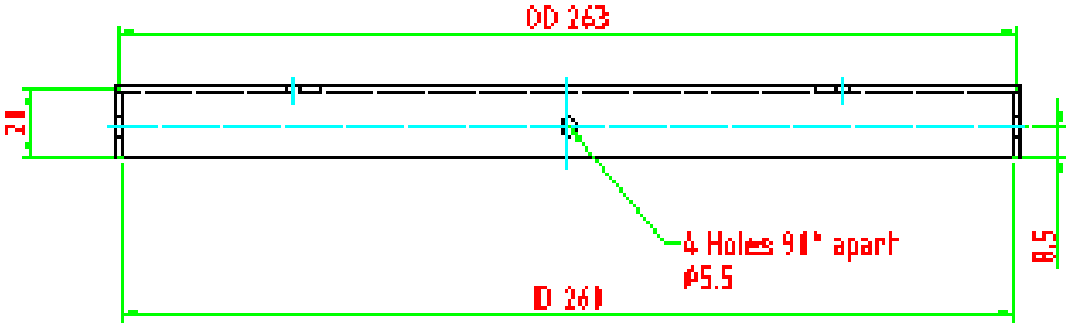

ITEM 3 SCALE 1:2

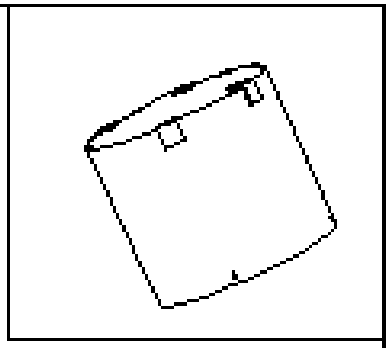

Use 1.5mm Plate

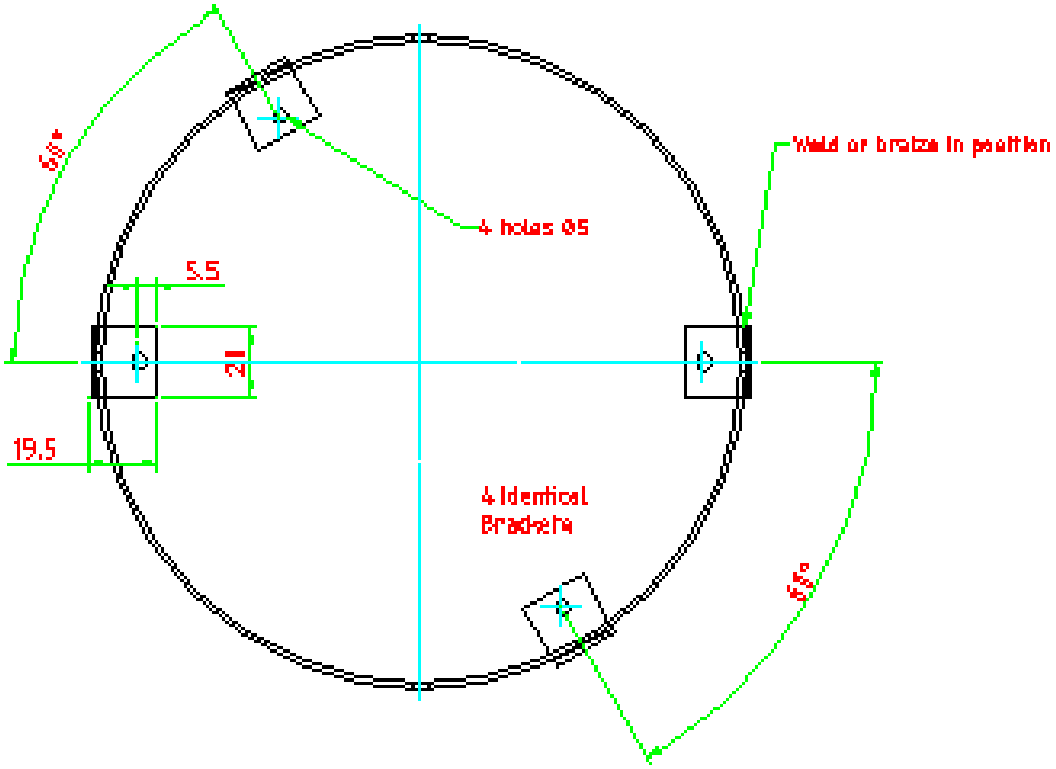

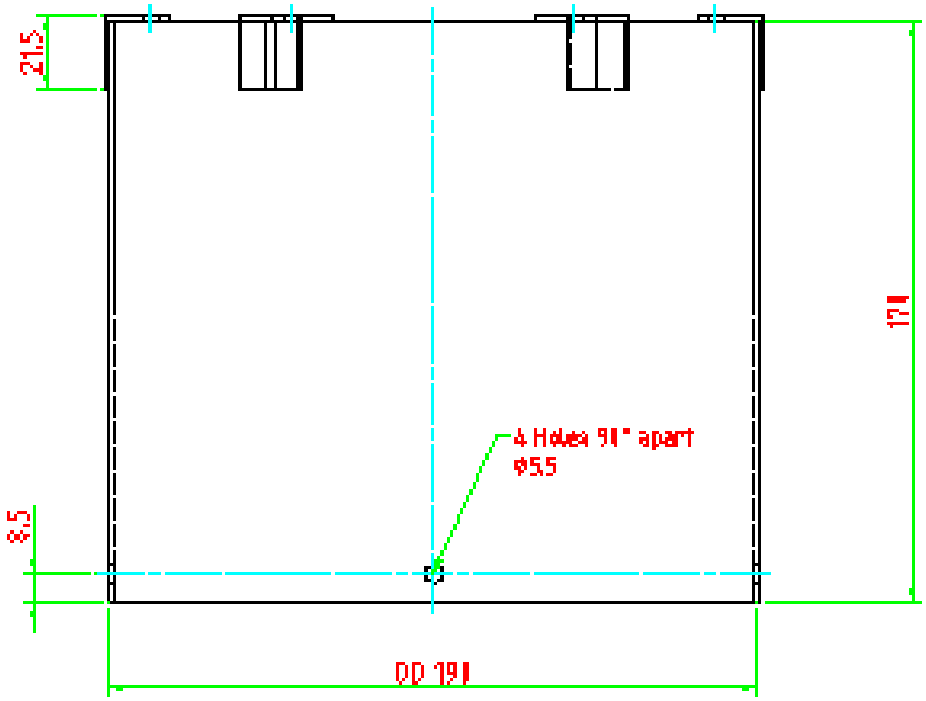

ITEM 4 SCALE 1:2

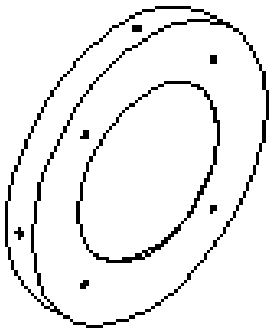

Use 15mm Plate

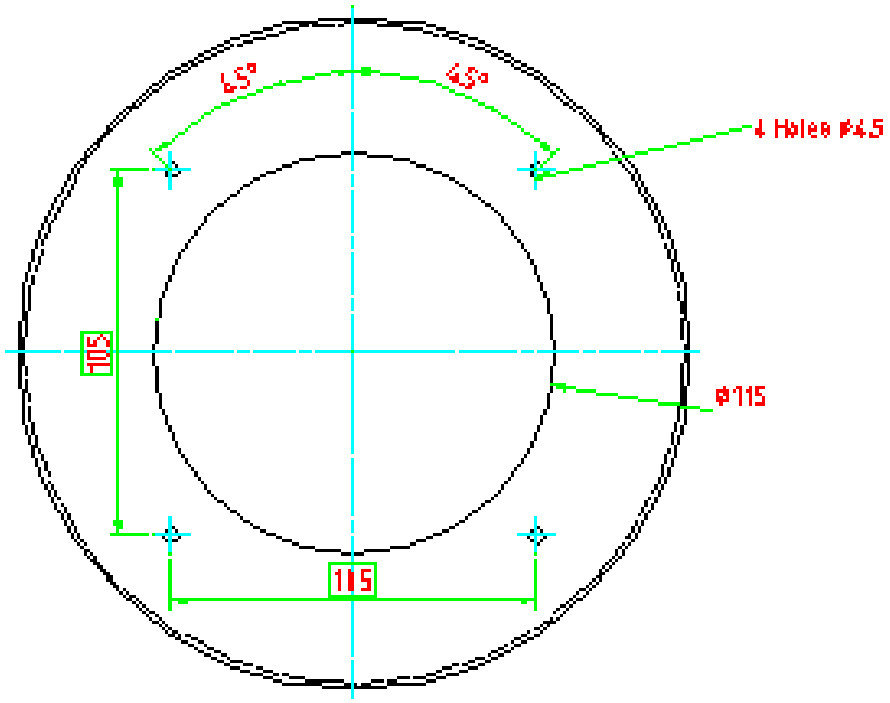

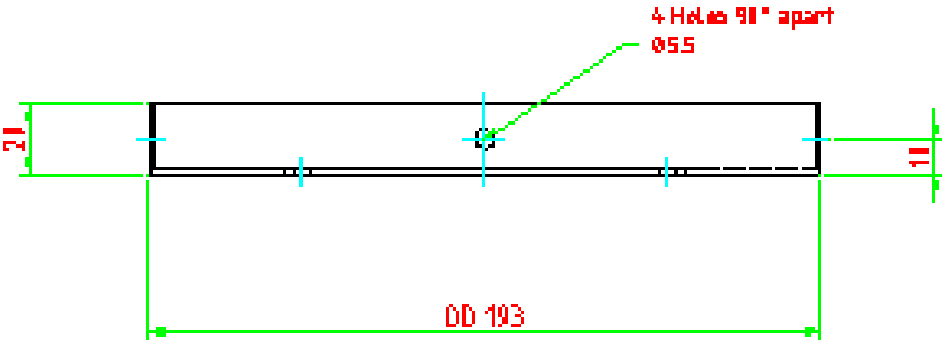

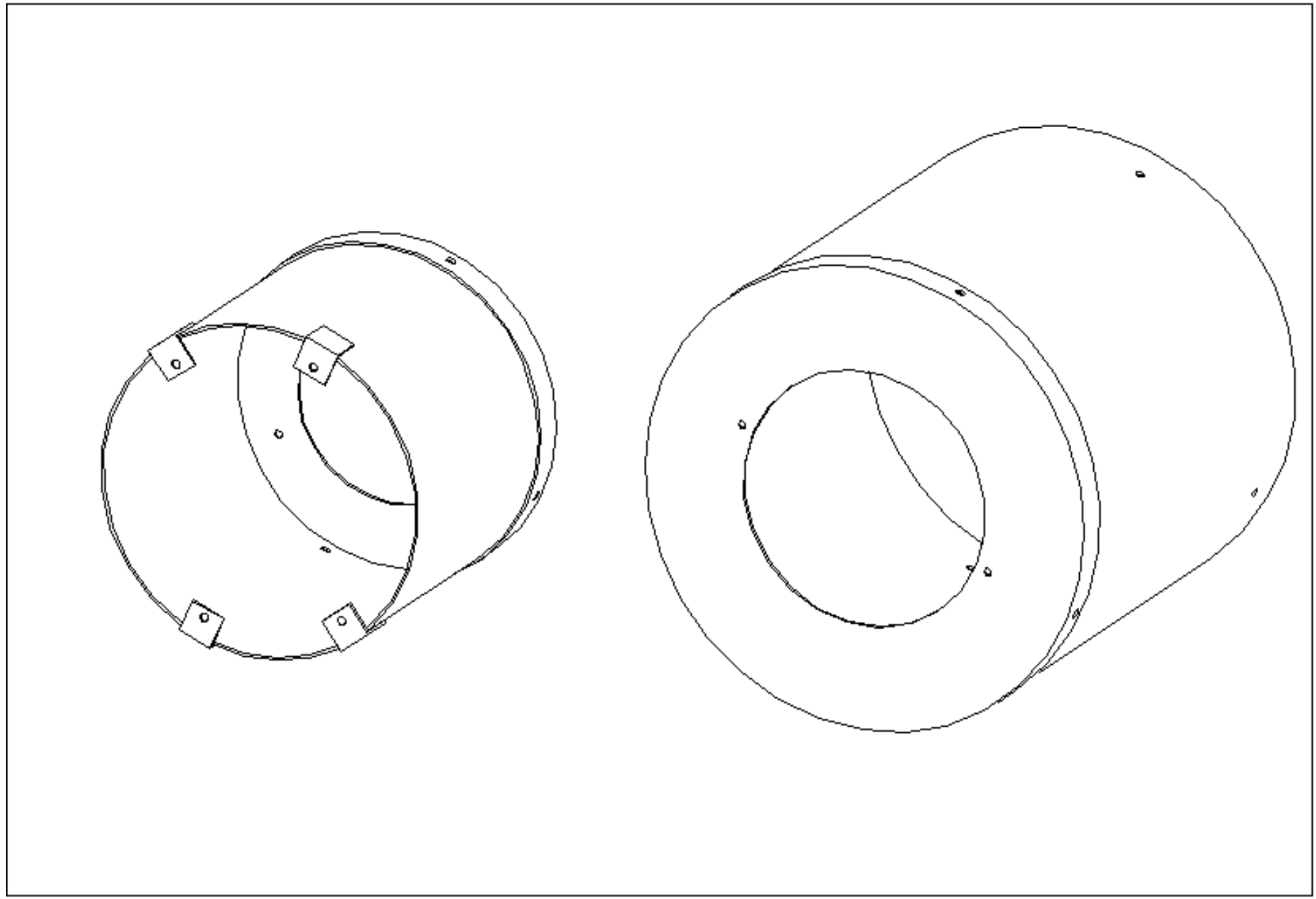

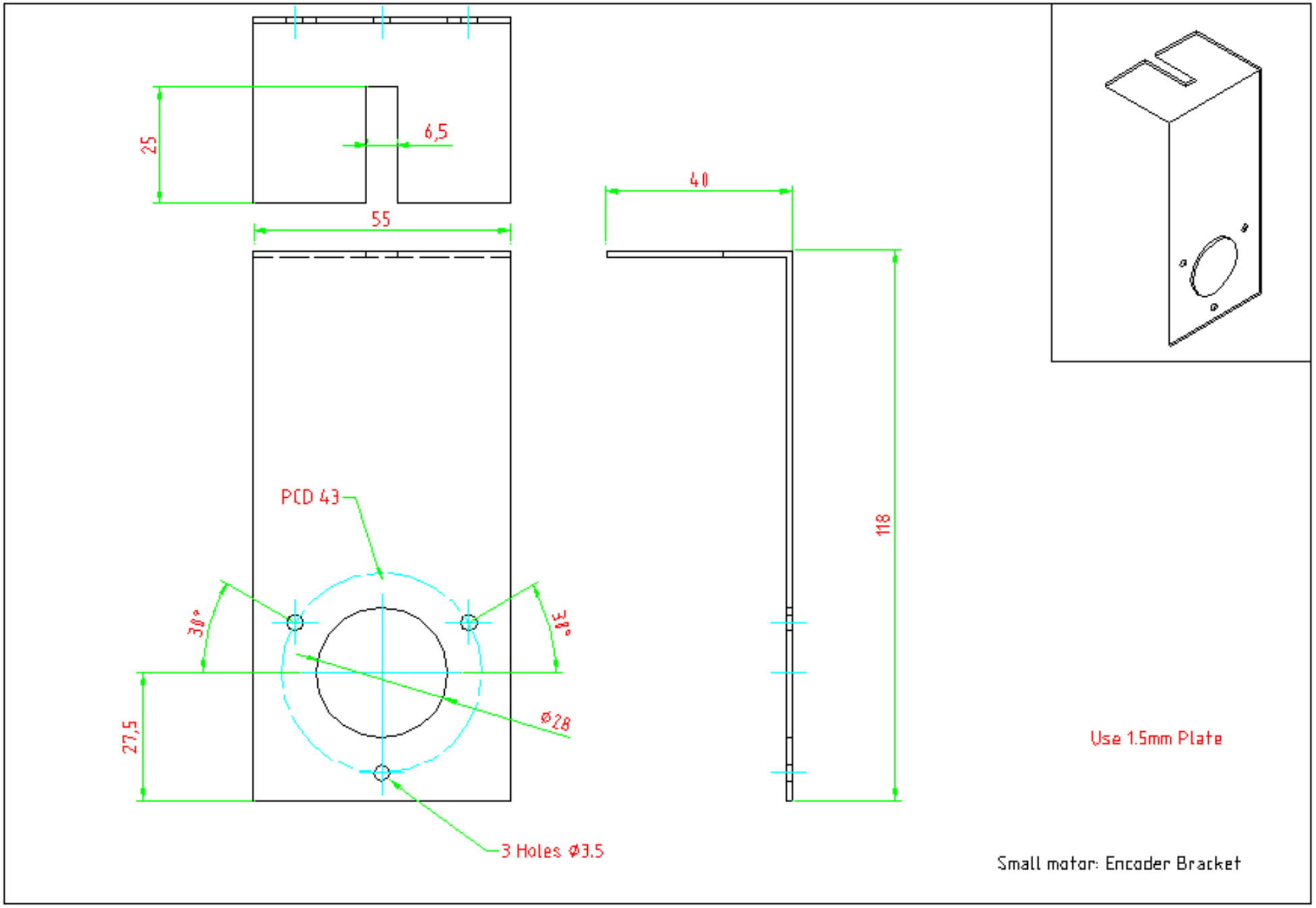
25
6,5
55
40
118
PCD 43
30°
30°
Ø28
27,5
3 Holes Ø3.5
Use 1.5mm Plate
Small motor: Encoder Bracket

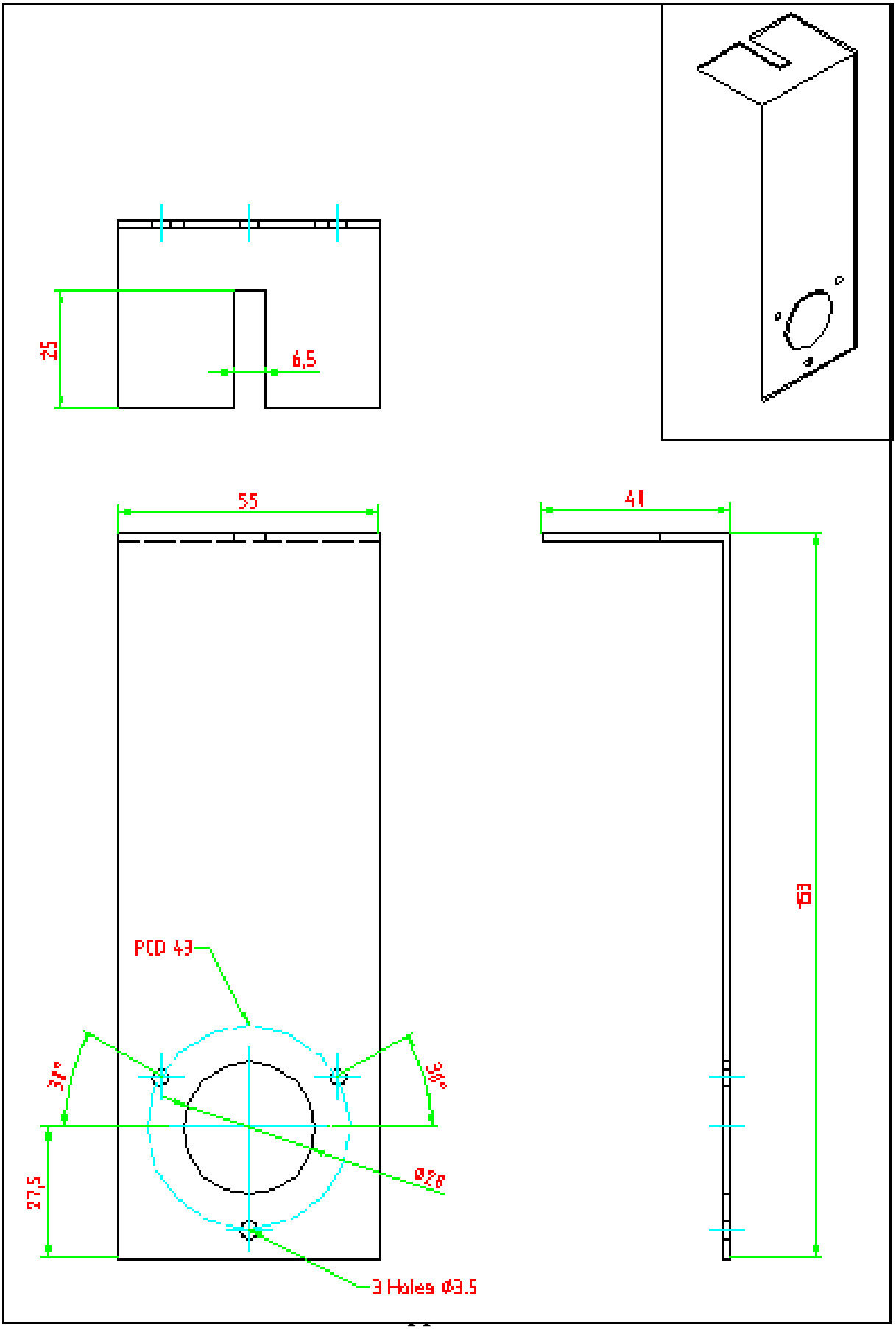
25
6.5
55
41
63
PCD 43
30°
30°
27.5
Ø26
3 Holes Ø3.5

In Combination with Chapter 4

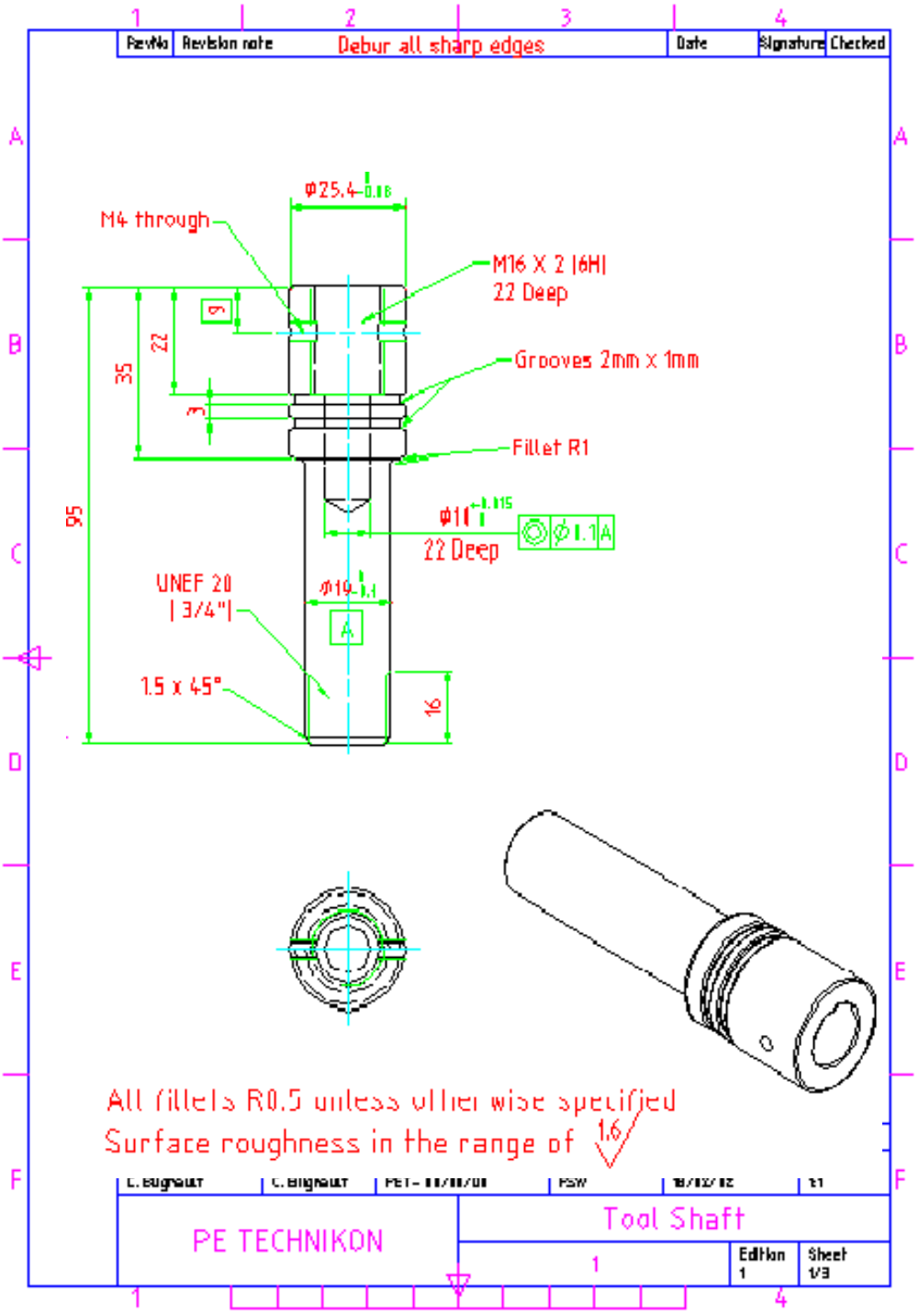
Rev.No
Revision note
Debur all sharp edges
Date
Signature
Checked
M4 through
M16 X 2 (6H)
22 Deep
Grooves 2mm X 1mm
Fillet R1
22 Deep
UNEF 20
(3/4")
1.5 x 45°
All fillets R0.5 unless other wise specified
Surface roughness in the range of
PE TECHNIKON
Tool Shaft
Edition
Sheet

Rev.No	Revision note		Date	Signature	Checked
		Debur all sharp edges			

All fillets R0.5 unless otherwise specified

Surface roughness in the range of 1.6

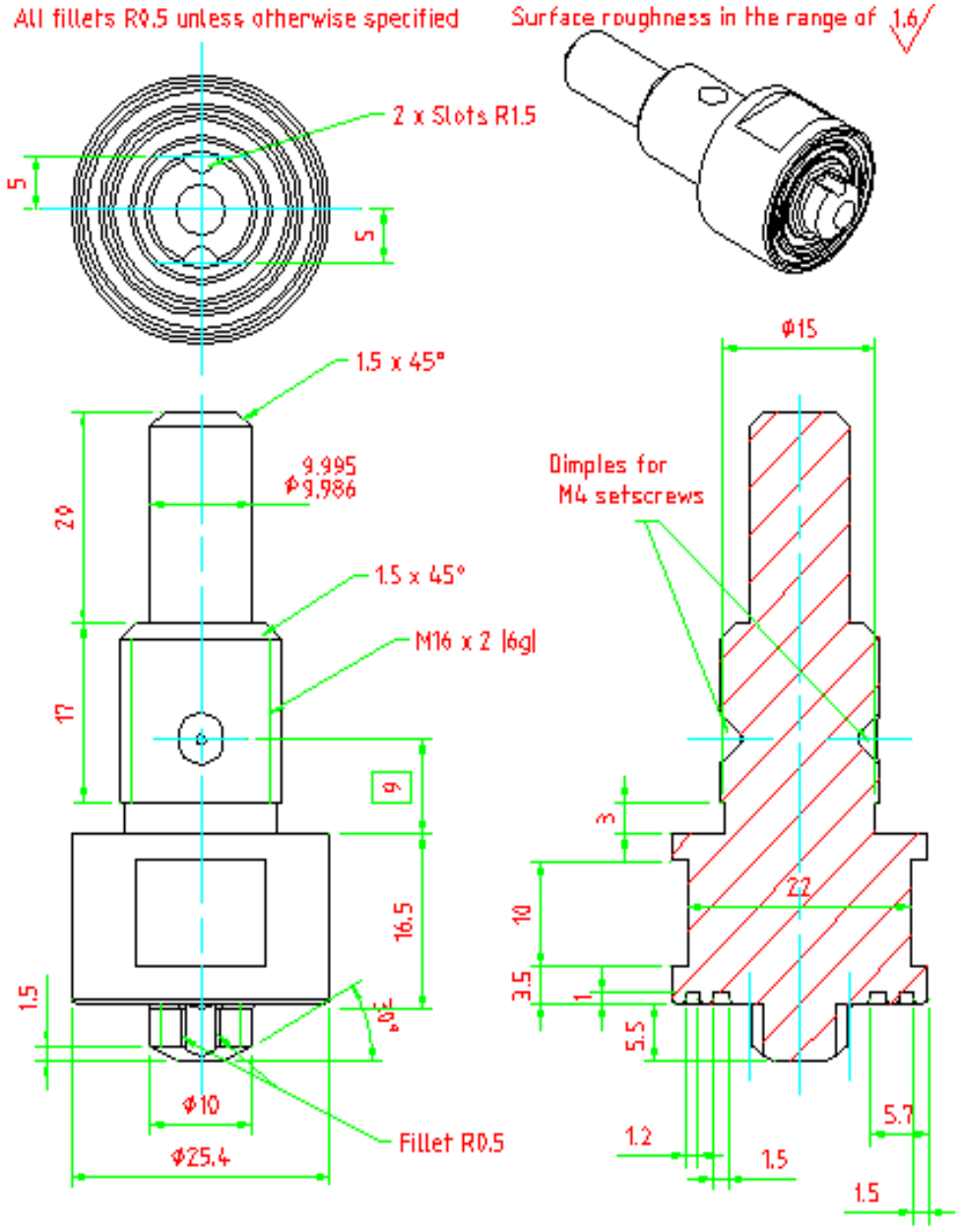

Item ref	Quantity	Title/Name, designation, material, dimension etc				Article No./Reference	
	1	MTR: W302 (H13) tool steel					
Designed by C Bilgneult		Checked by C Bilgneult	Approved by - date PET- 11/11/11	File name FSW		Date 16/12/12	Scale 2:1
PE TECHNIKON		Tool Tip					
			1			Edition 1	Sheet 2/3

Revision	Revision note		Date	Signature	Checked

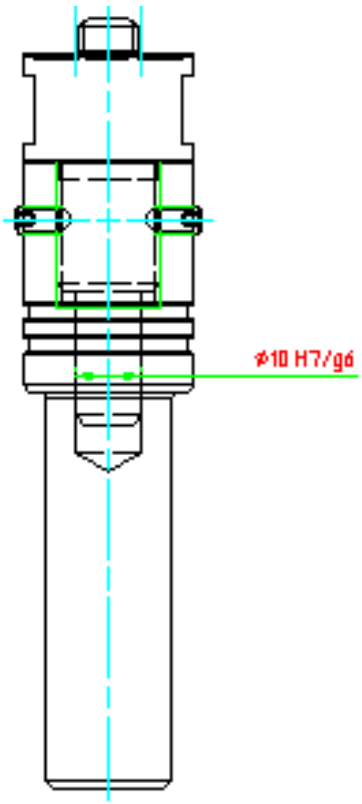

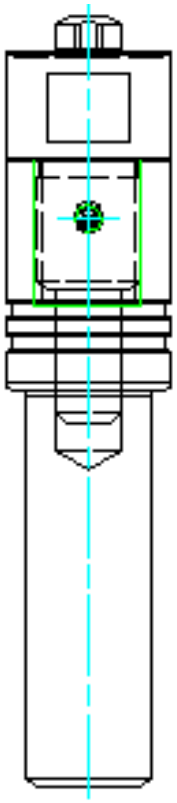

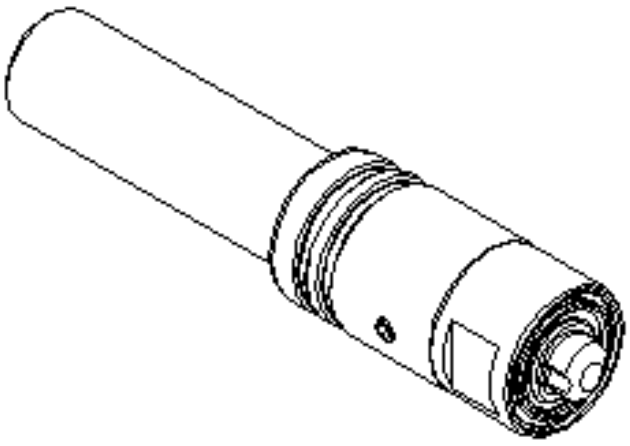

External threads not shown !
Setscrews indicated: M4 x 8

Item ref	Quantity	Title/Name, designation, material, dimension etc			Article No./Reference	
	1	MTR: W302 (H13) tool steel				
Designed by C. Bilgeri IT		Checked by C. Bilgeri IT	Approved by – date PET - 00/00/00	File name FSW	Date 18/12/12	Scale 1 : 1

PE TECHNIKON

Assembly

	Edition	Sheet
1	1	3/9

RevNo	Revision note		Date	Signature	Checked
		Debur all sharp edges			

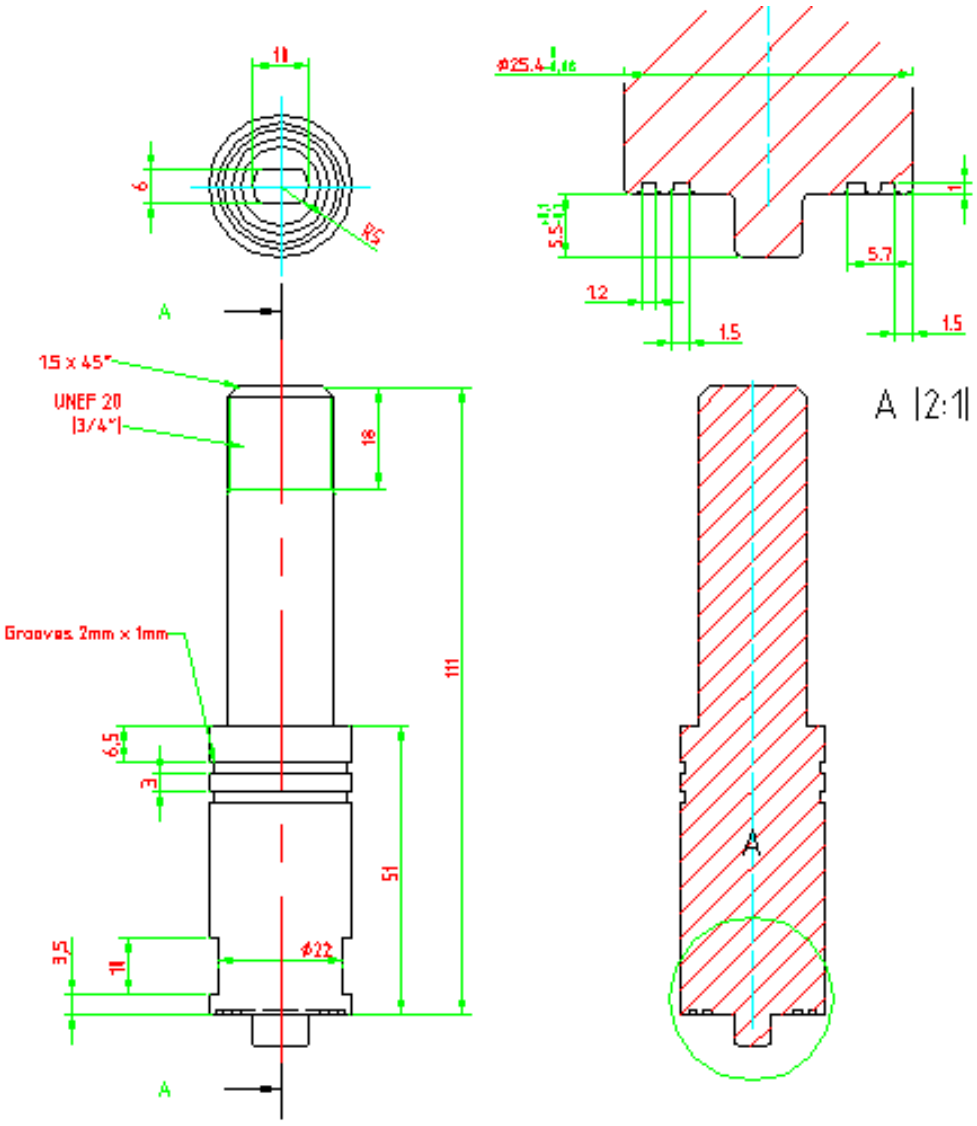

All fillets R0.5 unless otherwise specified

Surface roughness in the range of 1.6

	1	MTR: W312 (H13) tool steel				
Itemref	Quantity	Title/Name, designation, material, dimension etc			Article No./Reference	
Designed by C Bilgrout		Checked by C Bilgrout	Approved by - date PET- 00/00/00	File name PSW	Date 22/05/12	Scale 1:1
PE TECHNIKON		Tool Shaft				
		1			Edition 1	Sheet 1/1

RevNo

Checked

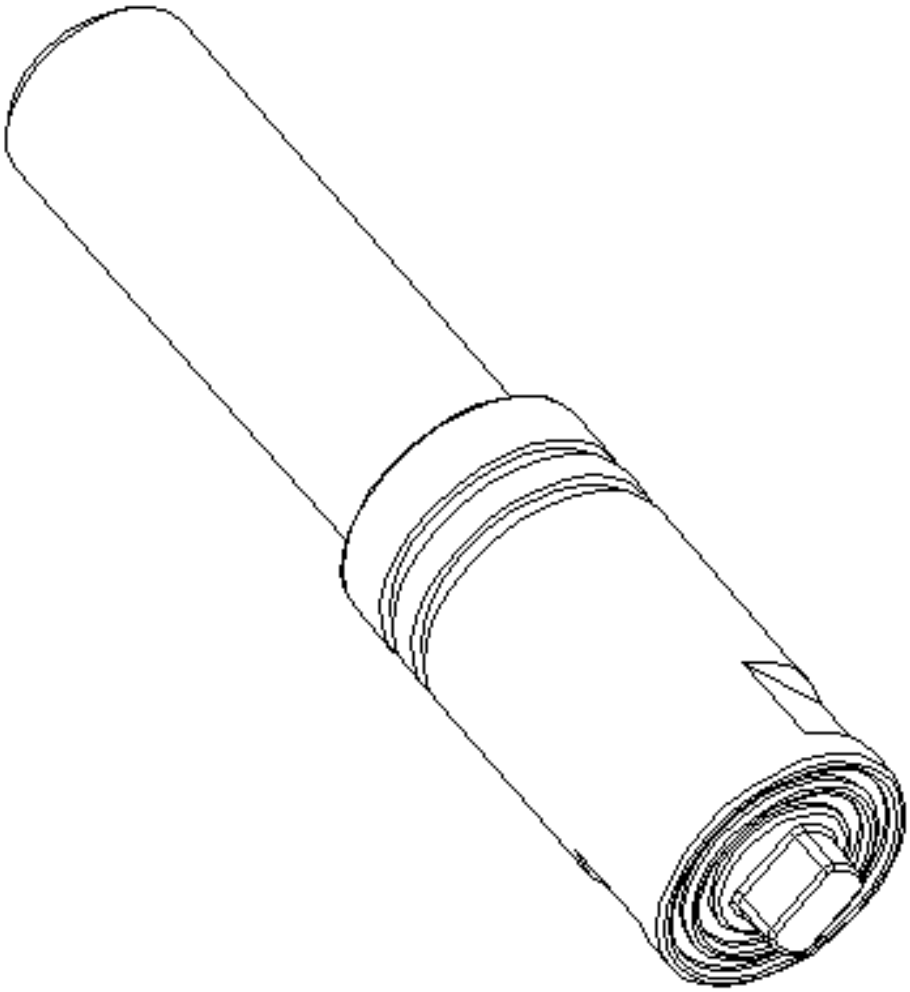

External threads not shown !

Itemref	Quantity	Title/Name, designation, material, dimension etc			Article No./Reference	
Designed by C. Bignault		Checked by C. Bignault	Approved by - date PET- 11/01/11	File name FSW	Date 22/15/12	Scale 2 : 1
PE TECHNIKON		Tool Tip				
		1			Edition 1	Sheet 2/2

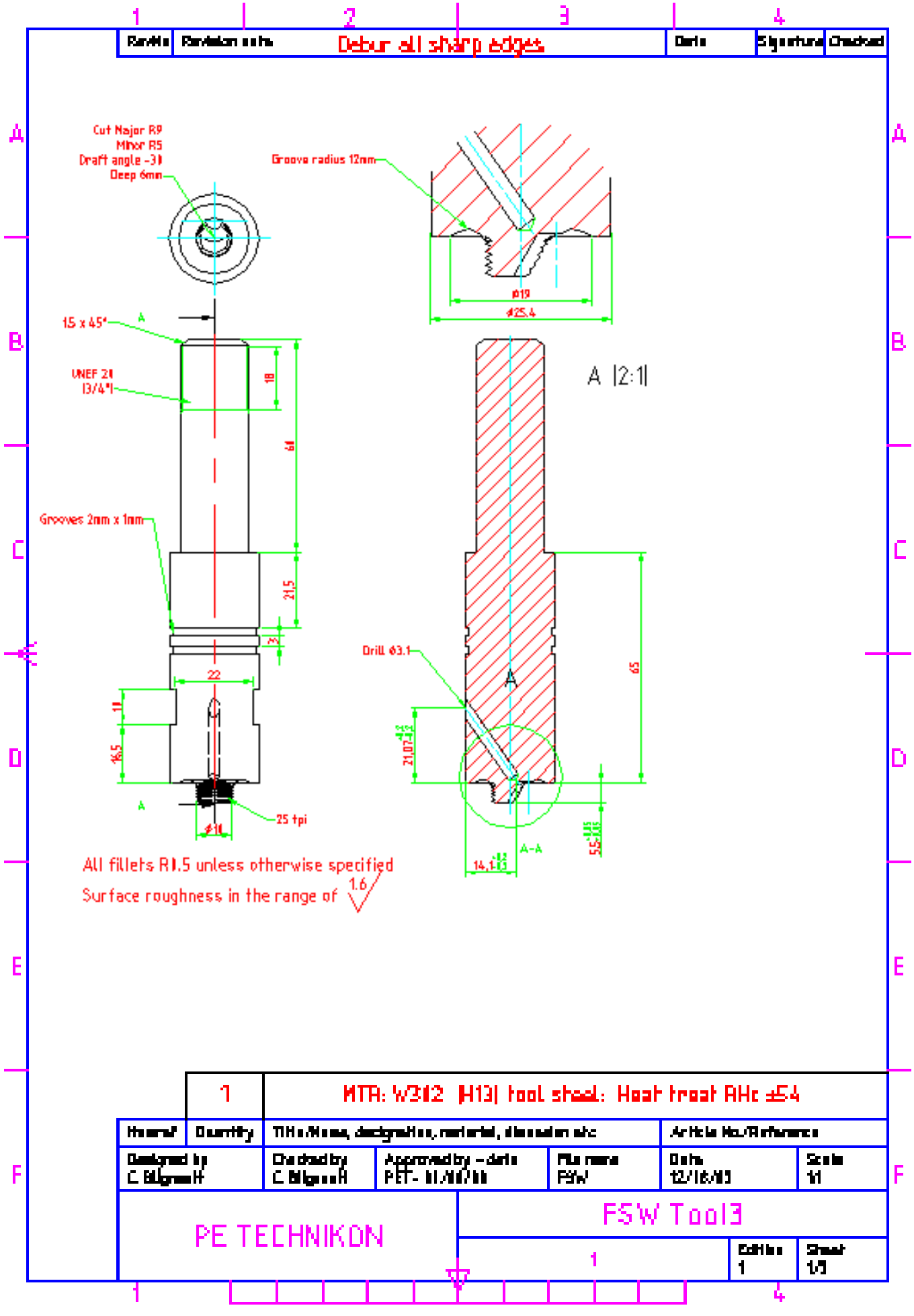
Deburr all sharp edges
Cut Major R9
Minor R5
Draft angle -3°
Deep 6mm
Groove radius 12mm
15 x 45°
UNEF 20
13/4"
Grooves 2mm x 1mm
25 tpi
A |2:1|
Drill ø3.1
All fillets R1.5 unless otherwise specified
Surface roughness in the range of 1.6
MTR: W302 |H13| tool steel: Heat treat RHc ±54
FSW Tool3
PE TECHNIKON

RevNo	Revision note	Debur all sharp edges	Date	Signature	Checked

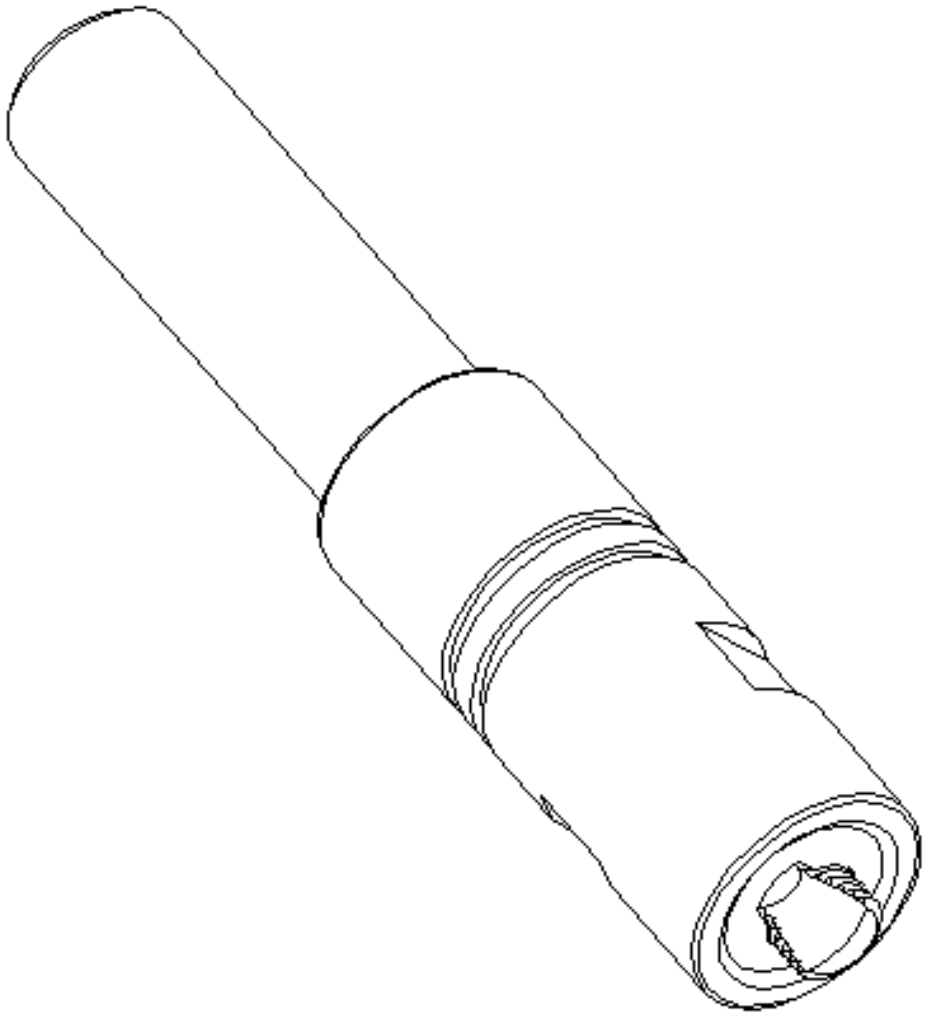

All fillets R0.5 unless otherwise specified

Surface roughness in the range of 1.6

	1	MTR: W302 (H13) tool steel : Heat treat RHc ± 54				
Item ref	Quantity	Title/Name, designation, material, dimension etc			Article No./Reference	
Designed by C. Blignaut		Checked by C. Blignaut	Approved by - date PET- 00/00/00	File name FSW	Date 12/03/02	Scale 1:1
PE TECHNIKON		FSW Tool3				
		1			Edition 1	Sheet 1/2

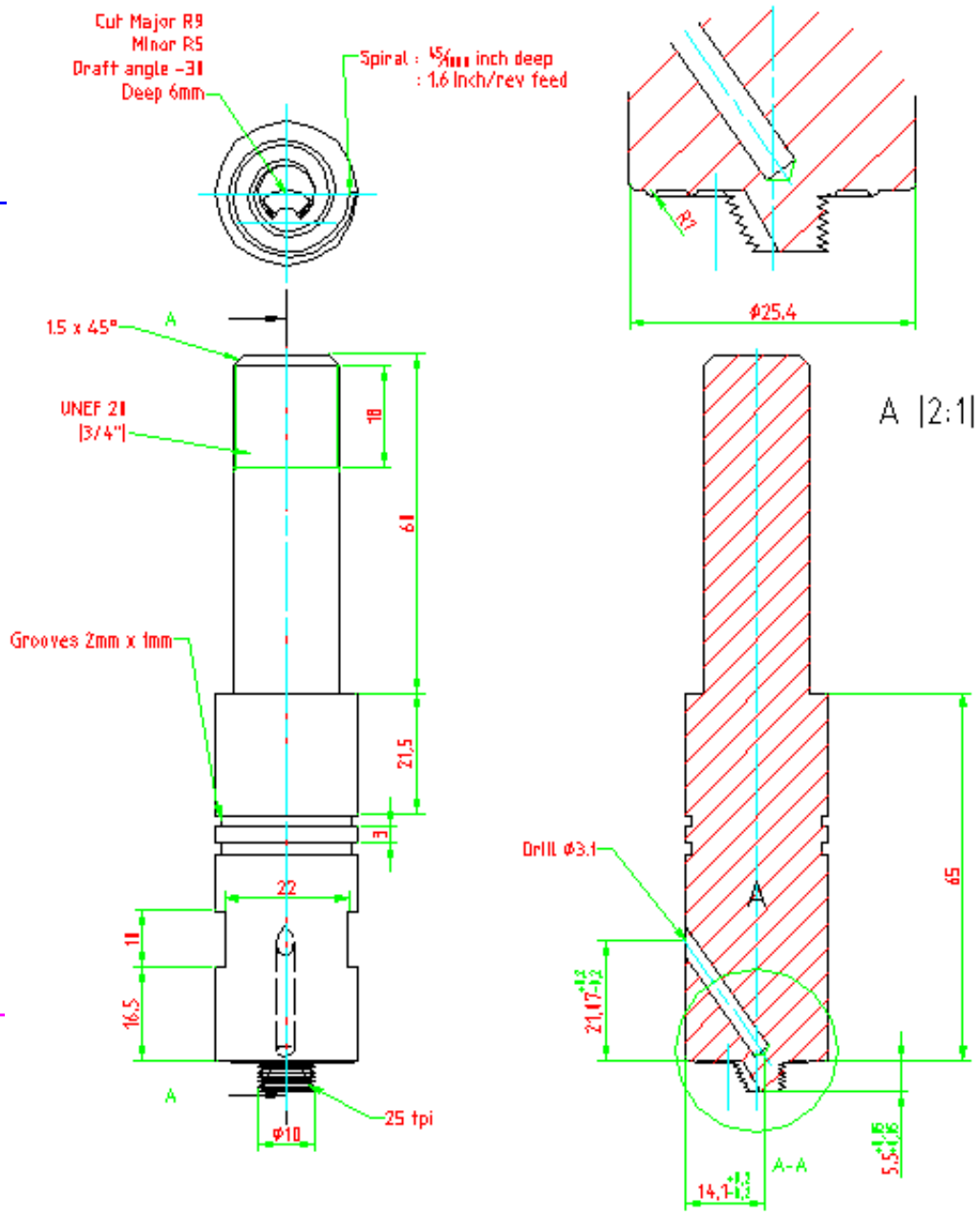

External shaft threads not shown !

Itemref	Quantity	Title/Name, designation, material, dimension etc			Article No./Reference	
Designed by C. Blignault		Checked by C. Blignault	Approved by - date PET- 00/00/00	File name FSW	Date 12/08/12	Scale 2 : 1
PE TECHNIKON		Overall View				
		1			Edition 1	Sheet 2/2

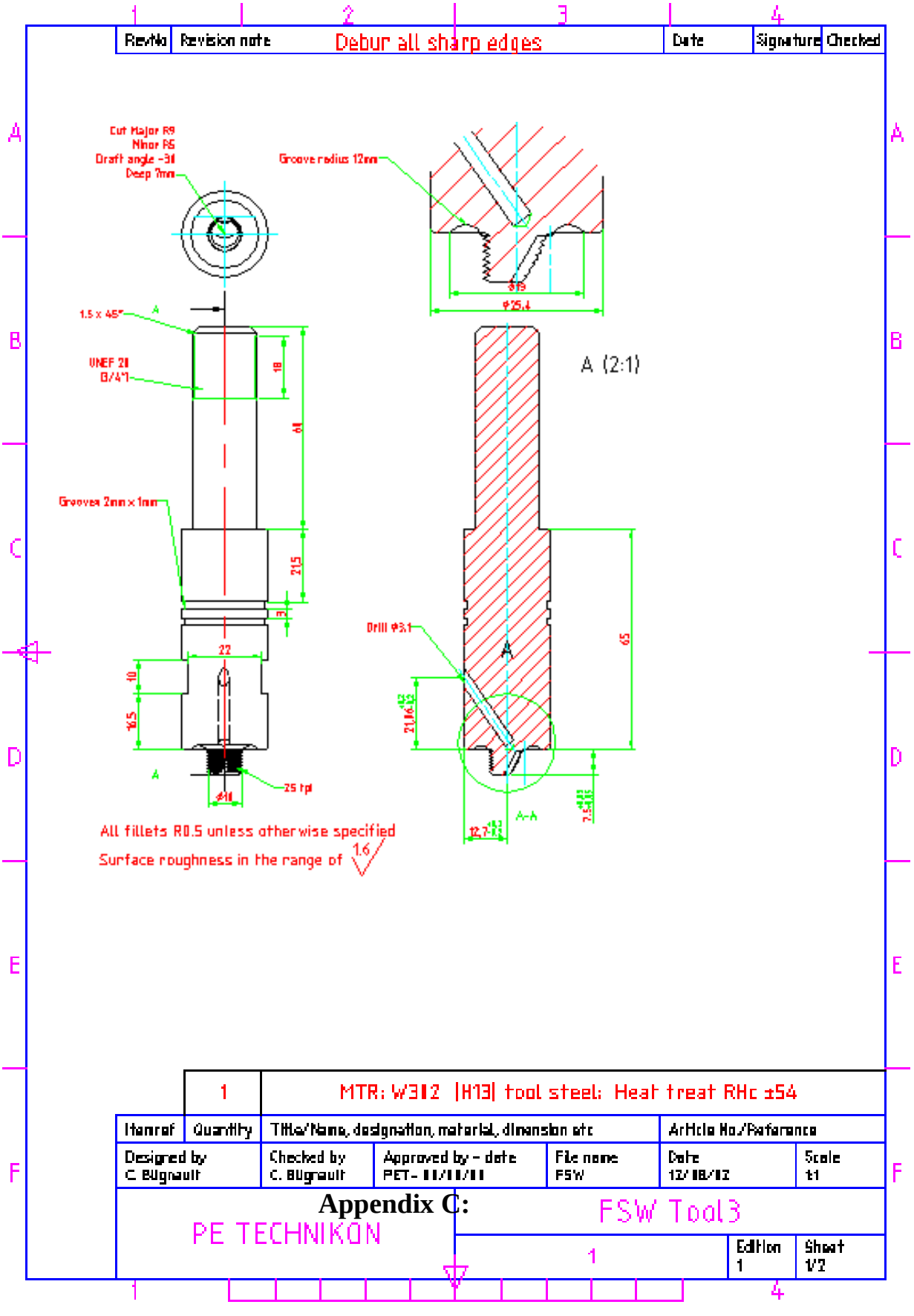
Rev/No
Revision note
Debur all sharp edges
Date
Signature
Checked
Cut Major R9
Minor R5
Draft angle -3°
Deep 7mm
Groove radius 12mm
1.5 x 45°
UNEF 2B
8/47"
Groove 2mm x 1mm
Drill Ø3.1
A (2:1)
A-A
All fillets R0.5 unless otherwise specified
Surface roughness in the range of 1.6
25 tpi
MTR: W302 (H13) tool steel: Heat treat RHc ±54
Item ref
Quantity
Title/Name, designation, material, dimension etc
Article No./Reference
Designed by
C. Bugnault
Checked by
C. Bugnault
Approved by - date
PET- 00/00/00
File name
FSW
Date
12/08/02
Scale
1:1
PE TECHNIKON
FSW Tool3
Edition
1
Sheet
1/2

Appendix C:

In Combination with Chapter 5

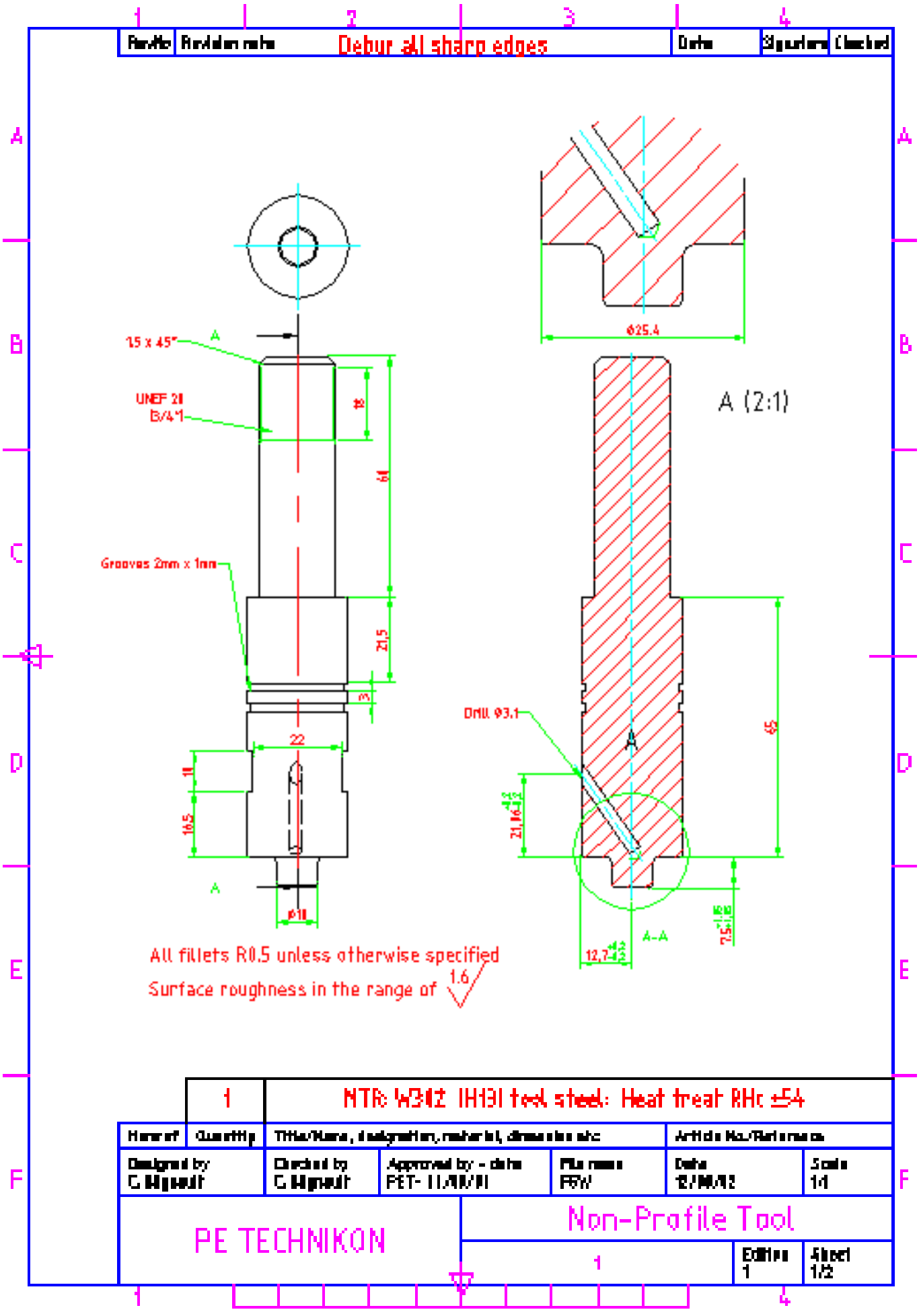
Rev.No
Revision note
Debur all sharp edges
Date
Signature
Checked
15 x 45°
A
UNEF 2B
5/8"-11
18
61
Grooves 2mm x 1mm
21,5
3
22
11
16,5
A
ø11
ø25.4
A (2:1)
Drill ø3.1
65
21,16
A-A
12,7
All fillets R0.5 unless otherwise specified
Surface roughness in the range of 1.6
1
NTR: W302 (H13) tool steel: Heat treat RHc ±54
Item ref
Quantity
Title/Name, designation, material, dimensions etc
Article No./Reference no.
Designed by
C. Mignault
Checked by
C. Mignault
Approved by - date
PET- 11/08/11
File name
PRW
Date
12/08/12
Scale
1:1
PE TECHNIKON
Non-Profile Tool
1
Edition
1
Sheet
1/2

Mark	Revision note	Deburr all sharp edges	Date	Signature	Checked

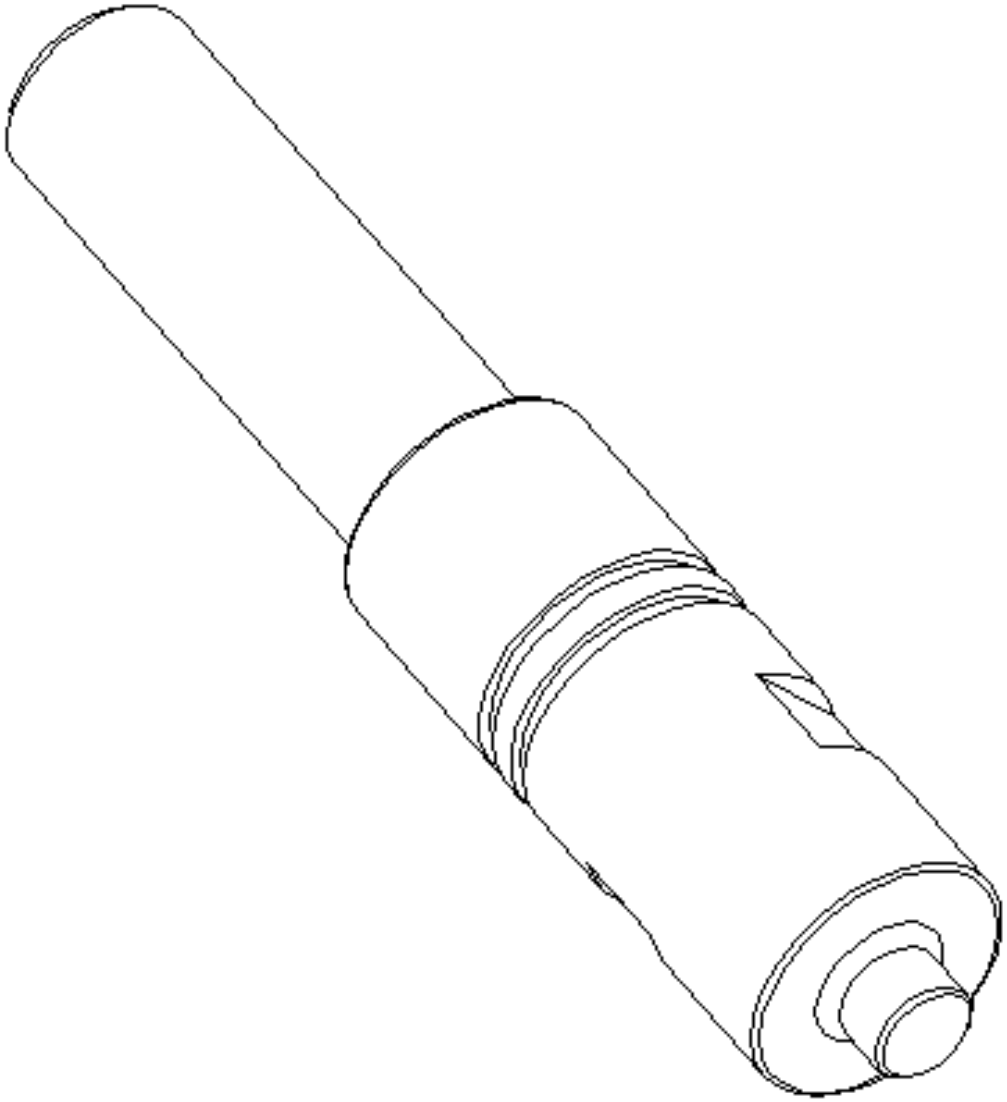

External threads not shown !

Itemref	Quantity	Title/Name, designation, material, dimension etc			Article No./Reference	
Designed by C. Bügnault		Checked by C. Bügnault	Approved by - date PET- 11/11/11	File name PSW	Date 12/08/12	Scale 2 : 1
PE TECHNIKON			Non-Profile Tool			
			1		Edition 1	Sheet 1/1

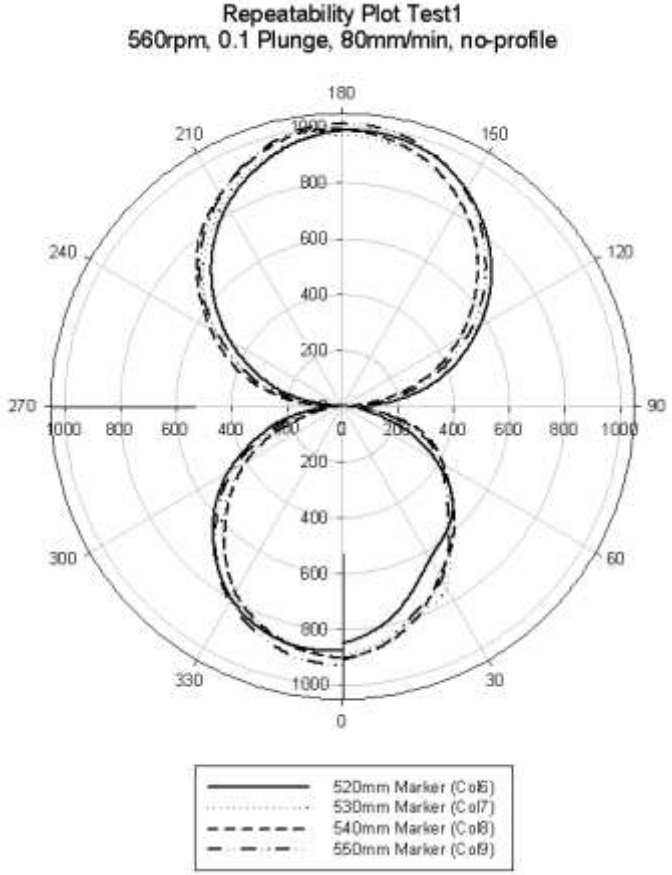
Repeatability Plot Test1
560rpm, 0.1 Plunge, 80mm/min, no-profile
520mm Marker (Col6)
530mm Marker (Col7)
540mm Marker (Col8)
550mm Marker (Col9)

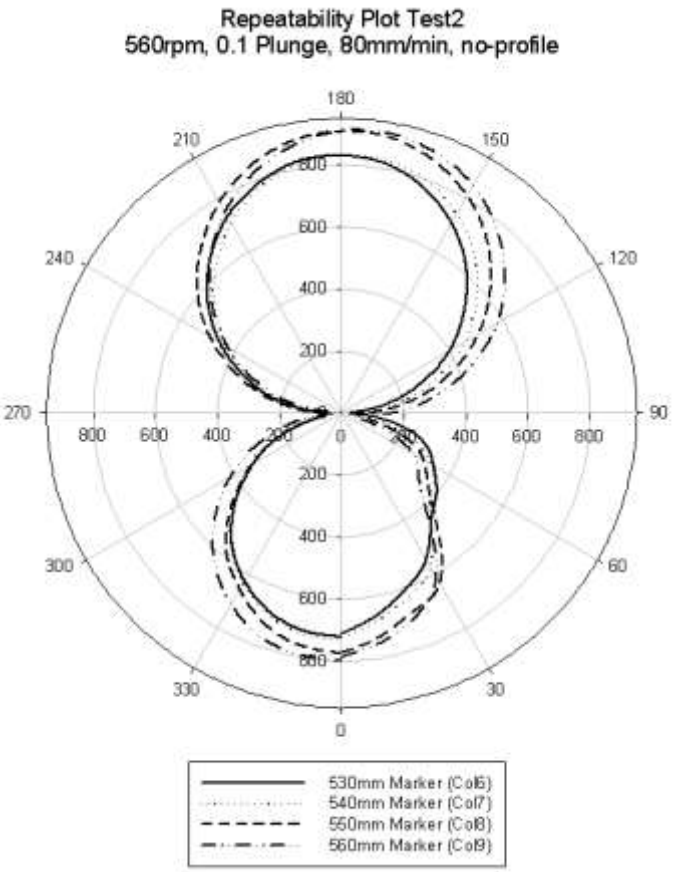
Repeatability Plot Test2
560rpm, 0.1 Plunge, 80mm/min, no-profile
530mm Marker (Col6)
540mm Marker (Col7)
550mm Marker (Col8)
560mm Marker (Col9)

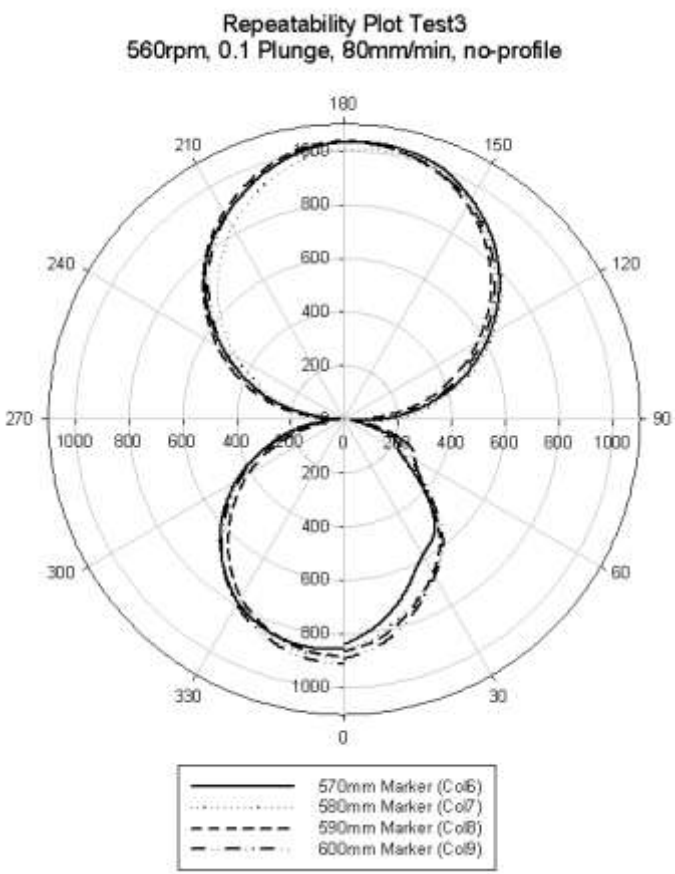
Repeatability Plot Test3
560rpm, 0.1 Plunge, 80mm/min, no-profile
570mm Marker (Col6)
580mm Marker (Col7)
590mm Marker (Col8)
600mm Marker (Col9)

Example of Sorted Weld Data Obtained - T2										
Feed X Position	440	450	460	470	480	490	500	510	520	530
Spindle Speed	537.5	495.1	484.1	477.6	472.2	457.4	443.5	427.3	421.7	417.6
Spindle Power	1812.7	5057.4	5072.7	5118.7	5166.2	5229	5279.8	5402.9	5438	5430.7
Spindle Torque	12.6	35.7	36.7	37.3	37.9	39.3	40.7	42.6	43.1	43.6
Spindle Current	4.8	13.3	13.3	13.4	13.5	13.7	13.9	14.3	14.3	14.3
Feedrate	8.1	96.4	96.6	96.7	96.7	96.7	96.7	96.7	96.7	67.8
Feed Power	100.1	543.8	542	543.6	543.7	545.5	544.1	548.2	544.9	409
Feed Torque	1.3	2	1.8	1.7	1.7	1.7	1.7	1.7	1.7	1.8
Feed Current	1.3	2.5	2.5	2.5	2.5	2.5	2.5	2.6	2.5	2.6
Tool Temperature	149.6	374.3	399.2	419	434.6	448.2	460.4	470.4	479.7	488.6
Tool Fx/Fy	1.2	4.2	3.7	2.7	2.37	2.48	2.78	2.31	2.38	1.89
Tool Fz	-2.9	-16.9	-16.9	-17.5	-18.6	-19.4	-19.5	-19.5	-19.6	-19.7
0	114.9	528.1	538.2	430.7	446.2	398	511.8	444.6	442.7	401.7
10	112.8	504.2	516.7	410.7	410.8	371.5	504.9	416.7	417.6	386.3
20	109.7	450.1	483	364.4	358.8	327.4	484.9	367.3	366.1	346.3
30	105.3	356	405.5	301.5	301.5	271	458.1	314.7	309.6	297.5
40	101.4	256.5	318.9	240.2	240.3	208.5	430	250.7	246.3	244
50	97.9	155.1	231.3	179.1	183.3	150	405.5	189.3	182.2	187.2
60	95.1	53.5	144.8	118	128.1	94.5	385.1	126.3	118.4	133.2
70	92.9	43.5	58.3	61.8	74.1	40.3	343.3	64.7	58.6	82.5
80	91.8	134.1	26.3	11.2	27.7	6.3	291.2	12.1	5.2	36.3
90	91.4	217.4	104.4	32.1	13.4	48.2	238	35.3	38.5	3.5
100	91.8	288.9	174.9	67.3	48.7	84	184	71.4	71.2	35.4
110	93.6	345	235.6	95.2	73.1	107.7	130.8	97.2	95.2	57.7
120	96.2	383.2	282.9	112.4	88.3	122.4	80	111.1	108.4	70.6
130	99.4	405.9	315.6	118.2	90.5	125.8	32.8	114.1	109.4	73.4
140	103.6	411.2	335.1	114.1	84.2	116.6	9.4	106.1	99.3	65.3
150	108.3	396.5	336.6	98.8	68.9	98.6	44.8	86.1	79.7	49.9
160	113.6	366.5	323.3	72.7	42.2	70.5	67.5	57.6	53.2	26.6
170	119	320.6	297.1	39.7	9.9	34.2	81.6	20.9	15.3	4.2
180	124.3	259	254.8	0.3	29.1	7.2	86.6	22.4	26.7	42.3
190	129.5	186.4	201.3	47	76.8	54.4	80.4	70.8	73.1	83.7
200	134.3	104.3	139.2	97.8	125.7	105.1	64.9	124.1	127.2	128.9
210	138.6	11.8	67.9	152.4	178.8	159.9	41.7	180.1	181.1	178.3
220	142.1	81.9	10.1	211.2	237	216.6	11.6	235.4	236.3	225.4
230	144.9	178	90.5	269.3	291.5	271.9	25.6	291.6	292.3	273.1
240	146.8	277.3	172.2	326.9	344.7	325.7	67.4	345.1	344.7	320.1
250	148	371.7	255.7	382.3	397.3	376.3	113.6	392.3	395.9	362.8
260	148.3	458.7	333.6	431.5	441.5	421.8	161.9	437.4	440.7	403.7
270	147.9	540.1	406	475.4	481.6	461.3	211.2	474.3	479.8	438.8
280	146.9	611.7	475	512.9	514.8	492.5	261	504.6	513.3	468.2
290	145.3	668	532.9	540.7	537.8	516.2	310.1	528.6	539.8	492.7
300	142.5	709.1	580.9	560.1	554.5	532.2	355.3	542	556.3	508.1
310	139.4	737.3	617.5	570.8	561.5	537.8	396	546.1	563.7	515.3
320	135.9	747.3	633.1	570.1	559.2	536.8	432.6	541.2	563.2	516
330	132	739.3	638.1	562.2	548.7	527.1	461.7	528.7	552.5	508.9
340	128	717.5	627.6	542.3	528.4	504.9	485.2	499.4	528.7	490.2
350	124	683.1	602.3	522.2	502.5	477.9	502.2	464.6	502.7	471.7
360	114.9	528.1	538.2	430.7	446.2	398	509.5	444.6	442.7	401.7

Training Exemplars: design of experiments

Welding Parameters					Process conditions			
Test No	N (rpm)	F (mm/min)	D (mm)		Oxide Layer (P)	Tool type (Y)	Material thickness (s)	Dwell time (t)
1	300	40	0.1		P1	Y1	s1	t1
2	600	100	0.4		P1	Y1	s1	t1
3	400	60	0.4		P1	Y1	s2	t2
4	500	80	0.1		P1	Y1	s2	t2
5	300	80	0.4		P3	Y2	s1	t2
6	600	60	0.1		P3	Y2	s1	t2
7	400	100	0.1		P3	Y2	s2	t1
8	500	40	0.4		P3	Y2	s2	t1
9	500	100	0.2		P1	Y2	s1	t2
10	400	40	0.3		P1	Y2	s1	t2
11	600	80	0.3		P1	Y2	s2	t1
12	300	60	0.2		P1	Y2	s2	t1
13	500	60	0.3		P3	Y1	s1	t1
14	400	80	0.2		P3	Y1	s1	t1
15	600	40	0.2		P3	Y1	s2	t2
16	300	100	0.3		P3	Y1	s2	t2

FSW PROCESS DATA for welds made on 6mm and 8mm Aluminum 5083 H321 plate with tool tilt angle of 2.5 degrees.

Training Exemplars: design of experiments

	Welding Parameters				Process conditions			
Test No	Actual RPM [N]	Actual feed (mm/min) [f]	Actual Plunge (mm) [D]		Oxide Layer [P]	Tool type [Y]	Material thickness [s]	Dwell time [t]
1	300.1	38.4	0.14		P1	Y1	s1	t1
2	443.5	97.6	0.43		P1	Y1	s1	t1
3	400.3	57.6	0.38		P1	Y1	s2	t2
4	495.6	77.3	0.11		P1	Y1	s2	t2
5	300.4	77.2	0.28		P3	Y2	s1	t2
6	600.1	57.6	0.08		P3	Y2	s1	t2
7	400.2	95.4	0.12		P3	Y2	s2	t1
8	448.6	37.2	0.01		P3	Y2	s2	t1
9	500.3	96	0.11		P1	Y2	s1	t2
10	400	38.1	0.2		P1	Y2	s1	t2
11	406.2	76	0.16		P1	Y2	s2	t1
12	300	57.3	0.03		P1	Y2	s2	t1
13	500	57.7	0.34		P3	Y1	s1	t1
14	400.1	77.2	0.23		P3	Y1	s1	t1
15	481.1	38.2	0.22		P3	Y1	s2	t2
16	299.8	97.6	0.25		P3	Y1	s2	t2

Training Exemplars: Sensor measurements and Surface appearance

Test No	Spindle Power (W) [Ps]	Spindle Torque (N.m) [Ts]	Spindle Current (A) [Cs]	Feed Power (W) [Pf]	Feed Torque (N.m) [Tf]	Feed Current (A) [Cf]	Tool Temp (oC) [T]	Force X (N) [Fx]	Force Y (N) [Fy]	Fx / Fy [R]	Z-Force (kN) [Fz]	Surface Appearance
1	2432.20	33.90	8.50	240.00	1.30	2.60	461.30	582.20	276.50	2.10	-9.70	Good, Smooth
2	5279.80	40.70	13.90	544.10	1.70	2.50	460.40	511.80	184.00	2.78	-19.50	No flash, Good
3	3408.40	37.10	9.60	336.20	1.80	2.50	501.70	695.40	175.10	3.97	-18.10	Slight flash, Good
4	4325.30	35.60	11.20	442.90	1.70	2.60	477.40	728.50	202.20	3.60	-15.60	Slight flash, Good
5	2526.40	35.80	8.70	453.20	1.60	2.60	410.70	847.50	107.40	7.89	-13.20	Shoulder void, Good
6	3012.70	23.40	7.70	341.90	1.80	2.60	449.60	647.00	66.40	9.74	-13.40	Worm hole, Bad
7	4235.50	43.70	11.20	541.30	3.80	2.50	496.40	1891.30	166.50	11.40	-28.20	Very Bad
8	5187.60	39.30	13.60	219.70	3.10	2.40	477.40	1220.10	95.50	12.78	-19.80	Very Bad
9	4238.30	35.40	11.00	545.80	2.90	2.50	414.50	1210.00	132.90	9.10	-23.70	Major flash, worm hole
10	2595.10	29.50	7.60	234.00	1.80	2.60	496.40	949.80	153.00	6.21	-14.70	Little flash, worm hole
11	5582.40	46.60	14.70	435.90	3.60	2.50	449.60	1724.50	70.90	24.30	-25.00	Major worm hole, Good
12	3268.10	43.30	10.60	328.00	2.30	2.50	410.70	1482.30	223.80	6.62	-16.50	Major worm hole, Good
13	2808.00	26.30	7.20	335.90	1.60	2.50	489.00	580.50	211.30	2.75	-11.30	Shoulder void, Good
14	3358.50	36.60	9.50	441.80	1.60	2.50	472.70	485.10	288.20	1.68	-17.10	Good, no flash
15	4964.10	36.50	13.00	237.40	1.60	2.60	523.70	640.40	242.20	2.64	-15.60	Bad flash, Good profile
16	4521.00	55.50	13.40	547.10	1.70	2.60	456.70	602.40	154.80	3.89	-19.20	Perfect, Good

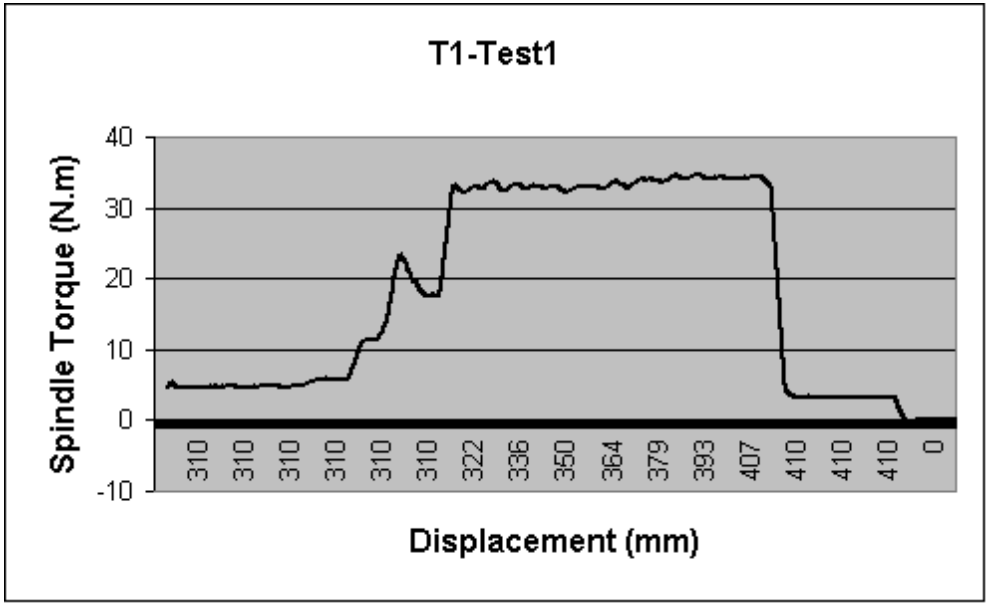
T1-Test1
Spindle Torque (N.m)
40
30
20
10
0
-10
310 310 310 310 310 310 322 336 350 364 379 393 407 410 410 410 0
Displacement (mm)

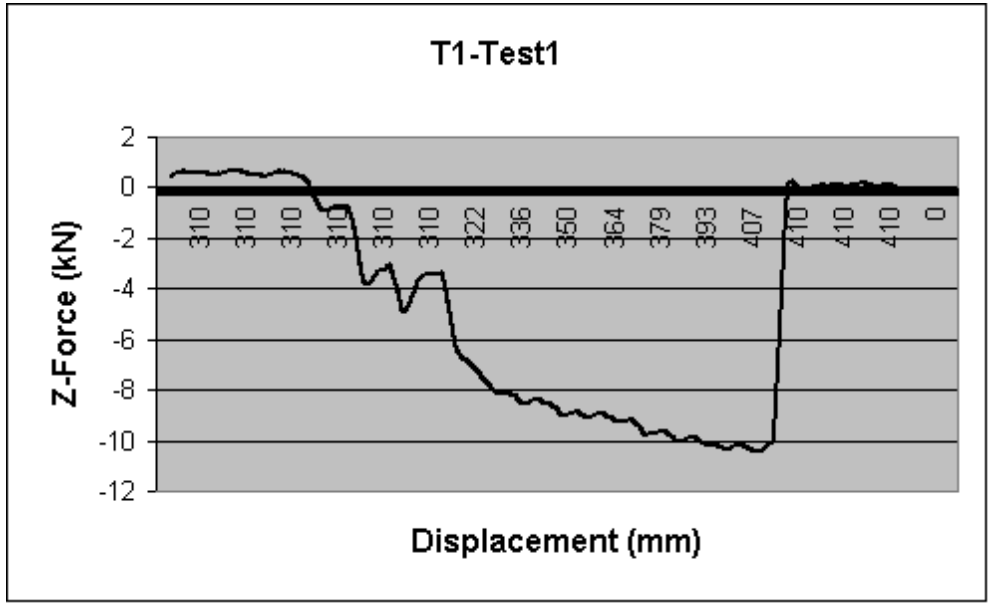
T1-Test1
Z-Force (kN)
2
0
-2
-4
-6
-8
-10
-12
310 310 310 310 310 310 322 336 350 364 379 393 407 410 410 410 0
Displacement (mm)

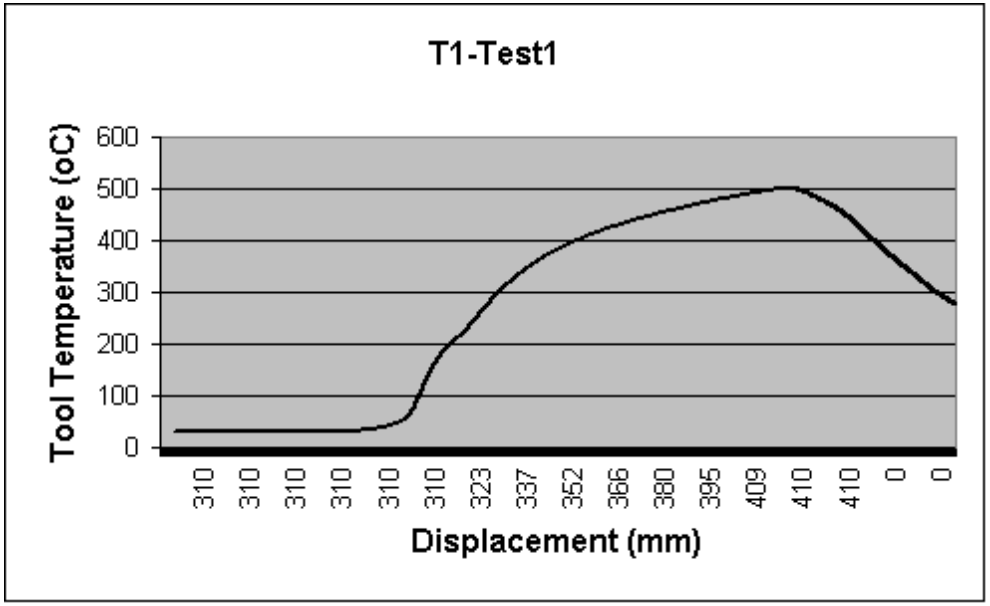
T1-Test1
Tool Temperature (oC)
600
500
400
300
200
100
0
310 310 310 310 310 310 323 337 352 366 380 395 409 410 410 0 0
Displacement (mm)

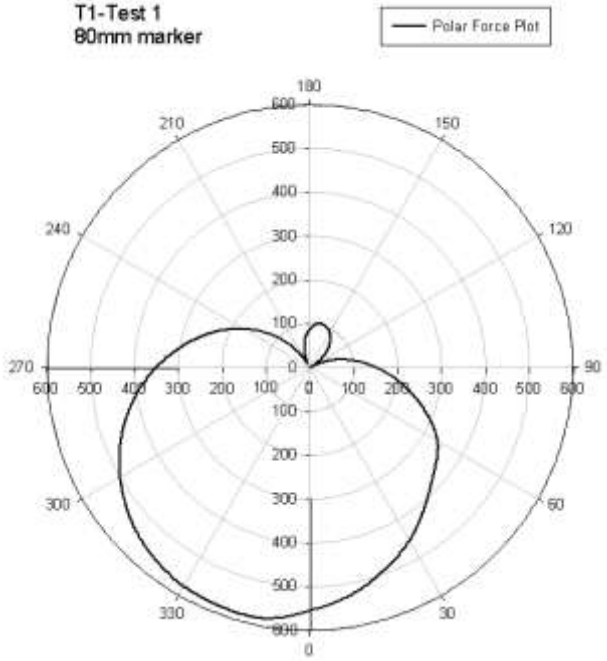
T1-Test 1
80mm marker
Polar Force Plot
180
150
120
90
60
30
0
210
240
270
300
330

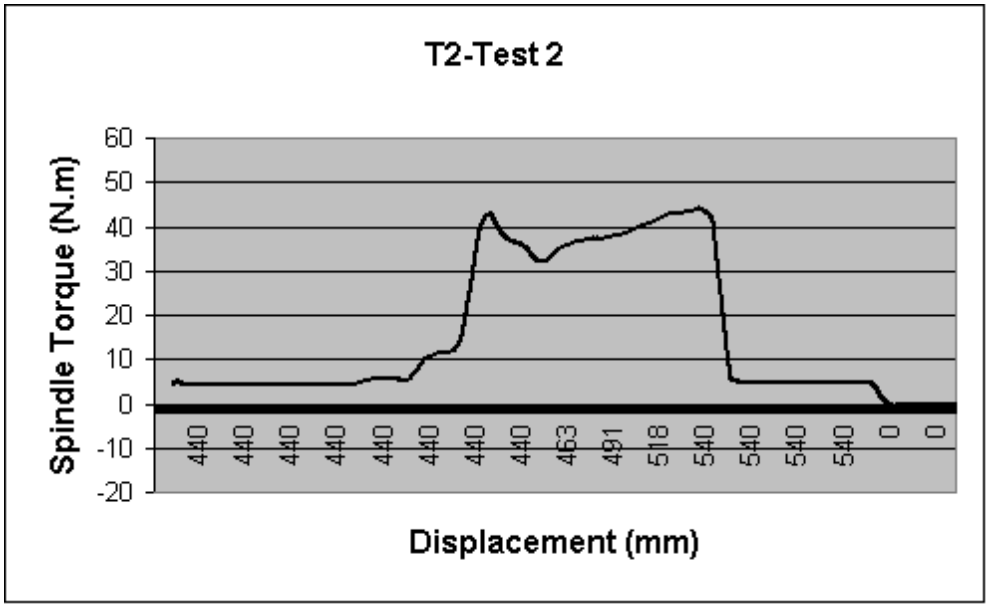
T2-Test 2
Spindle Torque (N.m)
60
50
40
30
20
10
0
-10
-20
440 440 440 440 440 440 440 440 463 491 518 540 540 540 540 0 0
Displacement (mm)

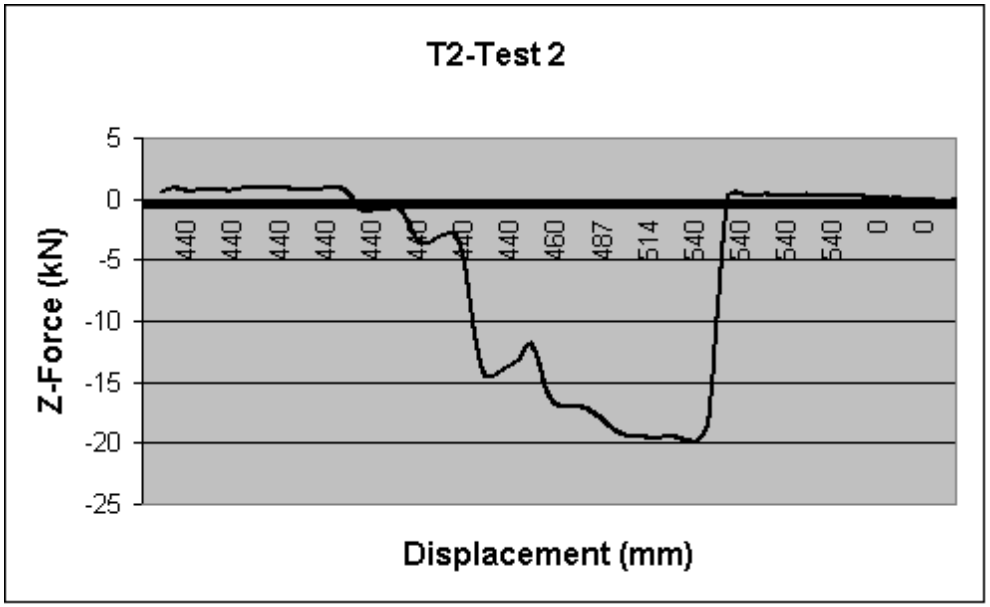
T2-Test 2
Z-Force (kN)
5
0
-5
-10
-15
-20
-25
440 440 440 440 440 440 440 440 460 487 514 540 540 540 540 0 0
Displacement (mm)

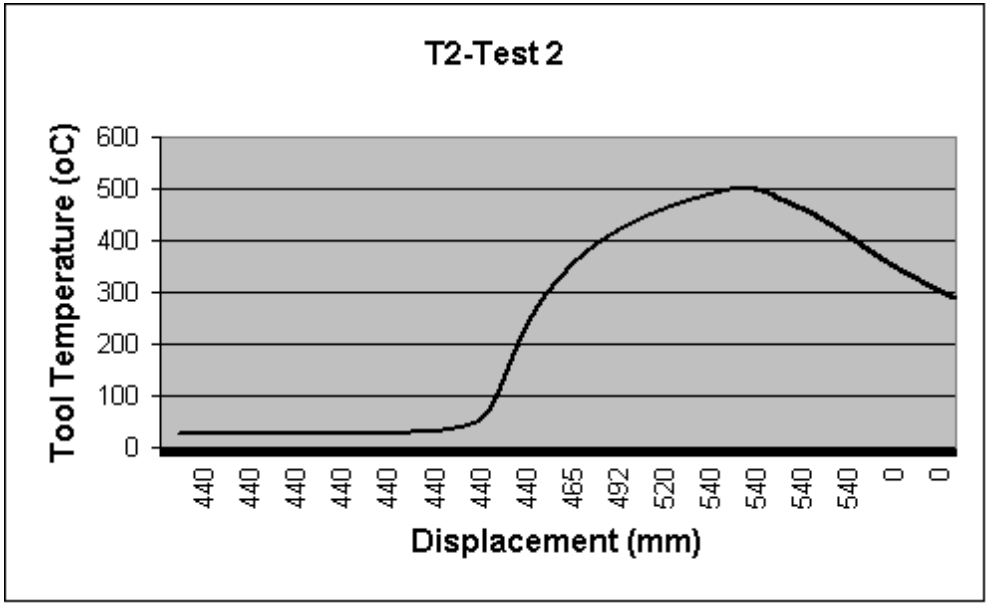
T2-Test 2
Tool Temperature (oC)
600
500
400
300
200
100
0
440 440 440 440 440 440 440 440 465 492 520 540 540 540 540 0 0
Displacement (mm)

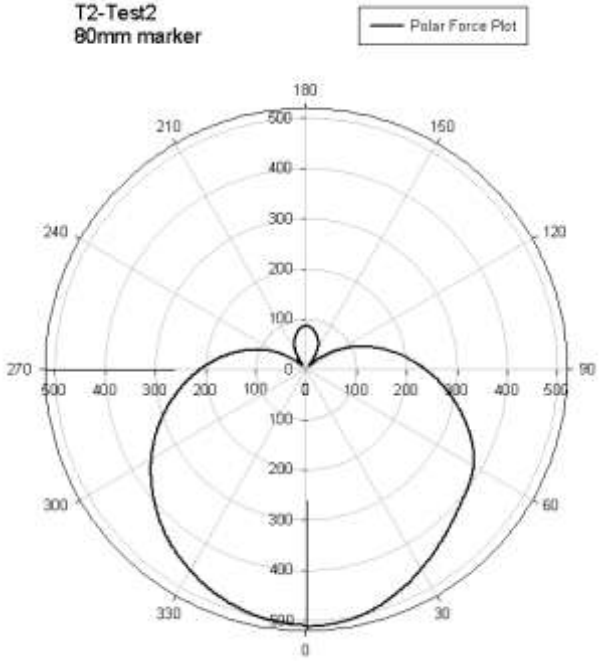
T2-Test2
80mm marker
Polar Force Plot
180
150
120
90
60
30
0
330
300
270
240
210
500
400
300
200
100
0

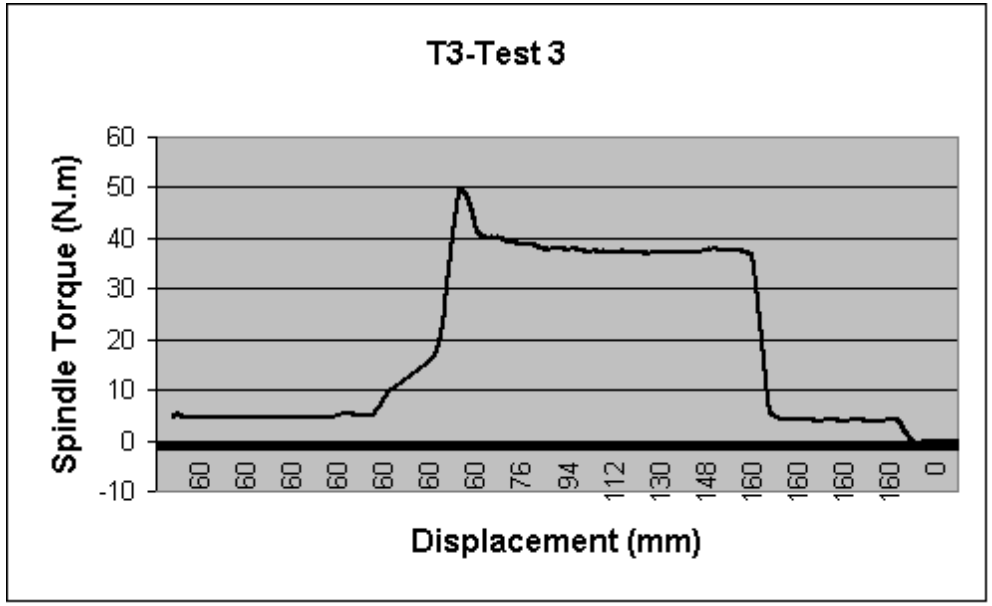
T3-Test 3
Spindle Torque (N.m)
60
50
40
30
20
10
0
-10
60 60 60 60 60 60 60 76 94 112 130 148 160 160 160 160 0
Displacement (mm)

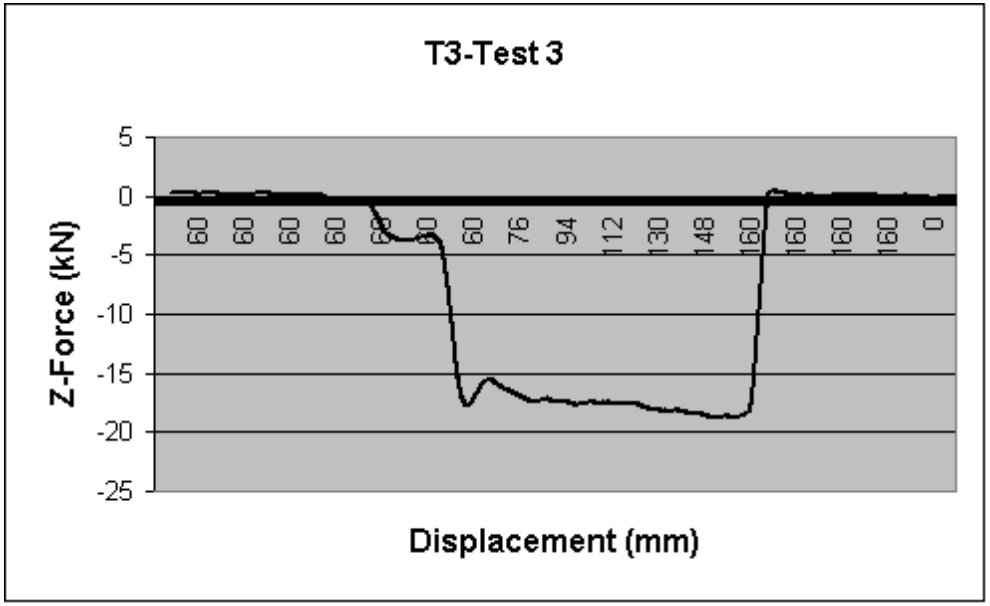
T3-Test 3
Z-Force (kN)
5
0
-5
-10
-15
-20
-25
60 60 60 60 60 60 60 76 94 112 130 148 160 160 160 160 0
Displacement (mm)

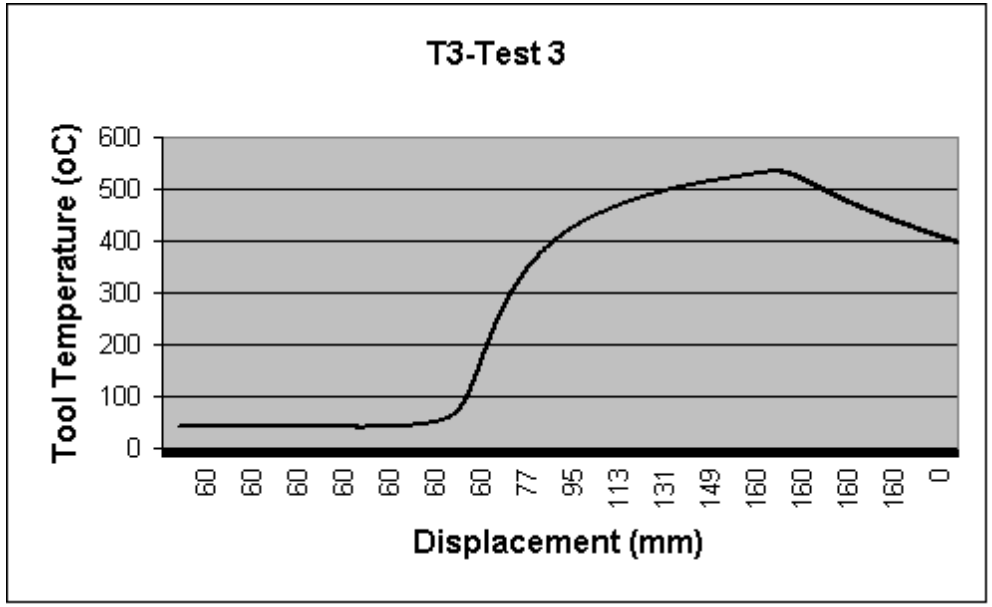
T3-Test 3
Tool Temperature (oC)
600
500
400
300
200
100
0
60 60 60 60 60 60 60 77 95 113 131 149 160 160 160 160 0
Displacement (mm)

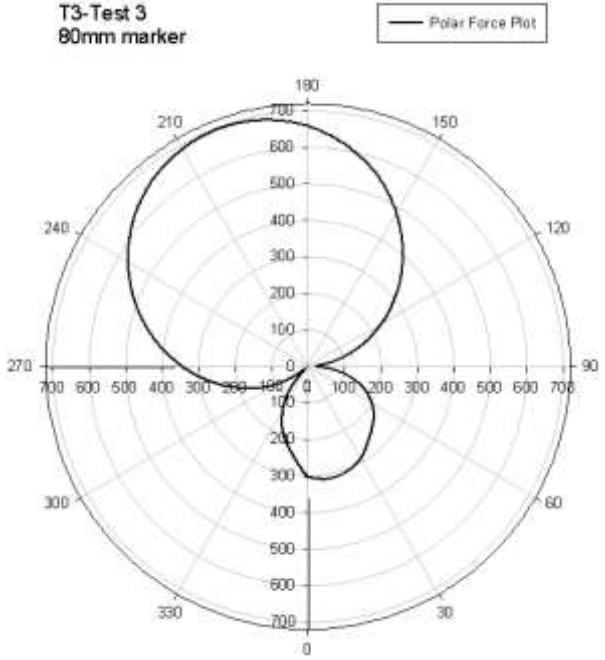
T3-Test 3
80mm marker
Polar Force Plot
180
150
120
90
60
30
0
210
240
270
300
330

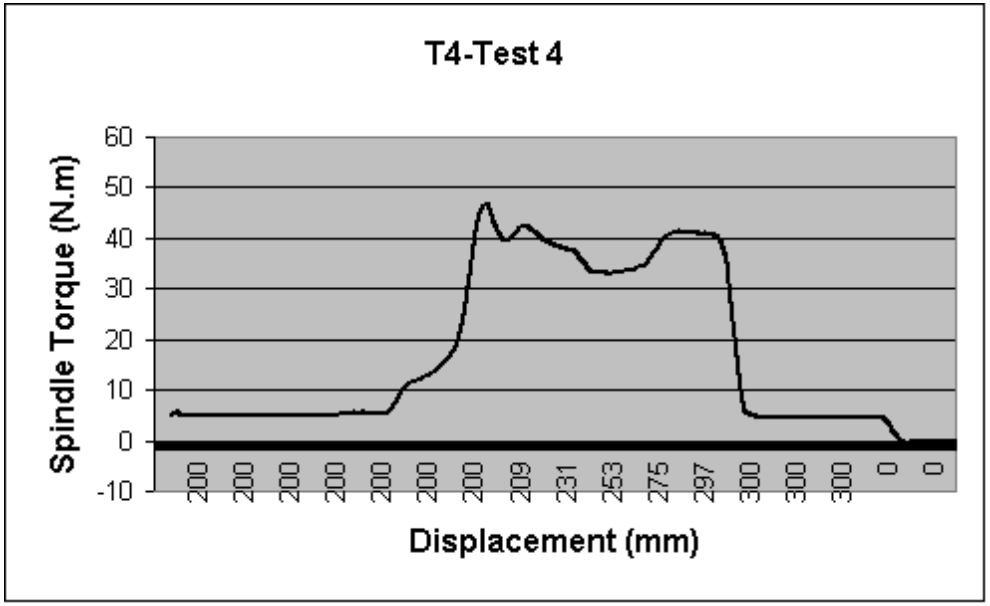
T4-Test 4
Spindle Torque (N.m)
60
50
40
30
20
10
0
-10
200 200 200 200 200 200 200 209 231 253 275 297 300 300 300 0 0
Displacement (mm)

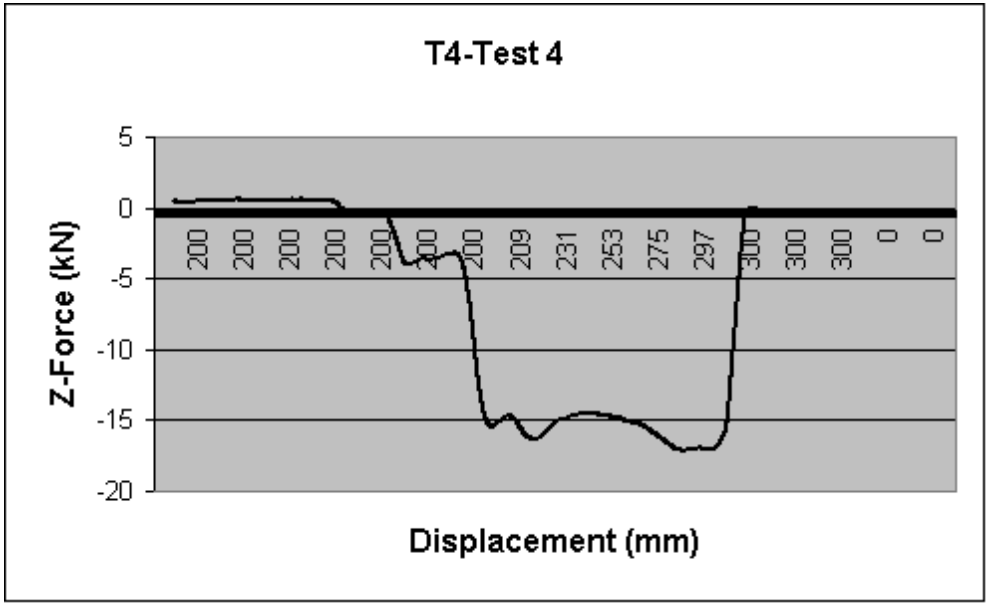
T4-Test 4
Z-Force (kN)
5
0
-5
-10
-15
-20
200 200 200 200 200 200 200 209 231 253 275 297 300 300 300 0 0
Displacement (mm)

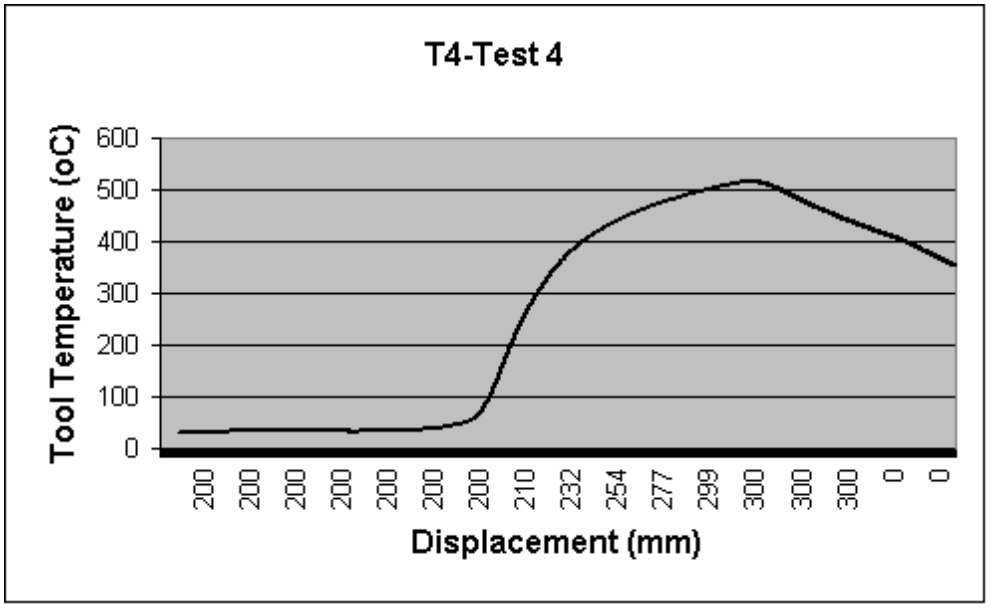
T4-Test 4
Tool Temperature (oC)
600
500
400
300
200
100
0
200 200 200 200 200 200 200 210 232 254 277 299 300 300 300 0 0
Displacement (mm)

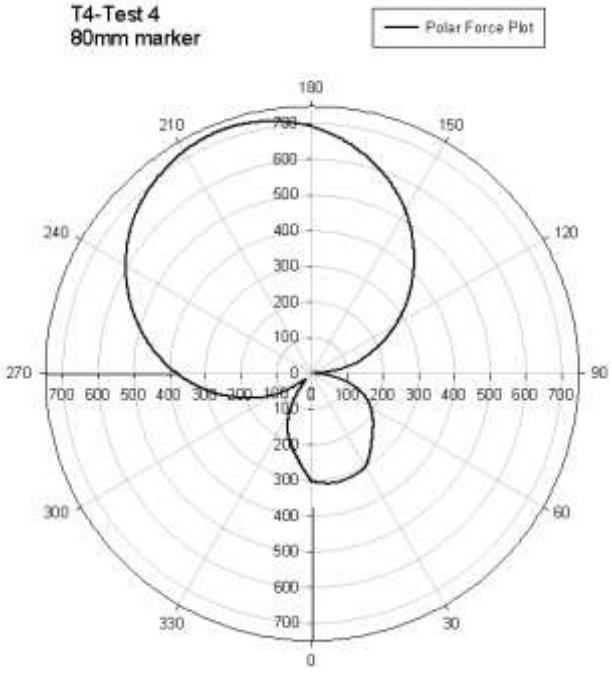
T4-Test 4
80mm marker
Polar Force Plot
180
150
120
90
60
30
0
330
300
270
240
210

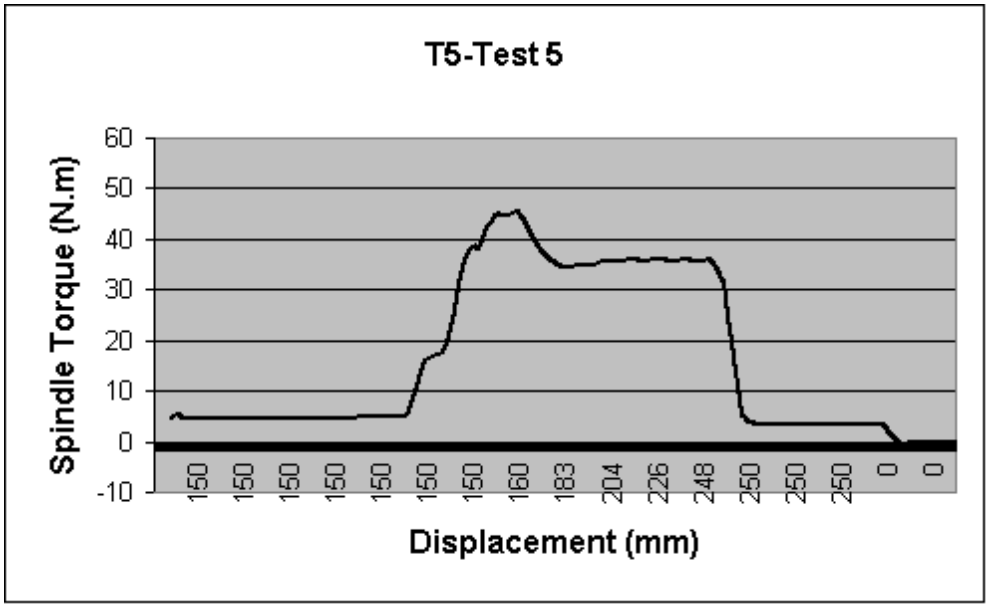
T5-Test 5
Spindle Torque (N.m)
60
50
40
30
20
10
0
-10
150 150 150 150 150 150 150 160 183 204 226 248 250 250 250 0 0
Displacement (mm)

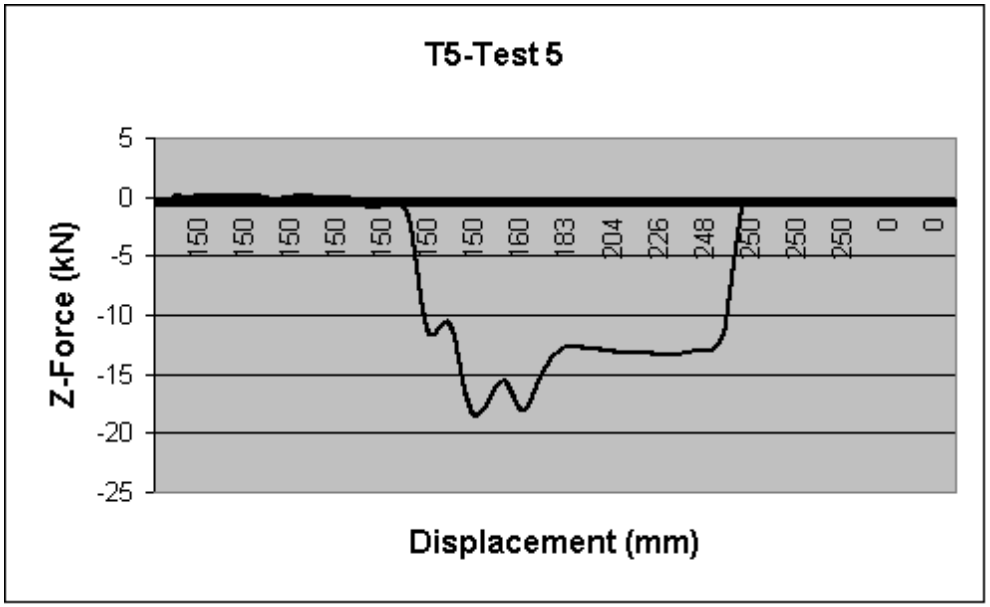
T5-Test 5
Z-Force (kN)
5
0
-5
-10
-15
-20
-25
150 150 150 150 150 150 150 160 183 204 226 248 250 250 250 0 0
Displacement (mm)

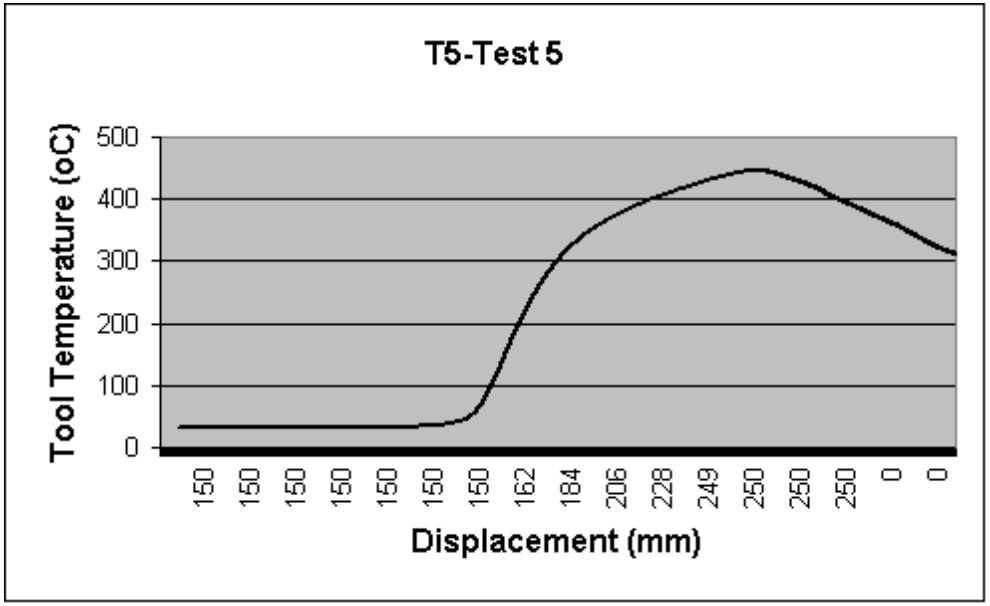
T5-Test 5
Tool Temperature (oC)
500
400
300
200
100
0
150 150 150 150 150 150 150 162 184 206 228 249 250 250 250 0 0
Displacement (mm)

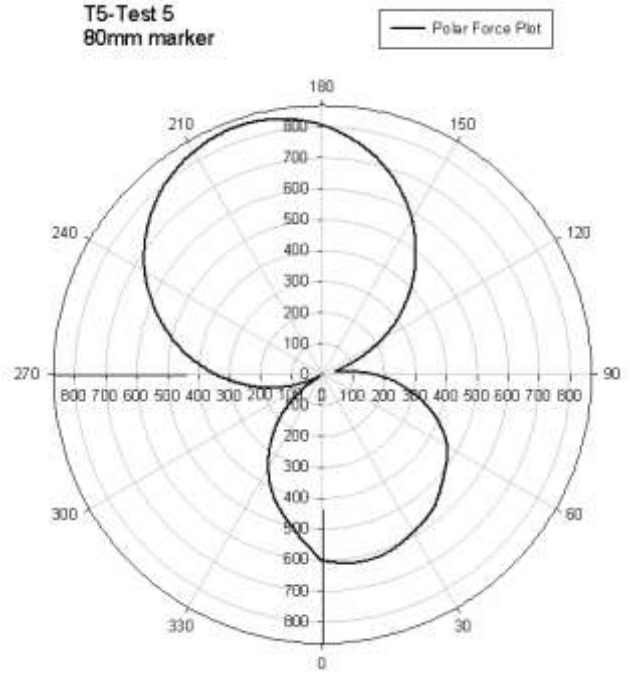
T5-Test 5
80mm marker
Polar Force Plot
180
210
150
240
120
270
90
300
60
330
30
0

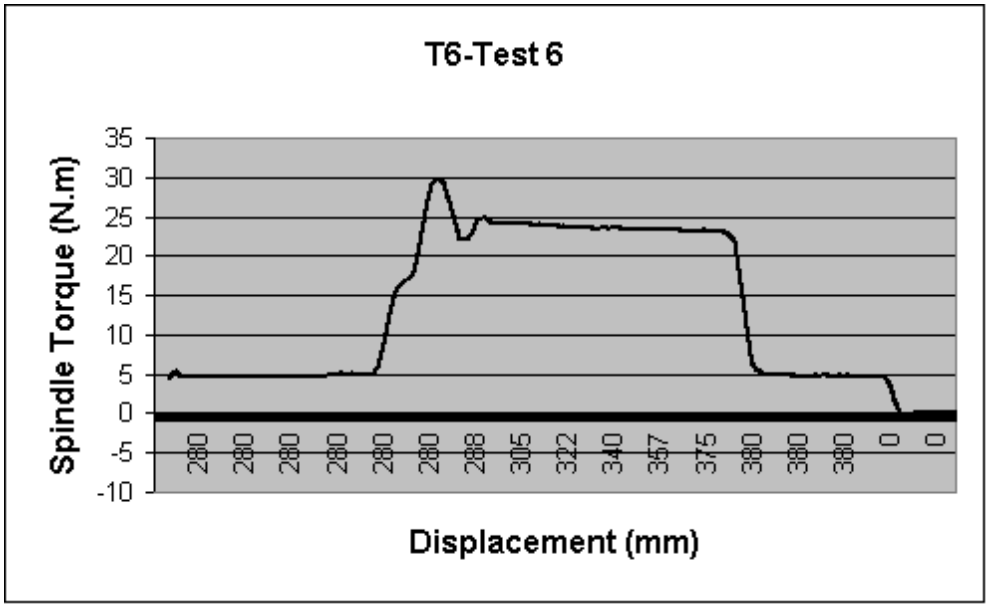
T6-Test 6
Spindle Torque (N.m)
35
30
25
20
15
10
5
0
-5
-10
280 280 280 280 280 280 288 305 322 340 357 375 380 380 380 0 0
Displacement (mm)

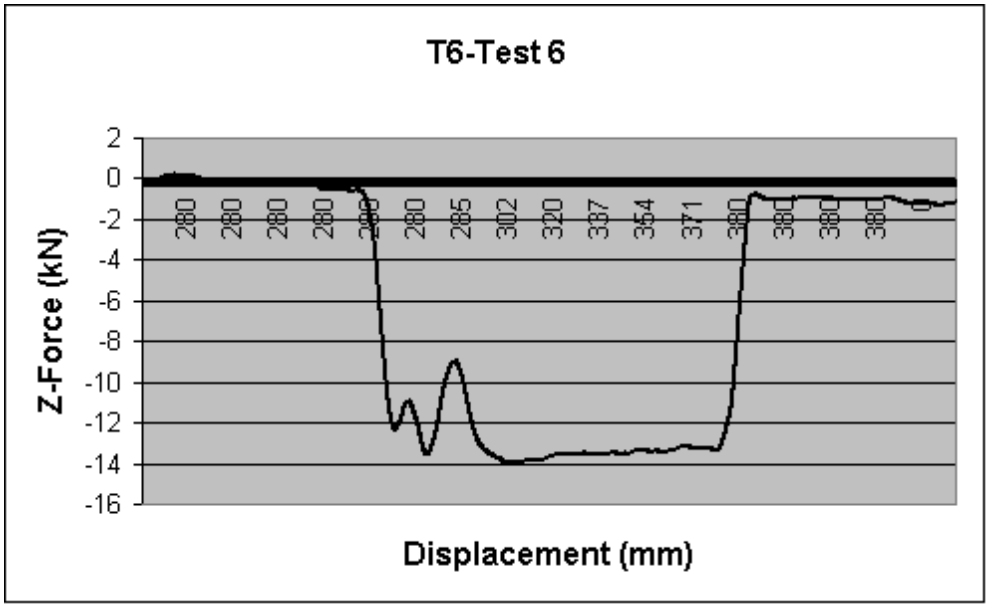
T6-Test 6
Z-Force (kN)
2
0
-2
-4
-6
-8
-10
-12
-14
-16
280 280 280 280 280 280 285 302 320 337 354 371 380 380 380 380 0
Displacement (mm)

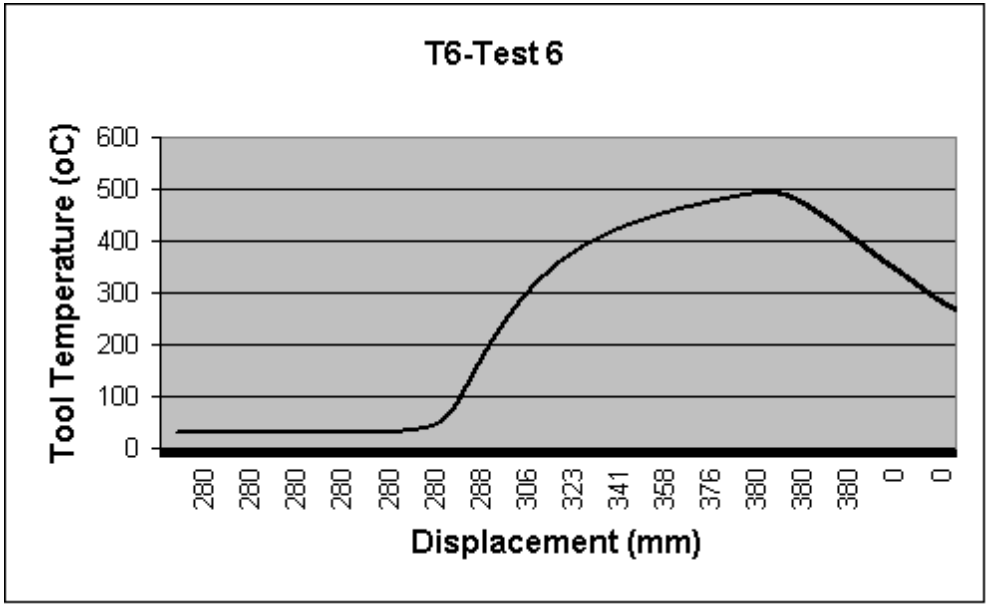
T6-Test 6
Tool Temperature (oC)
600
500
400
300
200
100
0
280 280 280 280 280 280 288 306 323 341 358 376 380 380 380 0 0
Displacement (mm)

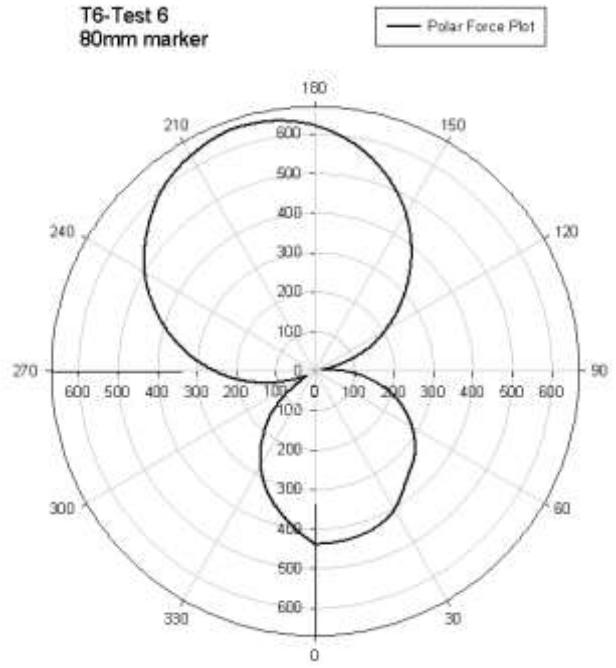
T6-Test 6
80mm marker
Polar Force Plot
180
210
150
240
120
270
90
300
60
330
30
0

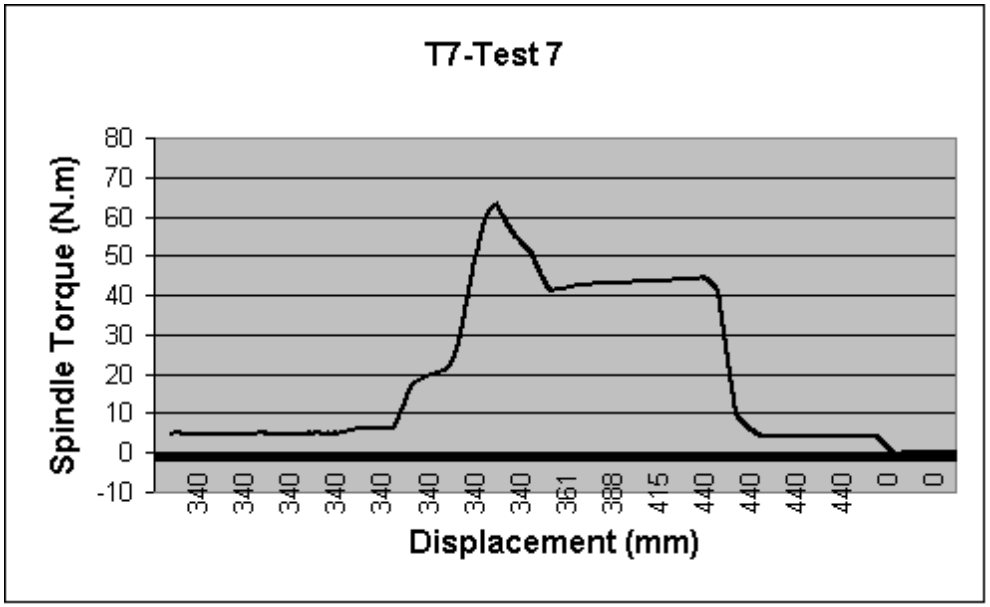
T7-Test 7
Spindle Torque (N.m)
80
70
60
50
40
30
20
10
0
-10
340 340 340 340 340 340 340 340 361 388 415 440 440 440 440 0 0
Displacement (mm)

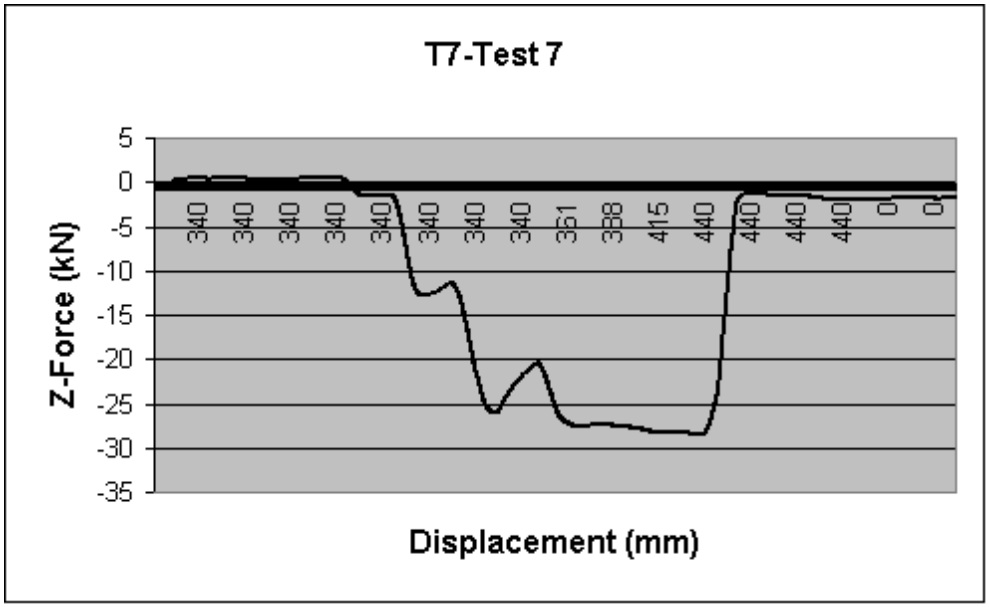
T7-Test 7
Z-Force (kN)
5
0
-5
-10
-15
-20
-25
-30
-35
340 340 340 340 340 340 340 340 361 388 415 440 440 440 440 0 0
Displacement (mm)

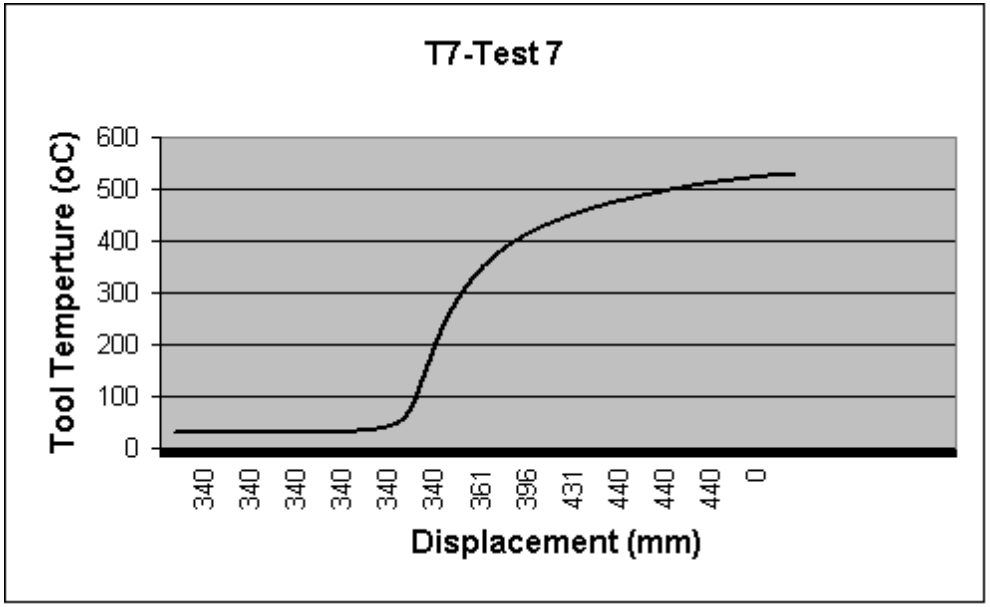
T7-Test 7
Tool Temperture (oC)
600
500
400
300
200
100
0
340 340 340 340 340 340 361 396 431 440 440 440 0
Displacement (mm)

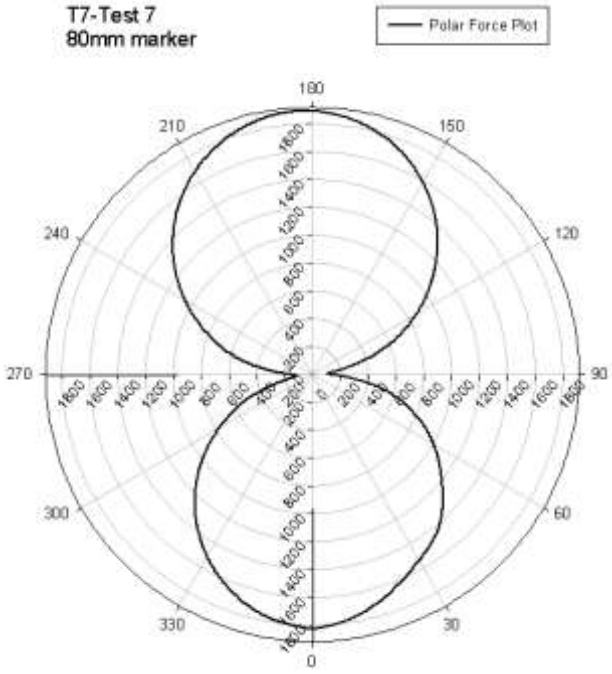
T7-Test 7
80mm marker
Polar Force Plot
180
210
150
240
120
270
90
300
60
330
30
0

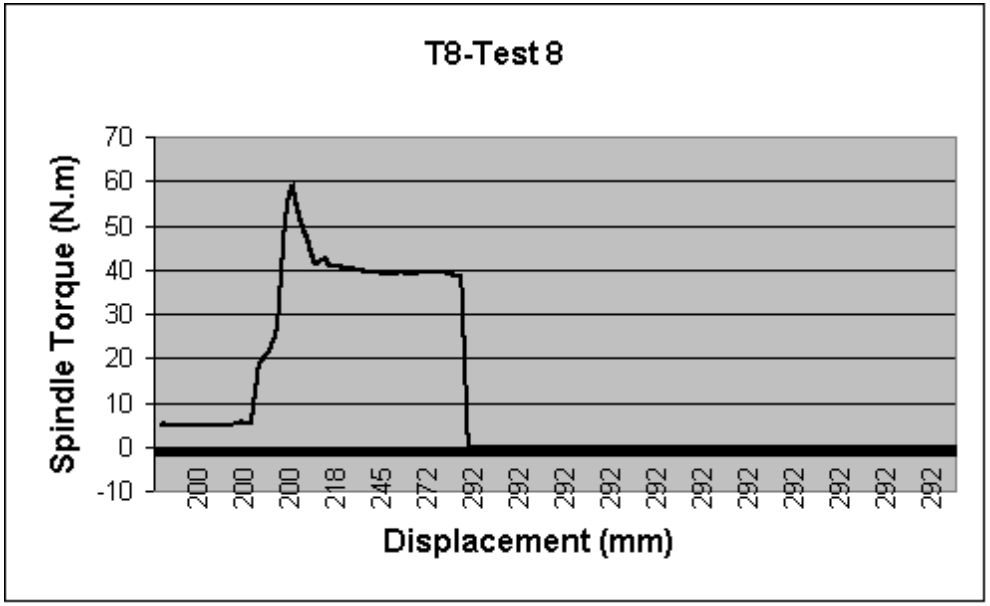
T8-Test 8
Spindle Torque (N.m)
70
60
50
40
30
20
10
0
-10
200 200 200 218 245 272 292 292 292 292 292 292 292 292 292 292
Displacement (mm)

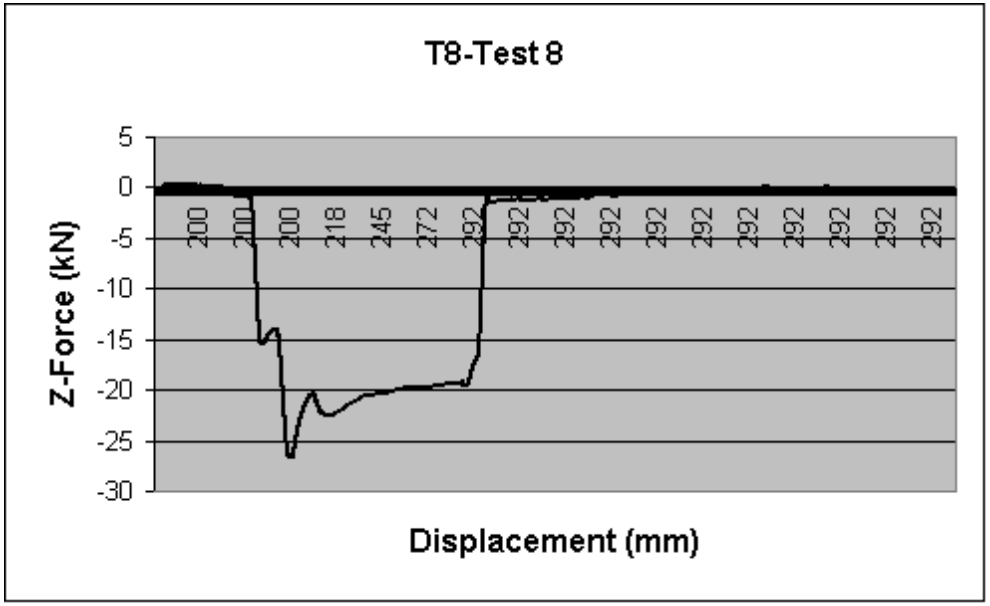
T8-Test 8
Z-Force (kN)
5
0
-5
-10
-15
-20
-25
-30
200 200 200 218 245 272 292 292 292 292 292 292 292 292 292 292
Displacement (mm)

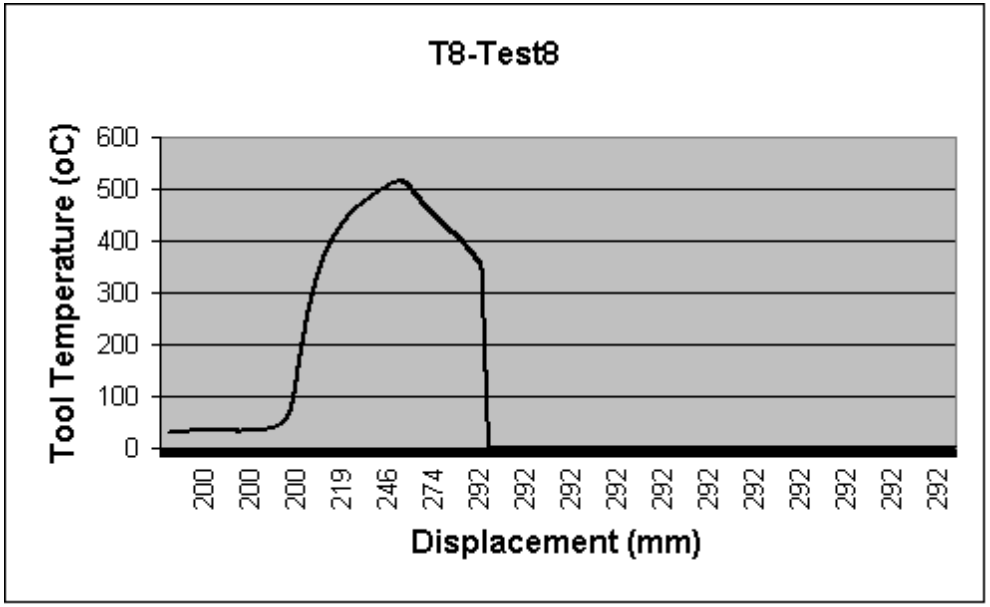
T8-Test8
Tool Temperature (oC)
600
500
400
300
200
100
0
200 200 200 219 246 274 292 292 292 292 292 292 292 292 292 292
Displacement (mm)

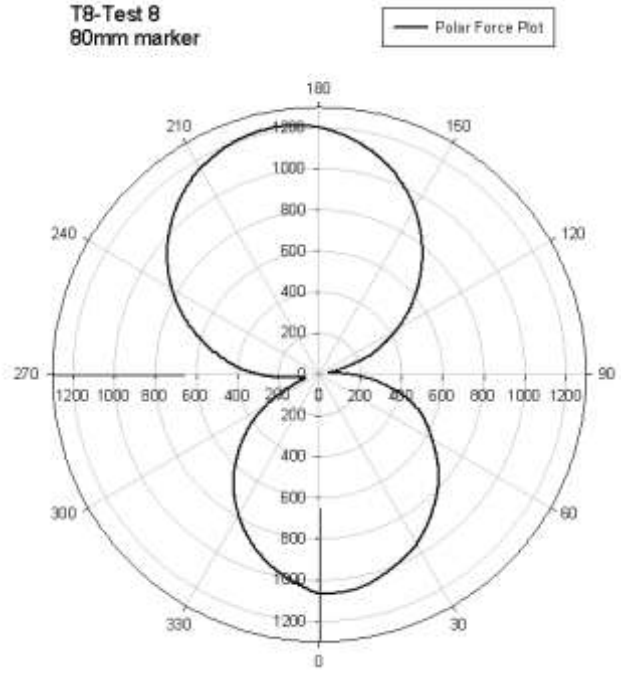
T8-Test 8
80mm marker
Polar Force Plot
180
210
150
240
120
270
90
300
60
330
30
0
1200 1000 800 600 400 200 0 200 400 600 800 1000 1200

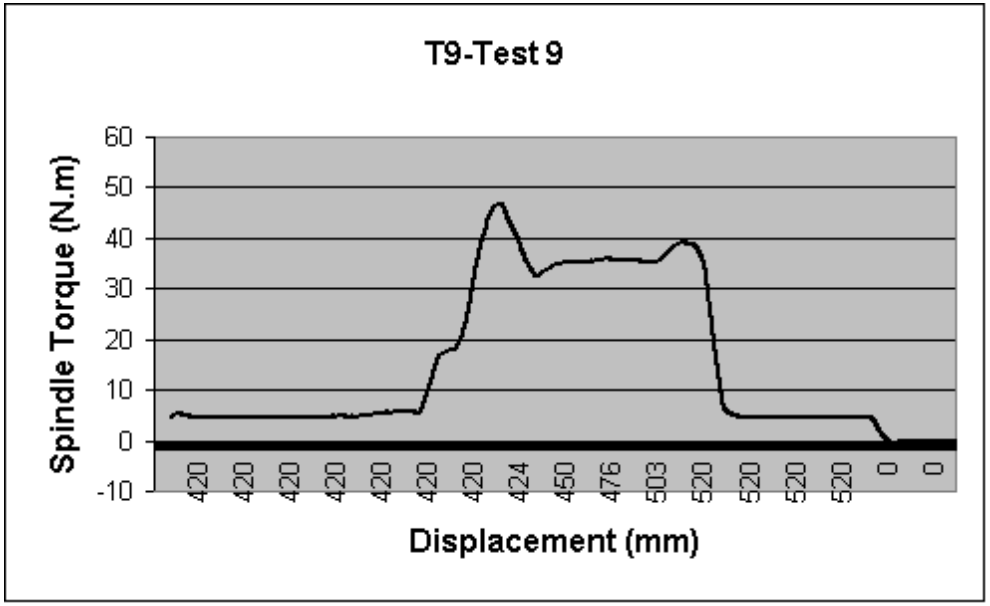
T9-Test 9
Spindle Torque (N.m)
60
50
40
30
20
10
0
-10
420 420 420 420 420 420 420 424 450 476 503 520 520 520 520 0 0
Displacement (mm)

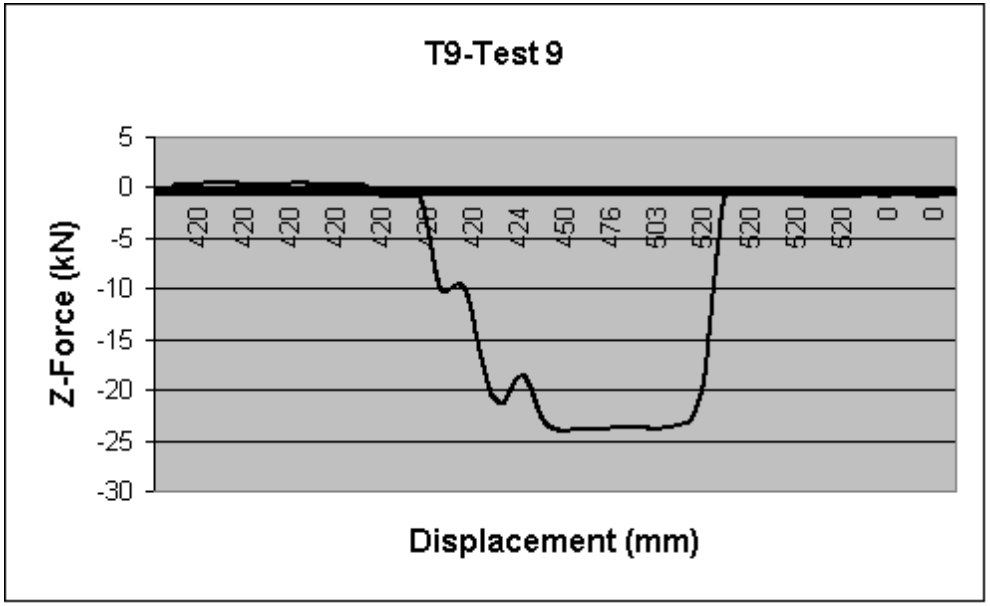
T9-Test 9
Z-Force (kN)
5
0
-5
-10
-15
-20
-25
-30
420 420 420 420 420 420 420 424 450 476 503 520 520 520 520 0 0
Displacement (mm)

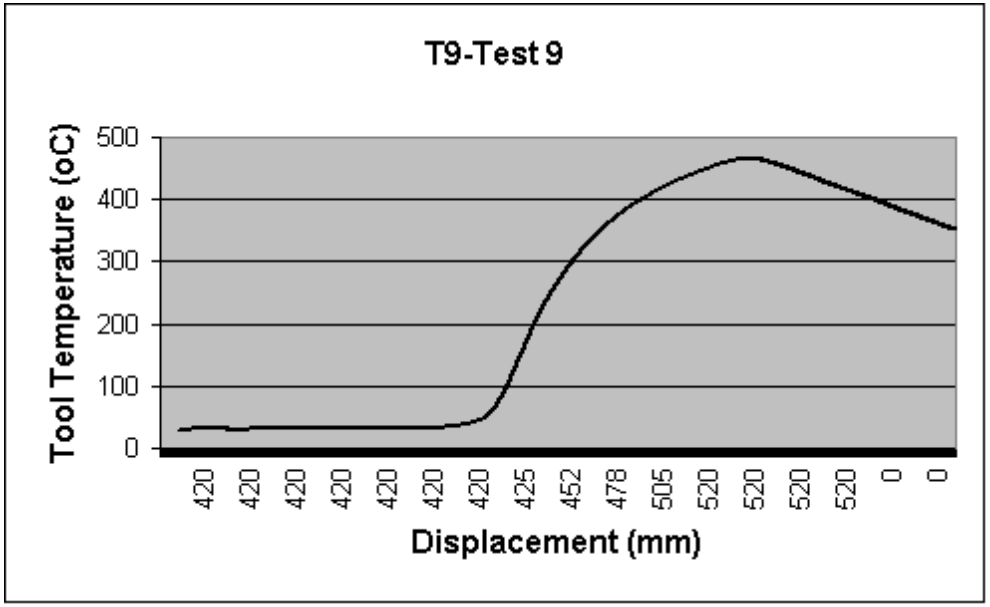
T9-Test 9
Tool Temperature (oC)
500
400
300
200
100
0
420 420 420 420 420 420 420 425 452 478 505 520 520 520 520 0 0
Displacement (mm)

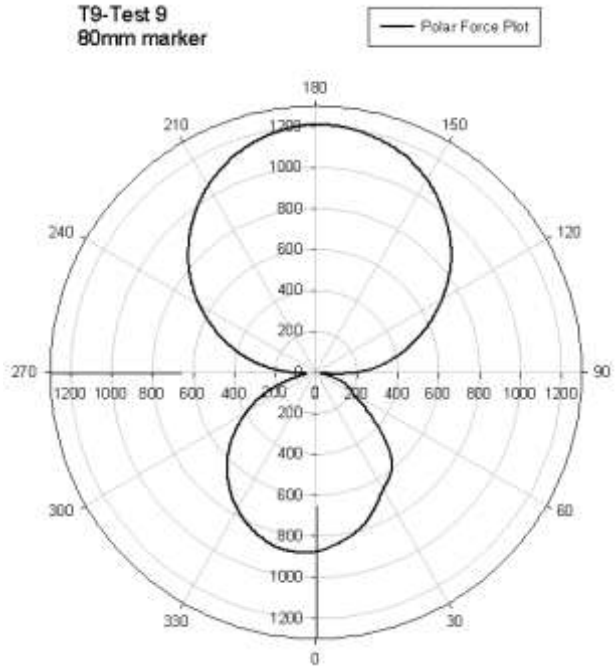
T9-Test 9
80mm marker
Polar Force Plot
180
150
120
90
60
30
0
210
240
270
300
330
1200 1000 800 600 400 200 0 200 400 600 800 1000 1200

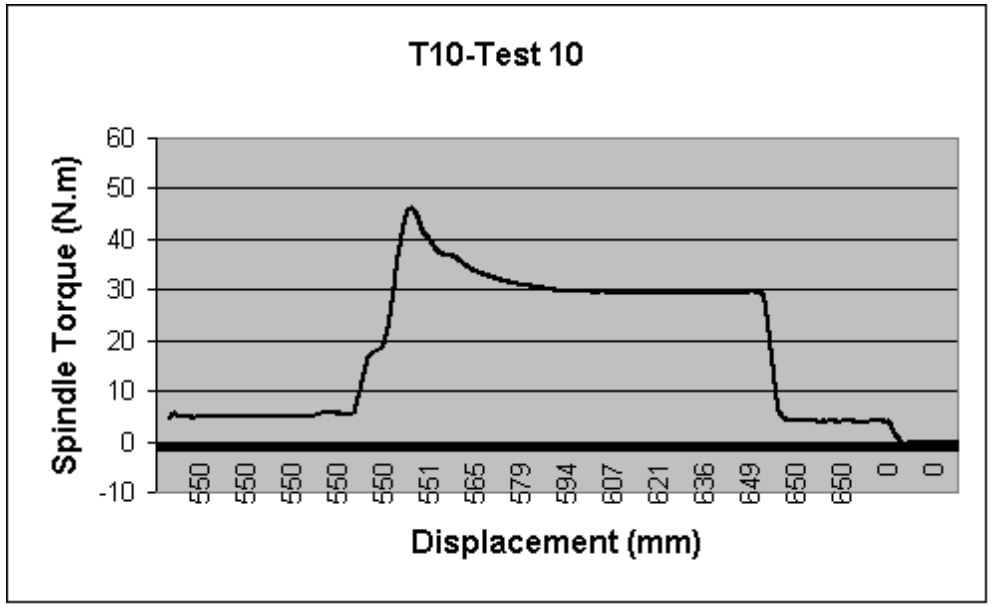
T10-Test 10
Spindle Torque (N.m)
60
50
40
30
20
10
0
-10
550 550 550 550 550 551 565 579 594 607 621 636 649 650 650 0 0
Displacement (mm)

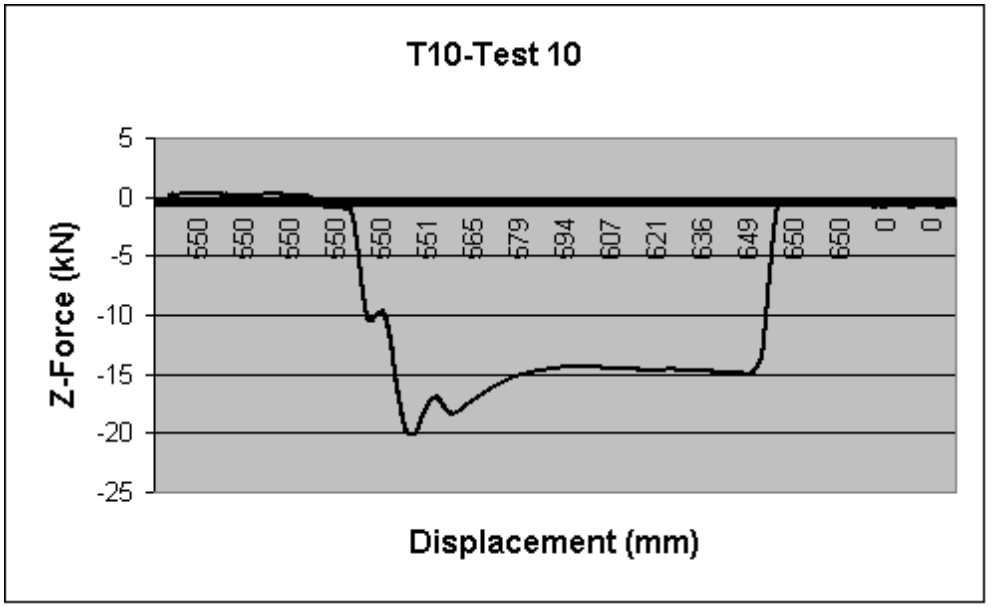
T10-Test 10
Z-Force (kN)
5
0
-5
-10
-15
-20
-25
550 550 550 550 550 551 565 579 594 607 621 636 649 650 650 0 0
Displacement (mm)

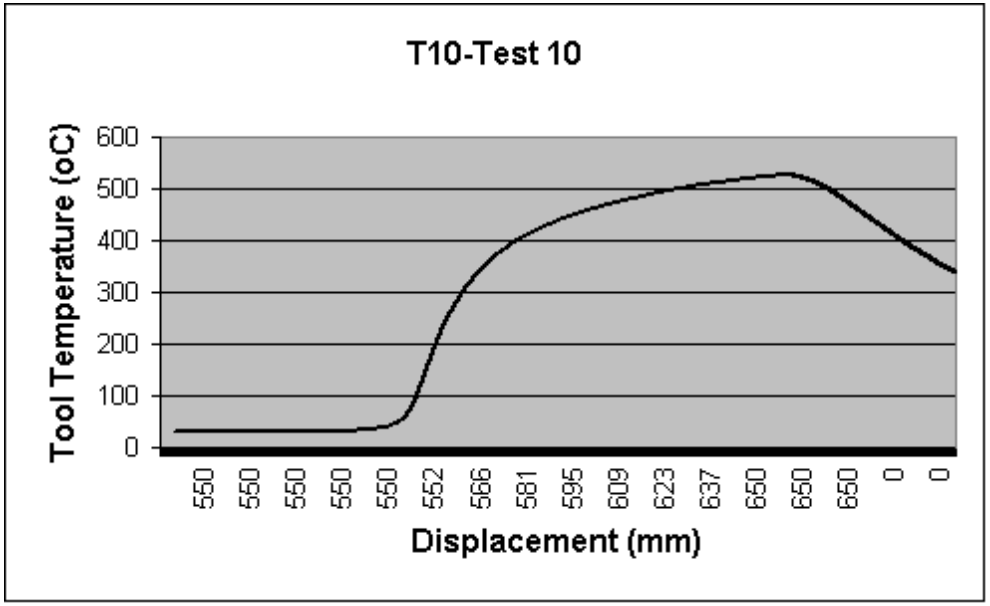
T10-Test 10
Tool Temperature (oC)
600
500
400
300
200
100
0
550 550 550 550 550 552 566 581 595 609 623 637 650 650 650 0 0
Displacement (mm)

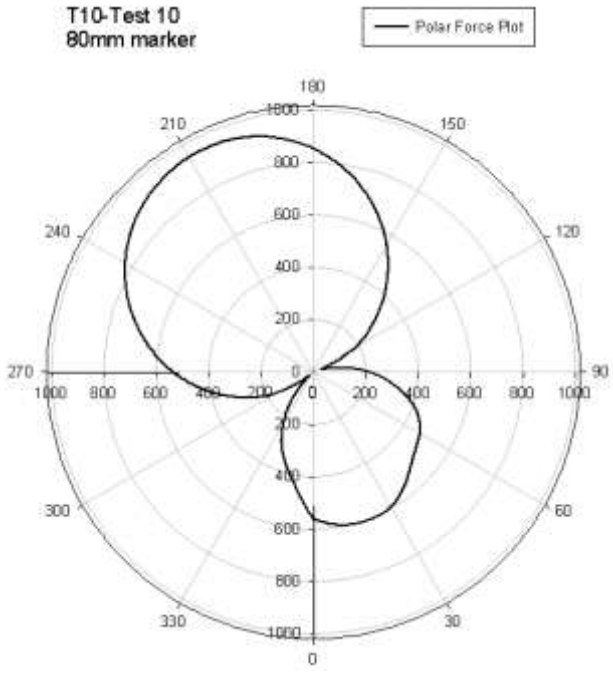
T10-Test 10
80mm marker
Polar Force Plot
180
210
150
240
120
270
90
300
60
330
30
0
200
400
600
800
1000

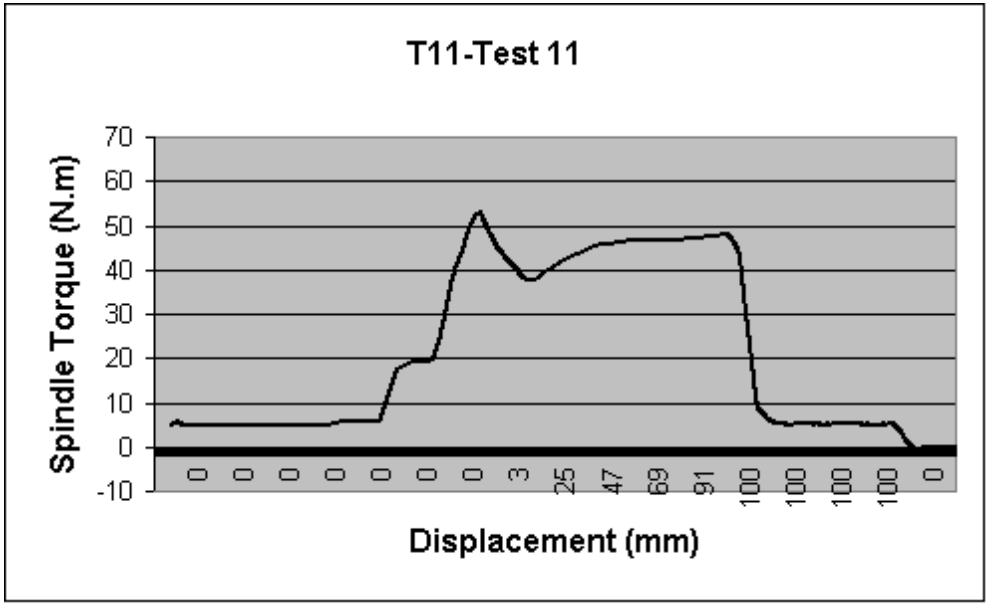
T11-Test 11
Spindle Torque (N.m)
70
60
50
40
30
20
10
0
-10
0 0 0 0 0 0 0 3 25 47 69 91 100 100 100 100 0
Displacement (mm)

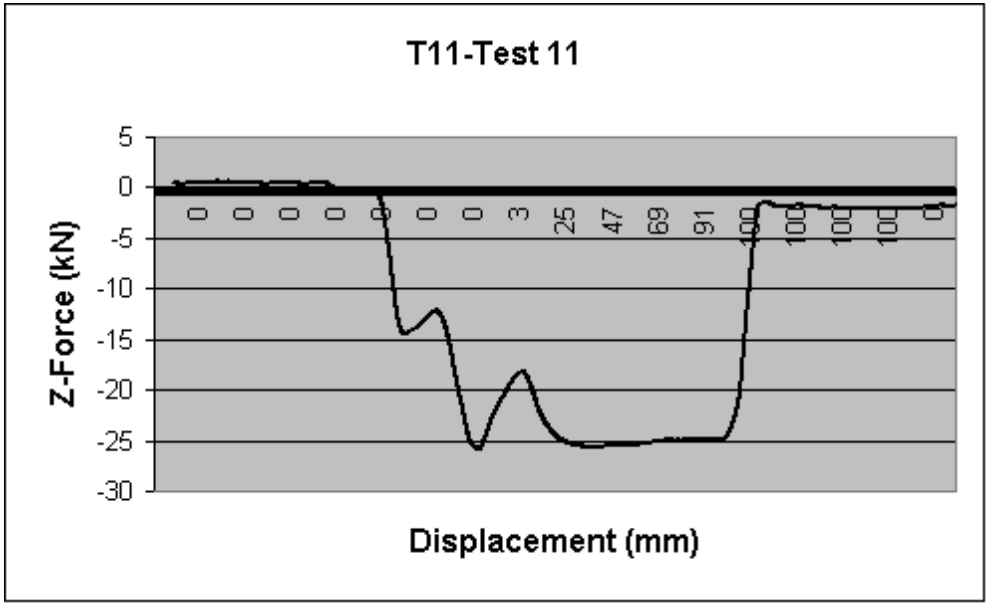
T11-Test 11
Z-Force (kN)
5
0
-5
-10
-15
-20
-25
-30
0 0 0 0 0 0 0 3 25 47 69 91 100 100 100 100 0
Displacement (mm)

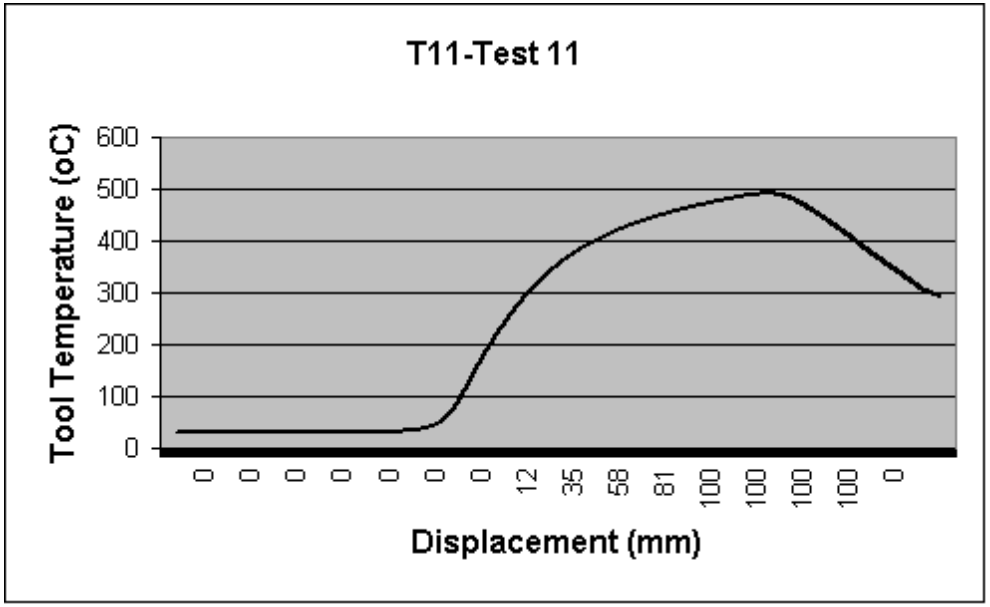
T11-Test 11
Tool Temperature (oC)
600
500
400
300
200
100
0
0 0 0 0 0 0 0 12 35 58 81 100 100 100 100 0
Displacement (mm)

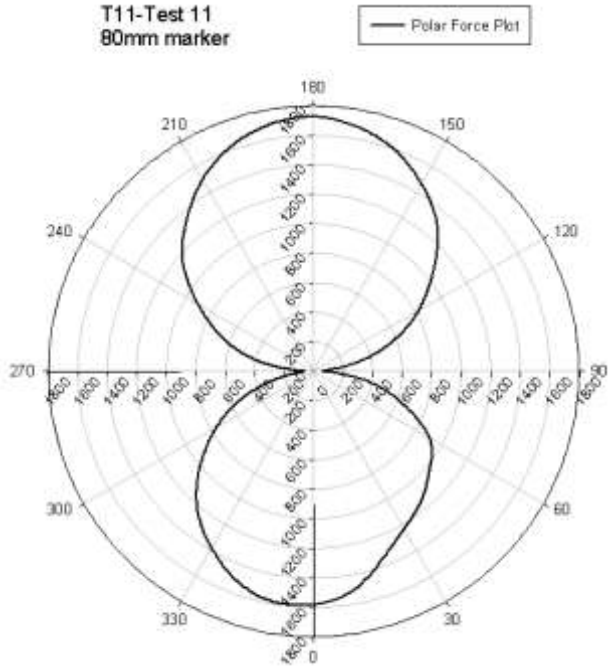
T11-Test 11
80mm marker
Polar Force Plot
180
210
150
240
120
270
90
300
60
330
30
0

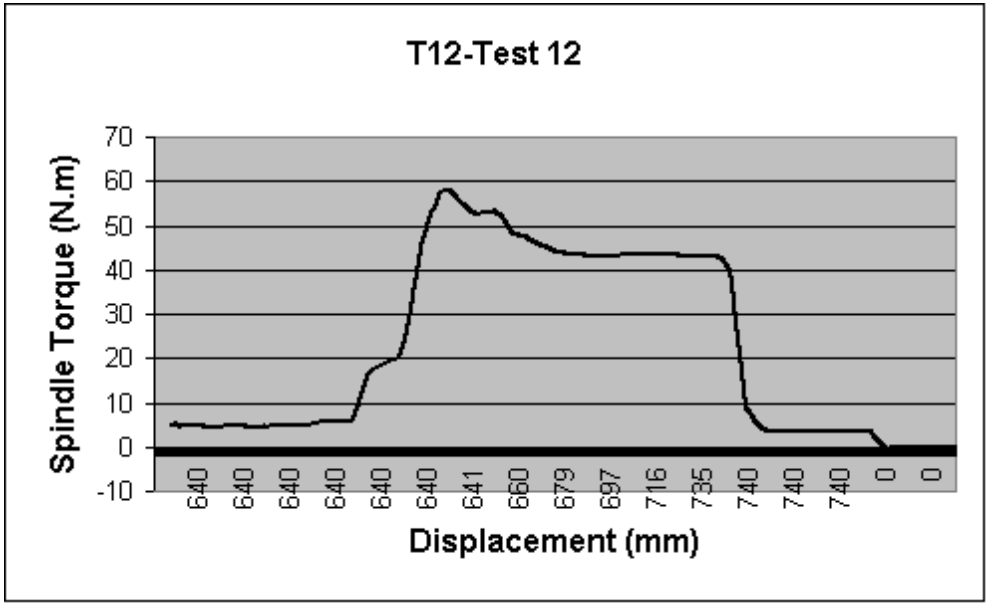
T12-Test 12
Spindle Torque (N.m)
70
60
50
40
30
20
10
0
-10
640 640 640 640 640 640 641 660 679 697 716 735 740 740 740 0 0
Displacement (mm)

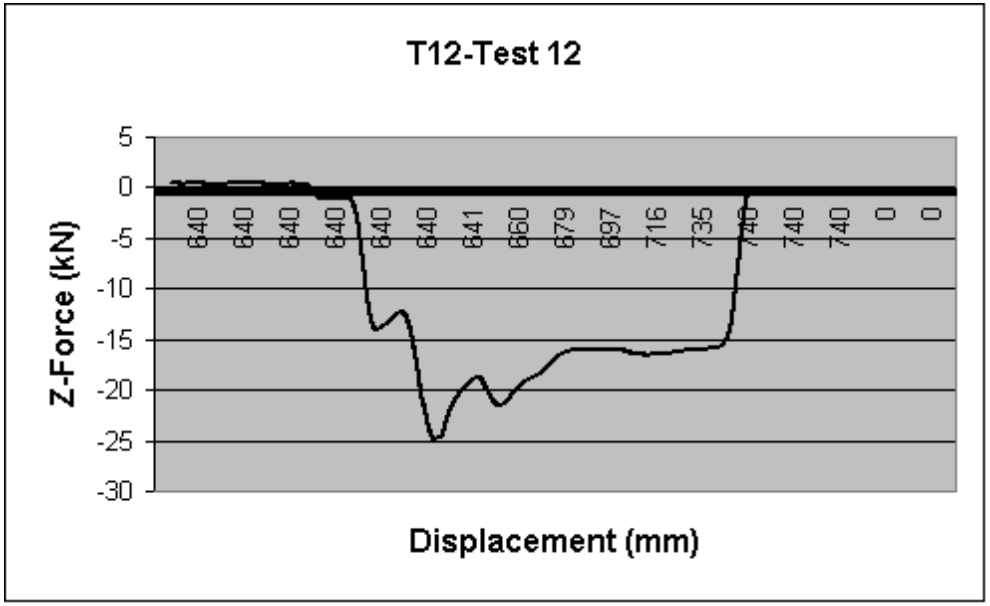
T12-Test 12
Z-Force (kN)
5
0
-5
-10
-15
-20
-25
-30
640 640 640 640 640 640 641 660 679 697 716 735 740 740 740 0 0
Displacement (mm)

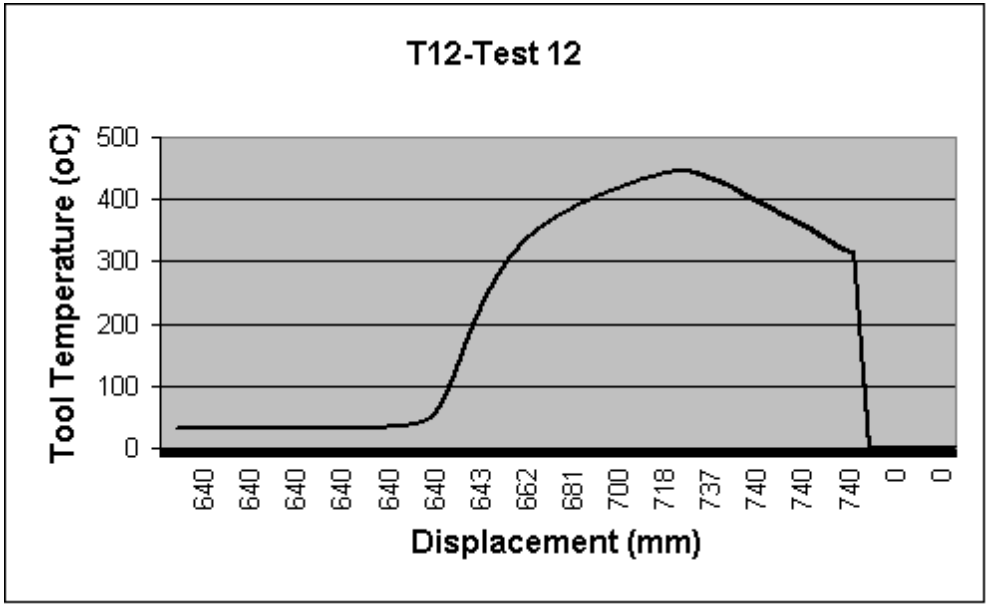
T12-Test 12
Tool Temperature (oC)
500
400
300
200
100
0
640 640 640 640 640 640 643 662 681 700 718 737 740 740 740 0 0
Displacement (mm)

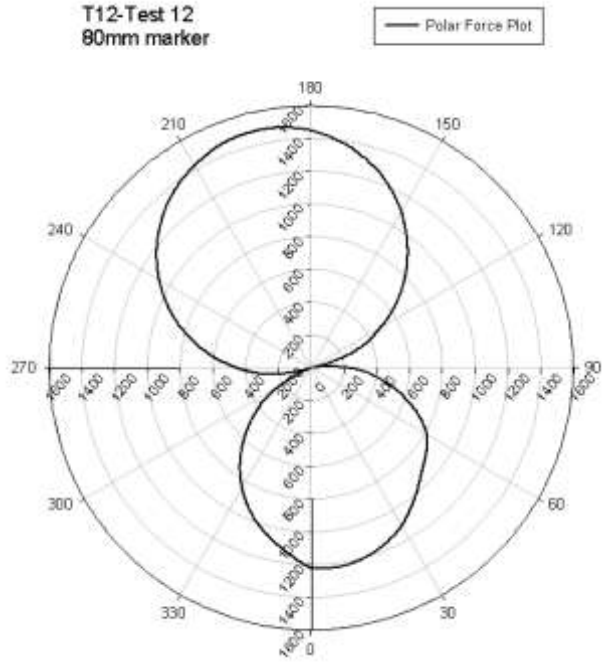
T12-Test 12
80mm marker
Polar Force Plot
180
210
150
240
120
270
90
300
60
330
30
0

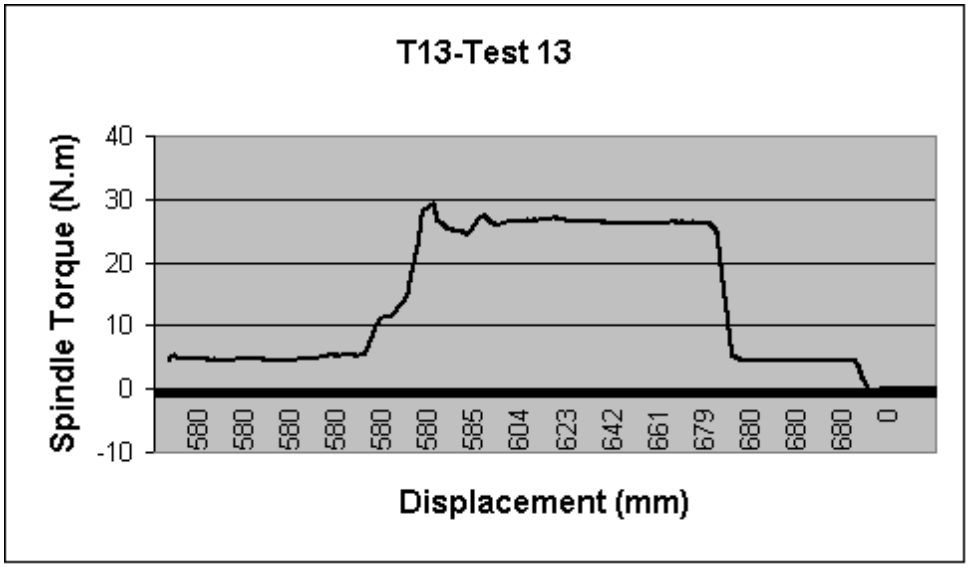
T13-Test 13
Spindle Torque (N.m)
40
30
20
10
0
-10
580 580 580 580 580 580 585 604 623 642 661 679 680 680 680 0
Displacement (mm)

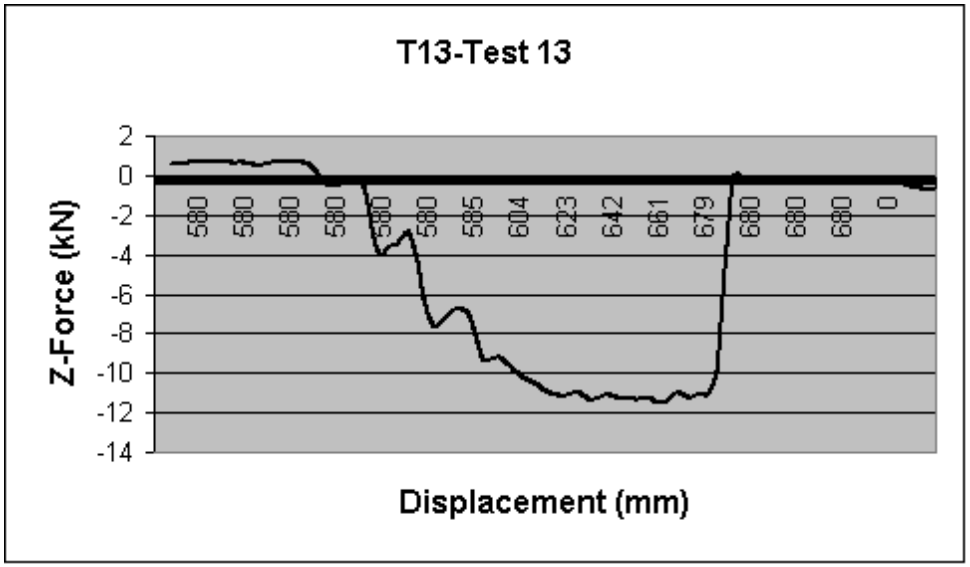
T13-Test 13
Z-Force (kN)
2
0
-2
-4
-6
-8
-10
-12
-14
580 580 580 580 580 580 585 604 623 642 661 679 680 680 680 0
Displacement (mm)

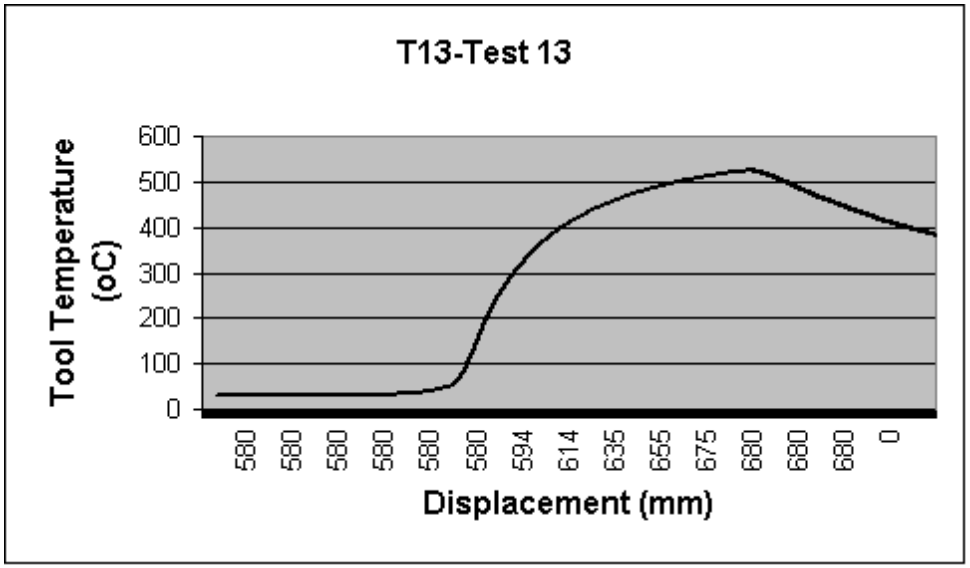
T13-Test 13
Tool Temperature (oC)
600
500
400
300
200
100
0
580 580 580 580 580 580 594 614 635 655 675 680 680 680 0
Displacement (mm)

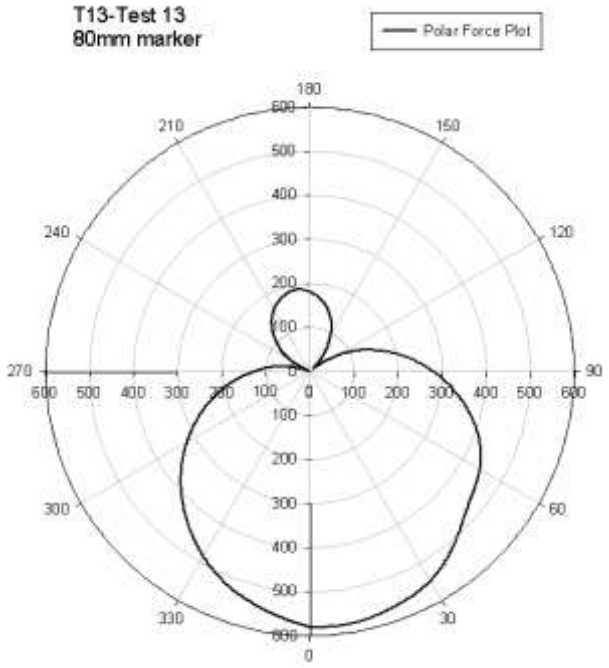
T13-Test 13
80mm marker
Polar Force Plot
180
210
150
240
120
270
90
300
60
330
30
0

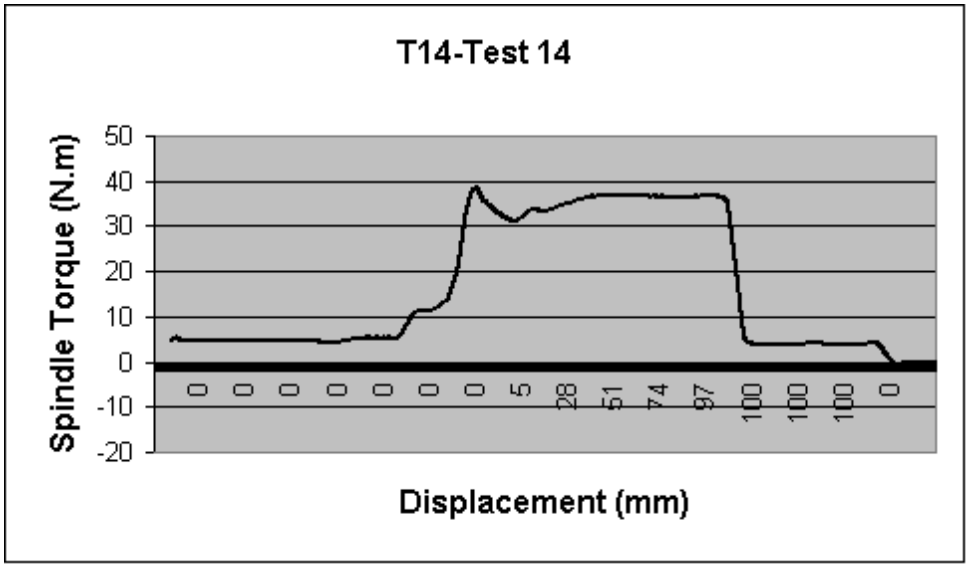
T14-Test 14
Spindle Torque (N.m)
50
40
30
20
10
0
-10
-20
0 0 0 0 0 0 0 5 28 51 74 97 100 100 100 0
Displacement (mm)

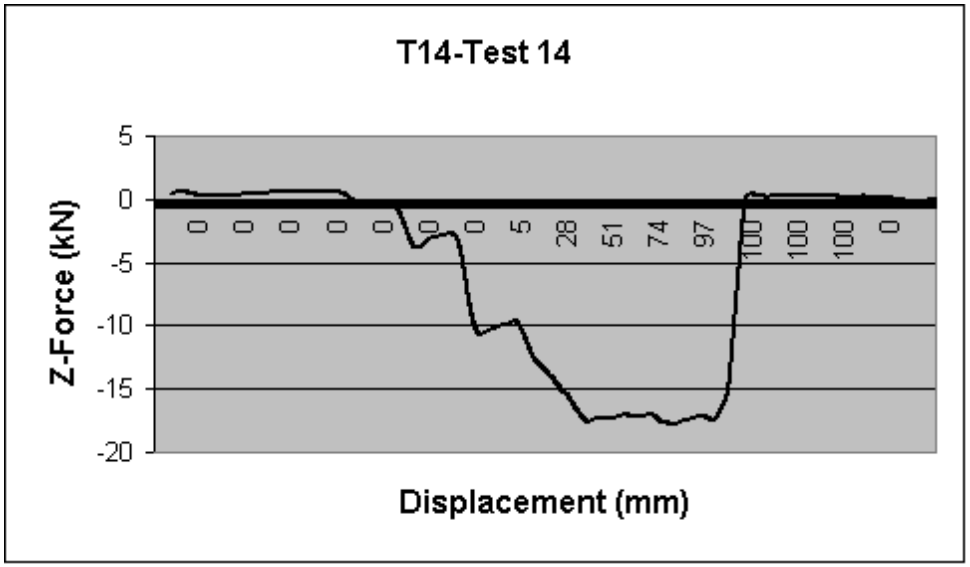
T14-Test 14
Z-Force (kN)
5
0
-5
-10
-15
-20
0 0 0 0 0 0 0 5 28 51 74 97 100 100 100 0
Displacement (mm)

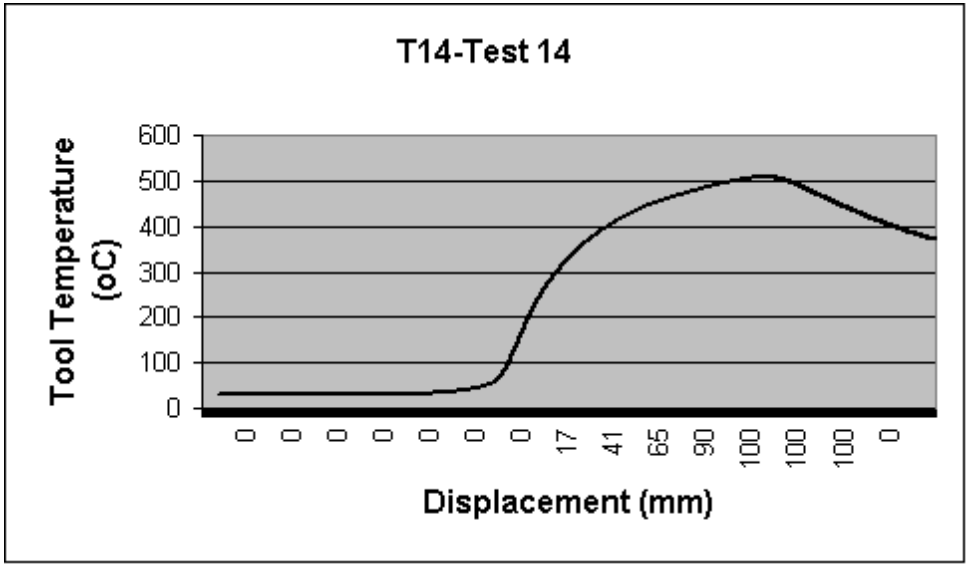
T14-Test 14
Tool Temperature (oC)
600
500
400
300
200
100
0
0 0 0 0 0 0 0 17 41 65 90 100 100 100 0
Displacement (mm)

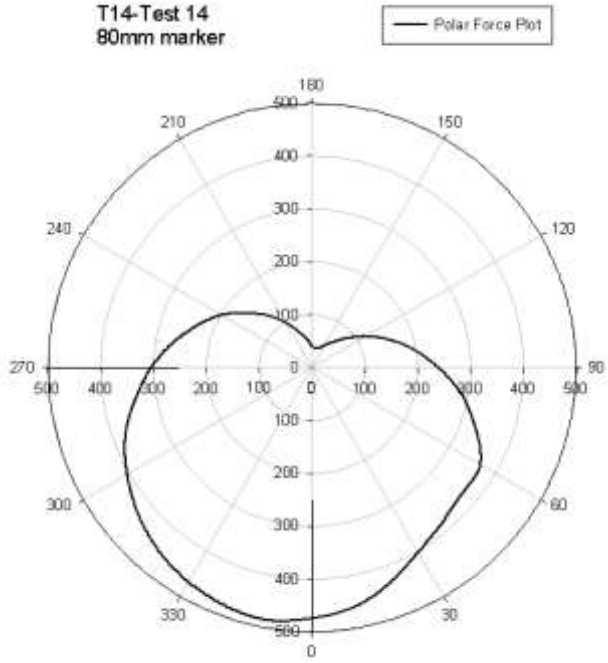
T14-Test 14
80mm marker
Polar Force Plot

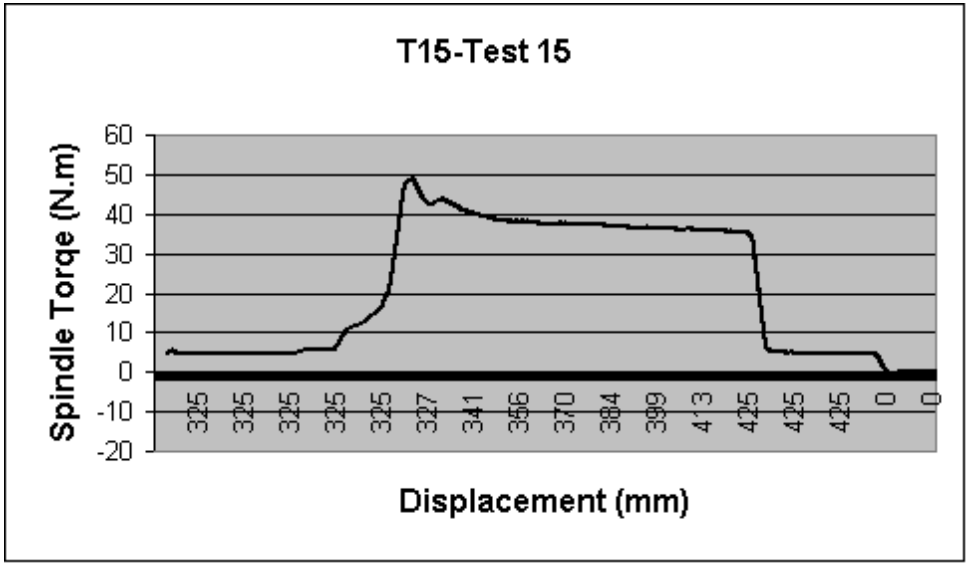
T15-Test 15
Spindle Torqe (N.m)
60
50
40
30
20
10
0
-10
-20
325 325 325 325 325 327 341 356 370 384 399 413 425 425 425 0 0
Displacement (mm)

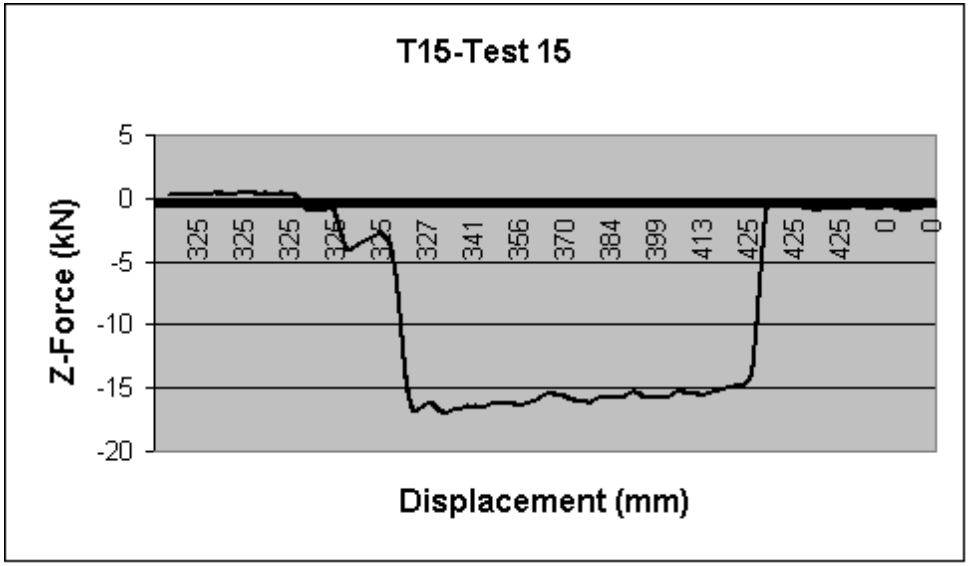
T15-Test 15
Z-Force (kN)
5
0
-5
-10
-15
-20
325 325 325 325 325 327 341 356 370 384 399 413 425 425 425 0 0
Displacement (mm)

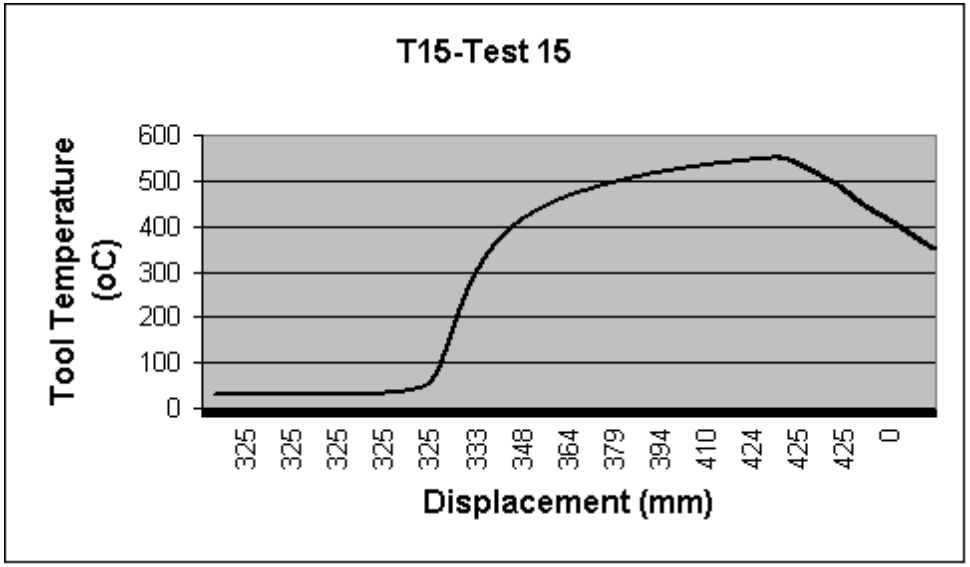
T15-Test 15
Tool Temperature (oC)
600
500
400
300
200
100
0
325 325 325 325 325 333 348 364 379 394 410 424 425 425 0
Displacement (mm)

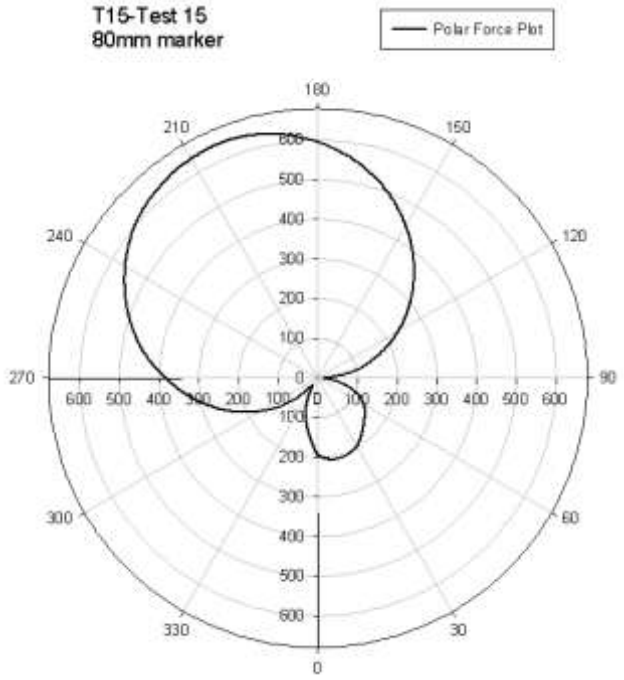
T15-Test 15
80mm marker
Polar Force Plot
180
210
150
240
120
270
90
300
60
330
30
0

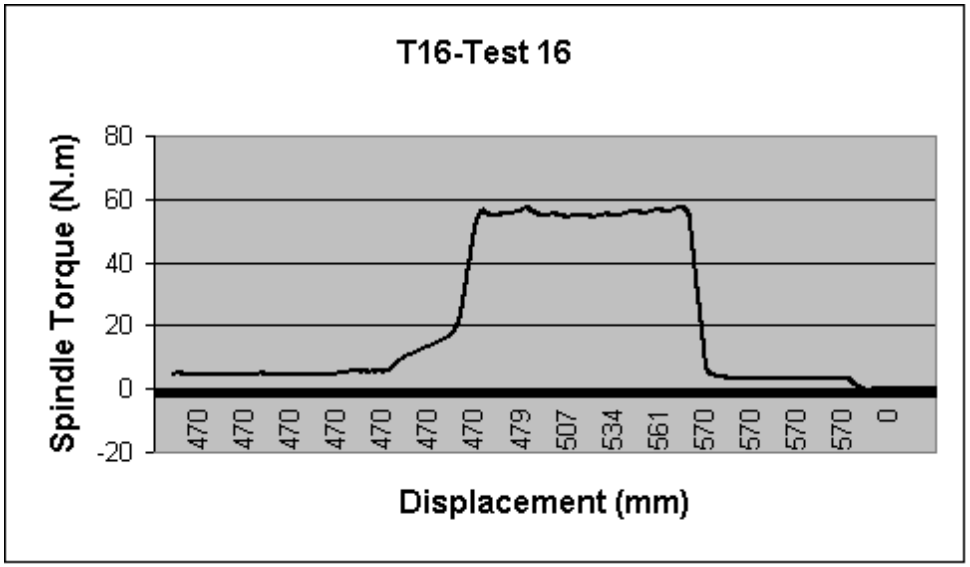
T16-Test 16
Spindle Torque (N.m)
80
60
40
20
0
-20
470 470 470 470 470 470 470 479 507 534 561 570 570 570 570 0
Displacement (mm)

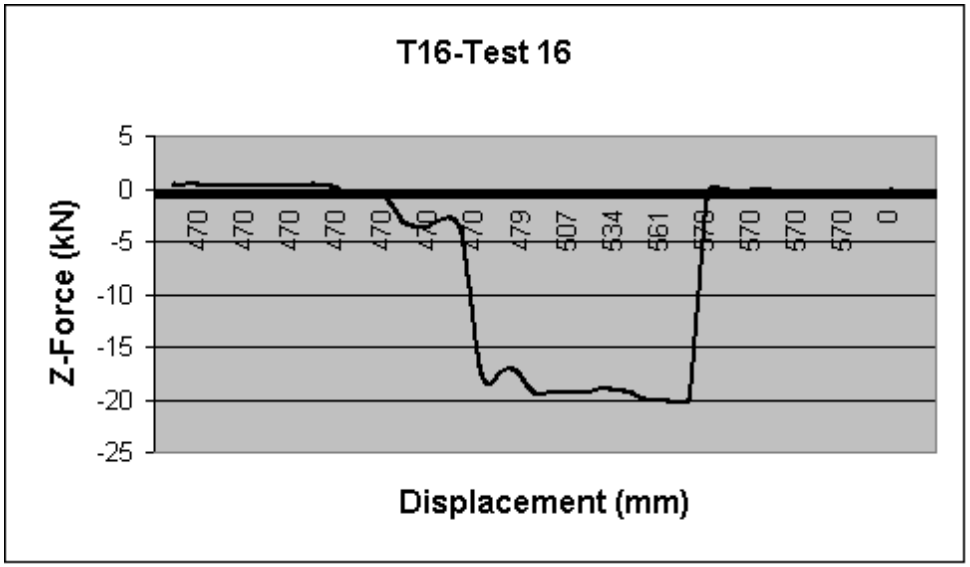
T16-Test 16
Z-Force (kN)
5
0
-5
-10
-15
-20
-25
470 470 470 470 470 470 470 479 507 534 561 570 570 570 570 0
Displacement (mm)

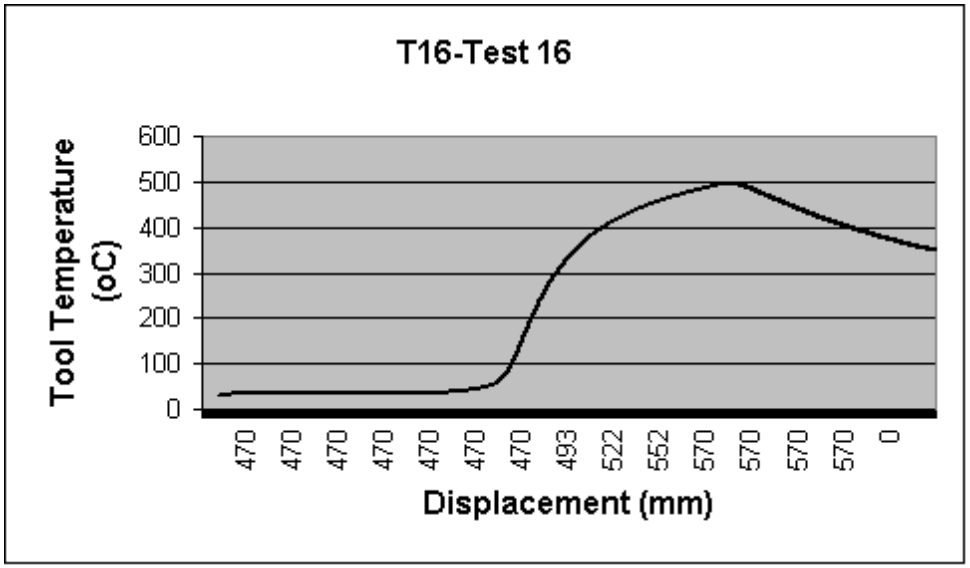
T16-Test 16
Tool Temperature (oC)
600
500
400
300
200
100
0
470 470 470 470 470 470 470 493 522 552 570 570 570 570 0
Displacement (mm)

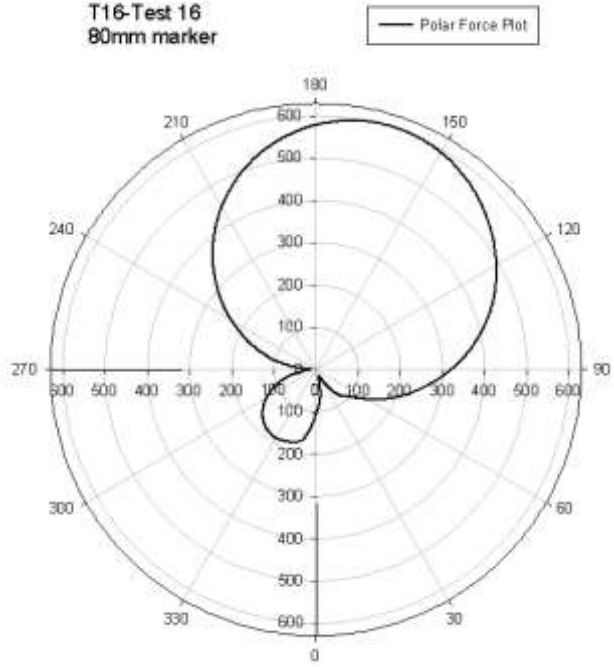
T16-Test 16
80mm marker
Polar Force Plot
180
150
120
90
60
30
0
210
240
270
300
330

Regression Summary for Dependent Variable: ps (Weld data Results for analysis.sta)
R= .78064883 R²= .60941259 Adjusted R²= .26764861
F(7,8)=1.7831 p<.21752 Std.Error of estimate: 909.68

N=16	Beta	Std.Err. of Beta	B	Std.Err. of B	t(8)	p-level
Intercept			-675.597	2263.135	-0.29852	0.772911
rpm	0.413695	0.234969	5.016	2.849	1.76064	0.116333
feed	0.333957	0.232332	15.727	10.941	1.43741	0.188539
plunge	0.134740	0.313676	1178.528	2743.625	0.42955	0.678857
oxide	-0.085124	0.223182	-175.224	459.412	-0.38141	0.712829
type	0.047781	0.286687	98.355	590.134	0.16666	0.871769
thick	0.666961	0.242850	1372.913	499.897	2.74639	0.025199
time	-0.255301	0.228895	-525.528	471.172	-1.11536	0.297076

Regression Summary for Dependent Variable: ts (Weld data Results for analysis.sta)
R= .93237423 R²= .86932170 Adjusted R²= .75497818
F(7,8)=7.6027 p<.00520 Std.Error of estimate: 3.8479

N=16	Beta	Std.Err. of Beta	B	Std.Err. of B	t(8)	p-level
Intercept			33.11654	9.57293	3.45939	0.008575
rpm	-0.455522	0.135910	-0.04039	0.01205	-3.35164	0.010056
feed	0.475613	0.134386	0.16380	0.04628	3.53917	0.007629
plunge	-0.016836	0.181436	-1.07690	11.60538	-0.09279	0.928350
oxide	0.020301	0.129093	0.30560	1.94329	0.15726	0.878938
type	-0.032017	0.165825	-0.48196	2.49623	-0.19307	0.851712
thick	0.559358	0.140469	8.42024	2.11453	3.98208	0.004050
time	-0.088104	0.132397	-1.32626	1.99303	-0.66545	0.524481

Regression Summary for Dependent Variable: cs (Weld data Results for analysis.sta)
R= .73986555 R²= .54740103 Adjusted R²= .15137693
F(7,8)=1.3822 p<.32818 Std.Error of estimate: 2.2587

N=16	Beta	Std.Err. of Beta	B	Std.Err. of B	t(8)	p-level
Intercept			4.03186	5.619328	0.717498	0.493482
rpm	0.113189	0.252934	0.00317	0.007074	0.447503	0.666381
feed	0.337462	0.250096	0.03666	0.027167	1.349329	0.214173
plunge	0.075732	0.337660	1.52791	6.812377	0.224284	0.828158
oxide	-0.087674	0.240247	-0.41629	1.140713	-0.364934	0.724619
type	0.016678	0.308607	0.07919	1.465294	0.054042	0.958227
thick	0.652906	0.261418	3.10006	1.241235	2.497558	0.037083
time	-0.217069	0.246397	-1.03066	1.169914	-0.880975	0.404021

Regression Summary for Dependent Variable: pf (Weld data Results for analysis.sta)
R= .99947192 R²= .99894413 Adjusted R²= .99802024
F(7,8)=1081.2 p<.00000 Std.Error of estimate: 5.3673

N=16	Beta	Std.Err. of Beta	B	Std.Err. of B	t(8)	p-level
Intercept			30.44096	13.35294	2.27972	0.052094
rpm	-0.007876	0.012217	-0.01084	0.01681	-0.64469	0.537170
feed	0.999503	0.012080	5.34155	0.06456	82.74221	0.000000
plunge	-0.004675	0.016309	-4.64065	16.18793	-0.28667	0.781647
oxide	0.007666	0.011604	1.79081	2.71062	0.66066	0.527391
type	0.003186	0.014906	0.74425	3.48191	0.21375	0.836091
thick	-0.019196	0.012627	-4.48396	2.94949	-1.52025	0.166937
time	0.021755	0.011901	5.08189	2.78001	1.82801	0.104956

Regression Summary for Dependent Variable: tf (Weld data Results for analysis.sta)
R= .92915152 R²= .86332254 Adjusted R²= .74372977
F(7,8)=7.2189 p<.00614 Std.Error of estimate: .39655

N=16	Beta	Std.Err. of Beta	B	Std.Err. of B	t(8)	p-level
Intercept			-1.18050	0.986561	-1.19658	0.265725
rpm	0.243602	0.138995	0.00218	0.001242	1.75259	0.117767
feed	0.286521	0.137436	0.00994	0.004770	2.08476	0.070591
plunge	0.057189	0.185554	0.36862	1.196020	0.30820	0.765799
oxide	-0.056703	0.132023	-0.08602	0.200270	-0.42950	0.678895
type	0.683940	0.169589	1.03749	0.257255	4.03293	0.003773
thick	0.493608	0.143657	0.74877	0.217918	3.43602	0.008876
time	-0.395336	0.135402	-0.59970	0.205397	-2.91971	0.019300

Regression Summary for Dependent Variable: cf (Weld data Results for analysis.sta)
R= .77632362 R²= .60267836 Adjusted R²= .25502192
F(7,8)=1.7335 p<.22857 Std.Error of estimate: .05344

N=16	Beta	Std.Err. of Beta	B	Std.Err. of B	t(8)	p-level
Intercept			2.662035	0.132949	20.02304	0.000000
rpm	-0.316866	0.236986	-0.000224	0.000167	-1.33707	0.217970
feed	-0.037222	0.234327	-0.000102	0.000643	-0.15885	0.877725
plunge	-0.304697	0.316369	-0.155229	0.161175	-0.96311	0.363698
oxide	0.038123	0.225098	0.004571	0.026988	0.16936	0.869715
type	-0.380642	0.289148	-0.045637	0.034668	-1.31643	0.224494
thick	-0.344255	0.244934	-0.041275	0.029367	-1.40550	0.197498
time	0.718425	0.230860	0.086136	0.027679	3.11195	0.014403

Regression Summary for Dependent Variable: t (Weld data Results for analysis.sta)
R= .79478862 R²= .63168895 Adjusted R²= .30941679
F(7,8)=1.9601 p<.18289 Std.Error of estimate: 27.752

N=16	Beta	Std.Err. of Beta	B	Std.Err. of B	t(8)	p-level
Intercept			406.7750	69.04195	5.89171	0.000365
rpm	0.360033	0.228170	0.1371	0.08692	1.57792	0.153237
feed	-0.449272	0.225610	-0.6647	0.33379	-1.99137	0.081600
plunge	0.391046	0.304600	107.4547	83.70036	1.28380	0.235144
oxide	0.158526	0.216724	10.2517	14.01538	0.73146	0.485367
type	-0.246808	0.278392	-15.9608	18.00336	-0.88655	0.401187
thick	0.431032	0.235823	27.8745	15.25045	1.82778	0.104994
time	-0.080133	0.222272	-5.1822	14.37416	-0.36052	0.727793

Regression Summary for Dependent Variable: fx (Weld data Results for analysis.sta)
R= .95228128 R²= .90683964 Adjusted R²= .82532432
F(7,8)=11.125 p<.00146 Std.Error of estimate: 187.30

N=16	Beta	Std.Err. of Beta	B	Std.Err. of B	t(8)	p-level
Intercept			-341.862	465.9749	-0.73365	0.484105
rpm	0.007358	0.114754	0.038	0.5866	0.06412	0.950450
feed	0.175219	0.113466	3.479	2.2528	1.54424	0.161110
plunge	0.023482	0.153193	86.591	564.9068	0.15328	0.881970
oxide	-0.140268	0.108997	-121.730	94.5920	-1.28689	0.234117
type	0.758299	0.140012	658.081	121.5075	5.41597	0.000634
thick	0.466105	0.118602	404.503	102.9277	3.92997	0.004357
time	-0.315692	0.111788	-273.969	97.0134	-2.82403	0.022355

Regression Summary for Dependent Variable: fy (Weld data Results for analysis.sta)
R= .84069276 R²= .70676432 Adjusted R²= .45018311
F(7,8)=2.7545 p<.08957 Std.Error of estimate: 50.020

N=16	Beta	Std.Err. of Beta	B	Std.Err. of B	t(8)	p-level
Intercept			589.722	124.4410	4.73897	0.001466
rpm	-0.275653	0.203591	-0.212	0.1567	-1.35395	0.212755
feed	-0.097832	0.201307	-0.292	0.6016	-0.48598	0.640010
plunge	-0.380534	0.271788	-211.222	150.8612	-1.40011	0.199048
oxide	-0.051101	0.193379	-6.675	25.2613	-0.26425	0.798265
type	-0.906042	0.248403	-118.357	32.4492	-3.64746	0.006518
thick	-0.236065	0.210420	-30.837	27.4874	-1.12188	0.294456
time	-0.178762	0.198329	-23.352	25.9079	-0.90134	0.393732

Regression Summary for Dependent Variable: r (Weld data Results for analysis.sta)
R= .84546614 R²= .71481300 Adjusted R²= .46527437
F(7,8)=2.8645 p<.08179 Std.Error of estimate: 4.2350

N=16	Beta	Std.Err. of Beta	B	Std.Err. of B	t(8)	p-level
Intercept			-16.8060	10.53612	-1.59508	0.149361
rpm	0.206791	0.200778	0.0137	0.01326	1.02995	0.333164
feed	0.086083	0.198525	0.0221	0.05094	0.43361	0.676024
plunge	0.198191	0.268032	9.4448	12.77306	0.73943	0.480779
oxide	-0.090725	0.190706	-1.0175	2.13881	-0.47573	0.646984
type	0.833485	0.244971	9.3477	2.74740	3.40239	0.009327
thick	0.389339	0.207512	4.3665	2.32729	1.87623	0.097470
time	-0.254650	0.195588	-2.8560	2.19356	-1.30197	0.229161

Regression Summary for Dependent Variable: fz (Weld data Results for analysis.sta)
R= .88689315 R²= .78657946 Adjusted R²= .59983649
F(7,8)=4.2121 p<.03058 Std.Error of estimate: 3.1524

N=16	Beta	Std.Err. of Beta	B	Std.Err. of B	t(8)	p-level
Intercept			7.34152	7.842569	0.93611	0.376609
rpm	-0.214346	0.173688	-0.01218	0.009873	-1.23409	0.252192
feed	-0.571013	0.171739	-0.12607	0.037916	-3.32489	0.010464
plunge	-0.170515	0.231868	-6.99188	9.507637	-0.73540	0.483098
oxide	0.090810	0.164975	0.87633	1.592026	0.55045	0.597043
type	-0.473935	0.211918	-4.57352	2.045026	-2.23641	0.055737
thick	-0.545341	0.179513	-5.26259	1.732320	-3.03789	0.016115
time	0.240151	0.169198	2.31748	1.632780	1.41934	0.193566

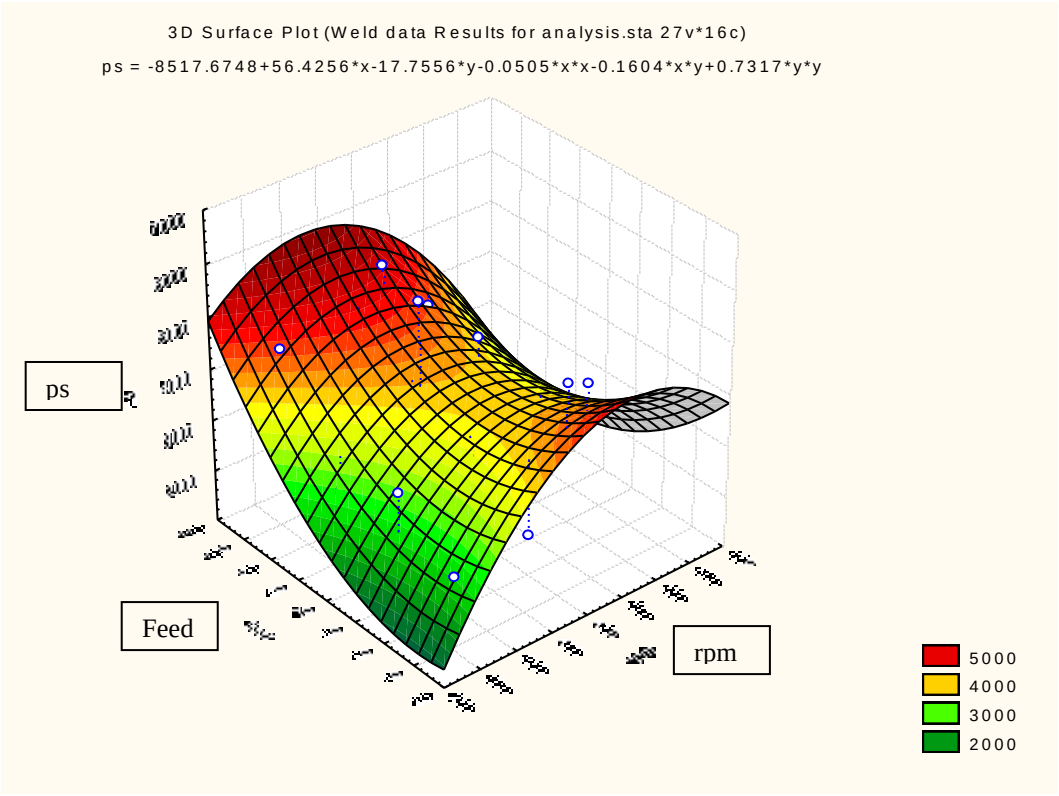
3D Surface Plot (Weld data Results for analysis.sta 27v*16c)
ps = -8517.6748+56.4256*x-17.7556*y-0.0505*x*x-0.1604*x*y+0.7317*y*y
ps
Feed
rpm
5000
4000
3000
2000

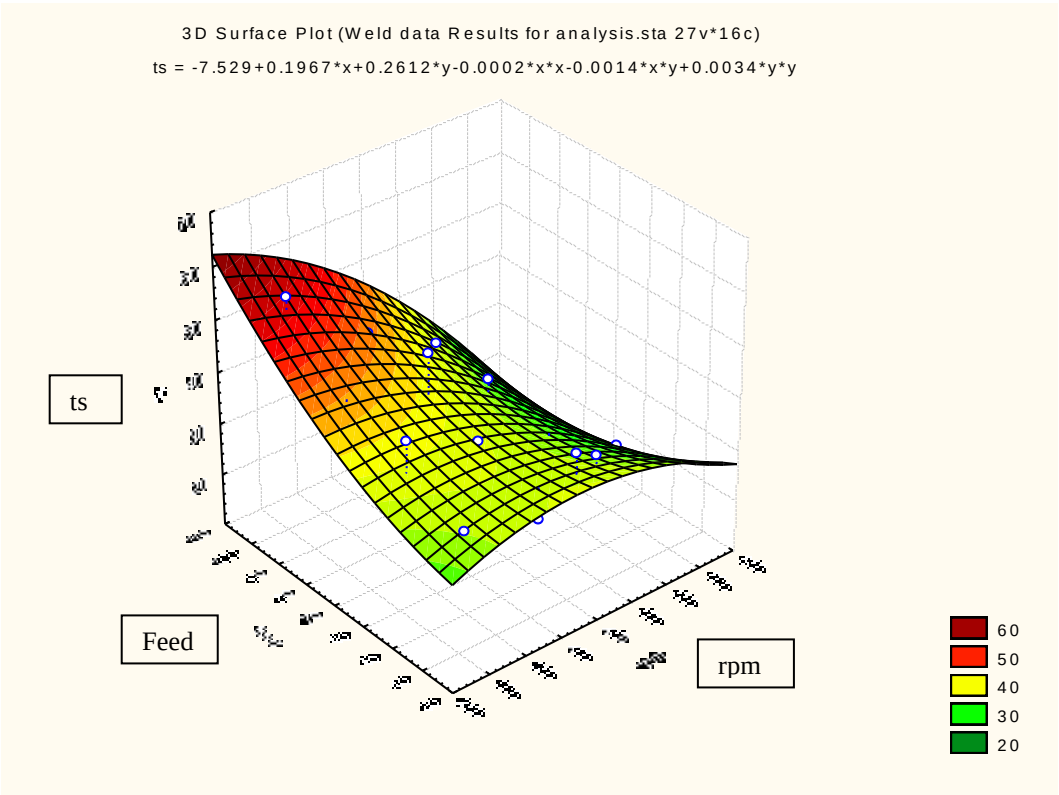
3D Surface Plot (Weld data Results for analysis.sta 27v*16c)
ts = -7.529+0.1967*x+0.2612*y-0.0002*x*x-0.0014*x*y+0.0034*y*y
ts
Feed
rpm
60
50
40
30
20

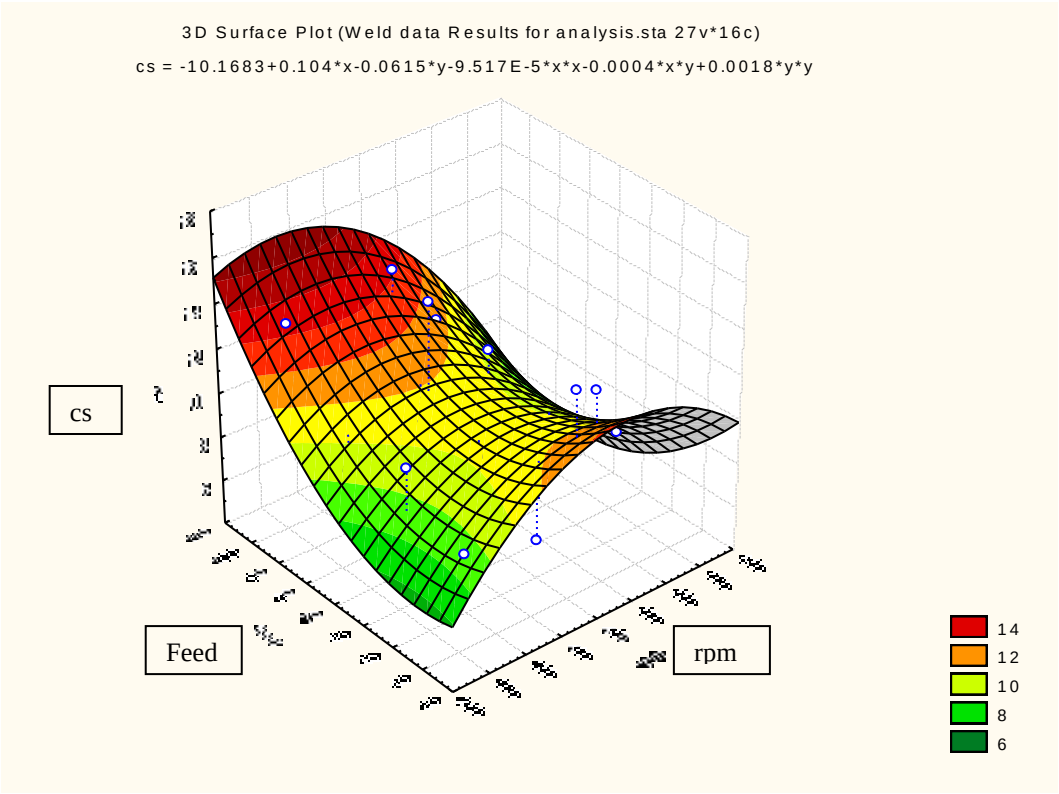
3D Surface Plot (Weld data Results for analysis.sta 27v*16c)
cs = -10.1683+0.104*x-0.0615*y-9.517E-5*x*x-0.0004*x*y+0.0018*y*y
cs
Feed
rpm
14
12
10
8
6

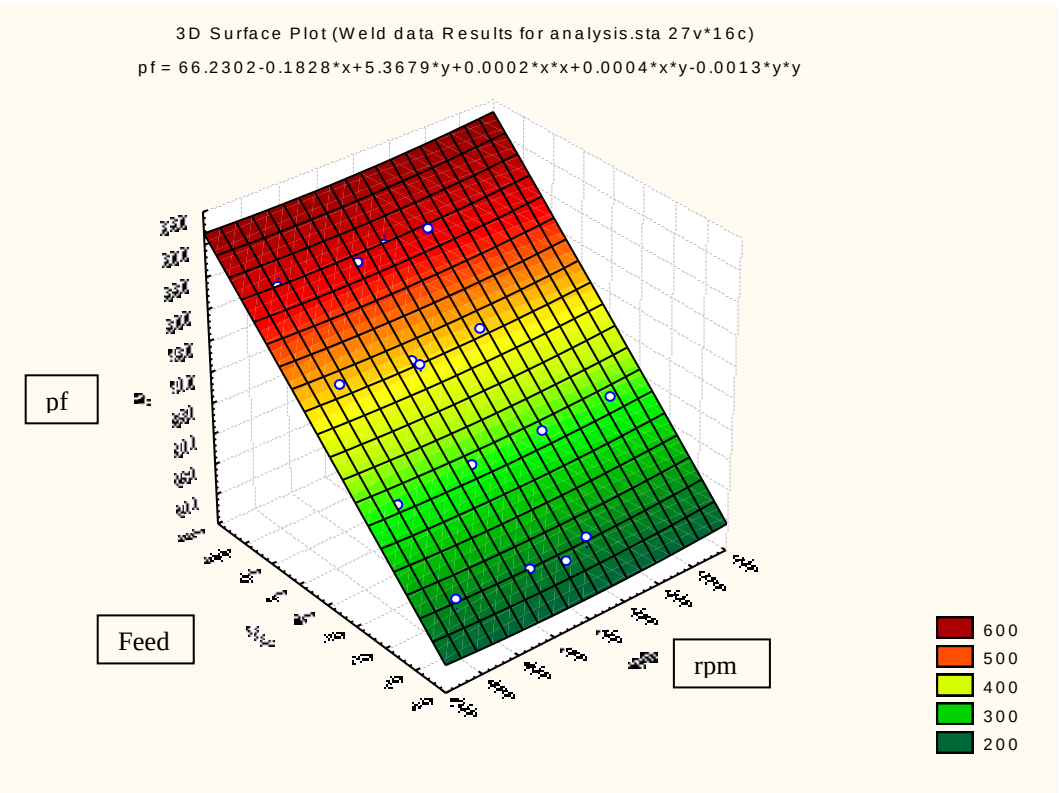
3D Surface Plot (Weld data Results for analysis.sta 27v*16c)
pf = 66.2302-0.1828*x+5.3679*y+0.0002*x*x+0.0004*x*y-0.0013*y*y
pf
Feed
rpm
600
500
400
300
200

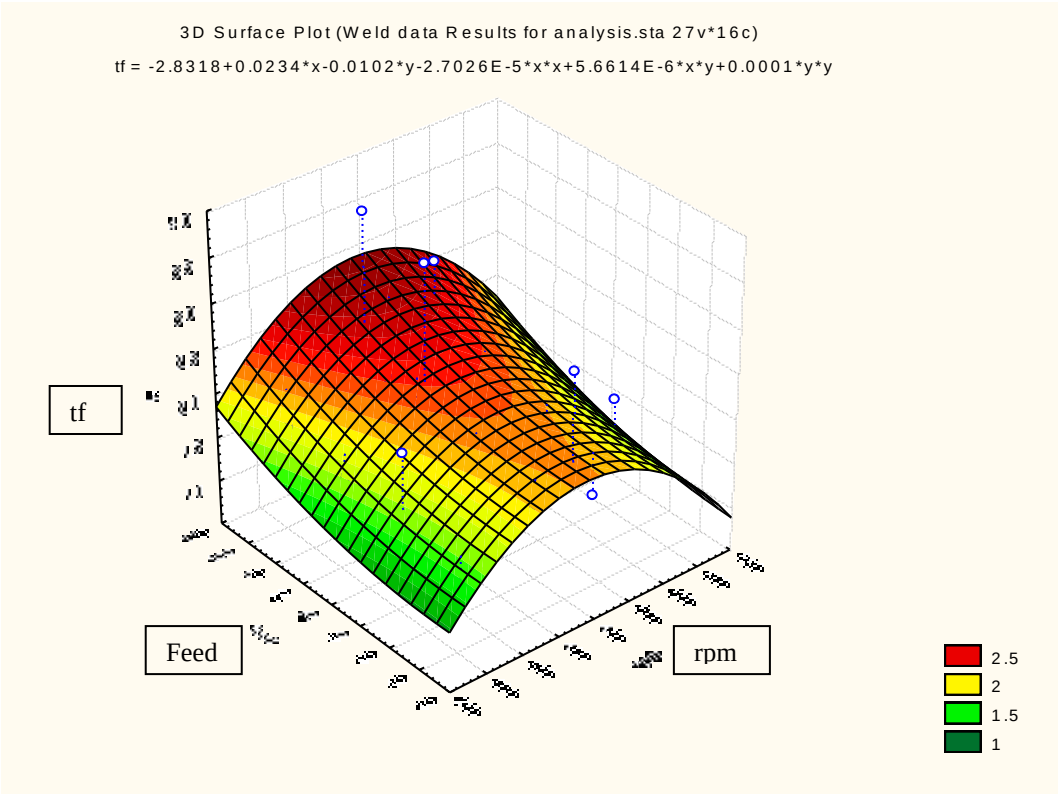
3D Surface Plot (Weld data Results for analysis.sta 27v*16c)
tf = -2.8318+0.0234*x-0.0102*y-2.7026E-5*x*x+5.6614E-6*x*y+0.0001*y*y
tf
Feed
rpm
2.5
2
1.5
1

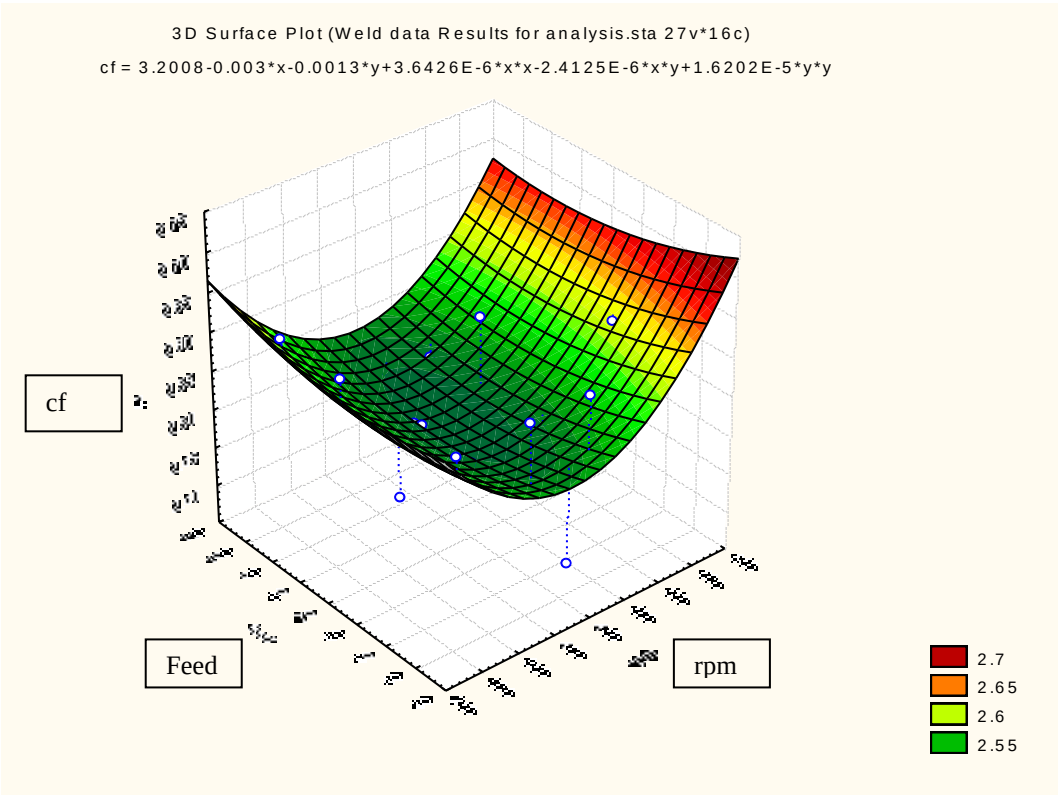
3D Surface Plot (Weld data Results for analysis.sta 27v*16c)
cf = 3.2008-0.003*x-0.0013*y+3.6426E-6*x*x-2.4125E-6*x*y+1.6202E-5*y*y
cf
Feed
rpm
2.7
2.65
2.6
2.55

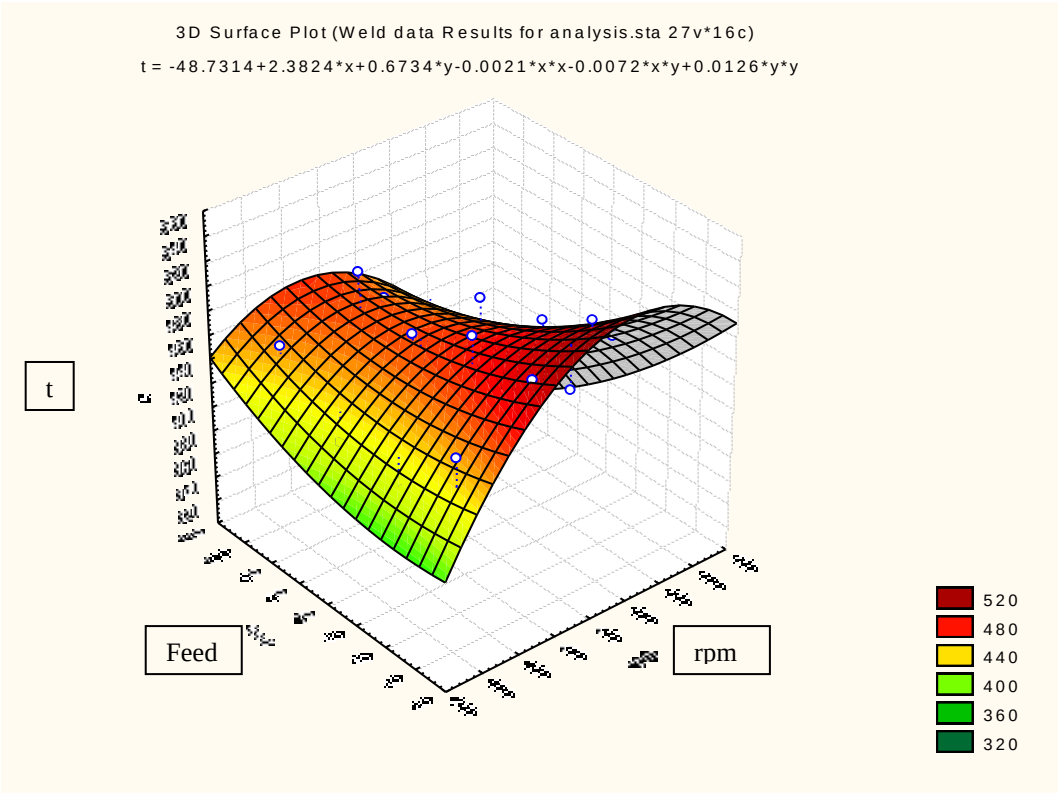
3D Surface Plot (Weld data Results for analysis.sta 27v*16c)
t = -48.7314+2.3824*x+0.6734*y-0.0021*x*x-0.0072*x*y+0.0126*y*y
t
Feed
rpm
520
480
440
400
360
320

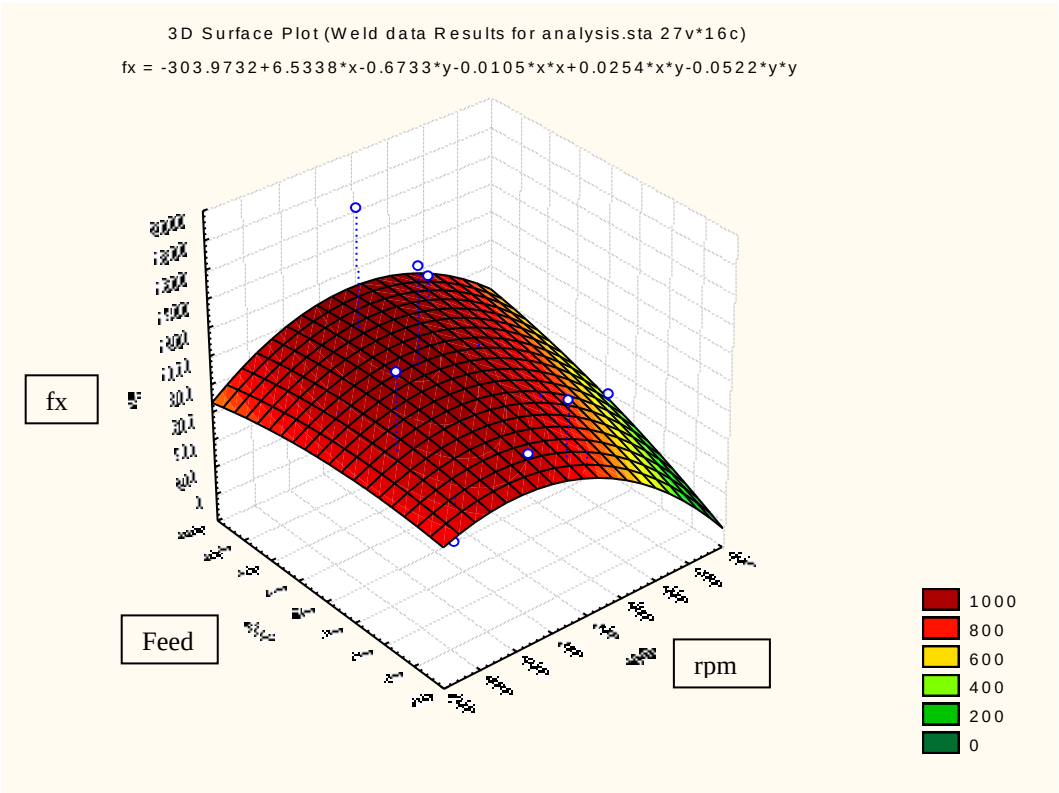
3D Surface Plot (Weld data Results for analysis.sta 27v*16c)
fx = -303.9732+6.5338*x-0.6733*y-0.0105*x*x+0.0254*x*y-0.0522*y*y
fx
Feed
rpm
1000
800
600
400
200
0

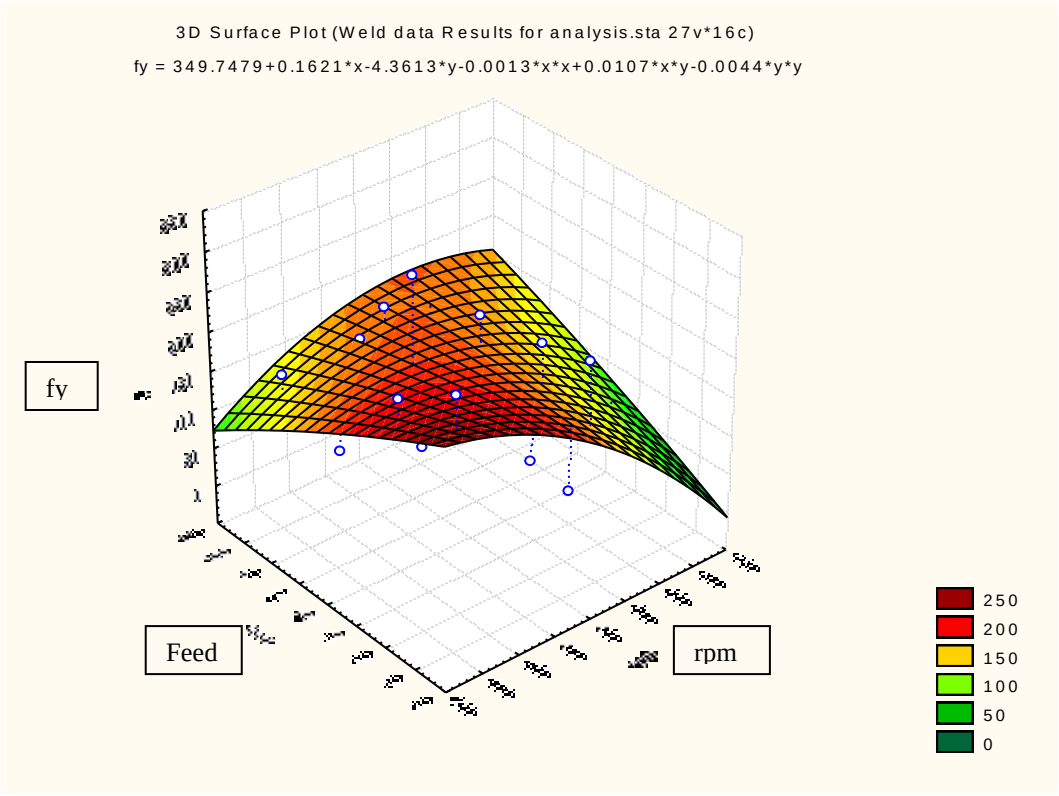
3D Surface Plot (Weld data Results for analysis.sta 27v*16c)
fy = 349.7479+0.1621*x-4.3613*y-0.0013*x*x+0.0107*x*y-0.0044*y*y
fy
Feed
rpm
250
200
150
100
50
0

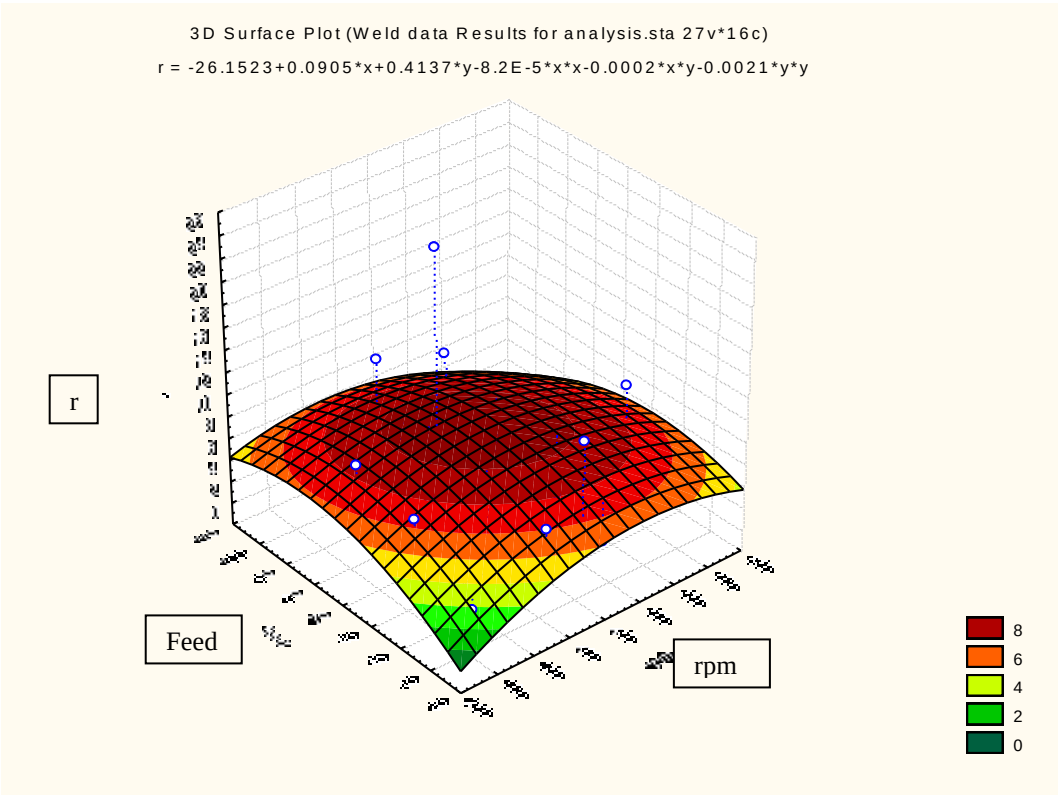
3D Surface Plot (Weld data Results for analysis.sta 27v*16c)
r = -26.1523+0.0905*x+0.4137*y-8.2E-5*x*x-0.0002*x*y-0.0021*y*y
r
Feed
rpm
8
6
4
2
0

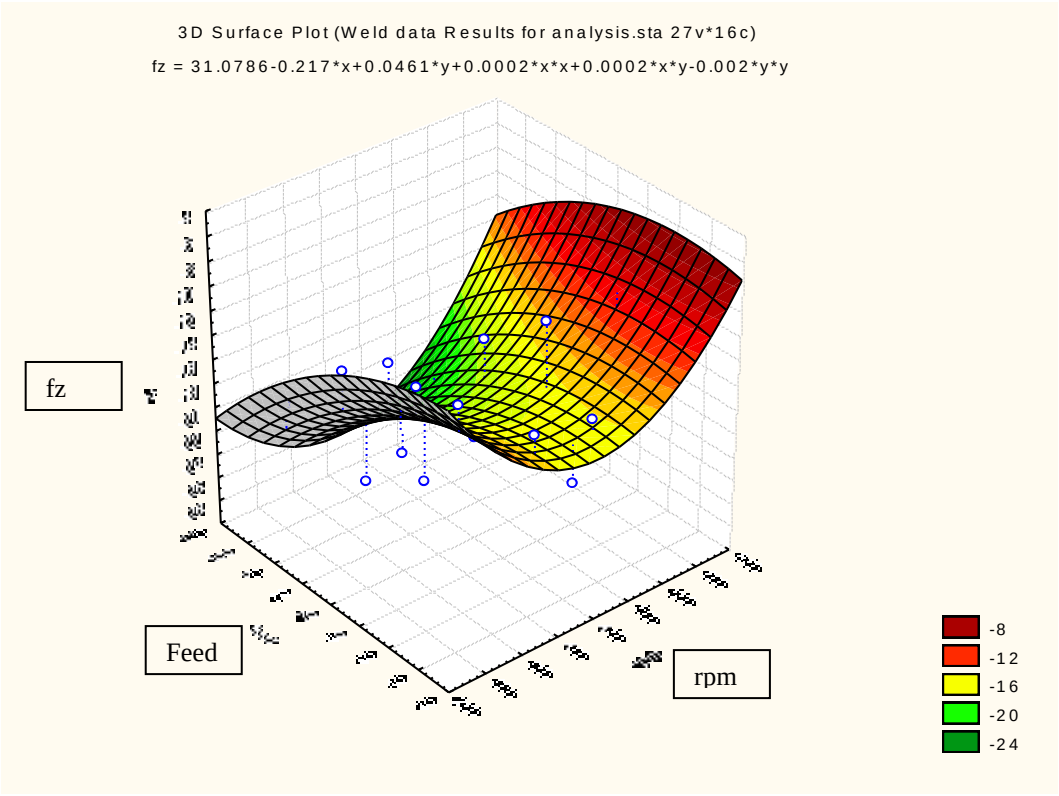
3D Surface Plot (Weld data Results for analysis.sta 27v*16c)
fz = 31.0786-0.217*x+0.0461*y+0.0002*x*x+0.0002*x*y-0.002*y*y
fz
Feed
rpm
-8
-12
-16
-20
-24

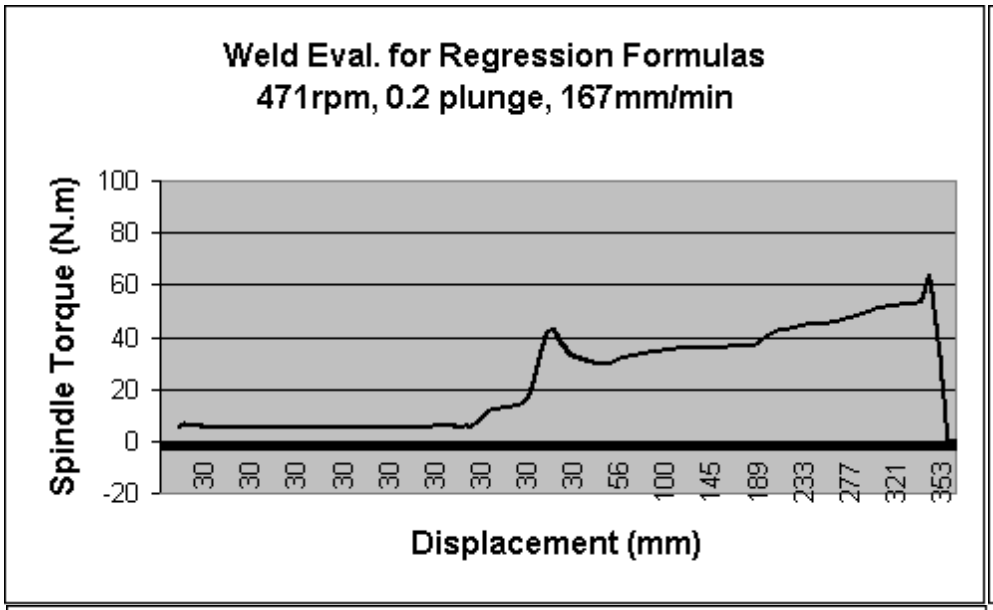
Weld Eval. for Regression Formulas
471rpm, 0.2 plunge, 167mm/min
Spindle Torque (N.m)
100
80
60
40
20
0
-20
30 30 30 30 30 30 30 30 30 56 100 145 189 233 277 321 353
Displacement (mm)

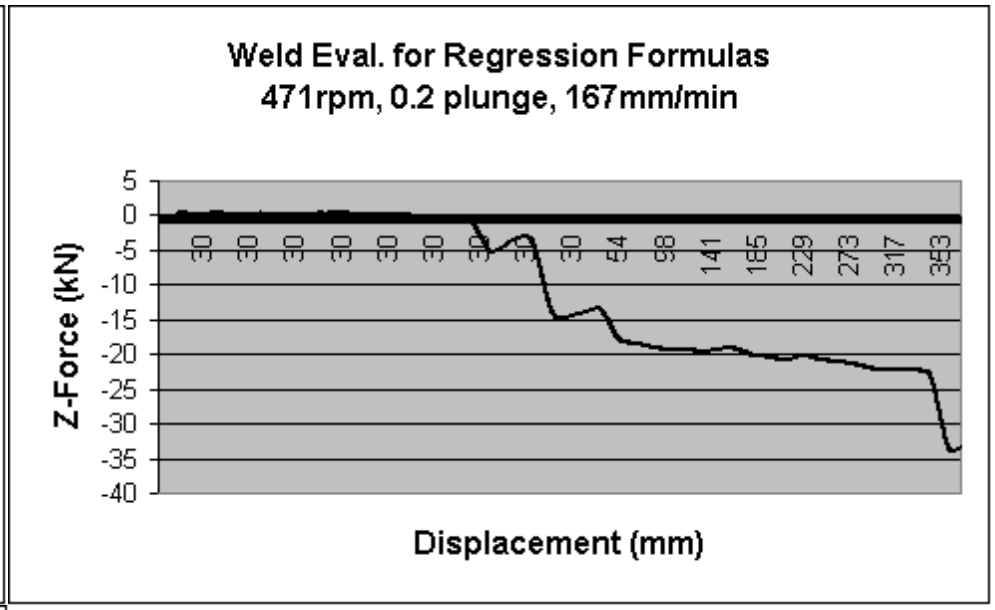
Weld Eval. for Regression Formulas
471rpm, 0.2 plunge, 167mm/min
Z-Force (kN)
5
0
-5
-10
-15
-20
-25
-30
-35
-40
30 30 30 30 30 30 30 30 30 54 98 141 185 229 273 317 353
Displacement (mm)

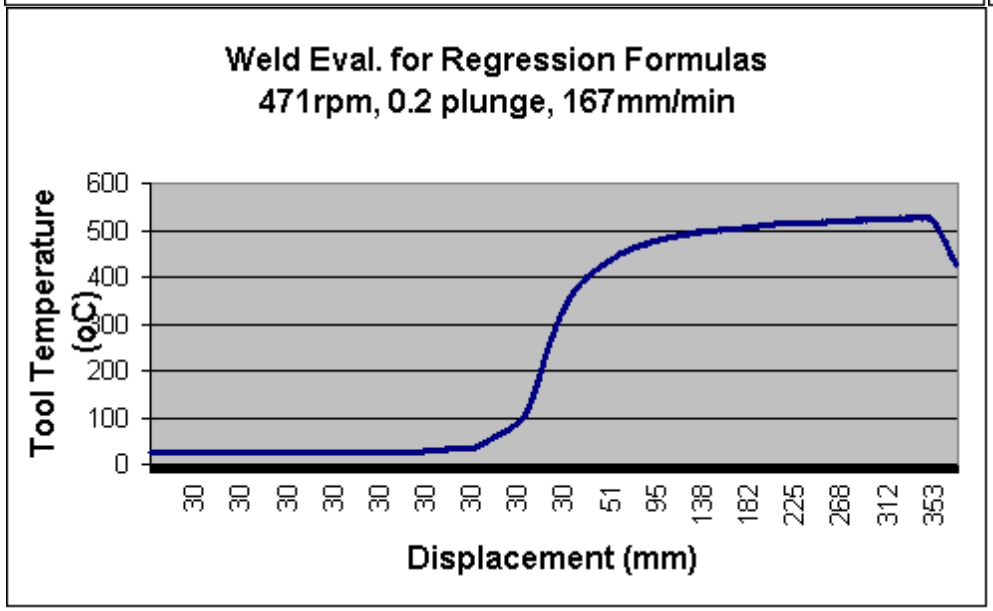
Weld Eval. for Regression Formulas
471rpm, 0.2 plunge, 167mm/min
Tool Temperature (oC)
600
500
400
300
200
100
0
30 30 30 30 30 30 30 30 30 51 95 138 182 225 268 312 353
Displacement (mm)

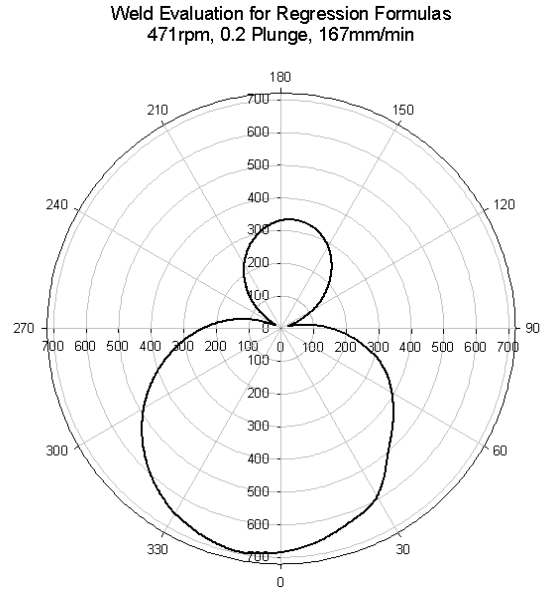
Weld Evaluation for Regression Formulas
471rpm, 0.2 Plunge, 167mm/min
180
210
150
240
120
270
90
300
60
330
30
0

Appendix D:

In Combination with Chapter 6

Page 229 – Important graphs obtained during a Weld evaluation

Page 230 – Successful Face and Root Bends at 180^0

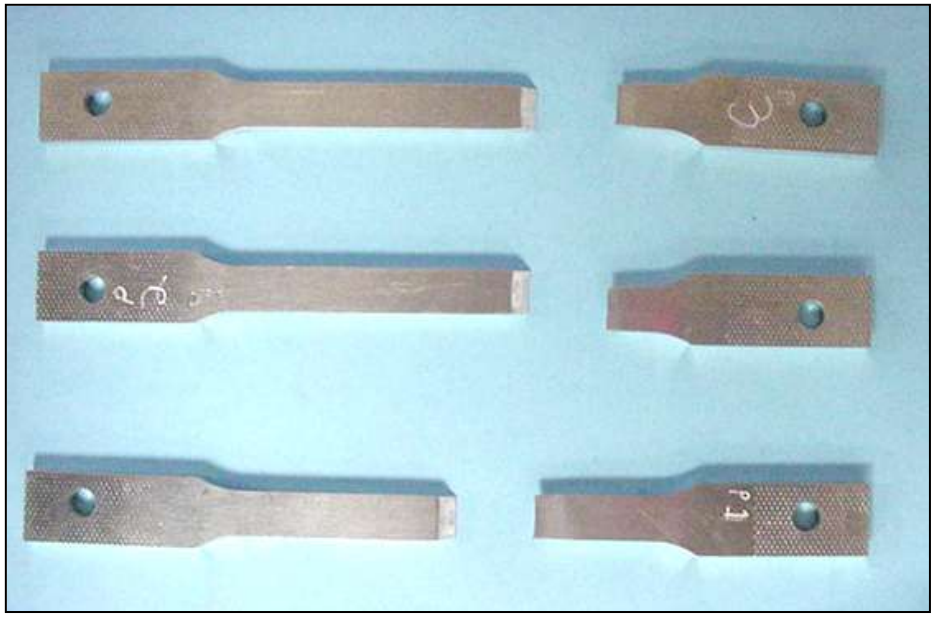

Parent Plate tensile specimens pulled and viewed after fracture.

Dimensions of tensile test specimens used for the analysis of the welded joint strength.

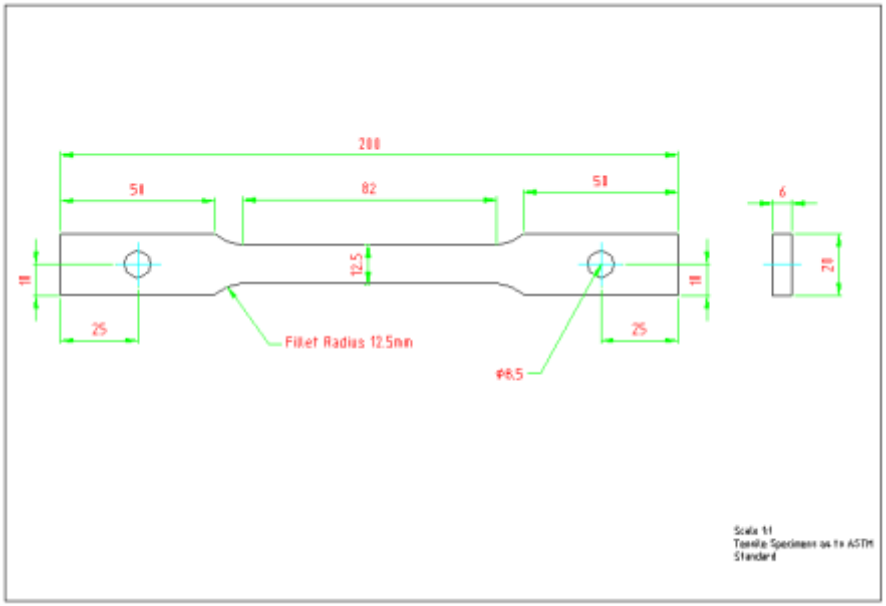

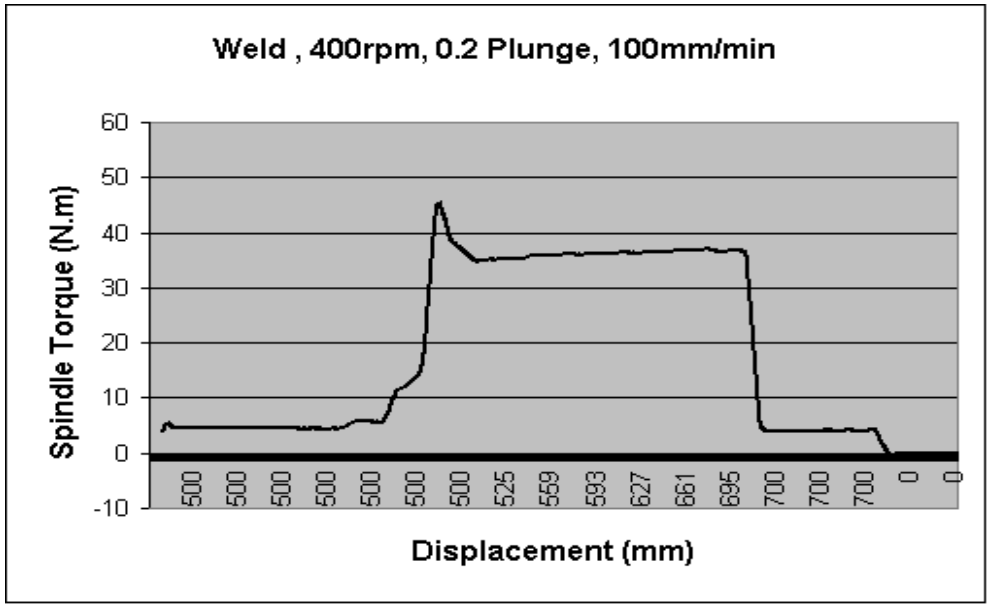
Weld , 400rpm, 0.2 Plunge, 100mm/min
Spindle Torque (N.m)
60
50
40
30
20
10
0
-10
500 500 500 500 500 500 500 525 559 593 627 661 695 700 700 700 0 0
Displacement (mm)

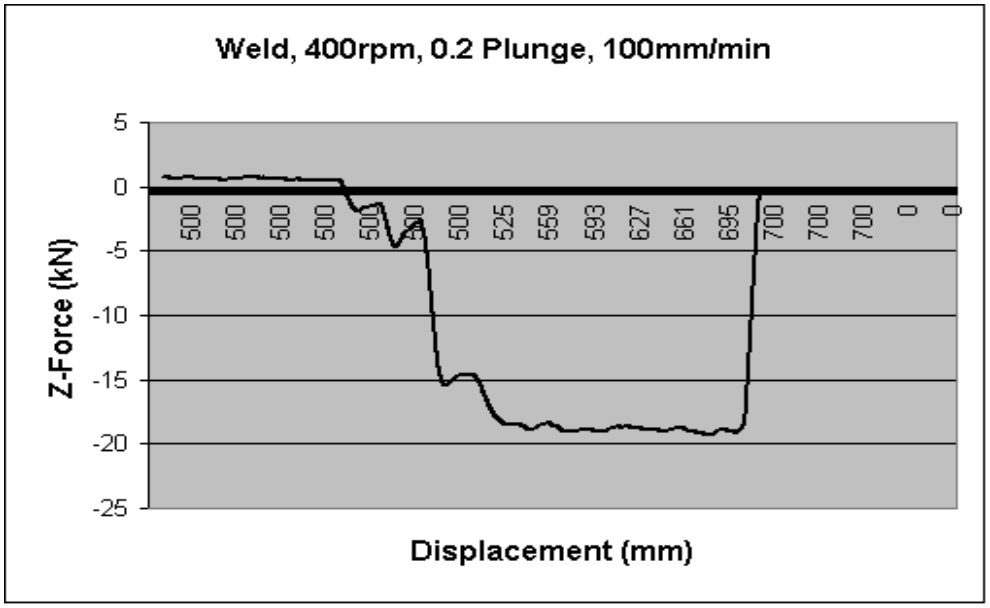
Weld, 400rpm, 0.2 Plunge, 100mm/min
Z-Force (kN)
5
0
-5
-10
-15
-20
-25
500 500 500 500 500 500 500 525 559 593 627 661 695 700 700 700 0 0
Displacement (mm)

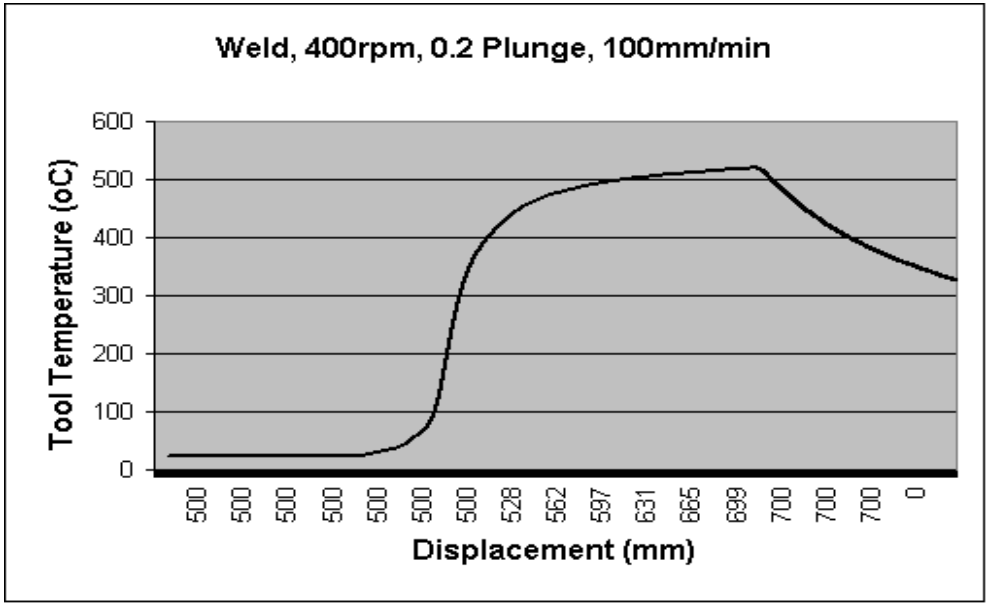
Weld, 400rpm, 0.2 Plunge, 100mm/min
Tool Temperature (oC)
600
500
400
300
200
100
0
500 500 500 500 500 500 500 528 562 597 631 665 699 700 700 700 0
Displacement (mm)

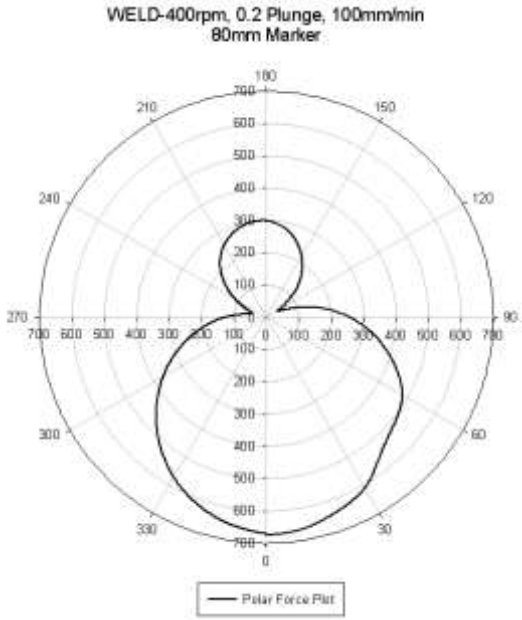
WELD-400rpm, 0.2 Plunge, 100mm/min
80mm Marker
Polar Force Plot

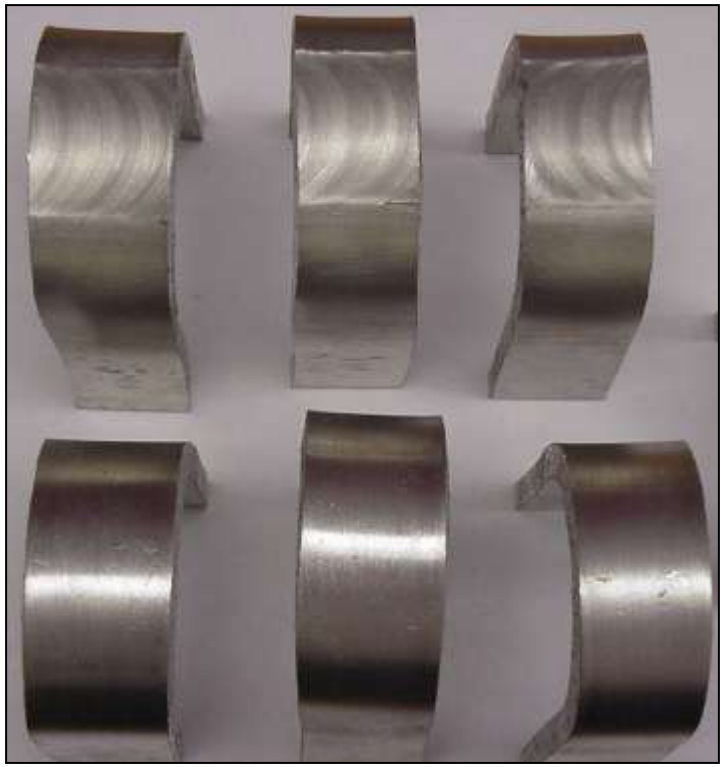

Successive Face (top) and Root (bottom) 180^0 bend tests perform on a weld made at 400rpm, 0.2 Plunge and 100mm/min.